Integrated benthic exchange dynamics and biogeochemical processes under varying environmental conditions

Dissertation
zur Erlangung des Doktorgrades
der Naturwissenschaften
- Dr. rer. nat. -

dem Fachbereich Biologie/Chemie
der Universität Bremen
vorgelegt von

Daphne Donis

November 2013

Die vorliegende Doktorarbeit wurde in Zeit von Januar 2010 bis November 2013 am Max-Planck Institut für Marine Mikrobiologie.

1. Gutachterin: Prof. Dr. Antje Boetius
2. Gutachter: Prof. Dr. Dieter Wolf-Gladrow

Tag des Promotionskolloquiums: 19. Dezember 2013

...E 'nt'a barca du vin ghe naveghiemu 'nsc'i scheuggi
emigranti du rìe cu'i cioi 'nt'i euggi
finché u matin crescià da puéilu rechéugge
frè di ganeuffeni e dè figge
bacan d'a corda marsa d'aegua e de sä
che a ne liga e a ne porta 'nte 'na creuza de mä...

Fabrizio De André

Summary

The early diagenetic processes that belong to the sea floor are determinant for the evolution of biogeochemical cycles in the ocean. The understanding of the sediment-water interface mechanisms, that control remineralization rates of organic matter in marine sediments, is essential for the assessment of carbon resevoirs, fluxes and turnover times. Those processes and their fashion, play a crucial role in regulating present Earth system dynamics.

Organic matter mineralization rates and burial efficiency in deep-sea sediments may be more dynamic than previously thought, as a response to changes in the carbon export from the water column (either from a seasonal point of view or as a possible consequence of climate change). Similarly, the contribution of coastal permeable sediments to global mineralization rates is not yet well quantified, due to the difficulty in accounting for complex factors that influence biogeochemical processes in sands (e.g. pore water advection and groundwater discharge).

A widely used proxy for carbon mineralization rates are oxygen benthic flux measurements, which, in order to be trustfully representative of the ongoing biogeochemical processes, need to be taken directly at the seafloor. Especially when studying deep-sea sediments and permeable sands, in situ flux measurements are necessary to account for conditions that could affect the reactions at the sediment-water interface (e.g. local hydrodynamics, flow topography, natural light condition), as well as to avoid artifacts generated by sediment core retrieval. In this context, pore water profilers, benthic chambers and eddy correlation systems, became fundamental technologies.

This work combines *in situ* measurements of benthic fluxes (particularly oxygen) with different methods in order to achieve a multiscale approach, from which it is possible to 1) point out methodological limits, 2) gain new insights into benthic biogeochemical processes. Most of the work presented in this thesis was focused on the eddy correlation (EC) technique. Among all the techniques used for quantifying benthic oxygen fluxes, this approach allows to quantitatively address benthic exchanges integrated over several square meters without interfering with the seafloor, thus usable in systems that are so far under-studied with respect to carbon mineralization. In addition the EC technique has the potential to perform long-term measurements under in situ conditions. However, general and objective evaluation criteria for its measurements are currently being defined.

In Chapter 2 it was investigated how, for EC measurements, the (necessary) distance between the oxygen sensor tip and the velocity sampling volume, and the response time of the oxygen sensor, can bias the derived benthic oxygen fluxes. The results indicate that some of the EC-flux variability, often encountered in field applications, can be

related to the orientation of the device with respect to the flow direction. We therefore provide suggestions for designing EC field deployments as well as for data processing, ameliorating knowledge for an accurate interpretation of the fluxes.

In Chapter 3 we examine the effect of non steady-state oxygen concentrations and current velocities on EC-fluxes. The results suggest that the velocity and oxygen concentration time series recorded during EC-deployments, as well as their rates of change, need to be carefully analyzed, in order to estimate how these factors may confound the true benthic flux. We show how the probability of erroneous flux estimations during transient conditions is higher for short deployments, while extended sampling periods would average out the biases leading to a trustworthy mean flux.

In Chapter 4 we present the deepest (2500 m) and lowest oxygen fluxes at the sediment-water interface (1 mmol m^{-2} d^{-1}) ever achieved with the EC technique. The applied post processing procedures and significance tests, were novel and necessary to deal with the limiting conditions that were found at this oligotrophic Arctic deep-sea site with low sediment respiration rates and low turbulence regimes (2-4 cm s^{-1}). Furthermore, the agreement of the obtained EC fluxes with other measurements (microprofiler and benthic chamber) allowed to confirm that deep-sea sediments in the Arctic have low oxygen uptake rates and faunal contribution to the remineralization of organic matter is rather small.

In Chapter 5 we evaluate the effect of submarine groundwater discharge (SGD) on mineralization pathways and net community production of sandy sediments. Benthic flux measurements (obtained by stirred benthic chambers) indicate that aerobic oxidation of organic matter represents the main mineralization pathway, and similar rates of total oxygen uptake are observed at two adjacent sites (impacted and non-impacted by SGD). Furthermore, the SGD supply of phosphate and silicate to the water column, that was observed at the seep site, was not reflected on net primary productivity. The main difference observed between biogeochemical processes at the two sites was driven by the supply of methane by SGD at the seep site, where anaerobic oxidation of methane (AOM) is indicated as an important process taking place in the surface sediment sublayers (7-10 cm).

In the perspective that in situ observations of benthic systems need to be disseminated more and improved in a way to be capable to determine whether a system is changing on long time scales, this work represents a next step for taking full advantage of one of the techniques that have this potential, i.e. aquatic eddy correlation. Furthermore, this work advances our understanding of dynamic benthic exchange processes in deep-sea and permeable sediments. The techniques that were applied and improved during

this thesis, can provide important information on the status of ecosystems, and may therefore also contribute to ecosystem based management strategies.

Zusammenfassung

Die Remineralisierung organischen Materials am Meeresboden ist ein wichtiger Teil des Kohlenstoffkreislaufs, weshalb die Bestimmung von Mineralisierungsraten notwendig ist, um das globale Kohlenstoffbudget besser einschätzen zu können.

Die Mineralisierungsraten und die Effizienz mit der organisches Material in Tiefseesedimenten langfristig gespeichert wird, sind möglicherweise dynamischer als bisher angenommen, abhängig von Veränderungen des Kohlenstoffexports aus der Wassersäule (entweder hervorgerufen durch saisonale Änderungen oder als Konsequenz des Klimawandels). Gleichzeitig ist es nur begrenzt möglich, den Beitrag küstennaher permeabler Sedimente zu den globalen Mineralisierungsraten abzuschätzen, da es schwierig ist, alle Faktoren, die die biogeochemischen Prozesse im Sand beeinflussen können, zu berücksichtigen. Zu diesen Faktoren zählen zum Beispiel die vorherrschenden hydrodynamischen Bedingungen oder das Auftreten von submarinen Grundwasseraustritten (SGD).

Benthische Sauerstoffflussmessungen werden häufig genutzt, um die Mineralisierung von Kohlenstoff zu berechnen. Die Anzahl von in situ Untersuchungen benthischer biogeochemischer Prozesse in marinen Sedimenten ist jedoch gering und meist nur auf bestimmte Regionen beschränkt. In situ Stoffflussmessungen werden direkt am Meeresboden ausgeführt, da es in einigen Ökosystemen (z.B. in der Tiefsee und in permeablen Sedimenten) nur so möglich ist, alle Faktoren, die die Vorgänge an der Sediment-Wasser-Grenzschicht beeinflussen können (z.B. lokale Hydrodynamik, Topographie, natürliche Lichtbedingungen), zu berücksichtigen. Außerdem werden so Artefakte vermieden, die während der Probenentnahme von Sedimentkernen entstehen können. In diesem Zusammenhang wurden Porenwasser-Microprofiler, Respirationskammern und Eddy Correlation Systeme zu fundamentalen Techniken.

Diese Arbeit kombiniert in situ Messungen benthischer Stoffflüsse (insbesondere Sauerstoff) mit verschiedenen anderen Methoden, um einen ganzheitlichen Ansatz zu erreichen, der es ermöglicht, 1) neue Einblicke in benthische biogeochemische Prozesse zu erhalten und 2) methodische Limitierungen aufzudecken. Die meisten Untersuchungen, die in dieser Arbeit vorgestellt werden, sind auf die Eddy Correlation (EC) Technik gestützt. Mit dieser Methode ist es möglich, benthische Austauschraten quantitativ über mehrere Quadratmeter zu integrieren, in Systemen, die in Bezug auf Kohlenstoffmineralisierung bisher nur wenig erforscht sind. Außerdem ermöglich die EC Technik Langzeit-, störungsfreie und nicht-invasive Messungen unter in situ Bedingungen. Es müssen jedoch noch allgemeingültige und objektive Evaluationskriterien für diese Form der Messung definiert werden.

In Kapitel 2 dieser Arbeit wurde untersucht inwiefern die Entfernung der Sauerstoffsensorspitze zum zu messenden Probenvolumen und die Reaktionsgeschwindigkeit des Sauerstoffsensors, die gemessenen benthischen Sauerstoffflüsse des EC Systems beeinflussen können. Die Ergebnisse deuten darauf hin, dass die Variabilität des EC-Flusses, die häufig in Feldversuchen auftritt, in Zusammenhang mit der Orientierung des Gerätes zur Fließrichtung steht. Wir machen daher Vorschläge für die Planung von EC Messstationen sowie für die Datenverarbeitung solcher Messungen, um eine akkuratere Interpretation von EC Daten zu ermöglichen.

In Kapitel 3 studieren wir den Effekt von nicht-stabilen (non steady state) Sauerstoffkonzentrationen und Fließgeschwindigkeiten auf den EC-Fluss. Die Ergebnisse zeigen, dass aufgezeichnete Zeitreihen von Geschwindigkeits- und Sauerstoffkonzentrationsmessungen während des Einsatzes des EC-Systems, sowie deren Änderungsraten sorgfältig analysiert werden müssen,, um deren Einfluss auf den tatsächlichen benthische Stoffffluss besser bewerten zu können. Wir zeigen, dass die Wahrscheinlichkeit von fehlerhaften Stoffffluss-Schätzungen während Übergangsbedingungen höher ist, wenn das System nur kurz zum Einsatz kommt, während längere Messungen eine geringere Verzerrung zeigen und somit zuverlässigere Flussraten ermitteln.

In Kapitel 4 präsentieren wird die tiefsten (2500 m) und niedrigsten Sauerstoffflüsse (1 mmol m^{-2} d−1), die mit der EC-Technik bisher an der Sediment-Wasser Grenzschicht gemessen wurden. Die verwendete Nachbearbeitung der Daten und Signifikanz-Tests stellen neue Ansätze dar, die notwendig waren, um die limitierenden Bedingungen in diesem oligotrophen, arktischen Ökosystem mit niedrigen Respirationsraten und geringer Turbulenz (2-4 cm s^{-1}) zu berücksichtigen. Durch die Übereinstimmung der gemessenen EC-Flüsse mit anderen Messungen (Mikrosensorprofile und benthische Kammern), konnten wir bestätigen, dass arktische Tiefseesedimente einen niedrigen Sauerstoffverbrauch aufzeigen und dass der Anteil der Fauna an der Remineralisierung organischen Materials gering ist.

Im Kapitel 5 evaluieren wir den Effekt von submarinen Grundwasseraustritten (submarine groundwater discharge, SGD) auf Mineralisierungsvorgänge und die Nettoprimär produktion von sandigen Sedimenten. Benthische Flussratenmessungen (ermittelt mit Hilfe von benthischen Respirationskammern) weisen darauf hin, dass die aerobe Oxidation organischen Materials für den Großteil der Mineralisierungsvorgänge verantwortlich ist. In zwei aneinander angrenzenden Untersuchungsgebieten (ein Gebiet unter Einfluss von Grundwasseraustritten, das andere ohne Einfluss von Grundwasseraustritten) wurden vergleichbare Sauerstoffverbrauchsraten ermittelt . Desweiteren wurden keine Auswirkungen auf die Nettoprimär produktion durch den Eintrag von Phosphat

und Silikat in die Wassersäule beobachtet, der durch den Grundwasseraustritt verursacht wurde. Unterschiede in den biogeochemischen Prozessen an beiden Untersuchungsorten wurden vor allem durch das Vorhandensein von Methan an der Grundwasseraustrittsstelle hervorgerufen, wo die anaerobe Oxidation von Methan (AOM) einen wichtigen Vorgang in Sedimentschichten (7-10 cm) unterhalb der Oberflächensedimente darstellt.

Da in situ Untersuchungen von benthischen Systemen optimiert werden müssen, um feststellen zu können, ob ein System Langzeitänderungen aufweist, stellt diese Arbeit einen wichtigen Schritt dar, um das volle Potential der vorhandenen Techniken nutzen zu können, z.B. der aquatischen Eddy Correlation. Außerdem trägt die Arbeit zu einem besseren Verständnis dynamischer Austauschprozesse in Tiefseesedimenten und permeablen Sanden bei. Die Techniken, die in dieser Arbeit angewendet und verbessert wurden, können wichtige Informationen zum Status eines Ökosystems liefern und so auch zu einem Ökosystem-basierten Management beitragen.

Contents

Chapter 1

Introduction

The sediment-water interface plays a key role in the Earth system, with crucial filter functions for the mass exchange between the seafloor and the water column. Early diagenetic processes, that take place at this separation line between ocean water and sediment, are determinant for the fate of solutes and particles that can be recycled or buried over geological time scales. Marine sediments are indeed the primary long term repository of organic matter, thus the systematic study of the control mechanisms of organic matter degradation is essential for the reconstruction of biogeochemical cycles in the ocean.

When studying the early diagenesis of sediments, of either deep-sea or coastal ecosystems, it is important to consider all features of the oceanic environment. Benthic biogeochemical processes show a mutable spectrum of variability, depending for instance, on the amount and composition of the available organic matter, on the solutes composition of the overlying and interstitial water and on the interaction between benthic boundary layer flows and seabed topography.

Due to the complexity, remoteness and spatio-temporal variability of the seafloor, the relationships between tightly coupled biological, physical and geochemical processes are still a matter of study and foster the development of new technologies, especially in order to achieve accurate carbon budgets.

1.1 Organic matter remineralization in marine sediments

Organic matter (OM) is supplied to the marine sediments by the overlying water column from either marine or terrestrial sources and constitutes the principal food source for most of the benthic fauna and microbes. Whereas the main source for OM is considered

to be phytoplankton detritus, whose supply to the seafloor is tightly coupled to the water column primary productivity, terrigenous OM is largely brought to the oceans by rivers, in either a dissolved or a particulate form (Burdige, 2007).

Thereby OM presents a wide range of sources and constituents, and its composition can be generalized by the following chemical formula (where (x), (y) and (z) values depend on the origin and age of the material):

$(CH_2\ O)x(NH_3)y(H_3PO_4)z$.

Detrital OM found in sediments typically contains similar proportions of compounds such as: carbohydrates (10-20%), nitrogenous compounds (mostly amino acids) (10%), lipids (5-15%) and humic substances that are relatively resistant to biological degradation (e.g. Schnitzer, 1991; Hedges and Oades, 1997; Burdige, 2007).

The degradation of OM starts immediately in the water column until it is then converted back into its inorganic constituents by heterotrophic organisms in a continuous process referred to as *remineralization*. This process serves as carbon source for heterotrophic organisms and controls the recycling of inorganic carbon and nutrients, the dissolution of carbonates, the flux of organic carbon to the deep biosphere and its burial in the sediment. (e.g. Canfield et al., 2005; Middelburg and Meysman, 2007). As a result, OM degradation determines the net CO_2 removal from the atmosphere, playing therefore a fundamental role in the global carbon cycle (e.g. Arthur et al., 1988; Berner and Canfield, 1989; Berner, 1990; Siegenthaler and Sarmiento, 1993; Archer and Maier-Reimer, 1994; Mackenzie, 2004; Ridgwell and Zeebe, 2005; Ridgwell and Hargreaves, 2007).

The OM that originates from biological photosynthetic activity in the photic zone, and escapes remineralization and grazers in the water column, rains onto the sediments (e.g. Berner, 1978; Jørgensen, 1978; Middelburg, 1989; Boudreau and Ruddick, 1991). The resulting percentages of deposited OM vary depending mainly on: water depth, primary production in the surface waters and processes of water column mixing (see sect. 1.1.1).

Once it reaches the seafloor, OM is remineralized by an array of aerobic and anaerobic processes. Although fauna contributes to the remineralization (see sect. 1.1.2.1), microorganisms and mainly bacteria are the dominant players in this context because of their versatile metabolism, covering both aerobic and anaerobic pathways.

Bacteria are sustained by the breakdown of large molecules of OM, eventually actively hydrolyzed into small mono- or oligomers (Munster and de Haan, 1998). This process is coupled to the sequential utilization of terminal electron acceptors with redox potentials that determine the energy yield of the individual metabolic pathways (Froelich et al.,

1979). The well-known order of electron acceptor utilization, based on the free energy yield available to the organisms is:

$$O_2 \rightarrow NO_2^- \rightarrow NO_3^- \rightarrow MnO_2 \rightarrow FeOOH \rightarrow SO_4^{2-} \rightarrow CO_2$$

Generally with increasing sediment depth, when a favorable electron acceptor is depleted, the next favorable will be used, although there may be some vertical overlap (Canfield and Thamdrup 2009). A large variety of metazoans and prokaryotes can mineralize organic matter completely into inorganic nutrients CO_2 and H_2O by using oxygen as the terminal electron acceptor, while anaerobic respiration is conducted by a consortia of organisms and can proceed via denitrification, manganese- and iron-reduction, sulfate reduction and methanogenesis (Table 1). Despite the relatively low rates, the two latter processes account for ca. 30% of global carbon remineralization and can extend down to hundred of meters into the sediment (Jørgensen 2000).

TABLE 1.1: Free energy changes for remineralization reaction (Morel and Hering, 1993). CH_2O represents sucrose.

Reaction	Free Energy Change kj mol^{-1} of CH_2O
$CH_2O + O_2 \rightarrow CO_2 + H_2O$	-476
$5CH_2O + 4NO_3^- \rightarrow 2N_2 + 4HCO_3^- O + CO_2 + H_2O$	-452
$CH_2O + 3CO_2 + H_2O + 2MnO_2 \rightarrow 2MnO_2 + 4HCO_3^-$	-388
$CH_2O + 7CO_2 + 4Fe(OH)_3 \rightarrow 4Fe^{2+} + 8HCO_3^- + 3H_2O$	-187
$2CH_2O + SO_4^{2-} \rightarrow HS^- + 2HCO_3^-$	-82
$2CH_2O \rightarrow CH_4 + CO_2$	-71

Characteristic solutes accompany most of the metabolic processes through sediments (Canfield and Thamdrup, 2009), molecular diffusivity being the most important mechanism by which these diffuse in pore water (see section 1.2.2.). Pore water properties are altered by remineralization of OM but also by dissolution or precipitation and adsorption or desorption of chemicals. These chemical and biological processes create concentration gradients (Fig. 1) that result in diffusion to and from the overlying water column, as well as to and from different regions of the sediments (Blackburn et al., 1994; Glud et al., 1994; Thamdrup et al., 1994b; Rysgaard and Berg, 1996).

Estimates of the global remineralization rates due to each of the oxidants indicate that aerobic respiration is by far the dominant process, accounting for 65% of the total remineralization (Canfield, 1993a). Sulfate reduction is the next (17.9%, Canfield, 1993b), followed by methanogenesis (9.8%, Hinrichs and Boetius, 2002) and denitrification (6.5% Dunne at al., 2005 and Gruber, 2004), while the reduction of manganese and iron makes a negligible contribution overall ($\sim$0.6%, $\sim$0.3% Bender and Heggie, 1984; Heggie at al 1997; Bender et al., 1989).

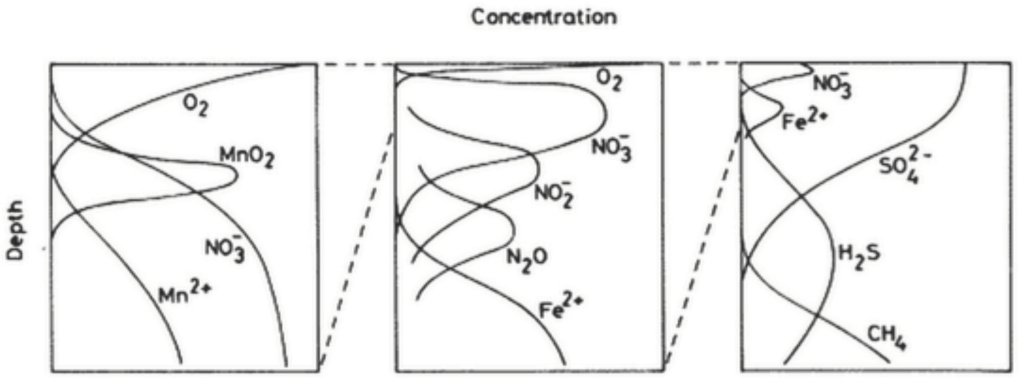

FIGURE 1.1: Idealized diagram of distribution of oxidants and their products in the pore waters of marine sediments. Reduction of oxygen gives the highest energy yield, while reduction of HCO_3 is barely an exergonic reaction. (from B. B. Jørgensen 1983).

The relative importance of the various remineralization pathways changes with sediment type and sedimentation rate. For instance aerobic respiration and sulfate reduction are the most important degradation processes in shelf sediments, where often of minor importance for organic matter mineralization are the rates of denitrification (Marinelli et al., 1998; Trimmer et al., 2000) and metal reduction (Jørgensen, 2000). In sandy sediments usually contents of Fe(III) and Mn(IV) are not high enough to support a significant heterotrophic metal reduction by bacteria (de Beer et al., 2005). However, denitrification and metal reduction can be enhanced by faunal activity and pore water advection (see Sect. 1.1.2). On the other hand,aerobic remineralization is the principal process for deep-sea sediments (>1000 m depth) that cover 90% of the area of oceans and seas (Jørgensen, 1983; Canfield, 1993a) (see Sect. 1.2).

This variety is determined by several factors, some of which have a direct effect on the degradation process efficiency, such as OM composition (e.g. Tegelaar et al., 1989; Dauwe et al., 2001), the ability of the microbial community to degrade it (Wetzel, 2001), the presence of grazers (Lee, 1992) and the availability of electron acceptors and redox conditions. Indirect factors are instead related to the water depth and the type of sediment, i.e. OM deposition rates and pore water advection.

1.1.1 Influence of deposition rates on organic matter remineralization

Organic matter supply to the seafloor is largely a function of productivity and water depth, however, vertical carbon transport velocities are highly variable and differ between ocean regions (e.g. Berelson, 2002). Thus, since most of the highly productive areas in the global ocean are adjacent to the continents, we can expect that benthic respiration intensity follows a decreasing gradient from coastal marine environments over

the continental shelves and slopes to the deep-sea (Wenzöfer and Glud, 2002). Fluxes of oxygen for instance, vary over orders of magnitude between oligotrophic open ocean areas and continental shelf areas (50 to 6000 mmol m^{-2} y^{-1}) (e.g. Devol and Christensen 1993; Glud et al. 1994; Berelson et al., 1994; Hammond et al., 1996; Luther et al., 1997; Hensen et al., 1998; Wenzöfer and Glud, 2002). Anyhow, lateral transport of organic material down-slope of margin sediments has been observed (e.g. Hecker, 1990) and probably explains intensified degradation activity along some ocean margins (Jahnke et al.,1990).

Annual primary production in the water column overlying sediments was estimated as 470 g C m^2 yr^{-1} (Wollast, 1998). About 20 % of this is produced in shallow waters, above the continental shelves (0 -200 m), although these regions cover only 7 % of the global seafloor (Wollast, 2002). Such high productivity is sustained by the upwelling of nutrient rich water near the shelf break, as well as by the input of nutrients from rivers, groundwater discharge and Aeolian input (Wollast, 1991; Gattuso et al., 1998; Herbert, 1999). Sediments at these depths receive and mineralize more than 95 % of the OM introduced to the continental shelf by primary production, that only in less extent is remineralized in the water column (de Haas et al., 2002).

Open oceans (depths > 1000 m), conversely, are mostly oligotrophic compared to coastal areas, but cover 90% of the global seafloor. On a global scale the majority of marine primary production is ascribed to these regions (Ryther, 1969; Antoine et al., 1996) but only a small fraction of the carbon produced at the surface reaches the seafloor. In this regard empirical results from sedimentation traps predict that over 90% of remineralization takes place within the upper hundreds of meters of the water column (assuming a surface primary production of 250 g C m^2 yr^{-1}) and at depth horizon of 1000 m only less than 5% of primary produced OM is left (Betzer et al., 1984; Berger et al., 1987; Martin et al., 1987). However, comparative measurements between primary production and benthic mineralization processes show that these empirical formulations are restricted to a limited regional use (Jahnke et al.1990; Rowe et al., 1994; Hensen et al., 2000). Indeed, patterns of decreased particulate OM at different depths deviate between ocean basins depending on the factors that control the particle transport through the water column (such as advection and water mixing), OM composition and its fractionation prior to deposition (Wakeham et al., 1997, Lee et al., 2004).

1.1.2 Influence of pore water advection on organic matter remineralization

When OM is present in the sediemnts, the mineralizazion process advances more or less intensively depending, for instance, on the oxygen penetration depth. The increased oxygen penetration depth due to advective pore water flow can largely increase aerobic mineralization (Lohse et al. 1996; Ziebis et al., 1996) as well as nitrification rates within oxic sediment layers that can by turn stimulate denitrification activity, and nitrogen release from the sediment (Kristensen et al. 1985; Huettel, 1990; Lohse et al. 1993). Oxygen penetration depth can strongly influence as well the fate of metals (Fe and Mn) and metal oxides, by the change of their oxidation state and consequent precipitation or complexation with reduced species (i.e. Fe(II) with S_2^-)(Shaw et al., 1990). These effects can be stimulated either by faunal activity (1.1.2.1) or by the interaction between the flow field and bottom topography of permeable sediments (1.1.2.2).

1.1.2.1 Role of fauna

Experimental studies demonstrate that fauna directly alter the fate of incoming fresh OM, either by feeding directly on it or producing irrigation and bioturbation of the sediments (Moodley et al., 2002, 2005a; Witte et al., 2003). Bioturbation causes a modification of the redox potential in the immediate surroundings of the burrow, by venting layers of sediment that oxygen would never reach if transport was restricted to molecular diffusion (see Section 1.2.2). As a result, large fauna acts to maintain habitat heterogeneity (Thrush et al., 2006a) and enhance OM recycling primarily through induced irrigation of deeper sediment layers and enhanced sediment-water solute exchange across the sediment-water interface (Huettel, 1990; Aller 1994; Graf and Rosenberg 1997; Biles et al., 2002; Lohrer et al., 2004; Mermillod Blondin et al. 2004; Michaud et al., 2005; Meysman et al., 2006; Thrush et al., 2006). In addition, benthic fauna decompose significant amounts of OM by digestion (Lopez and Levinton, 1987), leading to a fragmentation of OM hence an increased surface area for microbial colonization (Lee, 1992).

Altogether these processes can have a profound impact on sediment biogeochemistry (Davis 1974; Aller and Aller, 1998; Wenzöfer and Glud, 2004) and microbial ecology (Reichardt 1988; Marinelli et al., 2002) in both shelves and deep-sea sediments, although not with the same intensity. In fact Glud et al. (1994) found good correlation between the dry weight of macrofauna and the total oxygen consumption, with a decrease of faunal mediated oxygen uptake from shallow and productive areas towards less productive and deeper sites.

1.1.2.2 Current induced advection

As has been shown before, OM degradation efficiency can be enhanced by pore water advection, i.e. the net motion of water moving up and down in the sediments. The driving force behind advective pore water flow is always a pressure gradient, that may be caused by direct impact of orbital motion of waves, and tidal or bottom currents with the sediment topographic features (Huettel, 1996; Precht and Huettel, 2003) or, at high depths, by convective currents.

Advective pore water transport is particularly important in permeable, sandy sediments (Huettel et al., 2003). Indeed the intensity of the advective transport through the sediments, or pore water flow rate, is proportional to sediment permeability and to the pressure exerted on the seabed. In coastal areas pressure gradients can easily generate by bottom flow-topography interactions and undulating pressure differences between wave crests and troughs (e.g. Huettel and Gust, 1992, Huettel et al., 1996). These phenomena were studied first in laboratory flumes (Huettel and Gust, 1992; Huettel et al., 1996) and was found that pressure gradients scale both with flow velocity and obstacle height (e.g. a ripple). The horizontal pressure gradients that develop along seabed ripples will force an inflow of bottom water through the sides of the ripple, and an outflow of pore water close to the crest. Pore water velocities associated with current induced pressure gradients range from a only few to several centimeters per hour (Huettel and Gust 1992; Huettel et al., 1996), however would still produce an intense interfacial exchange of solutes, as it was shown that pore water can be transported upwards from <100 mm depth and released at the sediment surface.
The interaction between bottom flow and seabed topography were estimated both in lab experiments and in the field, (North Sea intertidal) showing that solutes exchange rates under moderate pressure gradients can be 7 to 50 times higher than diffusive exchange (Precht and Huettel 2003). However, it is worth noting that oxic organic matter mineralization, for instance, was shown to be stimulated only when the advective transport of oxygen is combined with supply of labile organic matter (Reimers et al., 2004; Cook et al., 2007b). Indeed a prompt stimulation of oxygen uptake at an increase in current flow cannot be used as a direct measure of an equivalent increase in carbon mineralization, in part because release in anoxic porewater and oxidation of stored reduced compounds will likely contribute to the measured oxygen flux (Glud, 2008) (see next section).

1.2 Oxygen dynamics at sediment water interface

Dissolved oxygen concentrations in natural water bodies are governed by the balance between oxygen supply (regulated by exchange with atmosphere, physical transport and photosynthesis) and removal (through biological consumption and oxidation of other reduced substances) (Zhang et al., 2010).

Oxygen saturation is only reached in surface waters, while below the productive layer, where biomass can be degraded, oxygen is depleted by microbial respiration processes that in most oceans are extended to a maximum depth of 1000 m. The distribution of oxygen then depends on how effectively it is redistributed by vertical and lateral advection of the water masses (Hensen et al., 2006).

The effect of oxygen on sediment biogeochemistry depends on the ecosystem. For instance, coastal sediments with active faunal communities and active iron and manganese cycles would respond differently to low-oxygen conditions than do sediments rich in sulphide and lacking oxidants other than sulphate (Middelburg and Levin, 2009). Indeed, if a large stock of reactive components is present in sediments, its responses to higher or lower oxygen levels may be delayed (Soetaert et al., 2000). In any case, in oxygenated bottom waters, sediments where OM is respired and mineralized are characterized by the stratification of oxidative zones (shown in Fig.1.1) that are majorly determined by oxygen's penetration depth in the sediments (Cai and Sayles 1995).

As a consequence of different oxygen consumption rates and transport mechanisms of this solute into the sediments, oxygen penetration depths can vary from less than 1 mm in active, muddy sediments and coastal depositional areas (e.g. Meysman et al., 2006), to a few cm in permeable sandy sediments (e.g. Cook et al., 2007). Nevertheless, oxygen penetration depths down to >10 cm were measured at abyssal sites and can even reach several meters in sediments where organic matter content is extremely low as in correspondence to the central oceanic gyres (Fischer et al., 2009).

Since oxygen concentration at the sediment-water interface depends on the concentration in the overlying water, the benthic exchange rates of this solute are strictly related to its distribution dynamics in the water column. Thus to the structure of the benthic boundary layer.

1.2.1 Benthic and Diffusive Boundary Layer

In the ocean, the interface between sediments and the overlying waters is defined as bottom (or benthic) boundary layer (Boudreau and Jørgensen, 2001) that by definition

is the water layer that is influenced by the friction between the sediment and the moving water column (Dade et al., 2001).

Molecular diffusion, pore-water advection, bioturbation and resuspension are affected by horizontal currents of the overlying water column (Wüest and Lorke 2003); therefore, to address and understand the dynamics of sediment-water exchange it is fundamental to consider the structure of the benthic boundary layer (BBL). Indeed, the transfer of particles and solutes through the BBL influences biological and geochemical processes in the upper sediments, such as the dissolution of calcium carbonate, the oxidation of organic matter and metals (iron, manganese, etc.), the removal of reactive nitrogen by denitrification and the supply of oxygen (McCave, 1984).

The BBL is the main location of the dissipation of energy of currents and waves as well as of turbulence and mixing in the stratified water column interior (Wüest and Lorke 2003). At solid boundary (in this context the sea floor) the flow goes to zero, while at some distance above the boundary the velocity reaches a constant value U. The height of a BBL is typically defined as the distance above the bed at which the mean flow equals 99% of U. The spatial variation of velocity over this distance is called *shear* i.e. the spatial gradient of the speed of a current in a direction normal to the direction in which it flows. Processes of shear act to increase interfacial areas of the water column and enhance the concentration gradients of advected solutes of fluid properties, thereby increasing the rate of molecular transfer (Thorpe, 2007).

The mean flow, as well as the characteristics of the seabed, defines different momentum (the quantity of motion of a moving body) and solute transport mechanisms. Indeed, the momentum is transported by the mean flow, by molecular transfer as well as by turbulence. An exchange coefficient, which is called *eddy viscosity* K_m can be assigned to the latter mechanism of momentum transfer (Boudreau, 1997), which is a function of the flow, not of the fluid. In the upper layer of the BBL (that starts at several meters over the sediment surface) the flow velocities follow the characteristic logarithmic profile described by the law of the wall (vonKarman, 1930)(Fig. 1.2). Here, turbulent flow determines the momentum transfer and $K_m$is of the order of 1 m^2 s^{-1}, or one hundred thousand times the molecular viscosity of a laminar flow (Wüest and Lorke, 2003). Consequently, in the water column (logarithmic layer), solute transport is dominated by turbulent mixing.

Close to the sediment-water interface, however, eddy transport is impeded by friction and viscous forces, and the logarithmic layer smoothes into the viscous sublayer (VBL), which starts above the seafloor, at a height that depends on the shear (Fig. 1.2).

The so-called viscous sublayer is defined as the height at which the turbulent mixing, becomes smaller than the molecular viscosity (10^{-2} cm^2 s^{-1}) which usually happens 5-10 mm above the sediment surface (Caldwell and Chriss, 1979; Boudreau, 2001). In this layer, viscous forces dominate, and in the lower part of this layer, trnasport is finally dominated by molecular diffusivity (10^{-5} cm^2 s^{-1}). For cohesive sediments this shift defines the upper boundary of the diffusive boundary layer (DBL) (Fig. 1.2). The DBL thickness typically accounts for one-tenth of the viscous sublayer thickness, but as it is defined by the molecular diffusion coefficient, it is solute dependent.

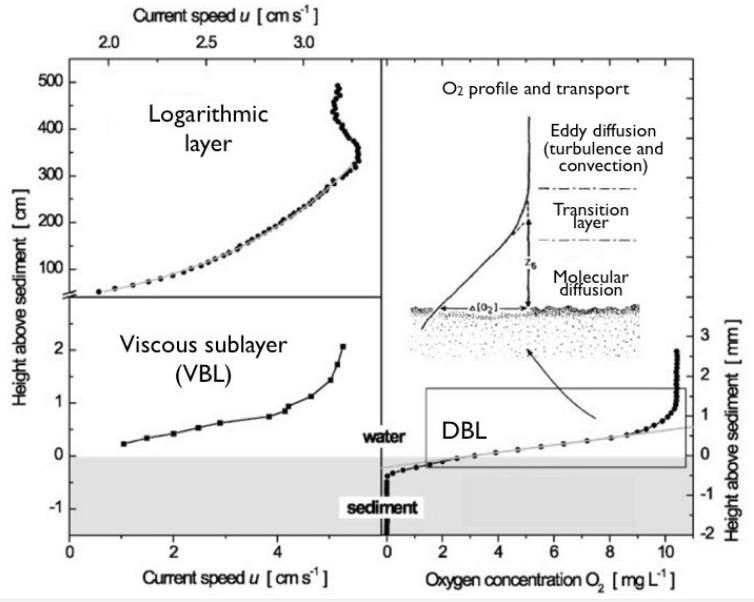

FIGURE 1.2: Measured currents showing a BBL logarithmic layer (Lorke 2002) and viscous sublayer (Caldwell and Chriss 1979). Oxygen profile shows a 0.5 mm thick diffusive boundary layer (DBL) (Muller et al. 2002). The schematic reproduced from Jørgensen and Des Marais (1990), shows with an oxygen profile (sub-millimeter scale) the transition between molecular, viscous and turbulent layer. Modified from Wüest and Lorke, 2003.

1.2.2 Molecular diffusion

Diffusive fluxes depend on the thickness of the DBL and the rate of consumption (or production) of solute in the sediment, the latter affecting the concentration driving force across the interface. As a result, processes that enhance the gradient also increase the magnitude of the flux (Jørgensen and de Marais, 1990). Fluxes across the DBL are governed by molecular diffusion, which intensity depends on the quasi linear concentration gradient across the boundary. The total diffusive flux J (mol m^{-2} s^{-1}) of a given solute

is proportional to the concentration gradient and can be described by Fick's first law:

$$J = -D_0 \frac{\delta C}{\delta x} \tag{1.1}$$

with D_0 denoting the temperature-, salinity- and substance-specific diffusion coefficient in seawater (m^2 s^{-1}) and $\delta C/\delta x$ the concentration gradient of the solute (mol m^{-3} m^{-1}). The ratio of the distance that a molecule travels around sediment particles and the direct path toward lower concentration is defined as the tortuosity of the sediment (Maerki et al., 2004). In order to calculate diffusive flux in sediments, D_0 must be reduced by the square of the sediment tortuosity to derive the diffusion coefficient in the sediment D_s (Boudreau, 1996). Diffusive transport is only effective over small distances (μm to mm scale) since the travel time of a molecule to a certain point increases with the square of the distance. Thus, molecular diffusion is particularly important in fine grained, cohesive sediments, since the mass transport of water is restricted by the low permeability of these sediments, even though fauna-induced irrigation can be important in some areas as mentioned before (e.g. Røy et al., 2004).

The in situ DBL thickness is regulated by the dissipation rate of turbulent energy in the benthic boundary layer (Higashino et al. 2003; Lorke et al., 2003), which is reflected by the trend of increasing in situ DBL thickness values with increasing water depth (i.e. lower current velocities, Boudreau and Jørgensen, 2001; Roberts and McMinn, 2004). Indeed, for the deep ocean, DBL values generally range between 450 and 950 μm, while values measured at the upper shelf or in coastal areas tend to be comparatively thinner between 200 and 700 μm (Boudreau and Jørgensen, 2001; Glud et al., 2003; Roberts and McMinn, 2004).

In systems where the diffusion time across the DBL limits the benthic O_2 consumption rate, a reduction of the DBL should increase the O_2 concentration at the sediment surface, enhancing the diffusive oxygen uptake and increasing the O_2 penetration depth (Gundersen and Jørgensen, 1990). For this reason the O_2 uptake rate of coastal sediments varies on short time scales (even minutes) as a result of changes in hydrodynamic forcing due to tidal currents, wind, and wave-induced water movements that affect the DBL thickness (Glud et al., 2007). However, the presence of a DBL was shown to have only a modest effect on the annual O_2 uptake even in diagentically relatively active sediments (a factor of 1.02-1.10 for DBL of 300- 900 μm, Glud et al., 2007).

The reason why the effect of DBL variations on the long-term O_2 uptake is minor, is that changes in the O_2 aerobic heterotrophic respiration, following changes in O_2 availability, are counterbalanced largely by corresponding changes in O_2 oxidation rate of reduced compounds. It was observed for instance, that during summer, the DBL impedes the O_2 uptake of the very active sediment, which is enriched with labile organic material

that stimulates the anaerobic activity and leads to an accumulation of a larger pool of reduced iron sulfides. This pool is subsequently oxidized during the winter period. Thus DBL thickness in coastal sediments influences mainly the relative importance of O_2 aerobic heterotrophic respiration versus the O_2 oxidation of reduced solutes and solids.

In deep-sea sediments with low organic carbon input, the oxygen uptake is dominated by aerobic heterotrophic respiration (Thamdrup, 2000), and O_2 penetration depth is usually in the order of centimeters. Here, the large interstitial O_2 pool has a lifetime of several hours or days (Wenzhöfer and Glud, 2002), thus, the diffusion time for O_2 across the DBL (i.e., 5-10 min) is short compared to the transport time down through the oxic zone. Consequently DBL variations do not have any major impact on the benthic O_2 uptake rate (e.g., Reimers et al., 2001).

1.2.3 Turbulent (eddy) diffusion

As we said, vertical transport of solutes and particulate matter across the BBL is operated by turbulence; this process promotes mixing and dispersion, extending the surfaces of contact between fluid volumes, hence increasing the area across which diffusive transfers of fluid properties may occur. As a result, turbulent diffusion generally exceeds molecular diffusion in the sediment, and is function of the flow field, varying with the flow velocity in the BBL.

The biogeochemical consequences of turbulence at the sediment water interface are thus related to the enhanced solute exchange and remineralization (provided that OM is also supplied). Indeed highly turbulent water columns (by wind-induced waves or tidal currents) can induce advective processes that flush surficial sediments (Riedl and Ott, 1972).

As mentioned in section 1.1.2.2, advective processes lead to the replacement of pore water with overlying water thus to an enhanced mixing of solutes, in a process that can result in up to three orders of magnitude higher than molecular diffusion.

The dynamics of turbulent transport in the BBL may be crucial to predict hypoxia in bottom waters and sulfide efflux from the sediments. In this regard, Holtappels and Lorke (2011) showed that even low turbulent diffusion in the BBL potentially controls the oxygen flux into the sediment. At high turbulence diffusion this is more obvious, indeed, variation in bottom shear stress induced by the tidal currents interacting with the microtopography of the seabed may cause an upward and downward moving anoxic-oxic boundary (Sect. 1.1.2.2).

As a consequence, solutes exchanges at the sediment water interface exhibit irregularities that cannot be explained by usual diffusion-reaction models based on molecular transport alone (Lohse, 1996). So, to get into a perspective of measuring turbulent solute exchanges, it should be explained that in turbulent diffusion at the boundary layer, mass is transferred through the mixing of *turbulent eddies* within the fluid (Fig. 1.3).

FIGURE 1.3: Simulation of a turbulent flow at the sediment/water interface (http://torroja.dmt.upm.es/jsillero) .

Turbulent eddies create fluctuations in velocity and in water properties, so that at a fixed point of measurement, past which turbulent eddies are being carried at a mean speed, the smaller ones will cause fluctuations in the measured properties, characterized by higher frequencies than those caused by large eddies (Kolmogorov, 1941). An energy frequency spectrum derived from analysis of the amplitude of the time variation of velocity at the fixed point can be converted to a wavenumber spectrum. The spectrum shows how the contribution of the energy of the turbulent eddies to the overall kinetic energy of the variable flow is distributed in wavenumber (or in eddy size).

It is important to recognize that turbulence is highly variable in the ocean and that spectra have to be derived from data obtained over a relatively large period of time, averaging over repeated samples (measurements) taken over periods larger than the energy containing eddy (Kaimal and Finnigan, 1994; Foken, 2008). This will be seen in detail later, at section 1.3.3, for application of EC technique.

1.3 Oxygen benthic fluxes measurements

Determination of consumptions/production rates in the pore water fraction serves to quantify the respiration processes that take place in the sediment sub layers, and define reactive horizons. Hence, oxygen is an excellent tracer to study biological activity because it is produced by photosynthesis and consumed directly or indirectly during the degradation of organic matter (e.g. Glud, 2008). However, there is no method, so far, to directly determine oxic respiration.

Total oxic respiration has to be calculated from the difference between 1) the oxygen demand of the sediment (i.e. aerobic heterotrophic activity of fauna and prokaryotes) and 2) the amount of oxygen consumed by oxidation of reduced species (i.e. reoxidation of reduced inorganic products released during the anaerobic heterotrophic degradation) (Canfield, 1993a; Glud, 2008). Nevertheless, the contribution to total oxygen uptake due to each of the two processes is difficult to quantify. The extreme cases are represented by the abyss, where benthic mineralization of the very low input of organic material can be almost completely covered by the available O_2 (Bender and Heggie, 1984), and by the mats of Beggiatoa sp., where $> 90\%$ of the O_2 is used for sulfide oxidation for these chemolitrophic bacteria (Jørgensen, 1982).

There is therefore a level of uncertainty in estimating respiration by only oxygen consumption, due to the presence of chemical processes which consume oxygen, that can be avoided by measuring the production of dissolved inorganic carbon (DIC), which is the final product of all respiration pathways (Anderson et al., 1986; Hulth et al., 1997). However, other processes such as precipitation and dissolution of calcium carbonate can also cause changes in the DIC concentration (e.g. Green et al., 1993) and have to be taken into account. At reactive sites, the contribution of carbonates dissolution to the total production of DIC can be estimated by concurrent determination of the Ca^{2+} or alkalinity exchange rate (Anderson et al., 1986; Stahl et al., 2004).

Even though total oxygen uptake (TOU) cannot directly be equated with aerobic respiration, when reduced inorganic solutes from anaerobic mineralization are fully oxidized within sediments (as is often the case in marine sediments), TOU represents a proxy of the total benthic carbon mineralization (Canfield et al., 1993a; Middelburg, 2005).

Total oxygen uptake measurement is the most widely used approach for assessing benthic carbon mineralization (Glud, 2008) and can be achieved using a variety of techniques, from *in situ* measurements to *ex situ* incubations of retrieved sediment cores. Concerning the in situ approach, within the past two decades benthic lander systems have been increasingly applied in the deep-sea (e.g. Berelson et al., 1987; Jahnke et al. 1997; Reimers et al., 1992; Wenzöfer et al., 2001a) to avoid artifacts resulting from sediment recovery. These platforms can host any of the majorly applied in situ techniques for the estimation of benthic fluxes (benthic chambers, microprofilers, eddy correlation system), that are described in the next sections.

1.3.1 Benthic chambers

Total benthic fluxes can be measured by chambers installed in the seafloor, or by incubating intact cores on board, isolating a specific volume of water and sediment and

measuring the concentration changes over time of target-compounds within the enclosed waterbody. The depletion or enrichment of the water inside the chamber is measured on water samples (for in situ deployments taken by pre-programmed syringes) and analyzed in the lab, or by sensors monitoring directly physical variables (i.e. temperature or conductivity) or solutes concentration (i.e. oxygen, sulphide). Samples and sensor readings are taken with a certain time interval and fluxes can be estimated by calculating the mean rate of change in concentration during the incubation period by regression analysis. This provides the total solute exchange across the sediment water interface J, as follows:

$$J = \frac{\delta C}{\delta t}\frac{\delta V}{\delta A} = \frac{\delta C}{\delta t}h \tag{1.2}$$

where $\delta C/\delta t$ is the change of concentration over time, and V is the volume of overlying water inside the incubator with area A. This calculation relies on a number of assumptions such as: (1) Steady-state conditions during the incubation, i.e. the flux of the solute across the sediment-water interface (SWI) is equal to the depth integrated production or consumption due to respiration, (2) respiration in the overlying water is negligible compared to that within the sediment and (3) Differences in hydrodynamic conditions between the inside of the incubator and ambient conditions have no influence on the fluxes across the SWI.

Although chambers isolate a certain water volume, a stirring system is used to generate known pressure gradients over the sediment surface, which mimic the natural hydrodynamic conditions (e.g. Huettel and Gust, 1992; Janssen et al., 2005a). In case of muddy sediments, the system can be set with a stirring mode reproducing the natural diffusive boundary conditions (Glud et al., 1995).

In case of permeable sediments, benthic exchange measurements with chambers conducted in the presence and absence of advection, showed that the benthic uptake of O_2 may be enhanced under conditions of advective flow as compared to purely diffusive conditions (Janssen et al., 2005b). Thus, for permeable sediments in situ incubations have to be performed with stirring velocities that reproduce pore water advection (e.g. Cook et al., 2007, Janssen et al., 2005). For this instance, it was shown that, by increasing the stirring velocity inside the chambers it is possible to reproduce a specific flushing rate generated by the advective flow (Glud et al., 1996). Nevertheless, the advection process partially depends on sediment topography and currents, both of which change rapidly in nature (Precht and Huettel, 2004). Therefore, when benthic chambers are deployed in sandy sediments the assumption of a steady state situation may not be valid.

However, in situ incubation may still be preferred to ex situ intact core incubations.

For permeable sand environments, the difficulty of sampling the sediments while retaining in situ gradients and intact pore waters, often yields inaccurate results (Boudreau et al., 2001). For example, even when cores are successfully recovered intact, near-surface pore water gradients cannot be used to estimate benthic solute fluxes because gradient-transport relationships have not been accurately parameterized in this environment (Jahnke, 2005).

In the case of deep-sea sediments, by comparing in situ incubations with cores incubated on deck, the latter have been shown to exhibit artificially high rates, probably due to sampling artifacts, such as the rise of temperature during the transit through the water column (Glud et al., 1994). Given this, in situ incubations are most clearly a necessary tool for deep-sea environments. The drawback is that deep-sea sediments usually have low consumption rates, thus the incubations have to be elongated to reach a statistically valid regression, and this can potentially determine conditions inside the chamber that can affect, for instance, the infauna activity.

1.3.2 Microsensor profiles

Microsensor profiles are widely used to calculate the diffusive oxygen exchange across the sediment water interface by measuring the oxygen concentration point by point (at fixed time steps) from the overlying water to a certain depth in the sediment (typically until the anoxic horizon is reached). An important result of the use of O_2 microsensors (Revsbech, 1989) has been the detailed characterization of the diffusive boundary layer properties via the measurement of oxygen profiles in the micrometer scale, across the sediment-water interface (Jørgensen and Revsbech, 1985; Jørgensen and Des Marais, 1990).

The diffusive flux is calculated based on Fick's first law of diffusion (Eq.1), where the negative sign indicates that the diffusive flux runs in opposition to the gradient's direction from high concentrations to lower concentrations (Schulz and Zabel, 2006).

In the oxic layer of the sediment, the volumetric oxygen consumption rate can be assumed constant, independent of the oxygen concentration, and described as a zero-order reaction (Bouldin, 1968). Below this layer, a thin layer of enhanced consumption often exists, because of overlap between oxygen and reduced substances such as Fe^{2+}, Mn^{2+} or HS^{-}, diffusing up from below, as shown in Figure 4 (Jørgensen, 1983; Soetaert et al., 1996; Berg et al., 1998).

Microsensor profiling can be applied for determining diffusive fluxes either in situ or on intact cores in the lab. Similarly to TOU measurements, comparison between O_2

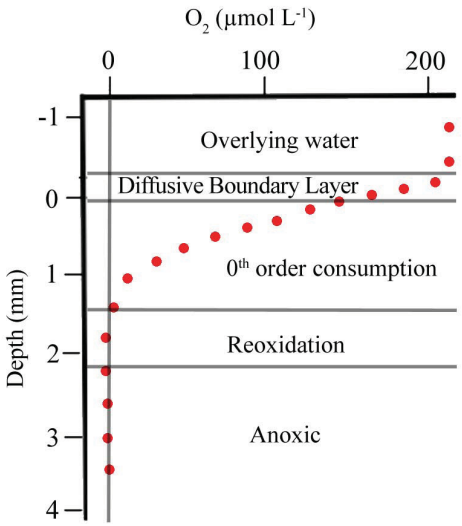

FIGURE 1.4: Benthic oxygen microprofile depicting the typical oxygen microdistribution in a continental shelf sediment.

microprofiles measured on shipboard and in situ at deep-sea indicated that core recovery introduced artifacts, that affected the benthic O_2 distribution (Reimers et al., 1986, 1987). Whereas, the differences were mainly explained by disturbance of the sediment structure during core recovery, closer agreements were achieved by applying extremely long pre-incubation periods. However, it was found that especially for diagenetically very active sediments it is problematic to fully reestablishing in situ profiles (Glud et al., 2003).

1.3.3 Eddy correlation technique

The eddy correlation (EC) technique allows a direct estimation of vertical fluxes by using the theory of turbulent bottom boundary layer flow to interpret measurements of the correlation between the fluctuations of vertical velocity and a constituent concentration (or a scalar). Applied to the sediment-water interface, this approach has the following unique characteristics: (1) it is non-invasive, (2) it integrates over a large footprint area, (3) it incorporates in situ hydrodynamics, and (4) it provides a long-term estimation of vertical fluxes (Berg et al., 2003).

Most of the EC technique applications in the marine biogeochemistry field were so far dedicated to the estimation of oxygen benthic fluxes (Kwae et al. 2006; McGinnis et al., 2008; Brand et al., 2008; Hume et al., 2010; Berg et al., 2009; Glud et al., 2010; Raimers et al., 2012; Long et al., 2013). However, the essential advantages of the technique

initiated many studies also on the boundary layer flux of other solutes such as nitrogen and phosphate (Holtappels et al. 2011), nitrate (Johnson et al., 2011) and sulphide (McGinnis et al., 2010). It was as well applied to estimate groundwater seepage rates through the measurement of heat fluxes (Crusius et al., 2007) or to couple oxygen fluxes to ice melt at the bottom sea-ice interface in polar regions (Long et al., 2012)

1.3.3.1 The eddy correlation system

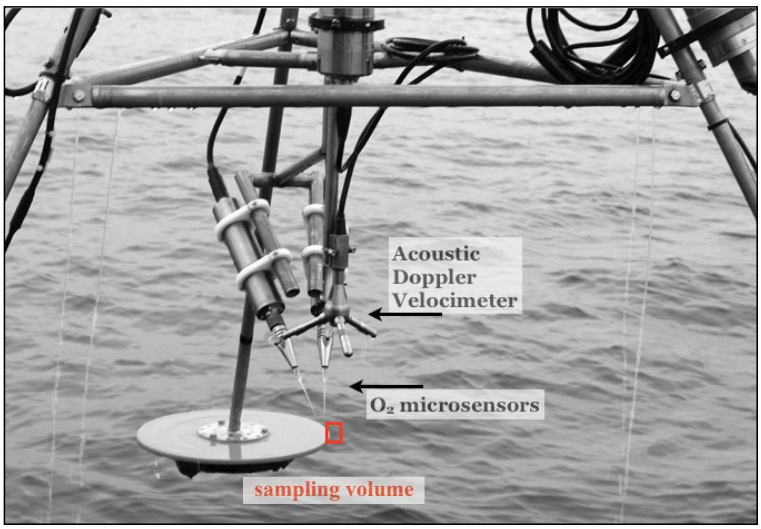

FIGURE 1.5: Picture of an eddy correlation system showing the acoustic Doppler velocimeter and 2 Clark type oxygen microsensors attached to their amplifiers. The red square indicates the approximate location of the sampling volume.

The EC system consists of an acoustic Doppler velocimeter (ADV, Nortek, Norway) with two analog inputs allowing two sensors to be simultaneously deployed (Fig. 1.5). Dissolved oxygen fluctuations are commonly measured with Clark type O_2 microelectrodes (Revsbech, 1989), given their fast response time down to 0.3 seconds (RT $<$ 0.3 s). However, the development of optodes (Klimant et al., 1995, Glud et al., 1999) and the improvement of their performance brought comparable response times, leading to promising applications for EC purposes (Chipman et al., 2012).

The ADV sampling volume, located 15.7 cm below the probe, has a hourglass shape with both base diameters and height of 14 mm, defined by the interception of the three beams, together with the width of the transmit pulse (Fig. 1.5). The O_2 sensor tips are positioned at the edge of the velocity sampling volume, without interfering with it. ADV and microsensors (with their amplifiers) are fixed to a frame allowing the least possible interference with the current field.

1.3.3.2 Principle of eddy correlation flux measurement and calculation

Eddy correlation measurements are made in the benthic boundary layer (BBL), where turbulence is the dominant transport mechanism. Assuming fluxes approximately constant with height, measurements taken in this layer are representative of the fluxes from the underlying surface (Swinbank 1951, Aubinet et al., 2000). Under those circumstances, fluxes are representative of an area with an extension that depends on the surface roughness and the height above the seafloor at which the measurements are taken (Berg et al. 2007).

When biogeochemical processes of surface sediments lead to O_2 consumption, over time, the covariance between vertical velocity (w) and O_2 concentration (C) gives rise to a net transport of O_2 toward the sediment. Accordingly, the reverse mechanism applies for sediment O_2 production (Berg et al., 2003). However in the BBL, no concentration gradients are visible when the dominant transport process shifts from molecular to turbulent diffusion (as in Fig. 1.4). Therefore, to determine the covariance of w and C, it is necessary to simultaneously resolve the turbulent fluctuations of these variables. To achieve this, we need to resolve turbulent motions, which requires the decomposition of the time-series of each variable into a time-mean part and a fluctuating part. This procedure is known as Reynolds decomposition (e.g. Reynolds, 1895, Boudreau, 1997) and is expressed as follows :

$$C(t) = \overline{C}(t) + C'(t); w(t) = \overline{w}(t) + w'(t) \tag{1.3}$$

Ideal conditions for measuring vertical fluxes require: (1) fluxes approximately constant with height in the surface layer, (2) horizontal and homogeneous flows (zero divergence) and (3) only gradual/slow changes of the background concentration C (quasi stationary), so that the conservation of momentum equation results in the following simplified form:

$$Flux = \overline{C'w'} \tag{1.4}$$

The above mentioned separation of turbulent fluctuations (w' and C') from the background means of the collected time series is a critical step in eddy flux measurement analysis. The reason is that the application of Reynolds decomposition requires averaging over many measurements, taken under identical conditions (Kaimal and Finnigan, 1994), which is certainly impossible in oceanic measurements. Thus, to fulfill this assumption, we need to verify that the fluctuations are statistically stationary during the averaging time. There comes the importance of the averaging window used to separate w' and C' from their corresponding means. To better understand this step, it is necessary to introduce how to visualize a turbulent signal.

Any turbulent flow may be thought of as a superposition of eddies over a wide range of sizes. As a result, the fluctuations of the the signals (in our case vertical velocity w' and oxygen concentration C') measured by sensors placed in such flow, vary over a wide range of frequencies (Brutsaert, 1982; Kaimal and Finnigan, 1994).

The frequency range encountered in the BBL can be divided into three major spectral regions (Fig. 1.6): at low frequencies (typically 10^{-4} Hz) is the advective range, where turbulent energy is produced; at intermediate frequencies is the inertial subrange (turbulence range), where energy is neither produced nor dissipated but transformed to smaller and smaller eddies due to an "energy cascade" process (see Stull, 1988); and at higher frequencies (> 1 Hz) is the dissipation range, where turbulent energy is dissipated through viscosity (Foken et al., 2012). Vertical flux carrying eddies belong to the inertial subrange, whose limits are not fixed, and depend basically on the kinematic viscosity and energy dissipation (Lorrai et al., 2010).

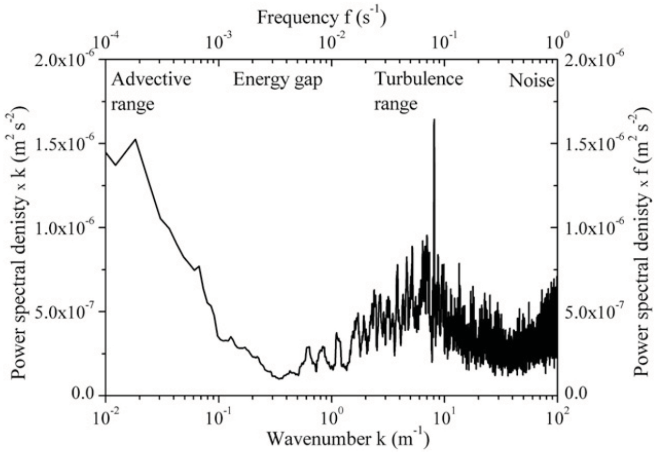

FIGURE 1.6: Variance-preserving spectrum of current (downstream component) in frequency and wavenumber domain for an average longitudinal velocity of 0.01 m s^{-1}. ADV data was recorded in Lake Alpnach at depth of 23 m (0.1 m above sediment). The advective range is clearly separated from the turbulent range by a prominent energy gap. (Lorrai et al. 2010).

In natural waters, large scale advective motions are not always clearly separated from the small-scale eddies (McGinnis et al., 2008). Therefore, as said, a major challenge with the EC technique is to separate turbulent fluctuations (higher frequency range) from advective motions (lower frequency range). A careful analysis of the relevant scales is thus necessary. This is done with signals spectral analysis, applying an integral transformation, which converts a function of time into a function of frequency (Fourier transform). This kind of analysis is used to determine the averaging window to be applied for the Reynolds decomposition, and separate turbulent from advective processes, using the firsts (w' C') to calculate their correlation, i.e. the eddy flux.

Of special usefulness for EC flux analysis are the power spectra of a signal (e.g. horizontal velocity component, Fig. 1.6) and the (co)spectrum of w' and C' (Fig. 1.7). The (co)spectrum, as an integral over the whole frequency range, expresses the magnitude of the vertical O_2 flux at different frequencies (e.g. Stull, 1988, Priestley, 1992):

$$\overline{Flux} = \int_0^\infty Co_{w'C'}(f)d(f) \tag{1.5}$$

where f is the frequency. This information, apart from giving the flux magnitude, can be used to evaluate if the O_2 microelectrode response time is sufficient to capture all turbulent fluctuations contributing to the vertical transport of O_2.

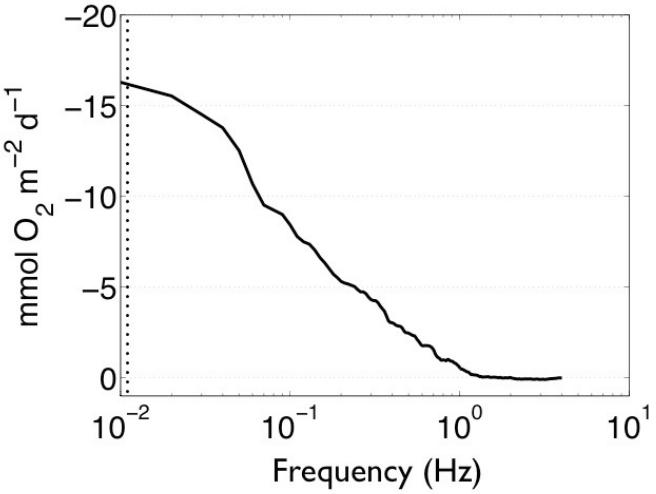

FIGURE 1.7: Cumulative (co)spectrum showing the frequency range of the flux-contributing eddies. The vertical dotted line marks the averaging window, i.e. Reynolds decomposition.

The detection limits of both the ADV and the oxygen sensor give an indication of flux-relevant resolution of the two signals. Under unfavorable conditions of especially weak turbulence or low oxygen gradients, the fluctuations may be too small to be resolved. However, the noise of the two sensor signals at the smallest scales (high frequencies) is mostly uncorrelated and does not contribute to the integral of the (co)spectrum. Therefore, the signal-to-noise ratio of the smallest fluctuations improves by several factors if only their correlation is considered (Goodman et al., 2006).

1.4 Comparison between in situ benthic flux methods

The selection of the most appropriate method to quantify benthic fluxes among benthic chambers, microsensor profiles and eddy correlation technique (Fig. 1.8), depends on the ecosystem and on the spatial-temporal scales that need to be addressed.

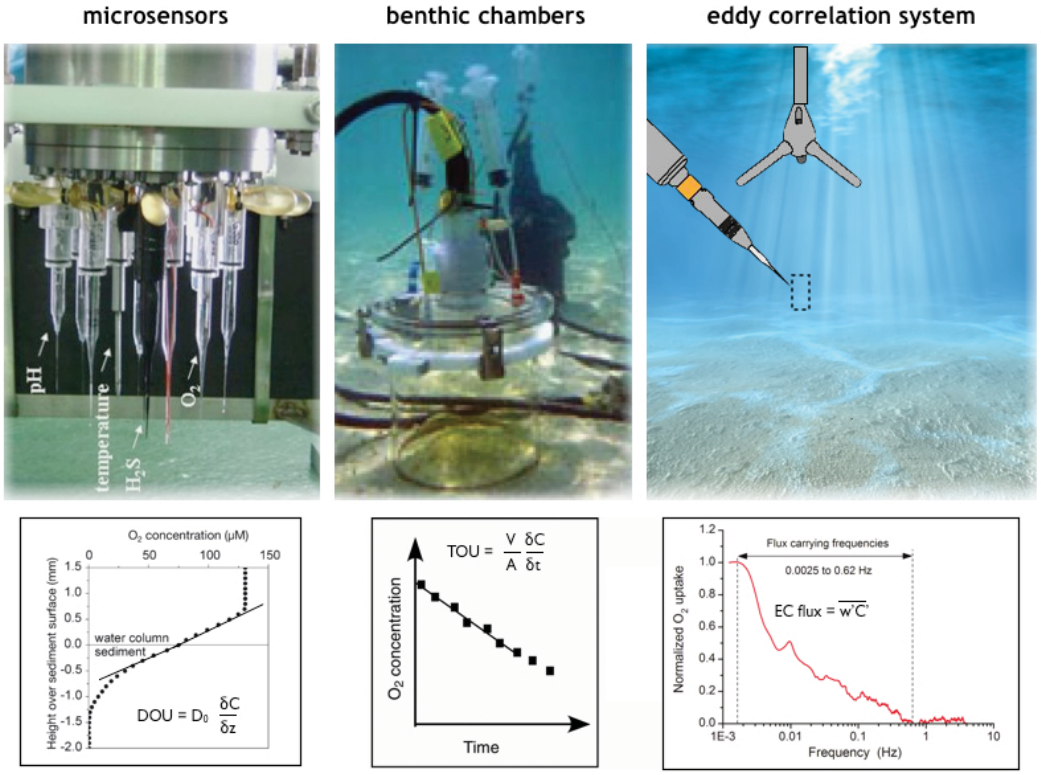

FIGURE 1.8: Comparison between in situ benthic flux methods. A set of microelectrodes connected to a profiler for in situ measurements (left), stirred benthic chamber deployed in shallow sandy sediments (middle), a sketch of eddy correlation where the dashed square indicates the sampling volume (right). Below, plots of the respective measurements used to infer dissolved oxygen uptake, total oxygen uptake and eddy-flux are shown..

On the other hand, the spatial and temporal scale at which benthic exchanges are measured may determine differences in the obtained fluxes, that can be attributed to the different factors that are taken into account by the selected method (e.g. bioturbation, water column dynamics).

In contrast to total fluxes measured by chamber incubations, fluxes measured by microprofiling represent the diffusive oxygen flux. This essential difference between microelectrode profiling and incubation measurement techniques often leads to a discrepancy in calculated oxygen fluxes (Grenz et al., 2003; Rabouille et al., 2003). The microprofiling method measures a local point flux, hence the effects of bioirrigation occurring away from the microsensor cannot be determined. Therefore the ratio between the total oxygen

uptake and diffusive oxygen uptake can be used as a measure of benthic fauna-mediated oxygen uptake (Glud et al., 1994; Wenzöfer and Glud, 2002), which includes the direct respiration by the macro- or meiofauna (Glud et al., 1994, Heip et al., 1995; Soetaert et al., 1997). Thus, the application of both methods is required to properly investigate the oxygen demand and the pathways of oxygen in the sediment. While benthic chamber incubations may represent better the flux estimation on meiofauna dominated systems, microsensors allow an insight into the sediment, providing information on the vertical zonation of biogeochemical processes.

Rasmussen and Jørgensen (1992) suggested that the ratio between total and diffusive oxygen uptake (TOU/DOU) varies from 1.5 to 2.6 in central Aarhus Bay, Denmark, and in the southern Kattegat area of the North Sea, and Archer and Devol (1992) found a TOU/DOU radio of 2-3 on the Washington shelf, attributing it to bioirrigation activities. By correlating TOU/DOU ratio with water depth it was shown how the diffusive-mediated oxygen uptake completely dominates below 3500 m depth, while the fauna-mediated oxygen uptake becomes quantitatively more important at water depths shallower than 1000 m (Wenzöfer and Glud, 2002, Glud, 2008). On average, the DOU only accounts for 43% of TOU in non-photic, cohesive sediments at water depths >100 m (Glud 2008).

Benthic chambers and microprofilers can provide reasonable flux estimates especially in non-bioturbated sediments of limited permeability. Moreover, these techniques cannot take into account the natural in situ variability of physical forcing on the sediment surface due to the water column motion. Indeed the dynamic conditions driven by meteorological forcing that seldom occur in shallow waters, which are extremely variable even on short time scales, cannot be truly reproduced for chamber incubations.

As reviewed by Reimers et al. (2001) and Viollier et al. (2003), the potential concerns on benthic chambers method's limitation are (1) changes in the hydrodynamic regime, including the diffusive sublayer adjacent to the sediment surface; (2) artificially inducing or blocking advective pore water flow (especially with permeable sediments); and (3) artifacts caused by chambers disturbing the water and sediment layers to be studied. Glud and Blackburn (2002) argued moreover that the insertion of small chambers will damage a greater number of fauna and burrows, which could enhance the oxygen flux. being these effects proportionally greater when overall oxygen fluxes are low. The greatest limitation for the application of benthic chambers is therefore related to coastal systems, since generally the dominating transport mechanism contributing to the sediment-water exchange of solutes at these sites is the pore water advection (see Sect.1.1.2.2). With this respect emerges the most advantageous feature of eddy correlation (EC) measurements,

i.e that are done under in situ conditions over nearly any kind of surface, with minimal disturbance of the sediment and benthic boundary layer.

Several studies were conducted obtaining comparative measurements between EC, microprofiles, and chamber incubations (Berg et al., 2003, 2009; Kuwae et al. 2006, Berg and Huettel, 2008; Reimers et al., 2012; present study).
For those ecosystems where advective processes and meiofauna mediated oxygen uptake is negligible, O_2 fluxes obtained by the three methods result in close agreement (Berg et al., 2003, 2009; present study). For permable sediments instead, it is not yet possible to define whether there is a relationship between O_2 fluxes obtained with EC and chamber incubations. It should be demonstrated whether there is a benefit gained by comparing EC with other methods, considering the uniqueness of this approach for the estimation of benthic fluxes. This is still a matter of debate, and will be discussed in the present work.

1.5 Objectives

The main focus of this thesis was on evaluating benthic exchange dynamics, and the relative consequences on carbon mineralization rates, from *in situ* and laboratory multiscale measurements.

Methods for in situ investigation of benthic fluxes have different spatial and temporal resolution: 1) **microprofilers** allow a high resolution description of pore water properties measurable by microsensors, and diffusive solute exchange rates at a single point, 2) **benthic chambers** allow total benthic exchange rates of any measurable property on incubated portions of sediments and overlying water, covering areas of approx. 30 cm^2, 3) **eddy correlation systems** measure total benthic exchange rates (so far mainly oxygen, temperature and conductivity) integrated on several m^2 of on undisturbed substrates.

Fluxes measured with each of these techniques can eventually include/exclude factors that may influence sediment mineralization rates, more or less severely, depending on the ecosystem under study. Therefore, the integration of the different techniques allows emerging insights on the biogeochemical processes of surface sediments. However important aspects, when evaluating flux measurements, are related to the method; is to say that is crucial to evaluate if the discrepancies between the measurements with different techniques are due to the distinct scales and processes addressed, or rather to method-related biases.

This context is carefully examined in this work, among the different settings where flux measurements were performed, especially in light of the fact that eddy correlation (EC) is a relatively new technique, which needs more case studies to assess the relationship with other flux measurements.

Laboratory studies, models and in situ data were used to identify and quantify errors introduced by sensor limitations and errors generated by the hydrodynamic context on EC flux measurements. By this, we aimed to achieve a more robust interpretation of EC-fluxes in general, as well as apply it to challenging environmental conditions, as oligotrophic deep-sea sediments.

On the other hand, by integrating different flux methods we wanted evaluate which limitations and advantages are related to the application of benthic chambers and EC. A further aim was to gain insights on biogeochemical processes for locations that are still overlooked in the context of global carbon budgets, such as Arctic deep-sea sediments and permeable sediments impacted by groundwater discharge.

The main questions:

- Is the variability that we encounter in EC-fluxes related to natural dynamics, or rather to uncertainties generated by the deployment design of the system? Can we detect biases and propose corrections? (Chapters 2,3)

- Can the EC technique be suitable for long-term benthic flux measurements in deep-sea sediments with clear waters and low turbulence? What are the benthic boundary layer conditions for the application of the state of the art EC technique? (Chapter 2,4)

- How the discharge of anoxic freshwater influences biogeochemical processes in coastal sands of a southern Baltic coast? Can we directly quantify seepage rates and their impact on benthic solute exchanges? (Chapter 5)

1.6 Outline of enclosed manuscripts

The thesis comprises 4 manuscripts presented as chapters.

Chapter 2: Improving precision and confidence of aquatic eddy correlation benthic solute exchange measurements

Daphne Donis, Moritz Holtappels, Christian Noss, Cecile Catalot, Andreas Lorke, Kasper Hancke, Filip Meysman, Frank Wenzhöfer, Ronnie N. Glud and Daniel F. McGinnis
(28.10.2013 - in preparation for Environmental Science and Technology)
D.D. analyzed and evaluated EC data from flume experiments and wrote the manuscript with editorial help and input from D.M.G., M.H. and F.W. This study was initiated by a group of EC users from different institutions (University of Southern Denmark-NordCEE, NIOZ, University of Landau, MPIMM). PIV-LIF measurements were performed, analyzed and evaluated by C.N., chamber incubations and microprofiles from C.C., model of oxygen microsensor from M.H.

Chapter 3: Effects of transient bottom water currents and oxygen concentrations on benthic exchange rates as assessed by eddy correlation measurements

Moritz Holtappels, Ronnie N. Glud, Daphne Donis, Bo Liu, Andrew Hume, Frank Wenzhöfer, and Marcel M. Kuypers
(2013-Published in Journal of Geophysical Research 118(3), 1157-1169)
D.D. carried out part of the measurements and provided comments and input to an earlier version of the MS written by M.H. This study was initiated by M.H. with input provided by the rest of the coauthors.

Chapter 4: Benthic boundary layer conditions for eddy correlation measurements in oligothrophic deep-sea: extremely low oxygen fluxes in Arctic sediments (HAUSGARTEN observatory)

Daphne Donis, Moritz Holtappels, Daniel F. McGinnis, Janine Felden and Frank Wenzhöfer
(28.10.2013 in preparation for Limnology and Oceanography Methods)
D.D. analyzed and evaluated EC data and wrote the manuscript with editorial help from F.W. who initiated the study and was responsible for the benthic deployment together with J.F, who provided microprofiler data.

Chapter 5: Biogeochemical impact of submarine groundwater discharge on coastal surface sands of the southern Baltic Sea as revealed by in-situ SBC (stirred-benthic chamber) measurements

Daphne Donis, Felix Janssen, Frank Wenzhöfer, Olaf Dwelling, Peter Escher and Michael Böttcher

(28.10.2013 in preparation for Estuarine Coastal and Shelf Science)

D.D. contributed to the organization of the two campaigns, to the deployment of the instruments, and collection of samples. She evaluated the data and wrote the manuscript with editorial help and input from F.J and comments of M.B. This study was initiated by M.B. (IOW) within the AMBER project. Samples were analyzed at IOW by O.D. and P.E.

This study was carried out within the framework of the 7 FP EU Project SENSEnet, a Marie Curie funded Initial Training Network which brought together leading scientists and researchers from across Europe with the aim of developing novel sensors for the marine environment. Work Package 2, at which this work was affiliated, was dedicated to the improvement and development of autonomous sensors, analysers and microsystem technology for chemical monitoring.
Financial support to this work was as well provided by the Helmholtz Alliance "ROBEX".

Chapter 2

Improving precision and confidence of aquatic eddy correlation measurements

Daphne Donis[1,♣], Moritz Holtappels[2],Christian Noss[3],Cecile Cathalot[4],Kasper Hancke[5], Pierre Polsenaere[4,6], Frank Wenzhöfer[1], Andreas Lorke[3] Filip Meysman[4], Ronnie N. Glud[5], and Daniel F. McGinnis [5,7]

[1]HGF-MPG Joint Research Group for Deep Sea Ecology and Technology, Alfred Wegener Institute for Marine and Polar Research, Bremerhaven, Germany
[2]Max Plank Institute for Marine Microbiology, Bremen, Germany
[3]Institute for Environmental Sciences, University of Koblenz-Landau, Landau, Germany
[4]Royal Netherland Institute for Sea Research (NIOZ), Yerseke, The Netherlands
[5]University of Southern Denmark, Institute of Biology and Nordic Center for Earth Evolution (NordCee), Odense, Denmark
[6]French research institute for exploitation of the sea Resources and Environment Laboratory, L'Homeau, France
[7]IGB - Leibniz-Institute of Freshwater Ecology and Inland Fisheries, Mggelseedamm, Berlin, Germany
♣Corresponding author

In Preparation for Environmental Science and Technology (28.10.2013)

2.1 Abstract

Eddy correlation (EC) measurements of benthic fluxes are based on simultaneous measurements of current velocity and a targeted constituent (i.e. O_2, H_2S, temperature, salinity). Measurements are collected at a fast sampling rate (64 Hz) at a single point above the seafloor using an acoustic Doppler velocimeter (ADV) and a fast microsensor. The EC advantages are that (i) is non-invasive, (ii) integrates over a large footprint area, (iii) incorporates in situ hydro-dynamics, and (iv) provides a long-term estimation of vertical fluxes. Aquatic EC has gained acceptance as a complementary and powerful technique for resolving in situ benthic exchange rates, however, there are no common protocols for data treatment to assess uncertainties or correct biases related to the nature of the method. Here, we present and discuss oxygen EC flux measurements that for the first time were conducted in well-constrained large-scale flume facilities. These novel observations aid in the understanding of the method, and are used to consolidate processing procedures and define deployment expedients for improving the precision (and confidence) of EC measurements.

2.2 Introduction

Aquatic eddy correlation is an increasingly common technique to infer exchange rates across the sediment-water interface. It allows a direct quantification of vertical fluxes from the correlation between the fluctuations of vertical velocity and a constituent concentration (or a scalar). Most of the EC applications in marine biogeochemistry were so far dedicated to estimate benthic oxygen fluxes (Berg et al., 2003; Kuwae et al. 2006; McGinnis et al. 2008; Brand et al. 2008; Berg et al. 2009; Reimers et al. 2012), showing promising results for substrates and ecosystems where conventional methods are difficult or impossible to apply (Glud et al., 2010; Hume et al. 2011; Long et al. 2012; Berg et al., 2013; Long et al. 2013).

The EC oxygen flux estimation is based on simultaneous high frequency measurements of the vertical (normal to the local streamline) component of flow velocity as well as oxygen concentration (Lorke et al., 2013). Performed at a single location just above the sediment, the resulting flux represents an areal average over a footprint area (Berg et al. 2007). Resolving instantaneous quantities and fluctuations of vertical velocity and oxygen concentration require that (i) the measurements have to refer to the same sampling volume and the same sampling time, and (ii) all "flux-carrying" eddies are resolved (Swinbank et al., 1951; Foken, 2004; Lorrai et al. 2010).

These requirements however are not always fulfilled, due to instrument, sensor and deployment limitations. The physical separation between the oxygen and velocity measurement locations causes systematic uncertainties that, if not eliminated or corrected, potentially produce biased flux estimates with poor accuracy (Billesbach, 2011). Therefore the respective times series must be aligned with a time-shift correction to correct for this systematic bias (McGinnis et al., 2008; Lorrai et al., 2010).

Additionally, the slower response time of the oxygen sensor compared to the velocity measurements also needs to be considered and, if necessary (and possible), also corrected. A longer response time of the oxygen sensor can mean that additional time-shifting is necessary. Furthermore, slower response times can dampen the high frequency fluctuations, and can lead to additional flux bias (Eugster and Senn, 1995; Aubinet et al., 2001; McGinnis et al 2008; Lorrai et al., 2010).

In general, the biases introduced to flux estimates due to the distance between the O_2 and velocity sensors and the response time of the oxygen sensor are difficult to estimate. Previous investigations (McGinnis et al., 2008; Lorrai et al., 2010) have demonstrated that the lag between concentration and velocity can be minimized with pre-measurement considerations (e.g. by knowing the response time of the oxygen sensor and the exact distance between the latter and the velocity sampling volume) and post-processing procedures (e.g. time-shift correction), however there exists no dedicated quantitative studies evaluating the potential effects of time-shifts or tools for dealing with this important

issue.

Our EC testing for this study encompass the results of two experimental workshops dedicated to EC flume studies: one centered around a large scale flume that could contain the EC setup in an unobstructed flow field, and one centered around a small-scale flume set up to perform Particle Image Velocimetry- Laser Induced Fluorescence (PIV-LIF) measurements combined with EC measurements. We present the results from experiments carried out during these two complementary workshops including: (i) direct EC measurements to investigate biases and signal loss resulting from flow direction and oxygen sensor response time, (ii) PIV-LIF measurements to visualize the advective and turbulent transport in the flow field and to verify how the time-shift is related to increasing the displacement between velocity and oxygen concentration measurements, and (iii) a numerical model of a Clark type microelectrode to quantify and compare EC fluxes obtained with different oxygen sensor response times. With these results, we improve the EC best practice knowledge and provide suggestions for designing EC field deployments as well as for data processing.

2.3 Materials and procedures

2.3.1 Workshop 1: EC measurements

2.3.2 NIOZ flume set up

An EC system (Berg et al., 2003) consisting of an acoustic Doppler velocimeter (ADV) and two O_2 microelectrodes was submerged into a large race-track flume facility (Fig. 2.1) with a total length of 17.55 m, 60 cm width, a straight working section of 10.8 m and a total capacity of about 10 m^3. The water flow was generated by a conveyor belt system, which uses a series of paddles to drive the flow at the sediment-water interface (for specifications see Bouma et al., 2005).

The flume was filled with a bed of natural cohesive sediment (porosity = 0.6 $\pm$ 0.09, organic carbon = 1.9 $\pm$ 0.4 wt%) obtained from an intertidal flat at Kapelle Bank (Westerschelde estuary, The Netherlands). Sediment collection took place 10 days prior the start of the experiments. At low tide, the top 10 cm of the surface sediment was collected, brought back to the flume facility and gently homogenized.

The sediment was subsequently used to cover the working section of the flume (8 m in front; Fig. 2.1) with a sediment layer of 5 cm thickness, ensuring a flat sediment-water interface. Seawater from the sampling site was added (salinity: 32 psu) and reached a depth of 30 cm layer in the working area. The sediment was allowed to equilibrate for 10 days to reach quasi steady state O_2 distribution. Temperature was kept constant at

17.4 °C. During the entire experiment, the temperature and O_2 concentrations in the flume water were monitored with macro optodes (Aanderraa ® Norway) located before the flow straighteners and at the end of the straight work section (Fig. 2.1).

2.3.3 EC system

The EC system consisted of an Acoustic Doppler Velocimeter (ADV, Nortek, Norway) with two analog inputs allowing two O_2 sensors to be simultaneously deployed. Dissolved O_2 fluctuations were measured with two Clark type O_2 microelectrodes (Revsbech, 1989) each connected to a gain adjustable, galvanically insulated amplifier (McGinnis et al., 2011). All O_2 microelectrodes used for the study were calibrated against the saturated flume water (with known salinity and temperature) and anoxic water at the same temperature (Gundersen et al. 1998).
The ADV sampling volume, located 15.7 cm below the probe, has a hourglass shape with both base diameters and height of 14 mm, defined by the interception of the three beams, together with the width of the transmit pulse (Lohrmann and Cabera, 1994). For simplicity we considered a cylindrical shape with the same dimensions, to set the distance of the O_2 sensor tips (taking into account that the velocity measurement takes place at the center of the cylinder).

2.3.4 Flux analysis

Both, O_2 concentrations and velocities, were sampled with 64 Hz and afterwards averaged to 8 Hz to improve the signal to noise ratio, and to increase the convenience of data handling. Single-point velocity spikes were replaced with values interpolated from neighboring data points. Velocity spikes were removed by the interpolation from neighboring data points (as described by Goring and Nikora, 2002) with an ADV beam correlation threshold of 70%.
The mean vertical velocity component $\overline{w}$ (w = w' + $\overline{w}$, where prime and overbar denote the temporal fluctuation and mean, respectively), as well as the mean O_2 concentration $\overline{C}$ (C = C' +$\overline{w}$) were calculated by moving average with a window length of 60 s. This interval, used for Reynolds decomposition, was based on the power spectral density of the vertical velocity component (data not shown), from which is indicated the inertial subrange. The chosen window size is sufficiently long to include the frequencies that contribute to the vertical flux.
The O_2 fluxes were calculated as follows:

$$\overline{C'_j w'_j} = \frac{1}{N}\sum_{j=1}^{N}[(C_j - \overline{C})(w_j - \overline{w})] = \frac{1}{N}\sum_{j=1}^{N} C'_j w'_j \tag{2.1}$$

where N is the number of samples, corresponding to the average interval of 5 minutes, used for cross correlation of w'C'. This average interval was chosen as a good balance between a clear data visualization and a high temporal resolution.

2.3.5 Time-shift correction and p-value

EC flux represents a temporal correlation of two measured quantities, the most straight forward assessment of uncertainties is determining the significance of the correlation between w' and C' (Holtappels et al. 2013).
We determined the probability for a non-significant cross correlation (p-value) to assess the uncertainty of the results. The significance of the cross correlation between w' and C' was evaluated by calculating the probability of receiving the same correlation (i.e. the same flux) from random data. The threshold for a significant flux was set to 5 %.
The time-shift correction was performed for each 5 minute interval by shifting the time series of C' and w' against each other using a step size of 0.125 s (defined by the sampling rate of 8 Hz) and a maximum shift based on the response time of the O_2 sensor of $\pm$ 2 s (or $\pm$ 4 s when the response time of the sensor required it). For each step, the correlation and the corresponding p-value were calculated. Time-shift with minimum p-value indicated maximum correlation, which was subsequently used to calculate the average eddy flux. The time-shift interval (ts) necessary to reach the maximum correlation is expected to be in the range of the theoretical ts given by the sum of O_2 sensor response time and the traveling time between O_2 sensor and ADV measuring volume.

2.3.6 Time-shift effect on O_2 fluxes measurement for different sensors distance and orientations: experiment 1 and 2 (Exp.1, Exp.2, Exp.3)

For Exp.1 and Exp.2 we used two O_2 sensors with similar response times of $\tau_{90} = 0.35$ s. The response time τ_{90} was defined and measured as the time required for the sensor signal to reach 90% of the steady-state signal after a sudden concentration change. The sensors were positioned at different distances from the edge of the ADV sampling volume: one at 10 mm and one at 23 mm. The EC system was turned in order to have the O_2 sensors oriented either downstream, upstream or normal to the flow direction (Fig. 2.2): these three configurations are expected to cause distinct time-shifts (ts) between w' and C'.
Table 2.1 summarizes the deployment duration, orientations and flow magnitude ranges for the presented experiments.

Exp.1. Downstream and upstream O_2 sensors orientation - The experiment consisted in a 210 minutes deployment during which the EC system was turned by 180 degrees after 60 min and re-positioned at starting orientation after 120 min of measurements. The bulk flow velocity was set at 7.4 cm s^{-1} for the first 30 minutes, 2.8 cm s^{-1} for the next 50 minutes, 8.4 cm s^{-1} for the following 20 minutes and at 7.4 cm s^{-1} for the remaining time.
Downstream case: the EC was positioned in a way that the flow passed first the velocity sampling volume before it reached the O_2 sensors. Therefore *ts* was given by the O_2 sensor response time added to the water parcel traveling time determined by the flow velocity.
Upstream case: the EC was positioned in a way that the flow passed first the tip of the O_2 sensor at 23 mm, then the tip of the O_2 sensor at 10 mm and at last the velocity sampling volume. The given *ts* was thus determined by the O_2 sensor response time minus the water parcel traveling time.

Exp.2. Normal O_2 sensors orientation - Exp.2 was carried out for 110 minutes in which the same EC system was positioned in a way that the flow was coming from the side of the O_2 sensors (normal orientation) for the entire time with the velocity fixed at 11 cm s^{-1}. In this case, the velocity sampling volume and the two tips encountered the flow at the same time, thus *ts* was determined only by the response time of the O_2 sensor.

O_2 sensors response time effect on EC fluxes measurements: experiment 3 (Exp. 3)
A third experiment was conducted to measure simultaneous fluxes with two O_2 sensors with different response times of 0.35 s and 3 s. Both sensors were positioned at 10 mm distance from the velocity sampling volume and oriented downstream with a fixed flow velocity of 7.4 cm s^{-1} for 50 minutes. The measurements were compared with results from a 1D numerical model of a O_2 microelectrode (see below).

2.3.7 Theoretical and calculated time-shifts

Theoretical and calculated time-shifts (T*ts* and C*ts*) were determined for each orientation of the O_2 sensors at different distances from the velocity sampling volume. T*ts* is the expected displacement of the time series w' and C', given by the sum of O_2 sensor response and traveling time (depending on the distance between the sensor, flow velocity and direction). C*ts* is calculated by selecting the most robust correlation over $\pm$ 2 seconds (for positive and negative correlations) for each 5 minutes burst.

2.3.8 Microprofiles and Dissolved O_2 Uptake (DOU) rates

Oxygen distributions in the sediment were measured directly in the flume (Yerseke) using Clark type microelectrodes (Revsbech, 1989). The sensors had a tip diameter of 50 μm and a 90% response time less than 5 s. A linear two point calibration was performed using air saturated wa-ter of the flume tank and the zero O_2 reading in the anoxic part of the sediment. The micro-electrodes were positioned using a motor-controlled micromanipulator controlled with a PC computer (Unisense, Denmark). Measurements were conducted at three different flow velocities (18, 7.1 and 2.7 cm s^{-1}, 0.4 m and 1.5 m and downstream and 1.5 m upstream from the EC device.
Diffusive O_2 uptake (DOU) rates were calculated from O_2 concentration gradients at the sediment-water interface using the 1-D Fick's first law of diffusion:

$$DOU = \phi D_{O_2} \frac{dO_2}{dx} \tag{2.2}$$

where ϕ is the porosity at the sediment-water interface (0.85 for these sediment), D_{O_2} is the molecular diffusion coefficient of O_2 (cm s^{-1}) at in situ temperature and salinity and $\frac{dO_2}{dx}$ is the O_2 gradient just below the sediment-water interface (estimated from the pro-files).

2.3.9 Incubations and Total O_2 Uptake (TOU) rates

To complement the calculated DOU measurements we also performed core incubations in the flume, 4 m upstream from the EC system (Fig. 2.1). Three of the acrylic chambers (∅: 11 cm, height: 7 cm) were gently pushed down to the bottom of the flume in order to enclose and seal the complete layer of sediment. One chamber was completely filled with flume water and sealed to assess for potential O_2 consumption of the water. All chambers were closed with a lid that contained a magnetic stirrer and O_2 sensor (Firesting oxygen optode, PyroScience GmbH, Germany). The O_2 concentration was continuously logged during incubations, which lasted for 20 h. Sediment total O_2 uptake (TOU) rates were computed by linear regression of the O_2 concentrations within each chamber over the first period of the incubation (O_2 decrease < 20 %).

2.3.10 Workshop 2: PIV-LIF measurement

2.3.11 Landau flume set up

To estimate the effect of a displacement between the velocity and concentration sampling vol-ume on the apparent fluxes we used a PIV-LIF (Particle Image Velocimetry- Laser

Induced Fluorescence) system (Dantec Dynamics, Denmark) to visualize simultaneously the flow field and concentration values. Simultaneous visualization of velocity vectors and concentrations in aquatic environments are frequently applied to estimate fluxes above smooth and rough boundary layer flows (Reidenbach et al. 2010), turbulent jets (Webster et al. 2001) or fluxes induced by animals (Noss and Lorke 2012).

Measurements were conducted in a small flume with a test section, 3 m long, 36 cm wide and 33 cm deep (University of Landau, Germany; www.uphysik.uni-landau.de). A continuous sink of O_2 was introduced by injecting 318 ml min^{-1} of O_2-depleted, rhodamine dyed (Rh6G, Sigma Aldrich, USA) water in front of the test section. The injection using a horizontal line source was placed behind an inlet flow-straightener and 5 cm above the wave-formed bottom roughness of the flume. The fluorescent dye was previously added to the anoxic water and simultaneously injected at a rate of 1.34 mg min^{-1}. After passing the test section, the water was pumped back to the inlet of the flume causing a continuous increase of background Rh6G con-centration over time. However, it is assumed that no spatial gradients of O_2 and Rh6G exist at the inlet of the test section, i.e. O_2 and Rhodamine were fully mixed after passing the re-circulating pump.

The injections lasted for 9 min and maximal observed dye concentrations (cRh6G $<$ 0.08 mg L^{-1}) were within the range of linear response (Arcoumanis et al. 1990; Shan et al. 2004), i.e. below the threshold of ambiguity of the fluorescent-concentration relationship. Hence, fluorescent intensity was directly proportional to O_2 concentrations after correcting for the continuously increasing background in Rh6G concentration.

PIV-LIF measurements- Instantaneous and mean turbulent fluxes were estimated for the entire field of view by multiplication of velocity and concentration fluctuations in each interrogation area (IA) and averaging the products over the sampling interval. Four locations at different vertical positions and with different mean flow velocities, turbulence intensities and shear stresses (Table 2.4) were selected to study how the displacement between sampling positions of flow velocity and O_2 concentration affect their correlation, i.e. the resulting flux. For the sake of simplicity, velocity and concentration measurements are taken from single interrogation areas, thereby neglecting the different sensor related sizes of the sampling volumes.

Temporal cross-correlation analyses were performed between vertical velocity fluctuations at a fixed longitudinal position x and concentration fluctuations at positions x + d_x, where d_x varies between 0 and 58 mm and denotes the longitudinal displacement of the concentration reading in the downstream direction. Time-shifts *ts* (corresponding to time-shifts of the maximal negative correlation) were estimated for all displacements at each location.

Instantaneous three-dimensional flow velocities were measured in a thin 21 cm times 21 cm laser-light sheet, which was aligned with the longitudinal and vertical axes of the flume using stereoscopic particle image velocimetry (Adrian 1991). Buoyancy neutral

seeding particles (20 m PE, Dantec Dynamics, Denmark) in this field of view were illuminated by a double pulsed 532 nm laser with 12 ms between the pulses at a measurement frequency of 7.4 Hz and recorded by two 4 megapixel CCD cameras. A two frame adaptive correlation analyses was conducted for 32 x 32 pixel interrogation areas (IA) with 50 % overlap for velocity vectors observed by each camera. Finally, three-dimensional velocity vectors were received with 1.92 mm longitudinal and 1.67 mm vertical resolution. Turbulent velocity fluctuations were computed by subtracting the temporal mean velocities from instantaneous velocities.

The planar laser induced fluorescence (Crimaldi 2008) of Rh6G was measured simultaneously to the PIV images. The wavelength of the maximum fluorescence intensity of Rh6G (555 nm) was transmitted while the green laser light was blocked by a band pass filter (Stemmer Imaging, Germany) and intensities recorded by a third 4 megapixel CCD camera similar to the PIV cameras. Raw LIF images had been pixel-wise post-processed to remove and compensate for (i) background illuminations and electronic noise of the camera, (ii) inhomogenous light distribution, (iii) temporal laser power fluctuations and (iv) the continuously increasing background con-centration of Rh6G. Beforehand Rh6G concentrations were estimated from an experimentally obtained fluorescence intensity-Rh6G concentration calibration. At last pixel-wise O_2 concentrations had been averaged to receive the respective O_2 concentration of each IA for further assessment of the fluxes.

2.3.12 Numerical model of a Clark type microelectrode

A numerical model was developed and applied to compare EC fluxes obtained with different O_2 sensor response times.

Two data sets measured during the 50 minutes run (Exp. 3) were used as O_2 input at the sensor tip for the model. First, the O_2 concentrations recorded by the fast sensor were used as input for the slow sensor model to analyze the effect of a long response time. However, this assumes that the fast sensor represents the true O_2 fluctuations in the sampling volume, which is not the case. To approximate realistic high frequency O_2 oscillations we used the measured vertical velocity fluctuations as a second input data set for the slow and fast sensor model. For this, the amplitude of the vertical velocity fluctuations was adjusted until the standard deviation matched those of the O_2 concentration fluctuations. The resulting artificial O_2 time series was multiplied by -1 assuming a maximum negative correlation with the vertical velocity fluctuations (i.e. a downward flux).

O_2 sensors for EC-measurements have a response time in the range of 0.1-0.5 s, whereas the time scale for small eddies of the Batchelor length scale (1-10 mm) to pass the sensor can be significantly faster. An eddy of 3 mm size has for instance a time scale of 0.2 s

(Kolmogorov 1941). It is therefore necessary to investigate the effect of the O_2 sensor response time on a dynamic O_2 signal. The design and function of an O_2 microsensor is described in detail by Revsbech (1989).

Microelectrodes are equipped with a guard cathode and an internal reference. Oxygen diffuses through a silicone membrane at the sensor tip into the electrolyte to the cathode, where it is reduced by consuming four electrons per O_2 molecule (Fig. 2.3-A). The measured flow between cathode and anode reflects the O_2 flux to the cathode, which is proportional to the concentration outside the sensor. The signal transfer from the sensor tip to the cathode was simulated by Gundersen et al. (1998) using an analytical diffusion model. However, steady state O_2 concentrations are a prerequisite for this model. The model applies only if the O_2 concentration at the sensor tip is constant for at least the time needed to reach a steady state flux between sensor tip and cathode. Therefore, we applied a numerical model using the finite element program COMSOL Multiphysics® 4.3 (www.comsol.com) to simulate the O_2 flux in fast (0.35 s) and slow (3 s) responding sensors.

The flux from the sensor tip through the membrane (ME) and the electrolyte (EL) to the cathode was modeled using a 1-D diffusion model. The governing equation was given by

$$\frac{\delta C_i}{\delta t} + \nabla \cdot (-D_i \nabla c_i) = 0 \tag{2.3}$$

The domain consists of two parts, membrane and electrolyte (Fig. 2.3-A), with diffusivities of 0.69 and 1.00 x 10^{-9} m^2s^{-1}, respectively. The applied physical dimension of the sensors were determined by microscope (Fig 3-A). The maximum element size in the domain was 0.05 m. The concentration at the cathode was set to zero, whereas the concentration at the tip was set to realistic O_2 concentrations. The concentrations in the domain were calculated using a time dependent solver. The output concentrations, C_{out}, of the sensor model were calculated from the modeled flux at the cathode J_{cath} and the mean input concentrations at the sensor tip $\overline{C_{in}}$.

The response time of the sensor models was estimated by applying abrupt changes of O_2 concentrations at their tip. The models were validated by comparing modeled and measured response times (Fig. 2.3-B and C).

2.4 Results

2.4.1 Workshop 1: EC measurements

2.4.2 Time-shift effect on O_2 fluxes measurement for different sensors distance and orientations: Exp.1 and Exp.2

To illustrate the effect of the time-shift on the EC fluxes, the results for both O_2 sensors (10 mm and 23 mm distant) and the three orientations (Fig. 2.2; downstream, upstream and normal) are presented together with the time-shifts and p-values over the entire deployment (Fig. 2.4 A-D).

The calculated time-shift (*ts*) required for optimal correlation between w' and C' for both sensors increases with decreasing flow velocity (Fig. 2.4-B). As expected the sign of *ts* also reversed when shifting the sensor orientation from down- to up-stream (grey area in Fig. 2.4-B). During the upstream orientation, *ts* decreases with increasing flow velocity. Figure 4-B also illustrates that the O_2 sensor at 10 mm from the velocity sampling volume has a more stable *ts* compared to the sensor at 23 mm, particularly with low velocities and normal orientation.

As the lag time is caused by both the travel time between the sampling volumes and by the response time of the O_2 sensor, we compare the calculated time-shift (C_{ts}) to the theoretical time-shift (T_{ts}) obtained by the sum of these two factors (Fig. 2.5).

All T_{ts} and C_{ts} are significantly different between downstream, upstream and normal flow, indicating that the applied correction closely reflects the theoretically expected time-shift (Fig. 2.5). However, all C_{ts} are larger than T_{ts} , with a larger discrepancy for the normal orientation, for which the times shift calculations also exhibit high variability for the farthest sensor (Fig. 2.5). We also find less robust fluxes associated to unstable *ts*, shown by the higher p-values (Fig. 2.4 C-D).

Averaged O_2 fluxes measured during Exp.1 and Exp.2 are listed in Table 2.2. The time-shift correction leads to an increase in the O_2 flux magnitude, however in both cases (with or without time-shift correction) there is no significant difference between the average fluxes obtained from the two sensors located at 10 and 23 mm from the velocity sampling volume (Table 2.2).

Nevertheless, fluxes magnitudes obtained for different distances are in good agreement only if all orientations are included in the average. Indeed, if the different orientations are examined separately, fluxes obtained for downstream orientation are significantly greater than those obtained from the upstream and normal orientation. The disagreement is likely related to the flow direction and most importantly not compensated by the time-shift correction (Table 2.2).

For all sensor orientations the corrected *ts* for the sensor placed at 10 mm distance

resulted in more robust correlations, supported by p-values lower than the 5% threshold (data not shown). Only for the normal orientation did non-shifted time series result in non-significant correlations (3 bursts over 21 for sensor at 10 mm, and 5 bursts over 21 for the sensor at 23 mm).

2.4.3 Fluxes obtained by microprofiles and incubations

Diffusive O_2 uptake (DOU) rates measured by microsensors did not show any statistical differences ($p < 0.05$) between sensors placed at different locations (-156, 40 and 158 cm see Fig. 2.1) in the flume (Table 2.3), with an overall average of -12.4 ± 2 mmol O_2 m^{-2} d^{-1}. Similarly, no difference in DOU (Table 2.3) was observed for varying flow velocities (18, 7.1 and 2.7 cm s^{-1}), with an overall averaged flux of -13.4 ± 2 mmol O_2 m^{-2} d^{-1}. TOU rates obtained by chamber incubations revealed similar values as compared to the DOU rates with fluxes of -12 ± 4 mmol O_2 m^{-2} d^{-1}.
These rates are closer to EC fluxes after time-shift correction (Table 2.2).

2.4.4 Analysis on single bursts

Spectral analyses is applied for a more in-depth evaluation of EC fluxes obtained for different sensor distances and orientations. The EC flux is expressed as the cross spectral density of w' and C' (cospectrum) represented in a frequency range that is constrained in its upper limit (higher frequencies) by the sampling frequency and response time of the sensors and in its lower limit by the 60 s running average used to calculate w' and C'. From the cumulative cospectra in Figure 2.6 A-C (for the three different orientation at flow magnitudes as close as possible) we see that all curves show turbulent eddy contributions at frequencies below 1 s^{-1}. Moving towards lower frequencies the curves of the cospectra show a gradient of increasing flux (between 10^{-1} and 10^{0} s^{-1}), representing the frequency range where the dominant contributions to the vertical O_2 flux are occurring.
The low and high frequency cutoff of the turbulent spectrum can be estimated theoretically (Lorrai et al., 2010). For the flume experimental conditions we can make a rough estimate considering a bottom drag coefficient (C_d) for muddy sediments of 0.0025 and a range of flow velocities between 7 and 11 cm s^{-1} (U_{1m}). Thus we calculate a range of friction velocities ($u_* = C_d^{1/2} * U_{1m}$) of $0.003 < u_* < 0.005$ m s^{-1} and energy dissipation ($\varepsilon = u_*^3 / 0.4 * h$) rates at 0.1 m above the bottom (h) of $1x10^{-6} < \varepsilon < 4x10^{-6}$ W Kg^{-1}. With these orders of magnitude one obtains turbulent time scales of ∼18 s for the largest eddies and ∼ 3 s for the smallest eddies. Thus the 60 seconds cutoff is sufficient to include all turbulent flux contributions and the slope of the cospectra confirms the

expected inertial subrange.
The correlation obtained for each *ts* step, and the corresponding p-values, (where the peak indicates the time-shift needed to reach the most significant correlation) are shown in Fig 2.6 D-F.
For the downstream case, the cumulative cospectra for both sensors have similar slopes indicating that the timescale of the smallest turbulent structures contributing to the flux is 1 s (10^0 s^{-1}) (Fig. 2.6-A). The peaks of the solid lines in the lower panel (Fig 2.6-D) for the sensor at 10 and 23 mm, indicate that time-shifts (0.7 s and 0.9 s, respectively) are essential to achieve the most significant correlation between w' and C'. In the upstream case (Figure 2.6-B), predominant contributions to the flux are in the same spectral range as for the downstream case (Figure 2.6-A). However, upstream cospectra reveal a less steep slope compared to the downstream case, indicating a smaller total flux. The upstream average flux before and after the time-shift correction is of the same magnitude (Table 2.2), indeed the cospectra also follow the same trend (Fig. 2.6-B). For this orientation the cross-correlation peak is not sharp, especially for the fluxes obtained for 23 mm distance between sampling volumes (Fig. 2.6-E).
In contrast, at normal orientation, the time-shift correction has a relevant effect on flux magnitude only for the 10 mm distance (Fig. 2.6-C). This is also visible from Figure 5-D where the bar plot indicates almost identical fluxes before and after the time-shift correction.
As shown from the smooth gradients in the cospectra, the poorly pronounced cross-correlation peaks (Fig. 2.6-F), and from the previous analysis (Fig. 2.5-C and D), the magnitude of the flux at normal orientation is remarkably smaller than the flux obtained for the downstream orientation (on average 70% less for 10 mm distance and 85% for 23 mm distance - Table 2.2).
We also observed that for all orientations, after shifting the time series, the significance of the fluxes is higher for the sensor at 10 mm.

2.4.5 Workshop 2: PIV-LIF measurements

The simultaneous visualization of the flow field and concentration values was performed with a PIV-LIF set up to determine the relationship between increasing displacement of the sampling volumes and evaluate the time-shift obtained by maximum (negative) cross-correlation of w' and C'. The relationships between apparent time-shifts *ts* and longitudinal displacements dx at all tested locations principally follow the reciprocal of the local mean longitudinal flow velocities $\overline{u}$, i.e.$ts \approx -dx/\overline{u}$, in vicinity of the sensor positions (Fig. 2.7-A). Thus the time-shifts represent the times for advective transport of O_2 from the velocity sampling positions to the O_2 sampling positions.

Cross-correlations of non-shifted time series, however, rapidly decrease with increasing displacement at all observed locations (Fig. 2.7-B). E.g., all non-shifted cross-correlations at dx = 23 mm (sensor displacement in Exp.1) decreased by at least 50% of the correlation measured at identical positions (d_x = 0 mm). In contrast, cross-correlations of shifted time series at the same position decreased only by 19% to 1% of the true flux.

However, taking the three-dimensionality of the turbulence into account, one recognizes that a time-shift may not simply be the time for a pure longitudinal transfer of O_2 concentrations from the velocity sampling position to the O_2 sampling position. In three-dimensional turbulent flow fields it is implausible that all correlated concentrations originate from the sampling volume of the velocity measurement. Pathways, i.e. x(t),y(t), ending at the O_2 sampling position were reversely constructed on the basis of the temporally resolved velocity vectors and the initial positions tracked at dt = ts. Although most of the initial positions of concentration values, which provide the maximal negative cross-correlation for dx = 10 mm and dx= 23 mm, e.g. observed at location B (Fig. 2.8-A), lay within the simulated ADV sampling volume, it is obvious that the scatter of concentration values increases with increasing displacements (Fig. 2.8-B). The time-shift indicates only the maximal negative correlation and may also lead to an overestimation of the apparent flux.

From the PIV-LIF experiment we observe that a 50 mm distance between the O_2 sensor and the velocity sampling volume (with O_2 sensors oriented downstream) still provide only a slightly underestimated flux between 80% and 90% of the true flux values when time-shifting is implemented (Fig. 2.7-B). However, if no time-shift correction is applied, the fluxes obtained e.g. for a 20 mm distance between the sampling volumes, would lead to a profound underestimation, e.g. only 40 % of the true flux would be estimated at location A (Fig. 2.7-B). For the same orientation (downstream) and distance (23 mm) from the direct EC measurements in Exp.1 we found a difference between shifted and non-shifted fluxes similar to the underestimation calculated with the PIV-LIF measurements (ca. 50% - Table 2.2).

2.4.6 Numerical model of a Clark type microelectrode

As the time delay between w' and C' is not only caused by the traveling time (visualized by PIV LIF) but also by the response time of the O_2 sensor, we now evaluate the effect of a slow sensor on the flux estimation through a numerical model that uses input data from Experiment 3.

The signal of the slow sensor used in Exp.3 was noisy and therefore the power spectrum (Figs. 2.9 A and C) showed an increased signal strength at high frequencies which was

above the signal strength of the fast sensor. When using the fast sensor signal as input for the slow sensor model, the signal strength decreases significantly at high frequencies indicating that the slow sensor acts as a low pass filter that strongly attenuates the signal above 0.1 Hz. The deviation of signal strength between the slow sensor model and the slow sensor measurement can be attributed to high frequency noise. This noise does not contribute to the flux as indicated by the good agreement between the measured and modeled slow sensor signal in the cumulative cospectrum and the cross- correlation (Figs. 2.9-E and G). However, compared to the fast sensor measurement the flux calculated from the slow sensor is reduced by 49%. The maximum cross correlation between vertical velocities and sensor signal is shifted by 0.4 s and 1.9 s for the fast and slow sensor, respectively (Fig. 2.9-G). The time-shifts of measured and modeled slow sensor signals agree indicating that a significant part of the time-shift can be attributed to the signal response time of the sensor. It should be noted that the signal response time (i.e. τ_{90}) itself is not necessarily equal to the time-shift in the cross correlation as the latter strongly depends on the frequency spectra of the signal strength.

Compared to low frequencies, the signal delay is less for high frequencies and thus the time-shift in the cross-correlation reflects always a combined delay of all frequencies in the spectrum. In summary, the model of the slow sensor was able to predict the signal loss of 49% and the time-shift of 1.9 s.

By using the artificial O_2 time series as input for the sensor models it was possible to test the potential signal loss of the fast sensor. The power spectra show a significant deviation of signal strength from the input signal at frequencies above 1 Hz (Figs. 2.9-B and D). The signal loss of the slow sensor model is comparable between the two different input data sets (Figs. 2.9 A-D). The resulting flux from the cumulative cross-spectrum is reduced by 15% and 65% for the fast and slow sensor models, respectively (Fig. 2.9-F). The maximum cross correlation between vertical velocities and model sensor signals are shifted by 0.2 s and 1.3 s for the fast and slow sensor model, respectively (Fig. 2.9-H). The time-shift is reduced compared to the measured O_2 time series (compare Figs. 2.9-G and H), which can be attributed to (i) the increased signal strength at high frequencies introduced by the artificial O_2 input (compare Figs 2.9-C and D) and (ii) the traveling time of the eddies, or better the fluid parcels, between the ADV and O_2 sensor which does not contribute to the time-shift in the artificial O_2 data set. It should be noted that the artificial O_2 data set imply maximum negative correlation between vertical velocity and O_2 concentrations, which is not necessarily the case under natural turbulent transport conditions. Therefore, model results from the artificial O_2 input represent only potential signal and flux reductions.

2.5 Discussion

The assessment of turbulent benthic solute exchanges with an EC system requires instantaneous measurements of velocities and a scalar at the same point. This is practically impossible to achieve with the currently available instrumentation, i.e. the combination of an ADV and a fast responding sensor (here, we examined the most used Clark type microelectrode for dissolved O_2 measurements). Previous work on aquatic EC measurements (McGinnis et al. 2008, Lorrai et al. 2010) have described how the flux measurements are systematically biased due to the different response time and the physical distance of the sensors. The authors introduced correction procedures which, however, were based only on theoretical assumptions. Moreover, the corrections were applied to data sets from EC deployments in natural systems with varying hydrodynamics and the unknown exact distance between the sensors and their orientation.
Benthic systems can exhibit highly variable fluxes in space and time when changing hydrodynamics or waves promote advection of oxygenated water in permeable sediments (Reimers et al., 2004, Cook et al. 2007, Berg et al., 2013, McGinnis et al., 2013) or when basin scale waves force intermittent turbulence (Brand et al. 2008; Bryant et al. 2010; Lorke et al. 2012).
Given that EC measurements are subject to the variability of natural conditions, standard deviation is not an appropriate statistical parameter for evaluating uncertainties, and becomes crucial to define cases where the measured variability is a method-related artifact.
We therefore designed ad hoc experiments in controlled environments (flume tanks) and a model of a Clark type microelectrode to systematically study the errors caused by sensor displacement and response times, and evaluate the correction procedures at hand.

2.5.1 Time-shift, sensors displacement and flow direction

By analyzing EC measurements in the well constrained conditions of a large scale flume facility, we could assess O_2 fluxes for different distances between the O_2 sensors and the velocity sampling volume at different flow magnitudes and directions.
When the flow is parallel to the sensors line (downstream or upstream orientation, Fig. 2.2), the turbulent structures are most probably passing the O_2 and velocity sensor with a delay that depends on the distance between sampling volumes for w' and C' measurements and the response time of the O_2 sensors.
However, eddy structures undergo changes in their sizes following an energy cascade

through a spectrum of smaller and smaller eddies (within which inertial forces are dominant). As demonstrated by the PIV-LIF experiment, an increasing distance between sampling volumes would lower the probability to sample the same eddy structure. This is likely the reason for the better correlations between w' and C' obtained in Exp.1 and Exp.2 for a distance between sampling volumes of 10 mm compared to 23 mm.

From the PIV-LIF experiment we observe that if no time-shift correction is applied, the fluxes obtained e.g. for 2 cm distance between the O_2 sensor and the velocity sampling volume (with O_2 sensor oriented downstream), we obtain a 40% underestimation of the true flux (determined by PIV-LIF). Although an almost identical underestimation in comparison to Exp.1 might have been observed by chance, Figure 2.7-B shows a surprisingly narrow range of decrease in fluxes of unshifted series. Hence similar underestimations are expected for unshifted correlations between velocities and concentrations with 2 cm measurement displacements, irrespective of the hydrodynamic conditions at the sampling spots.

However, the decrease, i.e. the underestimation of fluxes, appears stronger under low flow and turbulence conditions, if one considers larger displacements between the sampling positions.

When the flow is perpendicular to the sensors line (normal orientation), the probability for the ADV and O_2 sensors to detect the same structure depends on the size of the dominant turbulent eddies and both sensors have an increasing tendency to be decoupled. We can speculate that the two O_2 sensors positioned perpendicularly to the flow have a limited capability to detect the same structure that passes through the velocity sampling volume, compared to other orientations. We observed that when the flow is directed normal to the O_2 sensors, the flux is 70-85% smaller (depending on the sampling volumes distance) than the flux measured when O_2 sensors are oriented downstream.

The more robust correlations for the sensor at 10 mm, after time-shift correction, may confirm that a closer distance reduces the decoupling effect, i.e. O_2 and velocity sampling volumes have higher probability to share the same eddy structure than for the 23 mm distance.

We also observed that when the orientation of the O_2 sensors changes from downstream to upstream, i.e. the flow passes the microsensor tips first, the flux magnitude and the significance of the correlation decreased slightly. This effect could be generated by a disturbed flow imposed by the sensor amplifiers in front of the ADV sampling volume, even though we did not observe any major effect on the vertical turbulent intensity from the ADV data. In order to exclude this possibility, further experiments should address specifically the effect that obstacles, frames, and the EC hardware itself has on different flow fields.

The underestimation of the fluxes due to the EC system orientation is an aspect that was so far overlooked, assuming that the flux variability was due to natural variations

of the hydrodynamic conditions (hence their effect on the O_2 flux). Our results however indicate that some of the flux variability is instead related to the orientation of the sensor line with respect to the flow direction. This effect is not easily detected in natural environments, and the underestimation may be masked by a high variability in the flow field.

If all the orientations of the O_2 sensors with respect to the flow are considered for the flux average (equal deployment time of 60 min for downstream, upstream and normal), we observed 25-30% lower fluxes compared to DOU and TOU (EC= -9 ± 4; TOU= -12 ± 4; DOU= -13 ± 3 mmol O_2 m^2d^{-1}). However, the flux estimates are in good agreement with TOU and DOU when the EC instrument maintained its downstream orientation (EC = -14 ± 4 mmol O_2 m^2d^{-1}), while were significantly smaller if only normal orientation is considered (EC = -5 ± 1 mmol O_2 m^2d-1).

It was shown from several studies that the comparison between microelectrode profiling and incubation measurement techniques often leads to a discrepancy in calculated O_2 fluxes (e.g. Grenz et al., 2003, Glud et al 2003). This is because measurements by benthic chamber incubations represent the total O_2 flux including diffusion as well as advective O_2 transport across the sediment-water interface due to bioturbation, while the microprofiling method measures a local point diffusive flux (Archer Devol 1992; Wenzhöfer and Glud, 2002; Rabouille et al. 2003). However, for our experiments the visible fauna was removed and the sediment type does not facilitate advection, thus comparable fluxes between DOU and TOU are expected, and this is confirmed by the measurements.

The comparison between fluxes measured directly at the sediment-water interface (as for TOU and DOU) and measurements taken above the sediment (as for EC-flux) is reliable assuming measurements taken in the benthic boundary layer are representative of the fluxes from the underlying surfaces (Swinbank 1951, Aubinet et al. 2000), i.e. the fluxes are approximately constant with height. Given the dimensions of Yeserke flume, it is not possible to achieve a fully developed benthic boundary layer, thus the O_2 flux may not be constant over the vertical range. Nevertheless, the agreement between TOU, DOU and EC-fluxes at downstream orientation (that are moreover the more statistically robust) suggests that the comparison is trustworthy.

In summary, the flow direction appears as a predominant factor influencing EC-flux measurements. The time-shift correction does not lead to a uniform flux estimation between downstream and normal orientation, because the latter cannot compensate for the mis-sampling of flux carrying eddies. However, if all three orientations are equally included in the flux average, for our flume data set, the time-shift correction improved the confidence and precision of the obtained flux estimation up to 30%.

We can assess that for downstream configurations, the time-shift correction can compensate for the traveling time and response time bias, although increasing displacements

between the sampling volumes increase the mismatch of the spatial overlay of corresponding velocity-concentration pairs (Fig. 2.8), and may constitute a weak point of this method, especially under non-uniform flow conditions.
Applying a time-shift is thus a convenient procedure, and it was confirmed that it corresponds closely to the sum of traveling time and O_2 sensor response time for the case of downstream and upstream orientation of the EC system respect to the flow. The mismatch between calculated and theoretical time-shifts at normal orientation is most likely due to the decoupling effect previously described, that in our experiment flow conditions lead to weak correlations between w' and C' (as shown in Fig. 2.6-F).
The time-shift correction should compensate also for another source of bias between w' and C', that is the O_2 sensor response time. However, if the sensor is not fast enough for sampling the turbulence scales contributing to the benthic flux, the time-shift correction would be not sufficient.

2.5.2 Flux underestimation due to Clark type O_2 microsensor response time

By applying a 1-D model to simulate O_2 diffusion in a microsensor and imposing a vertical velocity signal with the same amplitude, we were able to reproduce the fluxes measured by microsensors with different response times. The simulations showed that an O_2 sensor with a 3 s response time (thus 10 times slower than sensors usually used for EC measurements) leads to an underestimation of 50% of the fluxes compared to the simulation with a sensor with 0.35 s response time. EC measurements in the flume (Exp. 3) indicated the same disagreement between the two response times.
The model allowed us to compare fluxes obtained by a fast sensor (0.1 s) with an artificial O_2 signal (thus no RT and no signal dampening), showing a 15 % underestimation of the true flux. This indicates that high frequency signal loss, intrinsic to any microelectrode measurement (dampening), cannot be corrected by the time-shift procedure. The dampening effect on vertical solute transport estimations by EC is however more or less significant depending on the frequency of the turbulent processes involved.
At lower flow magnitudes the signal loss would be less relevant because there will be less contributions to the flux from high frequencies. Conversely, the portion of missed turbulent contributions becomes more and more relevant with increasing response time of the O_2 sensor. The part of the spectral range that is mis-sampled could however be reconstructed with a theoretical approach by estimating the "true" cospectrum, either with in situ determination of the maximum frequency of the processes to be measured or a reasonable parameterization for it.

2.5.3 Theoretical correction with frequency-dependent dampening function

Similar to the modeling calculations, the O_2 spectra can be "rebuilt" to account for signal loss due to the sensor response time (McGinnis et al. 2008). The slower response time dampens the turbulent fluctuations, with increased dampening occurring at higher frequencies. The frequency dependent dampening function (Eugster and Senn 1995; Gregg 1999) is applied to the O_2 spectrum $S_O2\ ^{m}eas$ (muM^{2}s) and is expressed as:

$$S_{O_2}^{Corr}(f) = (1 + f^2\tau^2)S_{O_2}^{Obs} \tag{2.4}$$

where f is the frequency (Hz) and τ(s) is the response time. The corrected O_2 spectrum $S_{O_2}^{Corr}$ is then used to calculate the new cospectrum. This spectral enhancement, however, should only be applied up to the highest frequency of the inertial subrange and not beyond as it will enhance noise as well.

We applied the correction using equation 2.4 to the data set utilizing the 3-second response time sensor. The calculated correction factor is shown in Figure 2.10-A as a function of frequency. As shown, the corrections to the O_2 spectrum becomes quite substantial approaching high frequencies with slower responding sensors. However, the eddy contributions also decrease with increasing frequency, so while these corrections seem large, they are less (but still) significant when rebuilding the cospectra with the corrected O_2 spectra. Figure 2.10-B shows the calculated flux underestimation for the 7.4 cm s^{-1} case (Exp. 3) as a function of sensor response time, which was calculated by first multiplying the O_2 spectra with the correction factor as a function of frequency. Afterwards, the new cospectrum was calculated. Finally, the integral-average fluxes where calculated for each theoretic response time by integrating between the limits defined by the inertial subrange (5 Hz to 0.1 Hz). Note that the results are not sensitive to the lower frequency integration limit as the correction quickly decreases; however, it is very sensitive to the high frequency limit defined by the inertial subrange. The correction obviously has a tendency to amplify high frequency noise, so integrating beyond this limit may introduce artifacts. Thus, this example is only valid for the 7.4 cm s^{-1} case as the inertial subrange will shift with different velocities.

For the case of the 3 second response, we estimate a 67% correction would be needed. This is very close to the value obtained from the O_2 sensor model results. Again, this is dependent on the limits of integration. In low velocity conditions, the high frequency cut-off is lower and would result in less signal loss.

2.6 Conclusions and recommendations

Our flume and PIV-LIF experiments revealed that the distance between the eddy correlation (EC) O_2 sensor tip and the velocity sampling volume bias EC flux measurements, and that a closer distance leads to more robust flux estimation. We showed that applying a time-shift correction compensates for the traveling time and improves the precision of EC-flux estimation particularly when the O_2 sensors are oriented downstream.

When flow is normal (perpendicular) to the O_2 sensor-to-measuring volume line, the distance between the sampling volumes leads to a decoupling effect, i.e. measured time series are increasingly unlikely to refer to the same turbulent structure, which is translated into poor correlations and underestimated fluxes. Therefore, if the flow direction is expected to change during the deployment of an EC system, the O_2 sensor tip distance from the velocity sampling volume should be as small as possible (< 1 cm).

For downstream/upstream orientations the lower the flow and turbulence conditions the closer the sensors should be aligned, while for normal orientations a high turbulence regime (e.g. $u > 0.01$ m s^{-1}) and distances of 2 cm between the sampling volumes can lead to an 80% flux underestimation.

Accordingly, we recommend when deploying an EC system (given the good practice of recording the direction of the flow with respect to the orientation of the O_2 sensors) would be to discard the fluxes obtained for orientations other than downstream/upstream.

This could potentially lead to a remarkable loss of data. Therefore the most practical recommendation is that orientations should be accounted for (or tested) when assessing in situ data, hence, check if there is a relation between flux and direction, and if so, verify where lower fluxes correlate with the normal orientation.

The use a slow O_2 sensor may lead to the same issue of signal loss that is encountered when sensors are critically distant with respect to vertical flux turbulent structures. We showed how the response time of the O_2 sensor is crucial for the appropriate sampling of the turbulent processes that govern the sediment-water O_2 fluxes. However the error associated to a certain response time of the O_2 sensor depends on the turbulence level and distance of the sampling volume above the sediment surface. Hence, more than a recommended response time, it has to be clear that a greater underestimation of the flux is expected when coupling a sensor with RT > 0.2 s (the usual recommended RT for an EC measurement) with a high turbulence regime ($u_* > 0.01$ m s^{-1}) i.e. with eddy structures with a length scale < 3 mm, contributing mostly to the flux. Since this is quite likely to occur when using the EC for biogeochemical studies, we also show how, with frequency dependent dampening functions, it is possible to rebuild a data set where the high frequency signal loss leads to an underestimation of the true flux.

This is not suggested here to be a routine procedure because it requires exact knowledge

of the response time and careful consideration of sensor noise and turbulence time scale, rather it as a reliable way to correct potentially affected data series.
The EC is an extremely attractive approach for coupling turbulence driven benthic fluxes to biogeochemical processes and should not be restricted to "ideal" conditions.
Recent studies showed how for EC-flux measurements, steady state mean flow velocities and mean solute concentrations should prevail (Holtappels et al., 2013) and specific technical criteria for high resolution measurements are needed for application on heterogeneous substrates (Rheuban and Berg, 2013).
With the intent of improving confidence in EC-flux results, this work ameliorates knowledge for an accurate interpretation of data and deployment design, representing a next step for taking full advantage of this technique, and allowing an evaluation of the obtained fluxes without the need for supporting flux measurements obtained by other methods.

Acknowledgements

We thank the staff at Yerseke laboratories (NIOZ, The Netherlands) and Landau University for technical support in the use of the flume facilities and Anni Glud for manufacturing the microelectrodes. Support for this work was provided by EU 7th FP ?SENSEnet? (PITN-GA-2009-237868), the Helmholtz Alliance ?ROBEX?, the EU project ?HYPOX? (grant 226213), the Netherlands Organization for Scientific Research (NWO-VIDI grant to FJRM), Research Foundation Flanders (FWO-Odysseus grant to FJRM), University of Landau, Southern Danish University, Department of Biology and Nordic Center for Earth Evolution (NordCEE, DNRF53).

References

Adrian R.J. (1991): Particle-imaging techniques for experimental fluid-mechanics. Annual Review of Fluid Mechanics 23:261-304.

Archer, D. and Devol, A. (1992): Benthic oxygen fluxes on the Washington shelf and slope: A comparison of in situ microelectrode and camber flux measurements. Limnology and Oceanography, 37, 614-629

Arcoumanis C., McGuirk J.J. and Palma J.M.L.M. (1990): On the use of fluorescent dyes for concentration measurements in water flows. Experiments in Fluids 10 (2):177-180.

Aubinet M., A.Girelle, A., Ibrou, U., Rannik, J. Moncrieff, T. Foken, A.S. Kowalski, P.H. Martin, P. Berbigier, C. Bernhofer, R. Clement, J. Elbers, A. Granier, T.Grunwald, K.Morgenstern, K. Pilegaard, C. Rebmann, W.Snijders, R. Valentini, and T.Vesala (2000): Estimates of the annual net carbon and water exchange of forests: The EUROFLUX methodology. Advances in Ecology Research 30: 113-175

Aubinet M., Chermanne B., Vandenhaute M., Longdoz B., Yernaux M. and Laitat E. (2001): Long term carbon dioxide exchange above a mixed forest in the Belgian Ardennes. Agricultural And Forest Meteorology 108:293-315

Berg, P., Røy, H., Janssen, F., Meyer, V., Jorgensen, B., Huettel, M. and de Beer, D. (2003): Oxygen uptake by aquatic sediments measured with a novel non- invasive eddy-correlation technique. Marine Ecology Progress Series 261, 75-83

Berg, P., Røy, H. and Wiberg, P.L. (2007): Eddy correlation flux measurements: The sediment surface area that contributes to the flux. Limnology and Oceanography, 52(4), pp.1672-1684

Berg, P., R. N. Glud, A. Hume, H. Stahl, O. Kazumasa, V. Meyer and H. Kitazato (2009): Eddy correlation measurements of oxygen uptake in deep ocean sediments. Limnology and Oceanography Methods 7:576-584.

Berg, P. M. H. Long, M. Huettel, J. E. Rheuban, K. J. McGlathery, R. W. Howarth, K. H. Foreman, A. E. Giblin and R. Marino (2013): Eddy correlation measurements of oxygen fluxes in permeable sediments exposed to varying current flow and light. Limnology and Oceanography, 58(4), 1329-1343.

Billesbach, D.P. (2011): Estimating uncertainties in individual eddy covariance flux measurements: A comparison of methods and a proposed new method. Agricultural and Forest Meteorology, 151(3), pp.394-405

Bouma, T. J., M. B. De Vries et al. (2005): Trade-offs related to ecosystem engineering: a case study on stiffness of emerging macrophytes. Ecology 86(8): 2187-2199

Brand, A., D. F. McGinnis, B. Wehrli and A. Wuest (2008): Intermittent oxygen flux from the interior into the bottom boundary of lakes as observed by eddy correlation. Limnology and Oceanography, 53, 1997-2006

Bryant, L.D., C. Lorrai, D. F. McGinnis, A. Brand, A. Wuest and John C. Little (2010): Variable sediment oxygen uptake in response to dynamic forcing. Limnology and Oceanography, 55(2), 950-964

Cook, P. L. M., Wenzhoefer, F., Glud, R. N., Janssen, F. and Huettel, M. (2007): Benthic solute exchange and carbon mineralization in two shallow subtidal sandy sediments: Effect of advective pore-water exchange, Limnology and Oceanography, 52(5), 1943-1963

Crimaldi, J. (2008): Planar laser induced fluorescence in aqueous flows. Experiments in Fluids 44 (6):851-863.

Eugster, W. and W. Senn (1995): A cospectral correction model for measurement of turbulent NO_2 flux, Boundary Layer Meteorology, 74(4), 321-340

Foken T., Gockede M., Mauder M., Mahrt L., Amiro B.D. and Munger J.W. (2004): Post-field data quality control. In: Lee X et al. (eds) Handbook of micrometeorology: a guide for surface flux measurement and analysis. Kluwer, Dordrecht, pp 181-208

Glud R.N., J.K. Gundersen, H. Røy and B.B. Jrgensen (2003): Seasonal dynamics of benthic O_2 uptake in a semienclosed bay: Importance of diffusion and faunal activity. Limnology and Oceanography, 48: 1265-1276

Glud, R. N., P. Berg, A. Hume, P. Batty, M. E. Blicher, K. Lennert and S. Rysgaard (2010): Benthic O_2 exchange across hard-bottom substrates quantified by eddy correlation in a sub-Arctic fjord. Marine Ecology Progress Series, 417,1-12.

Goring, D. G. and V. I. Nikora (2002): Despiking acoustic Doppler velocimeter data. Journal of Hydraulic Engineering (ASCE), 128, 117-126.

Gregg, M. C. (1999): Uncertainties and limitation in measuring e and xT. Journal of Atmospheric and Oceanic Technology, 16(11), 1483-1490

Grenz, C., Denis, L., Boucher, G., Chauvaud, L., Clavier, J., Fichez, R. and Pringault, O. (2003): Spatial variability in sediment oxygen consumption under winter conditions in a lagoonal system in New Caledonia (South Pacific). Journal of Experimental Marine Biology and Ecology, 285, 33-47

Gundersen, J. K., N. B. Ramsing and R. N. Glud (1998): Predicting the signal of O_2 microsensors from physical dimensions, temperature, salinity, and O_2 concentration, Limnology and Oceanography, 43,1932-1937

Holtappels, M., R. N. Glud, D. Donis, B. Liu, A. Hume, F. Wenzhoefer and M. Kuypers. (2013): Effects of transient bottom water currents and oxygen concentrations on benthic exchange rates as assessed by eddy correlation measurements. Journal of Geophysical Research. Oceans 118:1-13

Hume, A.C., Berg, P. and McGlathery, K.J. (2011): Dissolved oxygen fluxes and ecosystem metabolism in an eelgrass (Zostera marina) meadow measured with the eddy correlation technique. Limnology and Oceanography, 56(1), pp.86-96

Kolmogorov, A. N. (1941): The local structure of turbulence in in- compressible viscous fluid for very large Reynolds numbers. Dokl. Akad. Nauk SSSR, 30, 301-305

Kuwae, T., K. Kamio, T. Inoue, E. Miyoshi and Y. Uchiyama (2006): Oxygen exchange flux between sediment and water in an intertidal sand- flat, measured in situ by the eddy-correlation method, Mar. Ecology Progress Series 307,59-68

Lohrmann, A. and Cabera, R. and Nicholas, C. K. (1994): Acoustic-Doppler Velocimeter (ADV) for laboratory use. In: Fundamentals and Advancements in Hydraulic Measurements and Experimentations, S. 351-365

Long, M. H., D. Koopmans, P. Berg, S. Rysgaard, R. N. Glud and D. H Sogaard (2012): Oxygen exchange and ice melt measured at the ice-water interface by eddy correlation. Biogeosciences 9(6):1957-1967

Long, M.H., P. Berg, D. de Beer and J. Zieman (2013): In situ coral reef oxygen metabolism: an eddy correlation study. PloS ONE 8(3):e58581

Lorke, A., D. F. McGinnis, A. Maeck and H. Fischer (2012): Effect of ship locking on sediment oxygen uptake in impounded rivers. Water Resources Research 48: W12514

Lorke, A., D. F. McGinnis and A. Maeck (2013): Eddy-correlation measurements of benthic fluxes under complex flow conditions: Effects of coordinate transformations and averaging time scales. Limnology and Oceanography: Methods: (in press)

Lorrai, C., D. F. McGinnis, A. Brand and A. Wuest (2010): Application of oxygen eddy correlation in aquatic systems. Journal of Atmospheric and Oceanic Technology. 27:1533-1546.

McGinnis, D. F., P. Berg, A. Brand, C. Lorrai, T. J. Edmonds and A. Wüest (2008): Measurements of eddy correlation oxygen fluxes in shallow freshwaters: Towards routine applications and analysis. Geophysical Research Letters 35:L04403.

McGinnis, D. F., S. Cherednichenko, S. Sommer, P. Berg, L. Rovelli, R. Schwarz, R. N. Glud and P. Linke (2011): Simple, robust eddy correlation amplifier for aquatic dissolved oxygen and hydrogen sulfide flux measurements, Limnology and Oceanography: Methods, 9, 340-347

Noss, C. and A. Lorke (2012): Zooplankton induced currents and fluxes in stratified waters. Water Quality Research Journal of Canada. 47: 276-285

Rabouille, C., Denis, L., Dedieu, K., Stora, G., Lansard, B. and Grenz, C., (2003): Oxygen demand in coastal marine sediments: comparing in situ microelectrodes and laboratory core incubation. Journal of Experimental Marine Biology and Ecology, 285, 49-69

Reidenbach, M.A., Limm, M., Hondzo, M. and Stacey, M.T. (2010): Effects of bed roughness on boundary layer mixing and mass flux across the sediment-water interface. Water Resources Research 46 (7):W07530.

Reimers, C. E., Stecher, III H. A., Taghon, G. L., Fuller, C. M., Huettel M., Rusch A., Ryckelynck N. and Wild C. (2004): In situ measurements of advective solute transport in permeable shelf sands. Continental Shelf Research, 24, 183-201

Reimers, C. E., H. T. Ozkan-Haller, P. Berg, A. Devol, K. McCann-Grosvenor and R. D. Sanders (2012): Benthic oxygen consumption rates during hypoxic conditions on the Oregon continental shelf: Evaluation of the eddy correlation method. Journal of Geophysical Research. 117:1-18

Revsbech, NP. (1989): An oxygen microsensor with a guard cathode. Limnology and Oceanography 34: 474-478

Rheuban, J.E. and Berg, P. (2013): The effects of spatial and temporal variability at the sediment surface on aquatic eddy correlation flux measurements. Limnology and Oceanography: Methods, 11, pp.351-359

Shan J., Lang D. and Dimotakis P. (2004): Scalar concentration measurements in liquid-phase flows with pulsed lasers. Experiments in Fluids 36 (2):268-273

Swinbank, W. C. (1951): The measurements of vertical transfer of heat and water vapor by eddies in the lower atmosphere. Journal of Meteorology, 8: 135-145

Webster, D.R., Roberts P.J.W. and Raad L. (2001): Simultaneous DPTV/PLIF measurements of a turbulent jet. Experiments in Fluids 30 (1):65-72.

Wenzhöfer, F. and R. N. Glud (2002): Benthic carbon mineralization in the Atlantic: A synthesis based on in situ data from the last decade, Deep-Sea Research I, 49(7), 1255-1279

Tables and Figures

Table 2.1 Experiments were conducted during Workshop 1, all showing concordant results concerning the time-shift. Here we report on three experiments in detail.

	Deployment duration (minutes)	O_2 sensors orientation	Flow magnitude
Exp. 1	210	downstream/upstream	2.8 - 8.4 cm s^{-1}
Exp. 2	110	normal	11 cm s^{-1}
Exp. 3	50	downstream	7.4 cm s^{-1}

Table 2.2 Average O_2 fluxes for experiment 1 and 2 for each orientation. Results before and after applying the time shift correction.

	Flux (mmol O_2 $m^{-2}d^{-1}$) shifted				Flux (mmol O_2 $m^{-2}d^{-1}$) non-shifted			
	Down-stream	Upstream	Normal	All	Down-stream	Upstream	Normal	All
O_2 sens. at 10 mm	-16 ± 3	-9 ± 1	-5 ± 1	-8 ± 3	-10 ± 2	-8 ± 1	-2 ± 1	-5 ± 2
O_2 sens. at 23 mm	-22 ± 3	-6 ± 4	-3 ± 2	-7 ± 2	-12 ± 2	-5 ± 1	-3 ± 2	-5 ± 4

Table 2.3 Diffusive oxygen uptake rates obtained by microprofiling in the flume.

flow magnitude (cm s^{-1})	profile position (cm)	DOU (mmol O_2 m^{-2} d^{-1})	
18	158	15.6 ± 1.9	n=8
7.1	158	12.8 ± 1.5	n=3
2.7	158	12.1 ± 0.6	n=4
2.7	-156	13.3 ± 1.5	n=3
2.7	40	12.4 ± 1.9	n=3
2.7	158	11.7	n=1

Table 2.4 Flow, turbulence and shear conditions at selected locations in the PIV-LIF field of view.

Location [1]	z [cm]	$\bar{u}(z)$ [cm·s^{-1}]	$K_{TKE}^{1/2}$ [cm·s^{-1}]	τ_{total} [N·m^{-2}]
A	6.7	1.9	0.8	0.014
B	10.9	2.4	1	0.020
C	15.9	2.9	1.3	0.032
D	19.3	4.2	1.5	0.066

with $K_{TKE}^{1/2} = \sqrt{\frac{\sigma_u^2 + \sigma_v^2 + \sigma_w^2}{2}}$ and $\tau_{total} = -\rho \times \sqrt{\overline{u'v'}^2 + \overline{u'w'}^2 + \overline{v'w'}^2}$

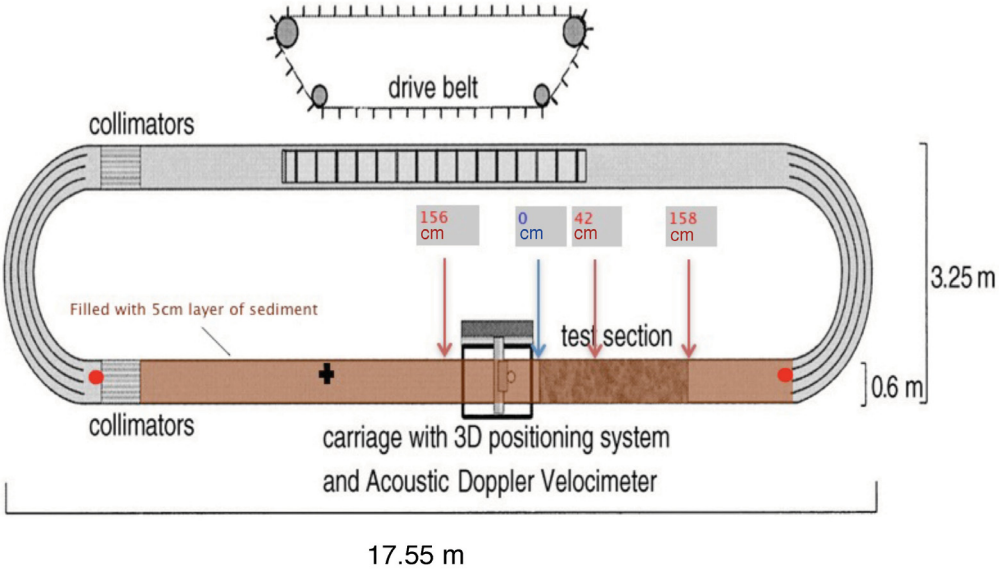

FIGURE 2.1: The race-track flume facility in NIOZ-Yerseke. The dark brown area represents the straight working part. Red arrows indicate the location where the O_2 microprofiles were performed. EC measurements were performed at position 0 (blue arrow). The two red dots mark the position of the optodes for monitoring the O_2 and temperature in the flume. The cross indicates where the incubations were performed. Scheme adapted from Bouma et al. (2005) (www.ceme.nioo.knaw.nl/en/content/dossier-nioo-flume).

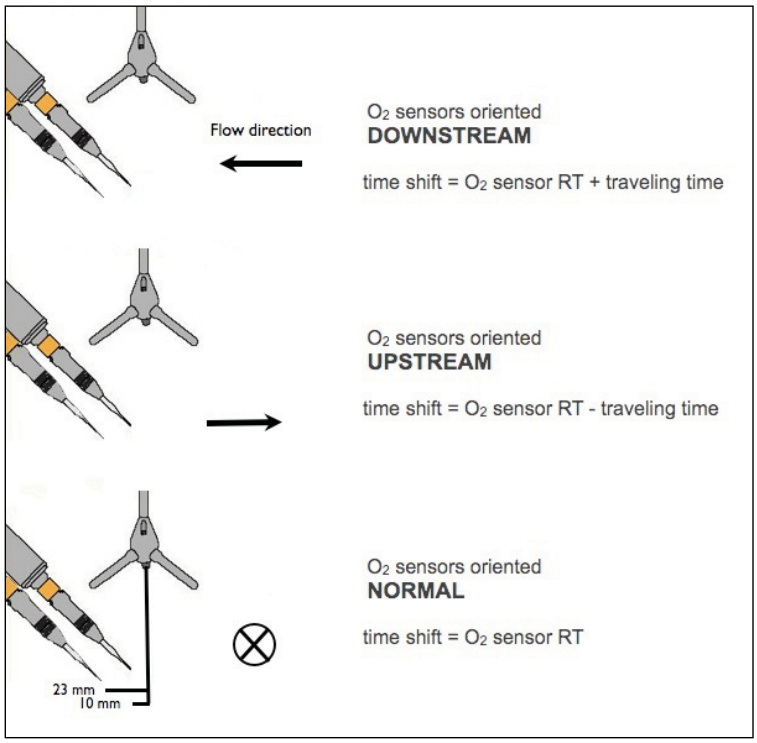

FIGURE 2.2: Sketch of the three configurations tested for experiment 1 and 2.

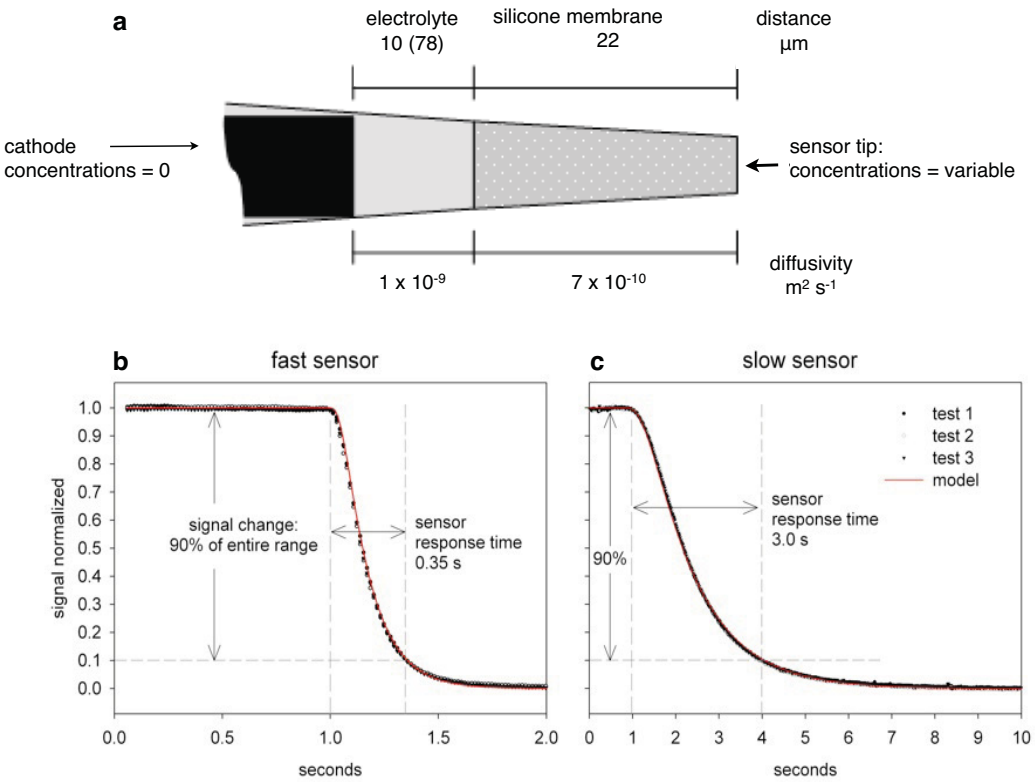

FIGURE 2.3: A) Schematic drawing of an O_2 microsensor and the dimensions and diffusivities used in the numerical model. B) Response times of a slow (3 s) and a C) fast (0.35 s) O_2 microelectrodes used for experiment 3 in the flume. The response time is defined as the time required to reach 90% of the steady-state signal (τ_{90}).

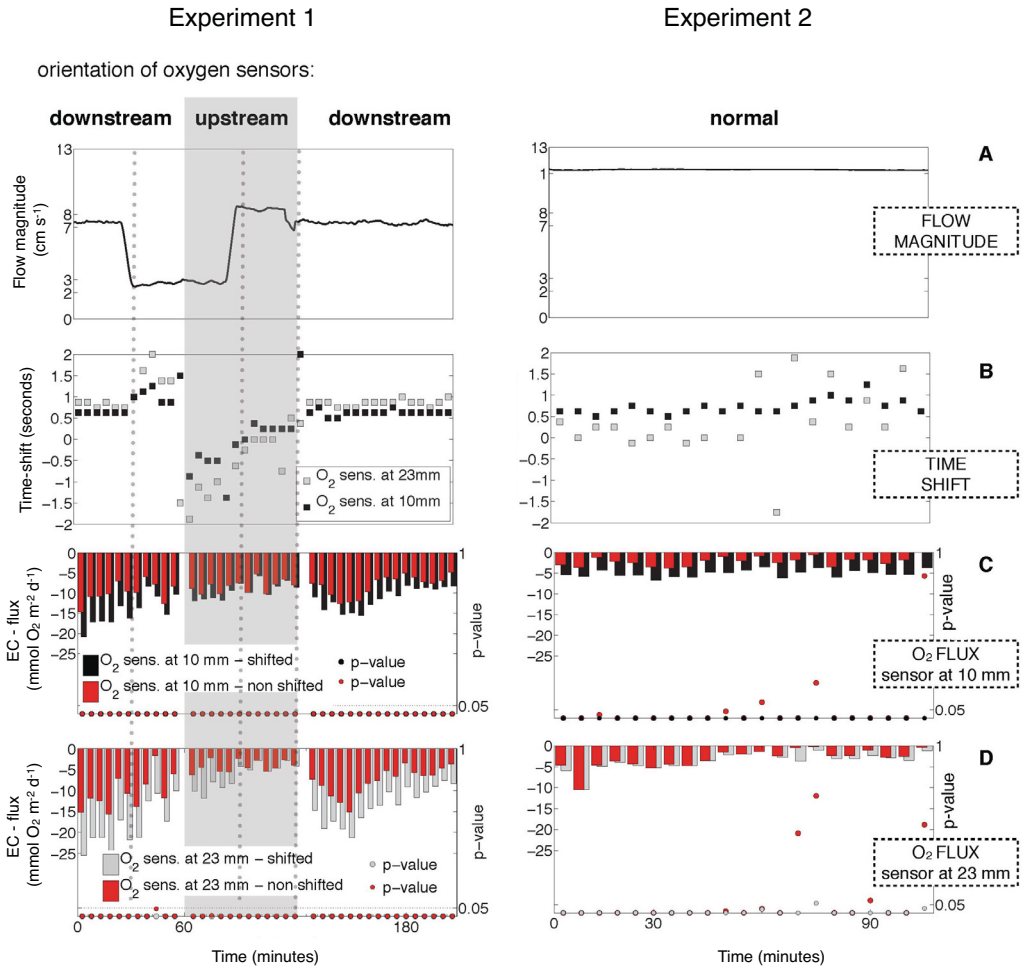

FIGURE 2.4: On left and right side results for experiment 1 and 2 respectively. A) Flow magnitude; B) time-shift calculated for the minimum p-value on 5 minutes interval for sensor at 10 mm (black), and sensor at 23 mm (grey); C) O_2 fluxes for sensor at 10 mm calculated before (red bars) and after (black bars) time-shift correction; p-values (dots) corresponding to shifted and non shifted fluxes are reported with the same color code; D) O_2 fluxes for sensor at 23 mm calculated before and after time-shift correction (red and grey bars, respectively) and p-values corresponding to shifted and non shifted fluxes (same color code). The grey area corresponds to upstream orientation of the O_2 sensors and the vertical dotted lines to the change in flow magnitude.

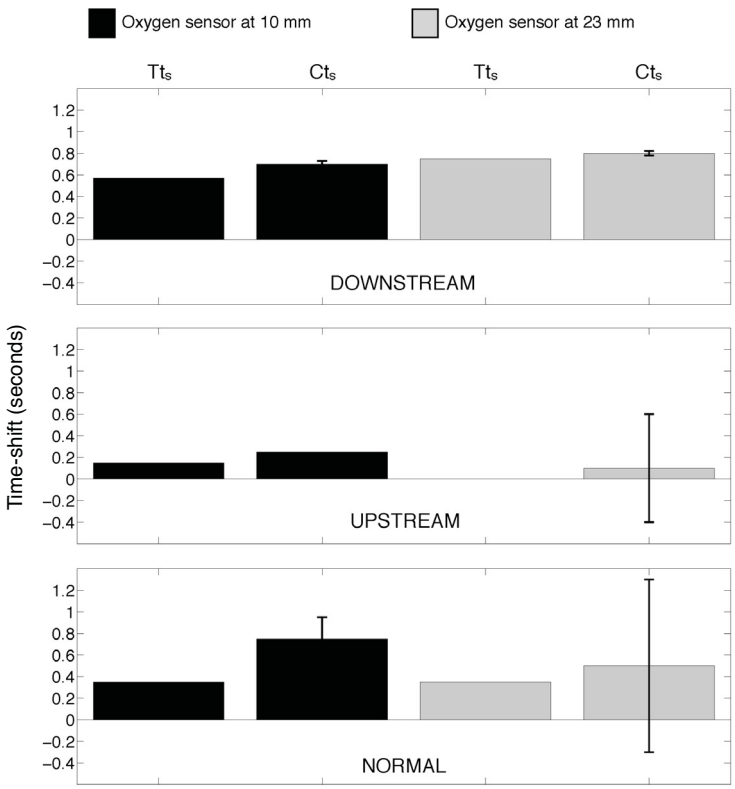

FIGURE 2.5: Theoretical time-shift (T_{ts}, i.e. sum of traveling time and sensor response time) and calculated time-shift (C_{ts} , i.e. shift of w' C' needed for achieving most significant correlation) for all orientations at comparable velocities.

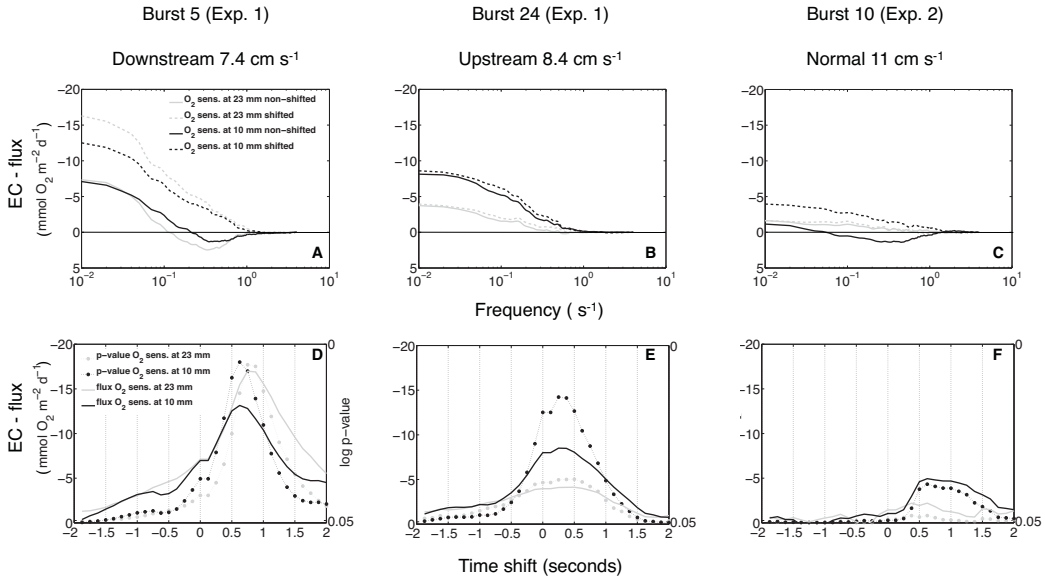

FIGURE 2.6: Upper panels (A-C): cumulative cospectra of 3 bursts, one for each case (downstream with flow velocity of 7.4 cm s^{-1}, upstream with 8.4 cm s^{-1}, normal with 11 cm s^{-1}) before (solid line) and after (dashed line) time-shift correction, for sensor at 23 mm (grey) and sensor at 10 mm (black). Lower panels (D-F): O_2 fluxes calculated for the same bursts for each time-shift (solid line) and corresponding p-values (dots); same color code as A-C for sensor at 10 mm and 23 mm from velocity sampling volume.

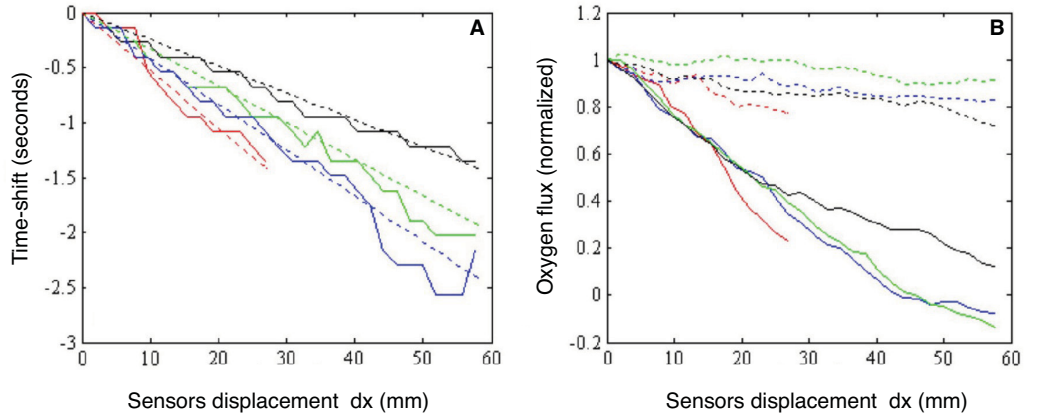

FIGURE 2.7: A) Time-shift for maximal negative cross-correlation between vertical velocity w' and concentration fluctuations C' observed at sampling volumes displaced by dx (velocity upstream, concentration downstream). Solid lines denote time-shifts as a function of dx (Location A - red, B - blue, C - green, D - black, see Table 4 for detailed information on the hydrodynamic conditions), while dashed lines denote the temporal displacement by mean flow velocities. B) Cross-correlations between non-shifted time series of w' and C' (solid lines, identical color code as A) and maximal negative cross-correlations of time-shifted time series of w' and C' (dashed lines) as a function of displacement dx. Correlations are normalized by the non-shifted correlation at dx = 0 mm.

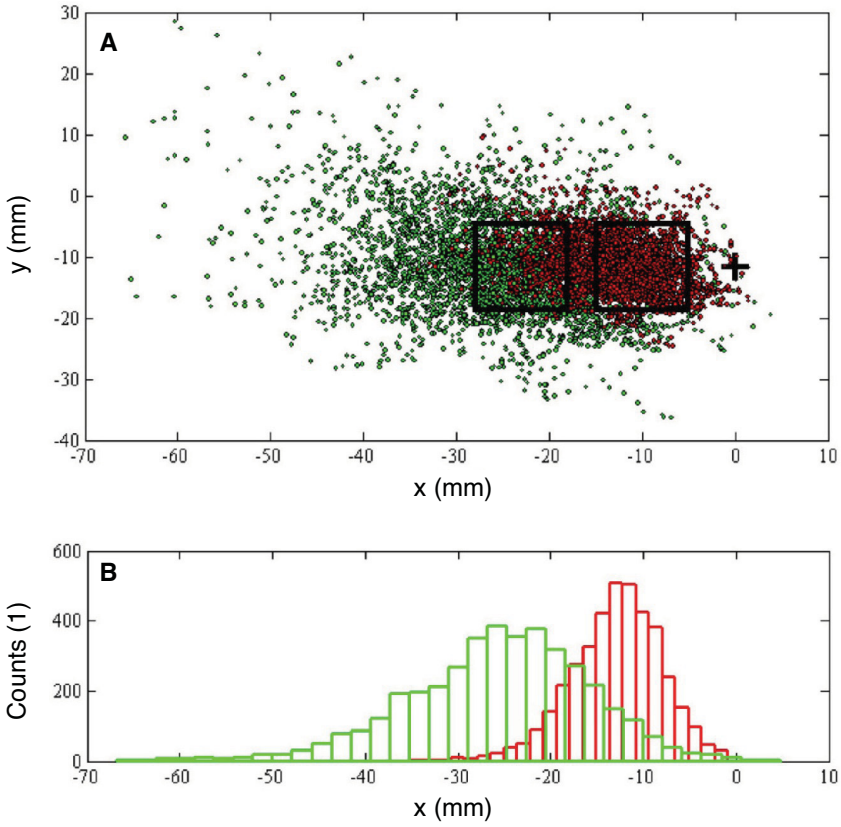

FIGURE 2.8: A) Origins of time-shifted concentration values providing maximal negative cross-correlation between vertical velocity and concentration fluctuations measured at sampling volumes with dx = 10 mm (red dots) and dx = 23 mm (green dots) displacement at Location B (Table 4). The black cross simulates the position of the tip of a Clark type electrode, while the black squares simulate the ADV sampling volume extension. B) Corresponding histogram of the longitudinal distributed positions of concentration origins (color code identical to A). Note that dots of dx = 10 mm overlay dots of dx = 23 mm in A), while bars of dx = 23 mm overlay bars of dx = 10 mm in B).

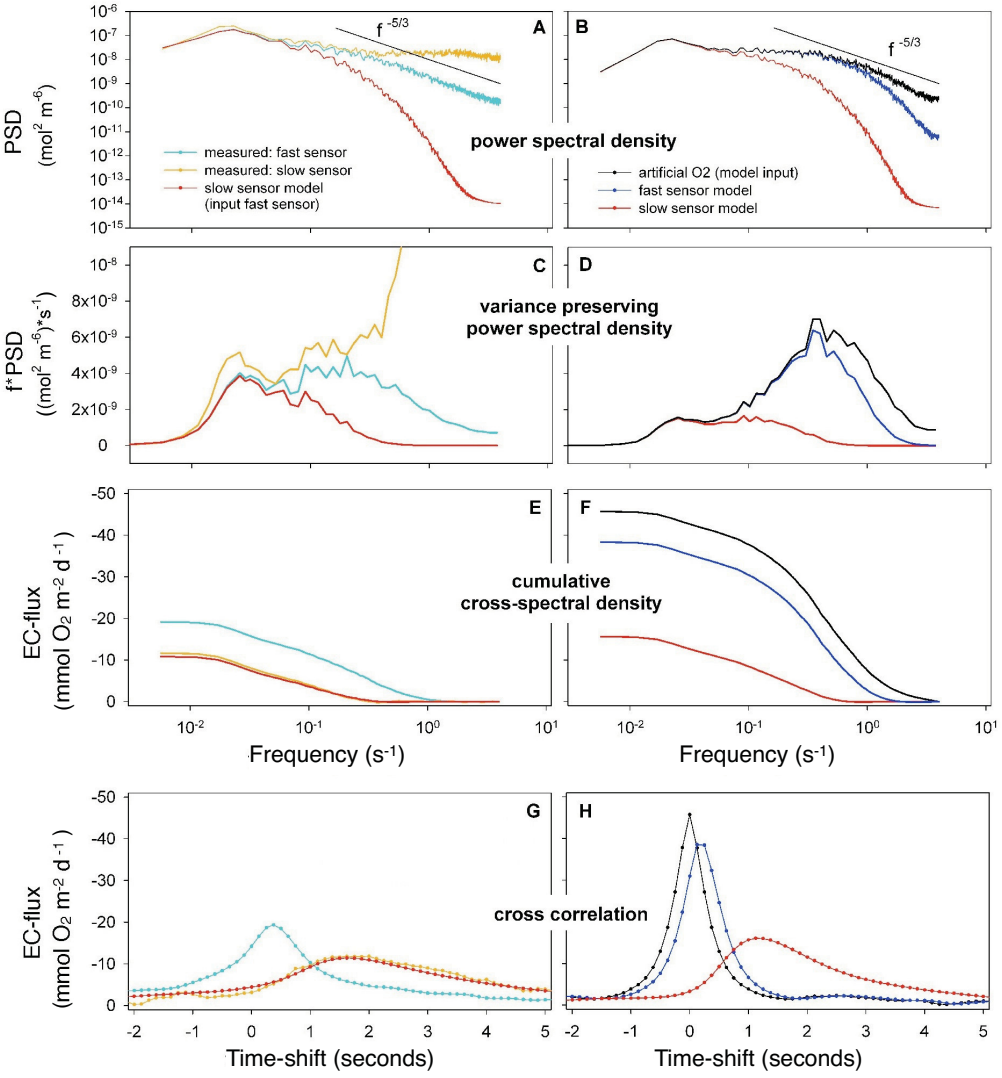

FIGURE 2.9: Measurements and model prediction of a slow (3 s RT -yellow line) a fast (0.35 s and 0.1 s RT - light blue and blue line, respectively) and an artificial (black line) O_2 sensor signal. Power spectral density (A-B), variance preserving power spectral density (C-D), cumulative cross-spectral density (E-F) and cross correlation of w' C' (G-H).

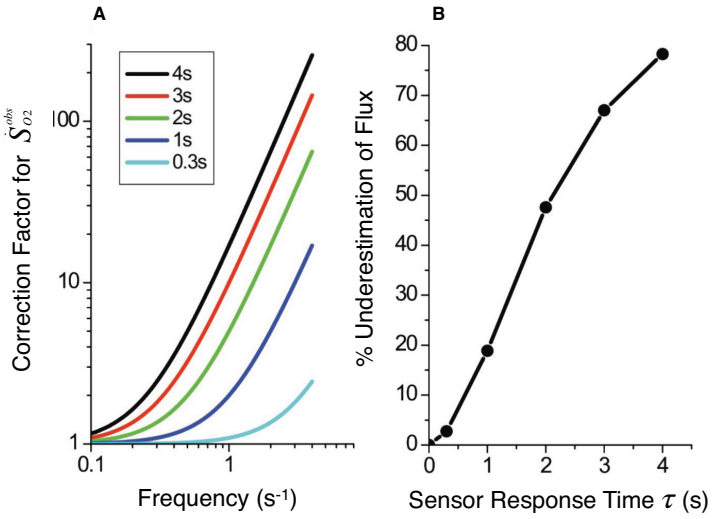

FIGURE 2.10: A) The frequency dependent correction factor applied to the O_2 spectrum. B) estimated underestimation of flux as a function of sensor response time.

Chapter 3

Effects of transient bottom water currents and oxygen concentrations on benthic exchange rates as assessed by eddy correlation measurements

Moritz Holtappels[1,♣], Ronnie N. Glud[2], Daphne Donis[1], Bo Liu[1],Andrew Hume[5],Frank Wenzhöfer[1,6] and Marcel M. M. Kuypers[1]

[1] Max Planck Institute for Marine Microbiology, Bremen, Germany.

[2]University of Southern Denmark, Nordic Centre for Earth Evolution, Odense M, Denmark.

[3]Scottish Association for Marine Science, Scottish Marine Institute, Oban, UK.

[4]Greenland Climate Research Centre, Nuuk, Greenland.

[5]Global Environment Facility, Washington, DC, USA.

[6]HGF-MPG Bridge Group for Deep Sea Ecology and Technology, Alfred-Wegener-Institute for Polar and Marine Research, Bremerhaven, Germany.

♣Corresponding author

Journal of Geophysical Research: Oceans 118, 1157-1169

JOURNAL OF GEOPHYSICAL RESEARCH: OCEANS, VOL. 118, 1157–1169, doi:10.1002/jgrc.20112, 2013

Effects of transient bottom water currents and oxygen concentrations on benthic exchange rates as assessed by eddy correlation measurements

Moritz Holtappels,[1] Ronnie N. Glud,[2,3,4] Daphne Donis,[1] Bo Liu,[1] Andrew Hume,[5] Frank Wenzhöfer,[1,6] and Marcel M. M. Kuypers[1]

Received 17 October 2012; revised 1 February 2013; accepted 5 February 2013; published 12 March 2013.

[1] Eddy correlation (EC) measurements in the benthic boundary layer (BBL) allow estimating benthic O_2 uptake from a point distant to the sediment surface. This noninvasive approach has clear advantages as it does not disturb natural hydrodynamic conditions, integrates the flux over a large foot-print area and allows many repetitive flux measurements. A drawback is, however, that the measured flux in the bottom water is not necessarily equal to the flux across the sediment-water interface. A fundamental assumption of the EC technique is that mean current velocities and mean O_2 concentrations in the bottom water are in steady state, which is seldom the case in highly dynamic environments like coastal waters. Therefore, it is of great importance to estimate the error introduced by nonsteady state conditions. We investigated two cases of transient conditions. First, the case of transient O_2 concentrations was examined using the theory of shear flow dispersion. A theoretical relationship between the change of O_2 concentrations and the induced vertical O_2 flux is introduced and applied to field measurements showing that changes of 5–10 μM O_2 h^{-1} result in transient EC-fluxes of 6–12 mmol O_2 m^{-2} d^{-1}, which is comparable to the O_2 uptake of shelf sediments. Second, the case of transient velocities was examined with a 2D k-ε turbulence model demonstrating that the vertical flux can be biased by 30–100% for several hours during changing current velocities from 2 to 10 cm s^{-1}. Results are compared to field measurements and possible ways to analyze and correct EC-flux estimates are discussed.

Citation: Holtappels, M., R. N. Glud, D. Donis, B. Liu, A. Hume, F. Wenzhöfer, and M. M. M. Kuypers (2013), Effects of transient bottom water currents and oxygen concentrations on benthic exchange rates as assessed by eddy correlation measurements, *J. Geophys. Res. Oceans*, *118*, 1157–1169, doi:10.1002/jgrc.20112.

1. Introduction

[2] In sediments underlying well oxygenated bottom waters, O_2 is the ultimate electron acceptor of almost all electron equivalents released during the oxidation of organic matter [*Canfield et al.*, 2005; *Thamdrup and Canfield*, 2000]. O_2 uptake of the sediment is therefore used as a robust proxy for benthic carbon mineralization [*Glud*, 2008]. Common approaches to measure the benthic O_2 uptake include O_2 microsensor profiles of surface sediments [*Jørgensen and Revsbech*, 1985] and incubations of sediment and overlying water in closed systems such as in situ chamber incubations [*Glud et al.*, 1995]. The two approaches are complementary: O_2 microsensor profiles consider the diffusive uptake, while the chamber approach includes convective contribution from bioirrigation; therefore, paired deployments allow assessment on the fauna mediated O_2 exchange [*Glud*, 2008; *Wenzhöfer and Glud*, 2002]. The incubation approach is, however, strongly invasive, and natural hydrodynamic conditions in the enclosed incubation volume are difficult to mimic, which can have severe affects not only on the O_2 transport in permeable sediments [*Huettel et al.*, 1996], but also on O_2 transport across the diffusive boundary layer above cohesive sediments [*Glud et al.*, 2007; *Lorke et al.*, 2003].

[3] In 2003, the eddy correlation (EC) approach was adapted from atmospheric sciences [*Berg et al.*, 2003] as an alternative way to estimate benthic fluxes. The method relies on natural hydrodynamic conditions as it measures the turbulent transport of O_2 a few centimeters above the sediment water interface, in the so-called benthic boundary

[1]Max Planck Institute for Marine Microbiology, Bremen, Germany.
[2]University of Southern Denmark, Nordic Centre for Earth Evolution, Odense M, Denmark.
[3]Scottish Association for Marine Science, Scottish Marine Institute, Oban, UK.
[4]Greenland Climate Research Centre, Nuuk, Greenland.
[5]Global Environment Facility, Washington, DC, USA.
[6]HGF-MPG Bridge Group for Deep Sea Ecology and Technology, Alfred-Wegener-Institute for Polar and Marine Research, Bremerhaven, Germany.

Corresponding author: M. Holtappels, Max Planck Institute for Marine Microbiology, Celsiusstrasse 1, 28359 Bremen, Germany. (mholtapp@mpi-bremen.de)

2169-9275/13/10.1002/jgrc.20112

layer (BBL). EC measurements combine high frequency measurements of flow velocities and O_2 concentrations in the same sampling volume, from which the instantaneous O_2 flux and a time averaged O_2 flux can be calculated. The EC approach combines several significant advantages: (1) because of its noninvasive nature, the EC approach allows continuous measurements to monitor the response of benthic O_2 uptake on changing environmental conditions [*Hume et al*., 2011]; (2) it is not confined by boundary interface conditions and allows to investigate O_2 sinks and sources at boundaries such as hard bottom substrate [*Glud et al*., 2010], sea ice [*Long et al*., 2011] and sandy sediments [*Reimers et al*., 2012]; (3) it integrates the flux across a large surface area [*Berg et al*., 2007] and thus integrates small to mesoscale heterogeneity of many benthic environments. These essential advantages initiated many studies on the boundary layer flux of other scalars such as dissolved nitrogen and phosphate [*Holtappels et al*., 2011], nitrate [*Johnson et al*., 2011], salinity [*Crusius et al*., 2008] and density [*Holtappels and Lorke*, 2011]. However, the downside of the EC approach is the complex data processing and interpretation, which requires knowledge in time series analysis and hydrodynamics. O_2 fluxes from EC measurements often show extensive short-term variability [*Lorrai et al*., 2010] that is poorly explained by benthic community response. So far, robust criteria to validate these fluxes are missing. It is therefore necessary to identify and quantify errors caused by sensor limitations such as slow response times and low signal to noise ratios as well as errors introduced by the hydrodynamic settings. Here, we focus on hydrodynamic conditions, which induce fluxes in the BBL that add to the true benthic flux estimate. It is useful to distinguish between the O_2 flux across the sediment-water interface and the flux at the sensor position, usually situated at 15–25 cm above the sediment. These fluxes should be identical if we can assume [*Baldocchi*, 2003; *Loescher et al*., 2006; *Lorrai et al*., 2010]: (1) negligible reaction rates in the water layer between sediment and measuring position; (2) a constant surface roughness of the measuring site, and unobstructed flow field ensuring uniform turbulent diffusivity upstream; (3) steady state (i.e., time invariant) mean current velocities, and; (4) steady state mean O_2 concentrations. If these assumptions are not met, the flux at the sensor position can significantly deviate from the flux across the sediment-water interface. The first assumption usually holds as the integrated O_2 consumption rates in the water layer below the sensor position are 1–2 orders of magnitude lower than benthic O_2 fluxes. The second assumption can be reviewed by additional observations from sediment sampling or video surveys, whereas the steady state assumptions for mean current velocities and mean O_2 concentrations can be evaluated from the EC measurement itself. In this study, the validation of the assumption of steady state concentrations and steady state velocities for typical coastal settings is examined and discussed on the basis of two case studies. *Case study 1*: Based on the theory of shear flow dispersion [*Fischer*, 1979; *Taylor*, 1953], we introduce a theoretical relationship between the temporal change of concentrations and the induced vertical flux. We present EC measurements from the Black Sea that are clearly affected by transient (i.e., nonsteady state) O_2 concentrations and validate the applicability of the analytical model. *Case study 2*: A 2D k-ε turbulence model is used to quantify the effect of transient velocities on the EC-flux. EC-measurements from a tidally influenced fjord (Loch Etive, Scotland) that show strong correlation between velocity and EC-flux are analyzed and compared with the numerical model.

2. Theory and Methods

2.1. Case Study 1—Transient O_2 Concentrations

[4] Water masses that move along the sediment can have different origins and can therefore carry different O_2 concentrations. Especially in stratified coastal seas and lakes, sediments intersect with the oxycline of the water column and are therefore exposed to waters with significant O_2 gradients. These water masses move along the sediment with mean current velocities that are decreasing towards the sediment (Figure 1a). The differential advection of water masses with a concentration gradient in the stream-wise direction will cause a vertical concentration gradient and thus a vertical flux (Figure 1b).

2.1.1. The Analytical Model

[5] The balance between differential advective transport in the streamwise direction and diffusive transport in the vertical direction is expressed according to *Fischer* [1979]:

$$\frac{\partial}{\partial z} D_t(z) \frac{\partial C'}{\partial z} = U' \frac{\partial \bar{C}}{\partial x} \tag{1}$$

where D_t denotes the turbulent diffusion coefficient. Here, the concentrations (C) and current velocities (U) are decomposed

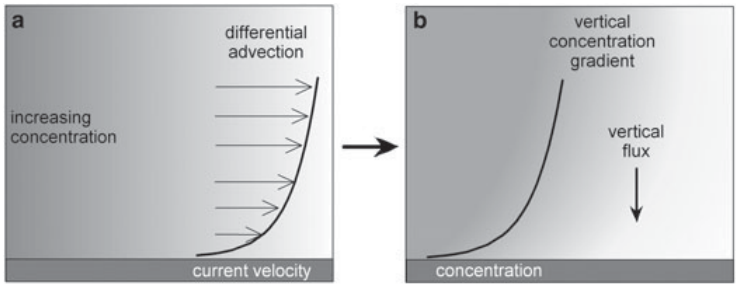

Figure 1. Schematic drawing of the flux caused by nonsteady state concentrations. Differential advection of horizontal concentration gradients (a) cause vertical gradients and (b) a vertical flux, which adds to the flux across the sediment water interface.

into depth averaged values and their deviations $C(x,z) = \bar{C}(x) + C'(x,z)$ and $U(z) = \bar{U} + U'(z)$ where x and z denote the streamwise and the vertical directions, respectively, and U is assumed to be uniform in the streamwise direction.

[6] The interaction between differential advection and vertical diffusion is known as shear flow dispersion. This phenomenon was first described by *Taylor* [1953], who initiated many studies on the spreading of contaminants in conduits and rivers. For a thorough description of shear flow dispersion, we refer to *Fischer* [1979]. In this study, we focus on the induced vertical flux in the BBL, which adds to any flux across the sediment water interface. For simplicity, we assume in the following zero flux at the bottom ($z = 0$). Then integration of equation (1) gives the vertical diffusive flux

$$J(z) = D_t(z)\frac{\partial C'}{\partial z} = \frac{\partial \bar{C}}{\partial x}\int_0^z U'(z)\mathrm{d}z \tag{2}$$

[7] Given Taylor's frozen turbulence assumption [*Taylor*, 1938], the concentration gradient in the streamwise direction, $\partial\bar{C}/\partial x$, can be expressed by the change of concentration over time divided by the mean current velocity, $(\partial C/\partial t)/\bar{U}$, so that equation (2) is rearranged to

$$J(z) = \frac{\partial C}{\partial t}\frac{1}{\bar{U}}\int_0^z U'(z)\mathrm{d}z \tag{3}$$

[8] In a fully developed turbulent flow, the logarithmic law of the wall (log-law) [*von Karman*, 1930] gives estimates of the current velocity profile

$$U(z) = \frac{u_*}{\kappa}\ln\left(\frac{z}{z_0}\right) \tag{4}$$

where u_* and z_o denote the shear velocity and the hydraulic roughness, respectively. Applying the log-law for the velocities in equation (3), we derive (see Appendix A for details)

$$J(z) = \frac{\partial C}{\partial t} z \frac{\ln(z/z_{up})}{\ln(z_{up}/z_0) - 1} \tag{5}$$

with z_{up} as the upper boundary of the BBL. The logarithmic expressions on the right side of equation (5) give negative values. Thus, concentrations that increase over time cause negative (downward) fluxes (Figure 1), and decreasing concentrations cause positive (upward) fluxes. It is evident from equation (5) that the vertical flux caused by transient concentrations is independent from the current velocity. Below, equation (5) is used to estimate the induced vertical flux derived from in situ data. From the time series of the in situ EC measurement, the change of concentration over time, $\partial C/\partial t$, was calculated, and the position z of the EC measuring volume was well constrained. The length scales z_{up} and z_o can be extracted by fitting equation (4) to measured velocity profiles (see below). If the velocity profile is not known, z_o can be calculated directly from equation (4), since U and u_* can be estimated from ADV data [*Inoue et al.*, 2011]. This procedure can be applied to most EC datasets.

2.2. Case Study 2—Transient Current Velocities

[9] In a turbulent steady state boundary layer flow, the profile of mean O_2 concentration depends on the turbulent diffusivity in the BBL and on the upper and lower boundary conditions, i.e., the flux across the sediment water interface and the O_2 concentration at the upper boundary of the BBL (Figure 2). The turbulent diffusivity depends on several factors such as bottom roughness, density stratification and flow velocity [*Holtappels and Lorke*, 2011]. For the sake of simplicity, and because flow velocity is the most dynamic factor, we only focus on the effect of transient current velocities on turbulent diffusivity and subsequently on the O_2 flux. Assuming constant boundary conditions, a change in current velocity over time will cause a change of the turbulent diffusivity and thus an adjustment of the O_2 concentration profile (Figure 2). Any adjustment of the O_2 concentration profile is ultimately linked to an O_2 flux in the bottom water that adds to the O_2 flux from benthic O_2 uptake. Increasing current velocities will cause the erosion of O_2 concentration gradients and increase the O_2 flux in the downward direction, whereas decreasing current velocities cause the buildup of concentration gradients and decrease the O_2 flux in the downward direction. It should be noted that the flux across the sediment-water interface is irrelevant for the induced flux in Case 1, but determines the induced flux in Case 2. If the O_2 flux across the sediment-water interface is positive (benthic primary production), the induced O_2 flux will change direction as well.

2.2.1. The Numerical Model

[10] Using the finite element program COMSOL Multiphysics® 4.3 (www.comsol.com), the turbulent boundary layer flow and the O_2 transport was modeled in a 2D channel of 6 m length and 1.5 m height. Within COMSOL, the low-Reynolds-number k-ε turbulence model was applied (see Appendix B for details), which uses dampening functions to solve for the region close to the wall, where viscous forces dominate. This allows the use of no slip boundary condition instead of wall functions [*Abe et al.*, 1994]. The k-ε turbulence model was coupled with a convection-diffusion model (see Appendix B for details) using the following domain and boundary settings. In the k-ε model, no slip boundary conditions were used

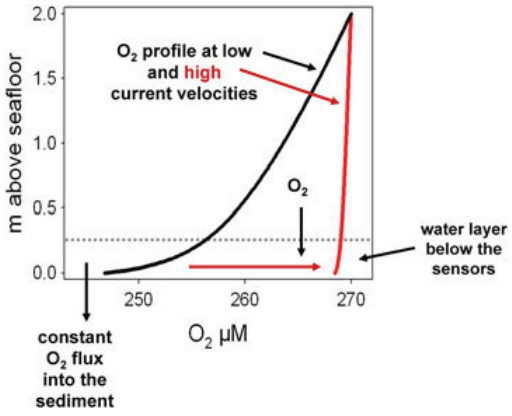

Figure 2. Schematic drawing of the flux caused by nonsteady state current velocities. Here, accelerating flow causes a vertical flux into the layer below the sensor (indicated by the horizontal line), which adds to the flux across the sediment water interface.

for the lower boundary, the upper boundary was set to symmetry condition, the left and right boundary were set to periodic boundary conditions, thus the variables solved for have the same value at the inflow and outflow boundary. In this way, an infinite long boundary flow could be simulated. Fluid motion was forced by a pressure gradient between the left and right boundaries. The pressure gradient was manually adjusted to give the intended velocity change. The pressure gradient was changing with time, thus forcing a transient current velocity. In the convection diffusion model, the upper boundary was set to a fixed O_2 concentration of 300 μM, whereas the lower boundary was set to a constant O_2 flux of -10 mmol m^{-2} d^{-1} to evaluate effects on a constant realistic background level. The left and right boundaries were set to periodic boundary conditions thus concentrations at the inflow boundary were taken from the outflow boundary. The output of the k-ε model, i.e., the velocity field and the turbulent viscosity, were used as input for the convective and diffusive transport. The coupled model was solved for a period of 14 h using a time dependent solver. Furthermore, the COMSOL model was used to estimate the deviation of the EC flux from the benthic O_2 uptake based on an EC deployment at Loch Etive, Scotland. For this, the pressure gradient in the model was adjusted to meet the measured current velocities, the EC flux measured in situ over 56 h was averaged and used as a lower boundary condition, and an average O_2 concentration of 170 μM was used as upper boundary condition.

2.3. Field Measurements

[11] Eddy correlation measurements were conducted at two different locations. Site 1 (for Case study 1) was located on the Crimean shelf, Black Sea, where O_2 dynamics were studied as part of the EU project HYPOX. During a cruise with the RV MS Merian in April/May 2010 a moored EC system was deployed for 14 h at 135 m depth (44°38.84′N, 33°0.18′E). At this depth, the oxycline intersects with the sediment, causing variable O_2 concentrations between 10 and 150 μM, as measured from a nearby mooring. The EC measurement at this site is therefore ideal for evaluating effects of transient O_2 concentrations on EC flux estimates. Video surveys and sediment coring were used to characterize the sediment as homogenous fine grained mud with no signs of benthic macrofauna, presumably as a consequence of low and variable O_2 concentrations.

[12] Site 2 (for Case study 2) was located in Loch Etive, on the west coast of Scotland (56°27.33′N; 5°15.25′W). Loch Etive is a 30 km long glacial fjord with a narrow opening to the sea and two main sills dividing the fjord into two basins. This work was undertaken in the lower marine-dominated basin at ~55 m water depth. The O_2 concentration was relatively constant varying between 169–176 μM during the 56 h long deployment. However, the flow velocity measured at 12 cm off the seabed ranged between 0.3 and 12.6 cm s^{-1} as a consequence of tidal forcing. The sediment was cohesive mud and hosted a dense community of the brittle star *Amphiura filliformis*.

[13] At both sites, the velocity in the x, y, and z directions was sampled using a downward facing acoustic Doppler velocimeter (ADV) (Vector, Nortek, Norway), placed on a tripod frame. The ADV measuring volume (1.5×1.5 cm) was situated 20 and 12 cm above the seabed at Sites 1 and 2, respectively. O_2 concentrations were sampled at the edge of the ADV measuring volume using a pressure compensated Clark-type O_2 microelectrode [*Gundersen et al.*, 1998; *Revsbech*, 1989] and a custom-built picoamperemeter, which was interfaced with the ADV electronics. Velocity and O_2 concentration were sampled with a frequency of 16 Hz (32 Hz at Site 2) in bursts of 15 min (14 min at Site 2) followed by a sleeping period of 15 min (1 min at Site 2). The O_2 microsensor was calibrated against zero and bottom water concentration using anoxic dithionite solution and the O_2 reading of an O_2 Optode (AADI, Norway) attached to a tripod deployed in parallel.

[14] At Site 1, approximately 300 m away from the EC system, a moored benthic-boundary-layer profiling system (BBL-Profiler) [*Holtappels et al.*, 2011] was deployed. The BBL profiler consisted of a tripod frame that has a slide attached to one of the three legs. The slide was equipped with an O_2 optode (Model 4330, Aanderaa), a sensor measuring conductivity, temperature, and depth (CTD) (SeaCat, SBE, US) and an ADV (Vectrino Nortek, Norway). The slider moved vertically across the first 2 m above the sediment surface, stopping at programmed positions to measure for a time interval of 2 min. Prior to the deployment, the O_2 optodes were calibrated using dithionite solution and 100% saturated fresh water. The O_2 readings were corrected for salinity using equations from *Garcia and Gordon* [1992].

[15] For both sites, ADV and O_2 data from the EC system were processed using the following procedure: (1) velocities with a beam correlation of less than 50% were discarded and replaced by an average of the two neighboring values; (2) the data set was despiked using the method described by *Goring and Nikora* [2002]; (3) the tilt of the ADV was corrected using the planar fit method by *Wilczak et al.* [2001]; (4) the power spectral density and the cumulative cospectrum of the vertical velocity and the O_2 concentration was calculated [*Lorrai et al.*, 2010]; (5) based on the cumulative cospectrum, which showed insignificant flux contributions below a frequency of 0.01 Hz, a running average with a window of 100 s was subtracted from the time series to calculate the fluctuating velocity w' and concentration C'; (6) the time series of w' and C' were cross-correlated for each burst allowing stepwise time shifts to a maximum 0.75 s of both, w' and C' [*Lorrai et al.*, 2010; *McGinnis et al.*, 2008], and the cross correlation with the highest correlation coefficient was used to calculate the flux; and (7) the cross correlations were subsequently evaluated by calculating the probability of receiving the same correlation (i.e., the same flux) from random data sets (corrcoef function in Matlab). The threshold for a significant flux was set to 5%.

3. Results

3.1. Case Study 1—Transient O_2 Concentrations

3.1.1. The Analytical Model

[16] For a known temporal change of O_2 concentration, the vertical flux can be calculated from equation (5). However, for a general analysis, it is more convenient to re-arrange equation (5) and introduce a proportionality factor R that depends only on the sensor position z and the dimensions of the logarithmic boundary-layer, i.e., z_0 and z_{up}. The

proportionality factor R is the ratio of the induced vertical flux (J) per temporal change of concentration ($\partial C/\partial t$):

$$R = \frac{J(z)}{(\partial C/\partial t)} = z\frac{\ln(z/z_{up})}{\ln(z_{up}/z_0) - 1} \quad (6)$$

[17] Using upper and lower estimates of z_o (10^{-3} and 10^{-5} m) and z_{up} (1 and 5 m), the range of the proportionality factor that can be expected at 15 cm above the sediment (the recommended position of the EC measuring volume) is calculated varying between −0.025 and −0.07 m (Figure 3). An increase of 10 µM O_2 h^{-1} would therefore result in a flux between −6.0 and −16.8 mmol O_2 m^{-2} d^{-1}, which is comparable to the O_2 uptake of typical shelf sediments. The negative sign indicates that the flux is directed towards the sediment. In contrast, decreasing O_2 concentrations would result in positive fluxes.

[18] From the field measurement, we estimated a bottom roughness (z_o) of 1×10^{-4} m by fitting the log-law (equation (4)) to the velocity profile of the BBL-profiler (Figure 4, left part). The upper boundary of the BBL (z_{up}) was assumed to be 2 m. The resulting proportionality factor R (Figure 4) decreases from zero at the lower and upper boundaries to −0.08 m at 70 cm above the sea floor. At 20 cm above the seafloor—the positions of the EC measuring volume at Site 1 (Black Sea)—the proportionality factor is still −0.05 m, and an increase of 10 µM O_2 h^{-1} results in a flux of −12.0 mmol O_2 m^{-2} d^{-1}.

3.1.2. Field Measurements

[19] During the 14 h of deployment, the average current velocities at Site 1 were varying between 5 and 9 cm s^{-1} (Figure 5a). A down-slope directed current carried O_2 concentrations, which increased on average by 1.2 µM h^{-1} (Figure 5B). However, the rate of change was not constant during the deployment. The change of O_2 over time was calculated for each burst by linear regression (Figure 5C), showing a strong increase of more than 4 µM h^{-1} in the first 2 h and between hour 8 and 11, whereas O_2 concentrations remain almost constant between hours 5 and 8. The O_2 flux from the EC measurement was calculated for each burst (Figure 5c). From a total of 27 bursts, two bursts were discarded due to insignificant correlation. The averaged O_2 flux of the remaining bursts was −6.0 mmol m^{-2} d^{-1}, which was greater than O_2 fluxes derived from microsensor

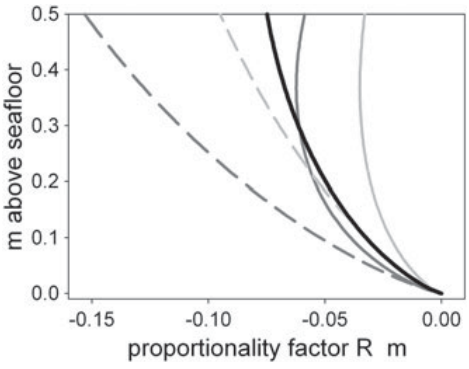

Figure 3. The proportionality factor (R) as a function of sensor position (z) and the following benthic boundary layer (BBL) dimensions: BBL height (z_{up}) of 1 m (solid lines) and 5 m (dashed lines) and roughness (z_0) of 10^{-5} m (light grey lines) and 10^{-3} m (dark grey lines). For Black Sea measurements, $z_0 = 10^{-4}$ and $z_{up} = 2$ m were assumed (black solid line).

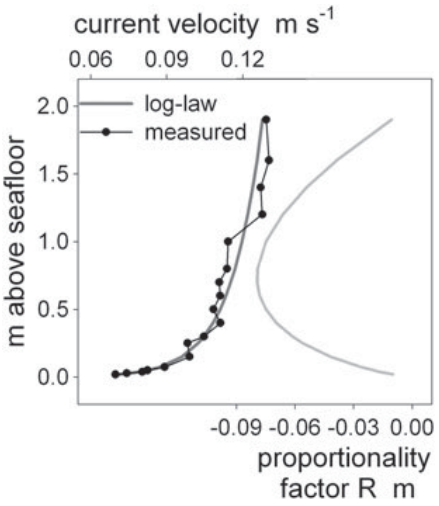

Figure 4. Black Sea deployment: left side: measured current velocity and fit with log-law. Right side: profile of R over the entire BBL of 2 m.

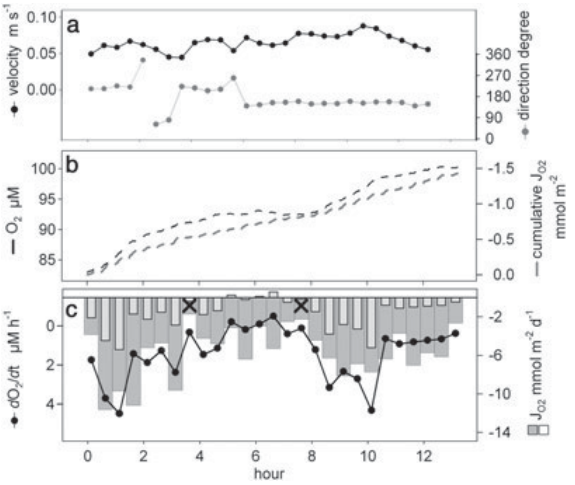

Figure 5. Results from the eddy correlation (EC)-measurement at the Crimean shelf, Black Sea show: (A) burst averages of current velocity and directions, (b) O_2 concentrations averaged over 100 s and the cumulative EC-flux, (c) the change of O_2 concentrations over time and the EC-flux, both averaged over the entire burst. The light grey bars in Figure 5C mark the O_2 flux induced by transient O_2 concentrations. Two bursts were discarded due to insignificant correlation (marked by **X**).

profiles ($-4.5 +/- 2.6$ mmol m^{-2} d^{-1}, $n = 7$) of a benthic lander at same station. Over the entire deployment, O_2 fluxes varied from -2.5 mmol m^{-2} d^{-1} to more than -11 mmol m^{-2} d^{-1}. Bursts with increased fluxes were found predominantly at times with strong O_2 increase, whereas decreased fluxes were found at times of constant or decreasing O_2. This is also observed when comparing the cumulative flux and the O_2 concentrations of individual bursts (Figure 5b), which show similar trends especially during the first 2 h and between hour 9 and 11. A significant linear relation ($p < 0.0005$) was found between the O_2 flux and the O_2 rate of change (Figure 6), which explains 42% of the O_2 flux variance. The slope of the linear regression, which gives the proportionality factor, was -0.05 m and matches the expected theoretical value (see above Figure 3, black line). The intercept of the linear regression (-4.2 mmol O_2 m^{-2} d^{-1}, Figure 6) gives the flux at steady state O_2 concentration, matching the O_2 flux derived from O_2-microsensor profiles. The flux due to changing O_2 concentrations was calculated from equation (5) and varied from +0.6 to -5.4 mmol O_2 m^{-2} d^{-1} (Figure 5c).

3.2. Case Study 2—Transient Current Velocities

3.2.1. The Numerical Model

[20] Two scenarios were simulated: accelerating and decelerating current velocities (Figure 7). The initial pressure gradient between the left and right boundaries of the model domain was adjusted to result velocities of 2 cm s^{-1} (and 10 cm s^{1}) at 15 cm above the lower boundary (Figures 7A and 7B). After simulating 3 h of steady state flow, the pressure gradient was readjusted to generate a 5 h increase (and decrease) of the velocity to 10 cm s^{-1} (and 2 cm s^{-1}). Thereafter, the velocity remained constant, and the flow returned to steady state. With changing velocities, the turbulent diffusivity (i.e., the turbulent viscosity) at the same depth varies between 0.4×10^{-4} and 2.2×10^{-4} m^2 s^{-1}. The transient conditions result in a phase shift between velocity and turbulent diffusivity. The initial increase of the turbulent diffusivity at hour 3 is delayed by 20 min compared to the initial velocity increase. Similarly, the turbulent diffusivity during deceleration is delayed by ~25 min. To follow the change during transient conditions, several vertical profiles of current velocity, turbulent diffusivity, O_2 concentration and O_2 flux were extracted from the model (Figures 7c–7j).

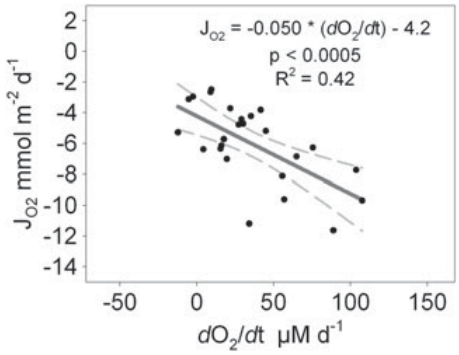

Figure 6. O_2 flux plotted against the change of O_2 concentration over time. The slope of the linear regression of -0.05 m gives an estimate of the proportionality factor *R*. Dashed lines mark the 95% confidence interval.

[21] During accelerating flow, vertical gradients of velocity and turbulent diffusivity increase, whereas the vertical gradient of O_2 decreases (Figures 7c, 7e and 7g). The shear stress at the lower boundary is the source for the turbulent kinetic energy. Therefore, the initial increase of turbulent diffusion starts at the lower boundary and is moving upwards causing transient maxima in the center of the domain (Figure 7e), which disappear as the flow field reaches steady state. This evolution of the turbulent diffusivity causes an initial decrease of concentrations at depths close to the lower boundary, before concentrations gradually increase at all depths. Similarly, the downward flux of O_2 starts increasing at the lower boundary (Figure 7i) showing transient maxima that move upward and increase before they finally decrease and disappear as the flux returns to steady state at -10 mmol m^{-2} d^{-1}. The temporal evolution of the O_2 flux at 15 cm above the lower boundary (Figure 7a) shows a high initial flux of -17.5 mmol m^{-2} d^{-1} which is gradually decreasing to steady state conditions over the following 3.5 h. Further away from the boundary, the maximum flux increases up to -19.5 mmol m^{-2} d^{-1} (at 0.5 m) and remains high for several hours. Temporal integration of the deviating O_2-flux over the interval of transient conditions gives the total amount of excess O_2 per area that is transported between the layer above and below the depth of interest. At 0.15, 0.25 and 0.5 m, the integrated O_2 flux due to transient conditions is -0.36, -0.47 and -0.69 mmol m^{-2}, respectively.

[22] During decelerating flow, vertical gradients of velocity and turbulent diffusivity decrease, whereas the vertical gradient of O_2 increases (Figures 7d, 7f and 7h). Different from accelerating flow, velocity, diffusivity and O_2 concentrations are monotonic functions of time and space as they continuously decrease with time and towards the lower boundary. Compared to accelerating flow, the resulting deviation of the O_2 flux is less pronounced (Figure 7j) but lasts twice as long. The temporal evolution of the O_2 flux at 15 cm above the lower boundary (Figure 7b) shows a moderate decrease over 4 h to -7.1 mmol m^{-2} d^{-1} followed by a 4 h increase to steady state conditions. Further away from the boundary, the O_2-flux minimum is lowered to -6.7 mmol m^{-2} d^{-1} (at 0.5 m) and the return to steady state conditions is delayed by another 3 h. Temporal integration of the deviating O_2 flux over the interval of transient conditions is the same as for accelerating flow, but with opposite signs.

3.2.2. Field Measurements

[23] Field measurements at Loch Etive were used to study the effect of transient current velocities on the EC flux. During the total of 56 h of deployment, 4 periods of low and high tide were observed that correlated with a change in current direction and current velocities (Figures 8a and 8b). Each period lasted 12.5 h in which 2.5 h of high velocities (8.5–13 cm s^{-1}) and high EC fluxes (-20 to -60 mmol m^{-2} d^{-1}) (Figure 8d) were followed by 10 h of low velocities (1–3 cm s^{-1}) and low EC fluxes (0 to -20 mmol m^{-2} d^{-1}). The mean EC-flux over 4 tidal cycles (50 h) was -10.2 mmol m^{-2} d^{-1}. A standard deviation of $+/-11.1$ mmol m^{-2} d^{-1} illustrates the natural high variability of the EC-flux. Parallel to the EC measurements, O_2 microprofiles were measured

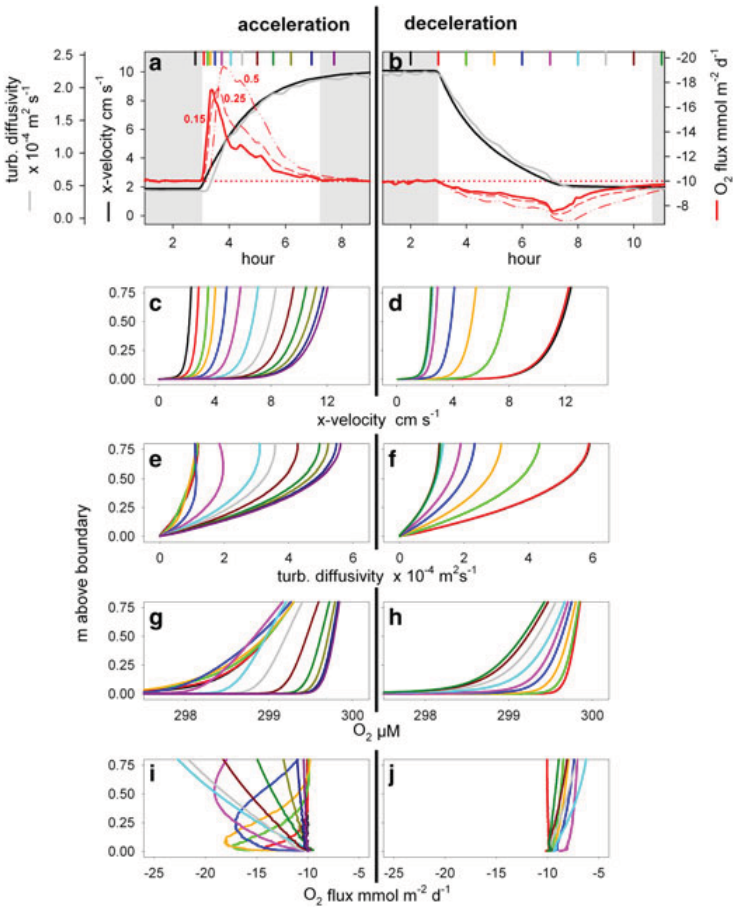

Figure 7. Results from the k-ε turbulent transport model show velocity, turbulent diffusivity and O_2-flux at 15 cm above the lower boundary during (a) accelerating and (b) decelerating flow conditions. The O_2-flux at 0 cm (dotted line), at 25 cm (dashed line) and at 50 cm (dashed-dotted line) above the lower boundary is also shown. Specific times are marked by colored bars in Figures 7a and 7b for which the vertical profiles of velocity (Figures 7c and 7d), turbulent diffusivity (Figures 7e and 7f), O_2 concentration (Figures 7g and 7h) and O_2-flux (Figures 7I and 7J) are shown.

using a transecting microprofiling instrument [*Glud et al*., 2009] and resolved a mean O_2 penetration depth of 3.7 +/− 1.1 mm (n = 16), a DBL thickness of 0.6 mm [*Inoue et al*., 2011] and a calculated average diffusive O_2 uptake of 7.9 +/− 1.2 mmol m^{-2} d^{-1}. Additionally, we deployed a benthic chamber lander right before and after the eddy measurement, and the chamber derived total O_2 uptake rates amounted to 10.4 and 16.8 mmol m^{-2} d^{-1}, respectively.

[24] During the EC deployment, O_2 concentration was relatively stable varying between 168 and 176 µM (Figure 8c). The change of O_2 over time ($\partial C/\partial t$) was calculated for each burst as described for the Black Sea data. However, the correlation between EC-flux and $\partial C/\partial t$ was weak, explaining less than 6% of the EC-flux variability. As such the flux due to transient O_2 concentrations was negligible, and on average, it amounted to −0.04 +/− 5 mmol m^{-2} d^{-1} (Figure 8c). The observed patterns of simultaneous increase and decrease of velocity and EC-flux, can be ascribed to several factors including changes in DBL resistance towards O_2 uptake, flow-induced shift in infauna behavior and flow dependent flushing of infauna burrows. However, it can also partly reflect an O_2-flux that deviates from the benthic O_2 uptake due to transient current velocities. To test this, we applied the numerical model and adjusted the input values for the pressure gradient to shorten the accelerating and decelerating intervals to 1 h (red line, Figure 8b). Upper and lower steady state current velocities were adjusted to 10 and 2 cm s^{-1}, respectively, which matches the measured current velocities over the first three tidal cycles. The measured average O_2-flux of the EC measurement (−10 mmol m^{-2} d^{-1}) and the average O_2 concentration (170 µM) were used as upper and lower boundary conditions. During acceleration, the modeled downward flux at the sensor position (12 cm above the lower boundary) increased by 100% up to −20 mmol m^{-2} d^{-1} and was elevated for 2.2 h. During deceleration, the flux decreased by 54% down to −4.6 mmol m^{-2} d^{-1} and was below the average flux for a total of 7 h. Temporal integration of the

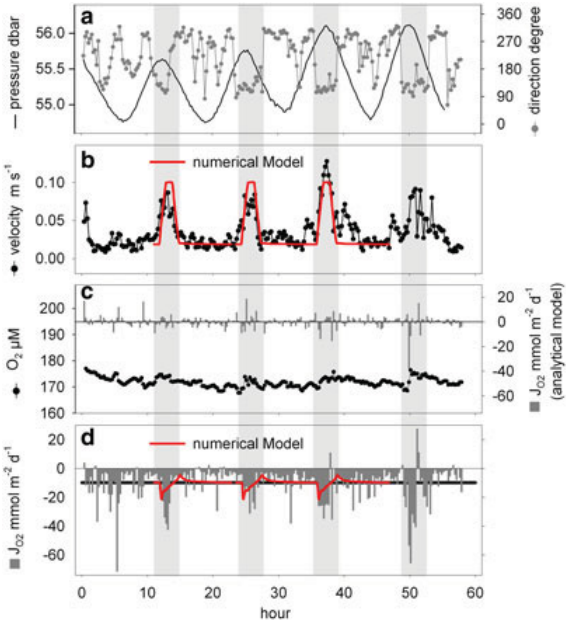

Figure 8. Results from the EC-measurement at Loch Etive show: (a) the pressure and current directions, (b) the current velocity, (c) the O_2 concentration and the estimated O_2-flux due to transient O_2 concentrations, (d) the EC-flux for each burst and the average EC-flux (black line). The total number of bursts was 231 of which five bursts were discarded due to insignificant correlation. Similar changes in current velocity were used in the k-ε transport model to estimate the O_2-flux at $z = 12$ cm (red lines).

deviating O_2 flux over the interval of transient conditions is the same for accelerating and decelerating flow, but with opposite signs. The modeled flux averaged over a full tidal cycle is therefore equal to the flux across the lower boundary (-10 mmol m^{-2} d^{-1}).

4. Discussion

[25] Both the analytical and the numerical model show that transient flow and O_2 concentrations can cause EC-fluxes that significantly deviate from the true flux across the sediment-water interface. For the case of transient O_2 concentrations it was possible to apply an analytical model because the flow field was constant and could be described by the log-law. However, the transient flow field in Case 2 results in phase shifts between velocity and turbulent diffusivity (Figures 7a and 7b), and transient maxima in turbulent diffusivity and O_2-flux profiles (Figures 7E and 7I), which are not reflected by analytical solutions derived from the log-law. Therefore, a k-ε turbulence model was necessary to capture the dynamics of turbulent transport across the BBL and the induced deviating EC flux. It should be mentioned that the flux across the sediment-water interface itself may show a temporal variability caused by, e.g., changing O_2 concentrations at the sediment surface, changing activity of the infauna or changing flushing rates in permeable sediments. However, in both models the variability of the flux across the sediment-water interface was neglected to allow an isolated examination of the potential errors due to transient conditions.

4.1. Case Study 1—Transient O_2 Concentrations

[26] The underlying assumption for the analytical model is a balance between differential advective transport and vertical diffusive transport (see equation (1)). This assumption may not be correct in case of abrupt changes of O_2 concentrations, which are occasionally recorded during EC measurements. To study how the balance is established after a sudden 5% increase of the O_2 concentration, we applied the COMSOL model and modified the following: (1) the domain was enlarged to 200 m length, 2 m height and 320,000 mesh elements; (2) in the k-ε module, a pressure difference between the left and right boundary was adjusted to a steady state velocity profile that matches the profile shown in Figure 4; (3) in the convection-diffusion model, the upper boundary was set to symmetry and the flux across the lower boundary was set to zero, and; (4) the inflow concentration at the left boundary was set to 105 µM, whereas the initial concentration in the domain was set to 100 µM. In this way, the evolution of a front with an abrupt 5% increase of O_2 concentration was modeled for 35 min using a time dependent solver. Figure 9 shows the temporal change of concentrations, the resulting downward flux and the proportionality factor, at 15 cm above the sediment and at different positions (20, 40, 80, 120, 160 and 200 m) downstream of the inflow boundary. The front slowly erodes as it propagates downstream (Figure 9A) and thus the maximum temporal change of O_2 concentration in the front decreases (Figure 9b) along with the induced vertical flux. The proportionality factor is approaching the theoretical value of -0.05 m as the front moves downstream (Figure 9C).

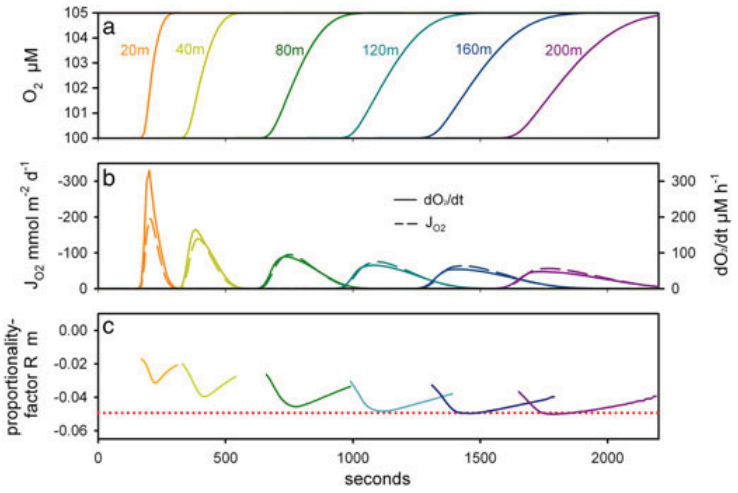

Figure 9. Results from a k-ε turbulent transport model simulating an abrupt increase of O_2 concentrations from 100 to 105 µM. The temporal change of (a) O_2 concentrations and (b) O_2 fluxes at 15 cm above the sediment is shown for different downstream-positions (color-coding). The (c) proportionality factor approaches the theoretical value of −0.05 m (red line) suggesting a balance between differential advective and vertical diffusive transport.

During the passage of the front at 200 m (i.e., 30 min after the initial change) the average value of the proportionality factor is −0.046 m (+/−0.004 m) suggesting that differential advective transport and vertical diffusive transport are nearly in balance. The numerical model shows that the analytical solution (equation (3)) is applicable already 30 min after the abrupt change of O_2 concentrations, which is, after all, an extreme nonsteady state situation causing extreme high vertical fluxes of up to −200 mmol m^{-2} d^{-1}.

[27] For the analytical model, we used the log-law to estimate the velocity profile and derive an exact solution that depends only on the boundary scales z, z_{up} and z_o. Strictly speaking, the log-law applies only for a specific layer within the entire boundary layer, but in many cases, it is also a reasonable model for the entire velocity profile (Figure 4). If the log-law is not applicable, which is the case in strongly stratified bottom waters [*Holtappels and Lorke*, 2011], equation (3) should be applied using measured current velocity profiles.

[28] Because the EC approach is based on the statistical analysis of two time series (i.e., the cross correlation of w' and C'), statistical measures should be used to evaluate the calculated fluxes. We introduced a probability test of the cross correlation of w' and C' to estimate the probability of deriving the same correlation from completely random data sets with similar mean values and standard deviations. Using a threshold of 5%, the fluxes of two bursts at Site 1 were flagged as not significant (Figure 5c). From a total of 27 bursts, these two bursts gave the lowest flux (~2 mmol m^{-2} d^{-1}, $p < 0.14$) most likely defining the detection limit of the deployed EC system at the given conditions. However, rejecting flux estimates that are below the detection limit would bias the average flux towards higher values. On the other hand, non significant correlations are not necessarily caused by low or zero fluxes, but could result also from sensor failure or flow disturbances. Here, the calculated EC fluxes are compared with other factors such as the O_2 change over time (Figure 6). For this kind of analysis, non significant fluxes have to be discarded. In general, longer burst intervals would improve the probability of a significant correlation. For future deployments, we therefore recommend continuous measurements if sufficient power supply and data memory is at hand.

[29] After rejecting two bursts due to non significant correlation, the fluxes of the remaining bursts were analyzed in light of the transient O_2 concentrations. The ratio of EC fluxes to changing O_2 concentrations (i.e., the proportionality factor R) was predicted by the analytical model, and could explain 42% of the flux variance. The flux caused by increasing O_2 concentrations was significant. On average, 30% of the measured EC-flux could be attributed to transient O_2 conditions and for individual bursts proportions of up to 70% were found (Figure 5c). If mean O_2 concentrations would have decreased over time, the induced O_2 flux would have been positive and the superposition with the benthic O_2 uptake would have caused extremely low or even positive EC-fluxes, most likely below the detection limit. Applying equation (5) to correct the EC flux resulted in an average EC flux of −4.2 mmol O_2 m^{-2} d^{-1}, which matched the flux calculated from O_2 microsensor profiles. Given that the impermeable sediment contained no fauna, this alignment put confidence in the analytic approach.

[30] It is recommended to equip the EC systems with additional sensors that continuously record O_2, temperature and salinity to provide a robust and independent measurement of mean O_2 concentrations and to detect water masses of different origin. This is particularly important in shallow coastal waters where a high short-term variability of O_2 concentrations is to be expected. Additionally, ADCP measurements would help to determine the velocity profile

applied in equation (3) and help improve any corrections of EC-derived O_2 fluxes.

4.2. Case Study 2—Transient Current Velocities

[31] In general, the O_2-flux caused by transient current velocities depends on (1) the flux across the sediment water interface, (2) the acceleration/deceleration of current velocity and (3) the current velocity itself, as described in the following. The O_2-flux caused by transient current velocities is proportional to the O_2-flux across the sediment-water interface (see Figure 2). Doubling the O_2-flux across the lower boundary results in a doubling of the EC-flux deviation. Thus, the EC-flux deviation can be expressed in percent of the flux across the sediment-water interface. In the model study, accelerating and decelerating flow resulted in EC-flux estimates that deviated by +75% and −30% from the true flux across the sediment-water interface (Figures 7a and 7b). Adjusting the model to the conditions found at Loch Etive resulted in EC-deviations of up to +100%. Increasing acceleration/deceleration also increases the deviation of the flux. If the change in current velocity by 8 cm s^{-1} takes place twice as fast (i.e., from 2 to10 cm s^{-1} within 2.5 h instead of 5 h), the deviation of the EC-flux is doubled. The deviation will even increase further if the same acceleration/deceleration takes place at lower current velocities (e.g., between 0.5 and 8.5 cm s^{-1}). On the other hand, the deviation strongly decreases for acceleration/deceleration at high velocities.

[32] The results of the numerical model reflected the overall dynamic of the measured EC-fluxes at Loch Etive (Figure 8d). During peak periods, the transient flow conditions could explain considerable parts of the observed flux variation, but not all. It is not surprising that the benthic O_2 uptake is flow dependent; it has previously been documented that enhanced flow velocities stimulate passive flushing of infauna burrows [*Munksby et al*., 2002] and change infauna behavior and irrigation [*Vopel et al*., 2003]. Further, flow driven variations in DBL thickness can affect the O_2 uptake in coastal waters [*Glud et al*., 2007]. The increase of the O_2-flux upon complete elimination of the DBL can be calculated according to *Boudreau and Guinasso* [1982]. Applying the conditions found at Loch Etive and assuming depth independent volumetric O_2 consumption rates in the sediment, the theoretical elimination of the DBL would increase the O_2-flux only by a factor of 1.3, which does not explain the observed variability. In conclusion, the EC-resolved flow dependence of the O_2 uptake is confounded by transient flow phenomena as described above, and the remaining response must be ascribed to a combination of several factors as described above. However, the general alignment between average values for the EC derived flux, chamber incubations and microprofiles put confidence in the approach as long as data are carefully evaluated and assessed.

[33] The current study documents that quantitative flow responses as derived from EC-measurements should be evaluated with care. Transient flow velocities could explain a significant fraction of the variable EC-flux during tidal cycles. However, the modeled response reflected an asymmetric maxima and minima that cannot be resolved by the field data. We cannot exclude that other effects also could have contributed to the flux variability. For instance, periods of enhanced fluxes did also correlate with current direction (Figures 8a and 8d), and local disturbances of the flow field from obstacles located upstream during the time of high current velocities could have increased the turbulent mixing and there are indeed some hints suggesting this to be the case. At increased current velocities (direction 100°), time series of turbulent diffusivities calculated directly from the velocity fluctuations according to *Holtappels and Lorke* [2011] are above turbulent diffusivities calculated from the log-law, the latter assuming a steady state velocity field. At other times, the calculated diffusivities agree. This suggests a direction dependent imbalance of eddy diffusivities and the mean flow field, which could be explained by upstream located disturbances of the flow.

[34] It should be noted that fluxes due to transient conditions complicate other noninvasive measurements as well. The measurement of mean concentration gradients in the BBL [*Holtappels et al*., 2011] in combination with measured or calculated turbulent diffusivities [*Holtappels and Lorke*, 2011] are affected in the same way. However, the determination of relative fluxes of two different solutes (e.g., O_2 and NO_3^-) from their concentration profiles remains unaffected by nonsteady state current velocities, because the transient turbulent diffusivities are the same for both solutes [*Holtappels et al*., 2011].

4.3. Consequences for EC-Measurements

[35] Strong O_2 gradients and rapid change of current velocities in the bottom water are most likely found in coastal waters where winds, tides and strong O_2 sinks and sources prevail. Thus, EC-measurements under these conditions are challenging. We show that moderate changes of mean current velocities and mean O_2 concentrations can cause EC-fluxes that deviate by up to 100% from the true benthic flux estimate (Figure 8). In both cases, the discrepancy increases with the distance between the measuring volume and the seabed. Therefore, measurements closer to the sediment are less prone to errors than measurements conducted further away from the surface, but this will at the same time reduce the size of the measuring foot print. In general, it is recommended to carefully analyze the velocity and O_2 concentration time series recorded during EC-deployments and resolve their rate of change to estimate how this may confound the true benthic flux. In addition, we recommend EC-measurements over extended periods to cover the site-specific natural variability of flow conditions and O_2 concentrations. Long sampling periods increase the probability that biases due to increasing and decreasing velocities or concentrations are averaged out and result in a trustworthy mean flux.

[36] Interpretation of EC-fluxes is complex, and there is the risk of a biased selection between valuable data and outliers, since common objective evaluation criteria are not well defined, so far. In general, there is a priori no reason to discard extremely high or low fluxes that may not fit into the expected range, unless there is evidence that the sensor performances were compromised during those periods. Instead, the measured fluxes have to be interpreted in light of the present hydrodynamic conditions. This study provides some important guidelines to reach this ultimate goal.

Appendix A

[37] Applying the logarithmic law of the wall, the current velocity profile is calculated:

$$U(z) = \frac{u_*}{\kappa} \ln\left(\frac{z}{z_0}\right) \tag{A1}$$

[38] The depth averaged velocity $\bar{U}$ can be obtained by integration of the current velocity between z_0 and z_{up}, where z_0 denotes the hydraulic roughness and z_{up} the upper boundary of the BBL:

$$\bar{U} = \frac{1}{z_{up}} \int_0^{z_{up}} U(z)\mathrm{d}z = \frac{1}{z_{up}} \int_0^{z_{up}} \frac{u_*}{\kappa} \ln(z/z_0)\mathrm{d}z \tag{A2}$$

$$\bar{U} = \frac{1}{z_{up}} \frac{u_*}{\kappa} \left(\ln\left(z_{up}/z_0\right) z_{up} - \int_0^{z_{up}} z\mathrm{d}[\ln(z/z_0)] \right) \tag{A3}$$

$$\bar{U} = \frac{1}{z_{up}} \frac{u_*}{\kappa} \left(\ln\left(z_{up}/z_0\right) z_{up} - z_{up} \right) \tag{A4}$$

$$\bar{U} = \frac{u_*}{\kappa} \left(\ln\left(z_{up}/z_0\right) - 1 \right) \tag{A5}$$

[39] The flux due to changing concentrations over time is given by

$$J(z) = \frac{\partial C}{\partial t} \frac{1}{\bar{U}} \int_0^z U'(z)\mathrm{d}z \tag{A6}$$

[40] Equation (A-5) is inserted into equation (A-6):

$$J(z) = \frac{\partial C}{\partial t} \frac{1}{\bar{U}} \int_0^z (U(z)\text{-}\bar{U})dz \tag{A7}$$

$$J(z) = \frac{\partial C}{\partial t} \int_0^z (U(z)/\bar{U}\text{-}1)\mathrm{d}z \tag{A8}$$

$$J(z) = \frac{\partial C}{\partial t} \frac{1}{\ln\left(z_{up}/z_0\right) - 1} \int_0^z \left(\ln(z/z_0)\text{-}\ln\left(z_{up}/z_0\right) + 1\right)\mathrm{d}z \tag{A9}$$

$$J(z) = \frac{\partial C}{\partial t} \frac{1}{\ln\left(z_{up}/z_0\right) - 1} \left[\ln(z/z_0)z - z\text{-}\left(\ln\left(z_{up}/z_0\right) - 1\right)z\right] \tag{A10}$$

$$J(z) = \frac{\partial C}{\partial t} z \frac{\ln\left(z/z_{up}\right)}{\ln\left(z_{up}/z_0\right) - 1} \tag{A11}$$

Appendix B: COMSOL 2D Model

[41] Low-Reynolds-Number Turbulent Flow (k-ε) coupled to Transport of Diluted Species

Turbulent Flow, k-ε:

Domain:

Reynolds-averaged Navier-Stokes equations:

$$\rho \frac{\partial \mathbf{u}}{\partial t} + \rho(\mathbf{u}\cdot\nabla)\mathbf{u} = \nabla\cdot\left[-p\mathbf{I} + (\mu+\mu_T)\left(\nabla\mathbf{u} + (\nabla\mathbf{u})^T\right) - \frac{2}{3}\rho k\mathbf{I}\right] + \mathbf{F}, \rho\nabla\cdot\mathbf{u} = 0$$

Transport equation for turbulent kinetic energy k:

$$\rho \frac{\partial k}{\partial t} + \rho(\mathbf{u}\cdot\nabla)k = \nabla\cdot\left[\left(\mu + \frac{\mu_T}{\sigma_k}\right)\nabla k\right] + P_k - \rho\varepsilon$$

Transport for the dissipation rate ε:

$$\rho \frac{\partial \varepsilon}{\partial t} + \rho(\mathbf{u}\cdot\nabla)\varepsilon = \nabla\cdot\left[\left(\mu + \frac{\mu_T}{\sigma_\varepsilon}\right)\nabla\varepsilon\right] + C_{\varepsilon 1}\frac{\varepsilon}{k}P_k - C_{\varepsilon 2}\rho\frac{\varepsilon^2}{k}f_\varepsilon$$

with

turbulent viscosity $\mu_T = \rho C\mu \frac{k^2}{\varepsilon} f_\mu$

production term $P_k = \mu_T[\nabla\mathbf{u} : (\nabla\mathbf{u} + (\nabla\mathbf{u})^T)]$

damping functions

$$f_\mu = \left(1 - e^{-l^*/14}\right)^2 \cdot \left(1 + \frac{5}{R_t^{3/4}} e^{-(R_t/200)^2}\right)$$

$$f_\varepsilon = \left(1 - e^{-l^*/3.1}\right)^2 \cdot \left(1 + 0.3e^{-(R_t/6.5)^2}\right)$$

turbulent Reynolds number $R_t = \frac{\rho k^2}{\mu\varepsilon}$

dimensionless wall distance $l^* = \frac{\rho u_\varepsilon L_W}{\mu}$, with $u_\varepsilon = \left(\frac{\mu\varepsilon}{\rho}\right)^{1/4}$

closest wall distance $L_W = \frac{1}{G} - \frac{L_{ref}}{2}$, with $L_{ref} = 0.75$

constants $C_{\varepsilon 1} = 1.5$ $C_{\varepsilon 2} = 1.9$

$C_\mu = 0.09$ $\sigma_k = 1.4$ $\sigma_\varepsilon = 1.5$

dynamic viscosity $\mu = 0.001$ Pa s

density $\rho = 999.6$ kg m^{-3}

The reciprocal wall distance is solved:
$\nabla G \cdot \nabla G + \sigma_w G(\nabla\cdot\nabla G) = (1+2\sigma_w)G^4$, $\sigma_w = 0.1$

Boundaries:

Wall:

$$\mathbf{u} = 0 \quad k = 0 \quad \varepsilon = \lim_{L_W \to 0} \frac{2\mu k}{\rho L_W{}^2} \quad G = \frac{2}{L_{ref}}$$

Symmetry:

$$\mathbf{u}\cdot\mathbf{n} = 0 \quad \mathbf{K} - (\mathbf{K}\cdot\mathbf{n})\mathbf{n} = 0$$

$$\mathbf{K} = \left[(\mu+\mu_T)\left(\nabla\mathbf{u} + (\nabla\mathbf{u})^T\right) - \frac{2}{3}\rho k\mathbf{I}\right]\mathbf{n}$$

$$\nabla k\cdot\mathbf{n} = 0 \quad \nabla\varepsilon\cdot\mathbf{n} = 0 \quad \nabla G\cdot\mathbf{n} = 0$$

Periodic Flow Conditions

$\mathbf{u}_{source} = \mathbf{u}_{dest}$ $k_{source} = k_{dest}$

$\varepsilon_{source} = \varepsilon_{dest}$ $G_{source} = G_{dest}$

Pressure difference $p_{source} - p_{dest}$: manually adjusted

Transport of Diluted Species:

Domain:

Convection-Diffusion Equations

$$\frac{\partial c_i}{\partial t} + \nabla\cdot(-D_i\nabla c_i) + \mathbf{u}\cdot\nabla c_i = R_i$$
$$\mathbf{N}_i = -D_i\nabla c_i + \mathbf{u}c_i$$

with

Reaction rate $R_i = 0$
Turbulent + Molecular Diffusivity: $D_i = \frac{\mu_T}{\rho} + 10^{-9}\ \mathrm{m^2\ s^{-1}}$

Boundaries:

Periodic Conditions

$$c_{i,\mathrm{source}} = c_{i,\mathrm{dest}}$$

Flux

$$-\mathbf{n}\cdot\mathbf{N}_i = -1.1574\ x\ 10^{-7}\mathrm{mol}\ m^{-2}s^{-1}\left(=10\ \mathrm{mmol}\ m^{-2}d^{-1}\right)$$

Concentration

$$c_i = 0.3\ \mathrm{mol}\ m^{-3}(\mathrm{model\ study}), 0.17\ \mathrm{mol}\ m^{-3}(\mathrm{Loch\ Etive})$$

Mesh:

Number of mesh elements 36,250
Resolution at the wall: 0.00027 m

[42] **Acknowledgments.** The study was funded by the European Union's Seventh Framework Program HYPOX, Grant Agreement No 226213 coordinated by Antje Boetius. We thank Antje Boetius for organizing the Black Sea cruise (MSM 15/1). We are grateful to the crew of R/V *MS Merian* for their excellent support. R.N.G. and A.H. were supported by the National Environmental Research Council (NERC; NE/F018612/1; NE/F0122991/1, NE/G006415/1), the Commission for Scientific Research in Greenland (KVUG; GCRC6507) and European Research Council through an Advanced Grant (ERC-2010-AdG20100224). We thank Lars Umlauf and Christian Noss for their helpful comments and discussion.

References

Abe, K., T. Kondoh, and Y. Nagano (1994), A New turbulence model for predicting fluid-flow and heat-transfer in separating and reattaching flows .1. Flow-field calculations, *Int. J. Heat Mass Transfer*, *37*, 139–151.

Baldocchi, D. D. (2003), Assessing the eddy covariance technique for evaluating carbon dioxide exchange rates of ecosystems: past, present and future, *Global Change Biol.*, *9*, 479–492. doi:10.1046/j.1365-2486.2003.00629.x.

Berg, P., et al. (2003), Oxygen uptake by aquatic sediments measured with a novel non-invasive eddy-correlation technique, *Mar. Ecol. Prog. Ser.*, *261*, 75–83.

Berg, P., H. Røy, and P. L. Wiberg (2007), Eddy correlation flux measurements: The sediment surface area that contributes to the flux, *Limnol. Oceanogr.*, *52*, 1672–1684.

Boudreau, B. P., and N. L. Guinasso Jr (1982), The influence of a diffusive sublayer on accretion, dissolution, and diagenesis at the seafloor, in *The Dynamic Environment at the Ocean Floor*, edited by K. A. Fanning, and F. T. Manheim p. 115–145, Lexington, Mass.

Canfield, D., B. Thamdrup, and E. Kristensen (eds.) (2005), *Aquatic Geomicrobiology* pp. 129–166, Elsevier, San Diego, Calif.

Crusius, J., P. Berg, D. J. Koopmans, and L. Erban (2008), Eddy correlation measurements of submarine groundwater discharge, *Mar. Chem.*, *109*, 77–85. doi:10.1016/j.marchem.2007.12.004.

Fischer, H. B. (1979), *Mixing in Inland and Coastal Waters*, pp. 81–104, Academic Press, San Diego, Calif.

Garcia, H. E., and L. I. Gordon (1992), Oxygen solubility in seawater: Better fitting equations, *Limnol. Oceanogr.*, *37*, 1307–1312.

Glud, R. N., J. K. Gundersen, N. P. Revsbech, B. B. Jørgensen, and M. Huettel (1995), Calibration and performance of the stirred flux chamber from the benthic lander Elinor, *Deep-Sea Res. Part I*, *42*, 1029–1042.

Glud, R. N., P. Berg, H. Fossing, and B. B. Jørgensen (2007), Effect of the diffusive boundary layer on benthic mineralization and O_2 distribution: A theoretical model analysis, *Limnol. Oceanogr.*, *52*, 547–557.

Glud, R. N. (2008), Oxygen dynamics of marine sediments, *Mar. Biol. Res.*, *4*, 243–289. doi:10.1080/17451000801888726.

Glud, R. N., H. Stahl, P. Berg, F. Wenzhoefer, K. Oguri, and H. Kitazato (2009), In situ microscale variation in distribution and consumption of O2: A case study from a deep ocean margin sediment (Sagami Bay, Japan), *Limnol. Oceanogr.*, *54*, 1–12.

Glud, R. N., et al. (2010), Benthic O_2 exchange across hard-bottom substrates quantified by eddy correlation in a sub-Arctic fjord, *Mar. Ecol. Prog. Ser.*, *417*, 1–12. doi:10.3354/meps08795.

Goring, D. G., and V. I. Nikora (2002), Despiking acoustic Doppler velocimeter data, *J. Hydraul. Eng.-Asce*, *128*, 117–126. doi:10.1061/(asce)0733-9429.

Gundersen, J. K., N. B. Ramsing, and R. N. Glud (1998), Predicting the signal of O_2 microsensors from physical dimensions, temperature, salinity, and O_2 concentration, *Limnol. Oceanogr.*, *43*, 1932–1937.

Holtappels, M., M. M. M. Kuypers, M. Schlueter, and V. Bruechert (2011), Measurement and interpretation of solute concentration gradients in the benthic boundary layer, *Limnol. Oceanogr.-Methods*, *9*, 1–13. doi:10.4319/lom.2011.9.1.

Holtappels, M., and A. Lorke (2011), Estimating turbulent diffusion in a benthic boundary layer, *Limnol. Oceanogr.-Methods*, *9*, 29–41. doi:10.4319/lom.2011.9.29.

Huettel, M., W. Ziebis, and S. Forster (1996), Flow-induced uptake of particulate matter in permeable sediments, *Limnol. Oceanogr.*, *41*, 309–322.

Hume, A. C., P. Berg, and K. J. McGlathery (2011), Dissolved oxygen fluxes and ecosystem metabolism in an eelgrass (Zostera marina) meadow measured with the eddy correlation technique, *Limnol. Oceanogr.*, *56*, 86–96. doi:10.4319/lo.2011.56.1.0086.

Inoue, T., R. N. Glud, H. Stahl, and A. Hume (2011), Comparison of three different methods for assessing in situ friction velocity: A case study from Loch Etive, Scotland, *Limnol. Oceanogr.-Methods*, *9*, 275–287, doi:10.4319/lom.2011.9.275

Johnson, K. S., J. P. Barry, L. J. Coletti, S. E. Fitzwater, H. W. Jannasch, and C. F. Lovera (2011), Nitrate and oxygen flux across the sediment-water interface observed by eddy correlation measurements on the open continental shelf, *Limnol. Oceanogr.-Methods*, *9*, 543–553. doi:10.4319/lom.2011.9.543.

Jørgensen, B. B., and N. P. Revsbech (1985), Diffusive boundary layers and the oxygen uptake of sediments and detritus, *Limnol. Oceanogr.*, *30*, 111–122.

Loescher, H. W., B. E. Law, L. Mahrt, D. Y. Hollinger, J. Campbell, and S. C. Wofsy (2006), Uncertainties in, and interpretation of, carbon flux estimates using the eddy covariance technique, *J. Geophys. Res.-Atmos.*, *111*, D21S90, doi:10.1029/2005JD006932.

Long, M. H., D. Koopmans, P. Berg, S. Rysgaard, R. N. Glud, and D. H. Sogaard (2011), Oxygen exchange and ice melt measured at the ice-water interface by eddy correlation, *Biogeosciences*, *9*, 1957–1967. doi:10.5194/bg-9-1957-2012.

Lorke, A., B. Muller, M. Maerki, and A. Wüest (2003), Breathing sediments: The control of diffusive transport across the sediment-water interface by periodic boundary-layer turbulence, *Limnol. Oceanogr.*, *48*, 2077–2085.

Lorrai, C., D. F. McGinnis, P. Berg, A. Brand, and A. Wüest (2010), Application of oxygen eddy correlation in aquatic systems, *J. Atmos. Oceanic Technol.*, *27*, 1533–1546. doi:10.1175/2010jtecho723.1.

McGinnis, D. F., P. Berg, A. Brand, C. Lorrai, T. J. Edmonds, and A. Wüest (2008), Measurements of eddy correlation oxygen fluxes in shallow freshwaters: Towards routine applications and analysis, *Geophys. Res. Lett.*, *35*, L04403, doi:10.1029/2007GL032747.

Munksby, N., M. Benthien, and R. N. Glud (2002), Flow-induced flushing of relict tube structures in the central Skagerrak (Norway), *Mar. Biol.*, *141*, 939–945. doi:10.1007/s00227-002-0874-x.

Reimers, C. E., H. T. Oezkan-Haller, P. Berg, A. Devol, K. McCann-Grosvenor, and R. D. Sanders (2012), Benthic oxygen consumption rates during hypoxic conditions on the Oregon continental shelf: Evaluation of the

eddy correlation method, *J. Geophys. Res.-Oceans*, *117*, C02021. doi:10.1029/2011JC007564.

Revsbech, N. P. (1989), An oxygen microsensor with a guard cathode, *Limnol. Oceanogr.*, *34*, 474–478.

Taylor, G. I. (1938), The spectrum of turbulence, *Proc. R. Soc. A*, *164*, 476–490.

Taylor, G. I. (1953), Dispersion of soluble matter in solvent flowing slowly through a tube, *Proc. R. Soc. Lond. A Math. Phys. Sci.*, *219*, 186–203.

Thamdrup, B., and D. Canfield (2000), Benthic respiration in aquatic sediments, in *Methods in Ecosystem Science*, edited by O. Sala, H. Mooney, R. Jackson, and R. Howarth, pp. 86–103, Springer, New York.

von Karman, T. (1930), Mechanische Ähnlichkeit und Turbulenz, pp. 85–105, Proceedings of the Third International Congress of Applied Mechanics.

Vopel, K., D. Thistle, and R. Rosenberg (2003), Effect of the brittle star *Amphiura filiformis* (*Amphiuridae*, *Echinodermata*) on oxygen flux into the sediment, *Limnol. Oceanogr.*, *48*, 2034–2045.

Wenzhöfer, F., and R. N. Glud (2002), Benthic carbon mineralization in the Atlantic: A synthesis based on in situ data from the last decade, *Deep-Sea Res. I*, *49*(7), 1255–1279.

Wilczak, J., S. Oncley, and S. Stage (2001), Sonic anemometer tilt correction algorithms, *Boundary-Layer Meteorol.*, *99*, 127–150.

Chapter 4

Benthic boundary layer conditions for eddy correlation measurements in oligothrophic deep sea: extremely low benthic oxygen fluxes in Arctic sediments (HAUSGARTEN observatory)

Daphne Donis[1,♣], Daniel F. McGinnis[2], Moritz Holtappels[3], Janine Felden1, 4, Frank Wenzhöfer[1]

[1]HGF-MPG Joint Research Group for Deep Sea Ecology and Technology, Alfred Wegener Institute for Marine and Polar Research, Bremerhaven, Germany
[2]IGB - Leibniz-Institute of Freshwater Ecology and Inland Fisheries, Müggelseedamm, Berlin, Germany
[3]Max Plank Institute for Marine Microbiology, Bremen, Germany
[4]MARUM Center for Marine Environmental Sciences, University Bremen, Germany

♣Corresponding author

In Preparation for Limnology and Oceanography: Methods (28.10.2013)

4.1 Abstract

Measuring benthic oxygen fluxes with eddy correlation has become a widely used technology in marine biogeochemistry. However, flux measurements in deep-sea sediments with low benthic consumption rates are rare, in fact only one other study (Berg et al., 2009) exists. Here we use the eddy correlation (EC) technique in combination with micoprofiler measurements and chamber incubations to estimate the benthic oxygen consumption of an oligotrophic Arctic deep-sea site. The results obtained with an EC system at 2500 m water depth at the HAUSGARTEN observatory represent the deepest and lowest in situ oxygen exchange measurements at the sediment-water interface ever achieved with this non-invasive stand-alone technique. But a considerable post processing procedure (e.g. lowering the acoustic Doppler velocimeter beam correlation threshold and evaluating the significance of the fluxes coupled to flow direction and magnitude) was necessary to account for the limiting conditions that were found at this oligotrophic Arctic deep-sea site, i.e. clear waters, low oxygen fluxes and low turbulence. The corrected EC oxygen flux compared well with simultaneous measurements carried out with a microprofiler and benthic chambers (DOU = -1.2 $\pm$ 0.1, TOU= -1.2 $\pm$ 0.3, EC-flux = -0.9 $\pm$ 0.2 mmol O_2 m^{-2} d^{-1}). Our results show that the EC technique is applicable to such extreme environments, and capable of measuring significant oxygen fluxes in the order of 1 mmol m^{-2} d^{-1} with low turbulence and clear waters.

4.2 Introduction

Flux measurements by eddy correlation (EC) systems together with state-of-the-art techniques contribute to investigations of benthic biogeochemical processes in sediments and thus in marine ecosystem studies. In situ flux measurements are a prerequisite for marine budget calculations and an important factor for our understanding of the marine cycle of matter. In 2003 the aquatic application of the EC technique was introduced for the estimation of benthic oxygen fluxes (Berg et al., 2003). The measuring principle of EC allows a direct estimation of vertical fluxes by the correlation between the measured fluctuations of vertical velocity (with an acoustic Doppler velocimeter, ADV) and oxygen concentration (with a fast responding microsensor) at a single point above the seafloor. Advantages of this approach are: (I) it is non-invasive, (II) it integrates over a large footprint area, (III) it incorporates in situ hydrodynamics, and (IV) it provides a long-term estimation of vertical fluxes.

Vertical oxygen flux can be calculated as the average over a period, significantly longer than the time scale of turbulent fluctuations and variations in the benthic boundary layer. For this instance EC instrumentation must be able to reasonably resolve the flux-relevant scales, which depend on the local dissolved oxygen gradients and turbulence (Lorrai et al., 2010). The technique's challenge is thereby the resolution of the two sensors under unfavorable conditions of especially weak turbulence or low oxygen gradients, that may determine fluctuations too small to be resolved.

So far most of the EC measurements were addressed to coastal or shelf ecosystems with a measured range of fluxes between 10 - 400 mmol O_2 m^{-2} d^{-1} (Kuwae et al., 2006; McGinnis, 2008; Glud et al., 2010; Hume et al., 2011; Reimers et al., 2012; Long et al., 2013), while there is lack of deep-sea applications. The only EC deployment in deep-sea sediments was carried out by Berg et.al. (2009) in Sagami Bay (Japan) at 1450 m depth, where they have measured the benthic oxygen-uptake with in situ benthic chambers, vertical sediment microprofiles and an EC system.

To quantify benthic oxygen consumption of deep-sea sediments, in situ measurements are preferable than measurements on retrieved intact cores, to avoid artifacts introduced by decompression and temperature changes, that may result in an overestimated oxygen consumption (Glud et al., 1994). For the interpretation of flux rates measured with different in situ methods, the different spatial and temporal scales that are addressed have to be taken into account. With oxygen microprofiles, the dissolved oxygen uptake (DOU) and the oxygen microdistribution within the sediment, are measured at a single point (Revsbech et al., 1980; Jørgensen and Revsbech, 1985; Reimers et al., 1986; Glud et al. 1994), excluding the fauna-mediated oxygen uptake. Thus several time-consuming sediment profiles have to be done before a certain area is covered. Fluxes measured by benthic chamber incubations (e.g. Jahnke and Christiansen, 1989; Archer and Devol,

1992), following the decrease in the enclosed water oxygen concentration over time, represent the total oxygen flux (TOU) including diffusion as well as advective oxygen transport across the sediment-water interface due to bioirrigation, even though larger fauna species may be excluded (Glud and Blackburn, 2002; Glud et al., 2003). Also, since chambers enclose a certain sediment area with the overlying water they can only mimic a certain hydrodynamic conditions neglecting natural variations in the flow field. The main advantage of the EC technique in respect to the other methods is that it allows estimating benthic exchange rates without disturbing the surface nor enclosing portions of sediment with the overlying water. EC measurements are also representative of for a larger seafloor area (in the order of tenths of m^2, Berg et al., 2007) in respect to chamber incubations (order of cm^2) and microprofiles (for which single profiles need to be reiterated many times to cover an area).

The benthic oxygen consumption at the seafloor depends on the amount of organic matter that can be mineralized (Seiter et al., 2005). In deep oceans most of the organic material produced in the water column is recycled in the upper 1000 m (e.g. Suess, 1980; Lee et al., 1998) and only a small fraction of it reaches the seafloor (Smith et al., 1994; Wenzhöfer and Glud, 2002 and references therein) where it is either remineralized or permanently buried in the sediment (Berner, 1980; Canfield, 1994). Quantitative measurements are therefore needed to estimate budgets of organic matter mineralization at the seafloor for which benthic oxygen uptake measurements are a commonly used proxy for the total benthic mineralization rate (e.g. Smith and Hinga, 1983). The Arctic Ocean, where primary production is limited by ice coverage (Ramseier et al. 1999; Hebbeln, 2000; Schlüter et al., 2000; Caroll and Caroll, 2003; Richardson et al., 2005), is characterized by low sedimentation rates to the sea floor (Rutgers et al., 1997; Schlüter et al., 2000; Schewe and Soltwedel, 2003; Sakshaug, 2004; Nodder et al., 2005; Bauerfeind, 2009), thus by low oxygen uptake rates, for which however, only a few studies exist.

Here we present EC flux measurements from an oligotrophic Arctic deep-sea site. Post processing procedures and analyses are introduced to account for I) the small fluctuations of oxygen at the sediment water interface (limiting condition for the oxygen fluctuation measurements) and II) the low amount of particles in the water column, thus low backscatter signal for the ADV (limiting condition for the velocity measurement). The corrected EC flux data are then compared to benthic chambers and microprofiler measurements.

4.3 Material and Methods

4.3.1 Site Description

The HAUSGARTEN observatory (Soltwedel et al., 2005) is located in the Fram Strait (Fig. 4.1) a large channel (ca. 500 km wide) that separates the northeast Greenland from the Svalbard archipelago. With a sill depth of ca. 2600 m, this is the deep-water connection where heat and mass exchanges takes place between the North Atlantic and the Arctic Ocean (Manley 1995; Fahrbach et al., 2001; Schauer et al., 2008). The hydrographic regime at HAUSGARTEN is therefore characterized by the inflow of relatively warm and nutrient-rich Atlantic water into the central Arctic Ocean, and outflow of less saline polar waters (East Greenland Current). Due to the heat exchange, the sea-ice cover in Fram Strait is variable, with permanently ice-covered areas in western parts, permanently ice-free areas in southeastern parts, and seasonally varying ice conditions in the central and northeastern parts of the Fram Strait (Vinje, 1977,1985) also influencing the export of organic matter to the seafloor (Bauerfeind et al., 2009). Despite the fact that the primary production export varies over a seasonal cycle, the overall amount of particulate organic material reaching the deep seafloor is low (Bauerfeind et al., 2009, Forest et al., 2010). Thus low particle concentrations are to be expected in the bottom water. During the ARK XXIV/2 cruise on the research ice-breaker RV Polarstern in July 2011, in situ benthic oxygen uptake measurements were performed at the central HAUSGARTEN sampling station (Fig. 4.1. 79° 4.83' N; 4° 5.41' E) at 2467 m water depth.

4.3.2 Benthic oxygen flux measurements

In situ benthic fluxes were measured with all presently available deep-sea instruments, including state-of-the-art benthic chambers (Jahnke and Christensen, 1989; Pfannkuche, 1993; Tengberg et al., 1995; Wenzhöfer and Glud, 2002) and microprofiler (Reimers et al., 1987; Glud et al., 1994; Wenzhöfer and Glud, 2002) as well as the recently introduced Eddy Correlation (EC) system (Berg et al., 2003, 2009). The instruments were mounted to two autonomous benthic lander systems (Witte and Pfannkuche 2000; Wenzhöfer and Glud, 2002) deployed next to each other for approx. 72 hours. One lander was equipped with a microprofiler unit, providing dissolved oxygen uptake (DOU) measurements, and the other carried 3 benthic chambers together with an Eddy Correlation (EC) system, providing total oxygen uptake (TOU_{Ch} and TOU_{EC}) data. The difference between TOU

and DOU is commonly dedicated to faunal-mediated consumption, including bioirrigation and bioturbation as well as the animal respiration itself (Glud, 2008 and references therein).

4.3.3 O_2 Microprofiles

During the high-resolution O_2 measurements in the sediments 5 Clark-type oxygen microelectrodes (Revsbech, 1989) mounted on an autonomous x-y-z microprofiler module were driven downwards with increments of 150 m steps from the water column to a sediment depth of 6.5 cm. The system allowed repeated profiles by horizontal repositioning of the module after each profile. Thus 16 O_2 profiles within an area of 625 cm^2 were obtained. The microsensors were calibrated by applying a two-point calibration from the O_2 concentration in the bottom water determined by Winkler titration (Grasshoff et al., 1983) and on-board signals recorded in anoxic, dithionite-spiked bottom water before instrument deployment. Diffusive Oxygen Uptake (DOU) was calculated from the linear concentration gradient in the Diffusive Boundary Layer (DBL) by applying Fick's first law of diffusion, as described in Jørgensen and Des Marais (1990). The diffusion coefficient of O_2 in seawater was corrected for salinity and temperature (Li and Gregory, 1974).

4.3.4 Benthic chamber incubations

The Chamber Total Oxygen Uptake (TOU_{Ch}) at the sediment-water interface was determined in situ with 3 squared benthic chambers (20 x 20 cm; Witte and Pfannkuche 2000). Changes in oxygen concentration were monitored over time by optode measurements (Glud et al., 1996). During the incubation the overlying water (water height 10 - 15 cm) was gently stirred to mimic the in situ hydrodynamic conditions. TOU_{Ch} flux (mmol O_2 m^{-2} d^{-1}) was calculated from the initial linear decrease in O_2 concentration versus time (Wenzhöfer and Glud, 2002).

4.3.5 EC instrument and deployment

The EC system consisted of a Nortek acoustic Doppler velocimeter (ADV) for the measurement of the three components of the flow field (x,y,z) and a Clark type O_2 microelectrode (Revsbech, 1989) connected to an amplifier for the measurement of dissolved oxygen concentration (Berg et al. 2003), both powered with an internal battery lasting for approx. 11 hours. The O_2 microelectrode (tip diameter 15m, response time < 0.2 s) was calibrated at in situ conditions (salinity and temperature) against oxygen saturated

and anoxic seawater (Gundersen et al., 1998). The EC system was fixed to one of the landers (Fig. 4.6), provided with a fin on the opposite side to initially help the orientations of the EC sensors towards the main current flow. However, during the 11 hour measuring time current direction varied which needs to be considered for EC oxygen flux calculations.

4.3.6 EC flux analysis

EC fluxes (equal to TOU_{EC}) were obtained by correlation of the instantaneous fluctuating components of vertical velocity (w') and O_2 concentration (C') at 15 cm above the seafloor, according to the following equation:

$$ECFlux = \overline{w'C'} \tag{4.1}$$

A multistep process was used to extract fluxes from the raw data. The first step was to average the 32 Hz recordings to 4 Hz to reduce the signal to noise ratio, and to increase the ease of handling the data set. In concomitance to the filtering process, velocity spikes were removed by the interpolation method by Goring and Nikora (2002) using an ADV beam correlation threshold of 0.5. At this stage the tilt of the ADV was corrected using the planar fit method by Wilczak (2001). This procedure is carried out to avoid components of horizontal velocities to be mapped onto the vertical velocities (Shaw and Trowbridge, 2001). By spectral analysis on the time series, it was verified that no flux contributions occurred below frequencies of 0.01 Hz (i.e. 100 s). This allowed the following step of separating the time series into time-average and fluctuating components (Reynolds decomposition) (Lee et al., 2004), using a window size of 5 minutes, which includes all turbulent flux contributions.

As both sensors are spatially separated, the delay between the time series w' and C' depends on the distance between the ADV velocity sampling volume and the O_2 sensor tip, the turbulent regime, and the response time of the O_2 microelectrode (McGinnis et al., 2008; Lorrai et al., 2010). Therefore the time series w' and C' were cross-correlated for each burst allowing stepwise time shifts of 0.25 s (for a maximum of ± 4 s) (Holtappels et al., 2013), and the flux was calculated by the highest correlation coefficient. The cross correlations were then evaluated by calculating the probability of receiving the same correlation (i.e., the same flux) from random data sets (corrcoef function in Matlab), setting at 0.05 the threshold for a significant flux.

4.4 Results

4.4.1 EC fluxes

The 11-hour EC measurement was performed between 2:00 and 13:00, where the current velocity varied between 0.2 and 4.4 cm s^{-1} with a mean of 2 cm s^{-1} (Fig. 4.2a). The decrease in current velocity below 1 cm s^{-1} during the last hours of the deployment was concomitant to several directional changes. Until 10:00 the current was coming from the front of the EC system, i.e. the O_2 sensor faced downstream with respect to the main current direction. After 10:00 abrupt changes in the current direction were associated to oscillations in the current magnitude (max $\pm$1 cm s^{-1}). This is ascribable to the interference that the lander frame caused with the flow as soon as the current was directed towards positive degrees (0-180 (Fig. 4.6). The O_2 concentration measured by the microelectrode decreased constantly during the 11 hours, from 305 to 296 μmol L^{-1}, which is most probably due to an electronic drift in the signal (Fig. 4.2b). A change in O_2 concentration (whether real or an artifact) can, however cause undesired contributions to the EC flux (Holtappels et al., 2013). In our case the small decrease can be removed by applying the running average to the time series, preventing any effect on the flux calculations (Berg et al. 2003).
The EC fluxes (Fig. 4.2c) from the entire data set revealed an average flux of -0.7 $\pm$0.3 mmol O_2 m^{-2} d^{-1}, while taking only the period until the current direction changed into account (first 28 bursts), the average flux results of -0.9 $\pm$0.2 mmol O_2 m^{-2} d^{-1}. As the statistical analysis on the 15 minutes interval cross correlation revealed 1 non-significant burst (marked with cross in Fig. 4.2c), this was not included in the average.

4.4.2 O_2 Microprofiles

A total of 16 O_2 profiles were recorded by the microprofiling instrument covering an area of 625 cm^2, with an average diffusive flux of -1.2 $\pm$0.1 mmol O_2 m^{-2} d^{-1}. All measured oxygen profiles showed a deeply oxygenated sediment (Fig. 4.3), with an oxygen penetration depth of approx. 8 cm. However, the single profiles reveal a deviation in the upper sediment layer indicating some heterogenic distribution of organic matter or bioturbation activity.

4.4.3 Benthic chamber incubation

TOU_{Ch} was estimated from 3 benthic chambers incubating a sediment area of 400 cm^2 over 48 hours. From the initial decrease in oxygen over time an average TOU_{Ch} of -1.2

± 0.3 mmol O_2 m^{-2} d^{-1} was calculated.

4.5 Discussion

Resolving low benthic fluxes with EC, as observed at the HAUSGARTEN deep-sea site HG IV, is challenging because they represent the lower limit of what can be resolved with this technique. Additionally, clear bottom water with lack of particles, which is often the case in oligotrophic areas, can compromise the quality of ADV data. In the following we describe the procedures that led to reliable EC fluxes and the assessment of their significance. The EC flux is compared with other benthic O_2 fluxes carried out by microprofiler and benthic chambers.

4.5.1 ADV beam correlation threshold

Although ADVs provide accurate estimates of water velocities, weak scatters in clear waters can reduce the return signal strength to the level of background noise (Elgar 2005). Weak scatters are associated to a low beam correlation (CORR) i.e. the coherence between the Doppler shift observed with successive pings (Cabrera et al. 1987, Lhermitte and Lemmin 1994), which lead to inaccurate velocity estimates (Zedel et al. 1996). The ADV correlation signal (ranging from 0 to 1.0) is therefore used to diagnose data quality (Zedel et al. 1996; SonTek 2004). To mark data points as bad, Elgar et al. (2005) proposed a correlation threshold γ_{CORR} as:

$$\gamma_{CORR} = 0.3 + 0.4\sqrt{\frac{f_s}{f_{max}}} \tag{4.2}$$

where *fs* is the sampling frequency for the measurements and $fmax$ is the maximum ADV sampling frequency. Data points where the correlation is lower than γCORR on any of the three beams (the three components of the current velocity) are marked bad. According to Eq. 2, with a sampling frequency of 32 Hz and a maximum capability for the ADV to sample at 64 Hz, the recommended CORR threshold is 0.6. However, when applying this threshold to our data to filter the data from 32 to 4 Hz and replace the outliers by interpolation, we could verify that more than 50% of the bins (composed by 8 data points) had to be replaced entirely. Therefore we lowered the CORR threshold to 0.5. Applying this threshold to our data increased the number of bins which had at least one original data point to 70%, thus allowing a more robust interpolation. However, we checked the variance preserving spectrum of the velocity component to verify if the filtered signal (from 32 to 4 Hz) was still capable to resolve the inertial subrange, i.e. the

scales that play a dominant role in energy and momentum transfer in the wavenumber space (Fig. 4). The spectral analysis on the vertical velocity component revealed that the frequencies of turbulent eddies contributing to the flux are still captured by the processed signal, and that the flux contributing turbulent structures have a lifetime between 1 and 100 s (Fig. 4).

4.5.2 Electronic noise and small O_2 fluctuations

Calculating EC fluxes from extremely small fluctuations of the O_2 concentration at the sediment-water interface, due to low consumption rates of the sediment, is challenging for EC flux calculations (Berg et al. 2009). The expected turbulent O_2 fluctuations depend on the local O_2 gradient and turbulence. As the sediment O_2 uptake is known (-1.2 ±0.1 mmol O_2 m^{-2} d^{-1}, DOU from microprofiles), the magnitude of O_2 fluctuations can be estimated based on the turbulent velocities (as in Lorrai et al., 2010). With a current velocity at 1 m above the seafloor of <0.03 m s^{-1} and a bottom friction coefficient for muddy sediments of 0.002, the expected O_2 fluctuations for our site result approx. ±0.01 mmol m^{-3}. This magnitude is close to the noise level of the used microelectrode (±0.06 mmol m^{-3}) calculated as the standard deviation of the difference of two consecutive data points of the measured O_2 concentration (Lorrai et al., 2010). However, electronic noise is by definition randomly distributed around the mean, therefore should not significantly correlate with the vertical velocity fluctuations (Berg et al., 2009). A first indication that the measurement consistently represented all eddy sizes that contributed to the flux is given by the cumulative cross-spectral density of C'w' (Fig. 4.5), that shows the range of the flux contributing eddies between 1 and 0.1 Hz (1-100 s). The correlation between C' and w' for the entire deployment, where fluxes were calculated on a 15 minute interval, shows that only one burst corresponded to non-significant flux. This confirms that the measurement represents consistently the vertical O_2 turbulent transport. However, an unsteady flow field may also lead to statistically strong correlations even when not related to sediment exchange rates (Holtappels et al., 2013) and needs to be verified.

4.5.3 Effect of current field on measured EC fluxes

In general, a time average of negative correlations between w' and C', i.e. negative flux, indicates a net transport of O_2 toward the sediment, while positive fluxes correspond to a net transport of O_2 from the sediment to the water column. Two out of the 43 bursts of the EC measurements showed positive fluxes (Fig. 4.2c), with $p<0.05$ (thus significant). This is unlikely to be the case for deep sea sediments at 2500 m water depth, where photosynthetic activity is excluded. Thus the measured flux is not related

to the sediment biogeochemical activity but rather to an effect of concomitant reversals in the direction of the current flow (Fig 2a), that may have led to positive correlations. Flux calculation might not only be compromised by the occurrence of rapid unsteady conditions in the current field (Holthappels et al., 2013), but also because the change in the current direction induced the flow to interfere with the lander frame, with consequent enhanced unsteady conditions.

Magnitude and direction of the current were calculated from ADV readings, respectively as the absolute value of the resultant of horizontal velocity components and the angular coordinate of the point (x,y). The position of the two sensors in respect to the current direction was inferred by the heading of the ADV compass.

Between 2:20 and 10:00 the current direction was -60 thus coming from the free area in front of the EC system (black arrow in Fig. 4.6). After 10:00 the current started turning towards the back of the lander frame at which the EC system was attached (green arrows in Fig. 4.6). Therefore, due to the shift in current direction, the frame disturbed the last part of the measurement. This abrupt change in current direction that occurred in the last part of the deployment (after 10:00) was also associated to low current magnitudes (< 1 cm s^{-1}), a decreasing EC O_2 flux magnitude and an increasing variance (average O_2 flux until 10:00 = -0.9 $\pm$0.2 mmol O_2 m^{-2} d^{-1}; average after 10:00 = -0.4 $\pm$0.4 mmol O_2 m^{-2} d^{-1}). Holtappels et al. (2013) showed that non steady state conditions such as a sudden change in current magnitude from 2 to 10 cm s^{-1} can bias EC fluxes by 30-100% for several hours. In our data set a current magnitude decrease of 3 cm s^{-1} occurred over 3 hours (from 7:00 to 10:00, Fig. 4.4a) and the average flux showed a concomitant decrease of about 30% (from -1 to -0.7 mmol O_2 m^{-2} d^{-1}). However, we do not observe the same effect on EC fluxes at the beginning of the deployment, when the current magnitude increased form 1 to 4 cm s^{-1}. Therefore, EC fluxes seems to be more affected by the abrupt changes in current direction, when the current reached magnitudes lower than 1 cm s^{-1}, than by the change in current magnitude that took place with the same trend at the beginning and in the second half of the deployment period. The low and unsteady current velocities most likely compromise the EC flux calculation, especially when associated to a weak O_2 gradient at the sediment-water interface. These conditions brought the technique to the limit of its detection possibilities, which were so far never assessed.

4.5.4 Time shift correction

It was shown that the time shift needed to achieve the most significant correlation (as described in the methods section) corresponds to the sum of the traveling time (the time that the water parcel needs to pass from the velocity sampling volume to the O_2 sensor

tip) and response time of the O_2 sensor (Donis et al. in prep.). Especially when the O_2 sensor is oriented parallel to the current flow, the time shift correction is a procedure that leads to a better precision of the EC flux estimation (Donis et al. in prep). The co-spectra in Fig. 4.7 reveal that the non-shifted data would underestimate the flux by almost 50 % (corresponding to a 15 minutes measurement). For EC deployments it is particularly important to assess the uncertainties when no reference measurement is available or possible (e.g. hard substrates) or when the comparison with other techniques is not reasonable (e.g. highly heterogeneous substrates).
For our data set the robustness of the EC fluxes is improved by applying the time shift, as shown by the significance of the correlations (Fig. 4.8). The non-corrected fluxes produced a total of 19 bursts corresponding to non-significant fluxes ($p > 0.05$), while after correction only one burst was non-significant. The correction allows to preserve almost the entire data set, otherwise it would be required to discard (as non-significant) more than 40% of the total bursts.

4.5.5 Assessment of uncertainties

A statistical approach is probably the most straight forward tool to determine the level of uncertainty of EC fluxes, since these are given by a mathematical expression (the correlation). In light of this, to determine the level of uncertainty and the detection limit of the technique for the conditions that we encountered at HAUSGARTEN, the significance of the flux calculation as functions of the flux magnitude is presented in Fig. 9. The significance of the correlation decreased in correspondence to fluxes between ± 0.4 mmol O_2 m^{-2} d^{-1}. This also coincided with the unstable flow regime and flow velocities < 1 cm s^{-1}, indicating that fluxes measured during the last 3 hours of the deployment were statistically scarcely robust. Therefore we consider the first 8 hours of the deployment as a reliable representation of the benthic oxygen consumption, which results in a average EC flux of -0.9 ± 0.2 mmol O_2 m^{-2} d^{-1} .

4.5.6 Comparison between methods

Oxygen benthic fluxes obtained by the three techniques used for this study at 2500 m depth in Arctic sediments at HAUSGARTEN (microprofiler, benthic chambers, eddy correlation) are in good agreement. From the microprofiles performed, the average O_2 flux (DOU) is -1.2 ± 0.1 mmol O_2 m^{-2} d^{-1} (N=16), the TOU obtained form benthic chamber incubations is -1.2 ± 0.3 mmol O_2 m^{-2} d^{-1} (N=3) and the corrected average EC flux is -0.9 ± 0.2 mmol O_2 m^{-2} d^{-1}. As known, the EC measurement integrates over a larger area than any other instrument that measures benthic fluxes. This area,

called footprint, can be estimated knowing the bottom roughness and the distance of the measurement from the seafloor (Berg et al. 2007). Using the senor height above seafloor of 15 cm and a relatively smooth sediment surface, the estimated footprint area at our study site is approx. 150 m^2. The comparison between the three methods might be limited by sediment heterogeneity that can be encountered within the area integrated by the EC measurement, compared to the smaller area used for microprofiling (625 cm^2) and benthic chamber incubations (400 cm^2) which also excludes any in situ hydrodynamics. However, the investigated sediment area at HAUSGARTEN is known to be very homogene, with respiration rates comparable to abyssal plain food webs that are under strong energy limitation (Soltwedel et al., 2005; VanOevelen et al., 2011). The cohesive sediments and the low benthic oxygen consumption lead to an oxygen penetration that is poorly affected by the hydrodynamics of the overlying water. This makes the comparison between the three methods trustworthy. The difference between DOU and TOU is generally assigned to fauna-mediated oxygen consumption, that includes respiration activity of the organisms and the increase of oxygen penetration in deeper sediment layers through their borrows (Wenzhöfer and Glud, 2002; Grenz et al., 2003; Rabouille et al., 2003). At HAUSGARTEN central station HG-IV (2500 m) sediment respiration is clearly dominated by prokaryotes (VanOevelen et al., 2011), with a small faunal contribution mainly due to the energy limitation. However, the ice melting in the summer season determines a stratified euphotic marginal ice zone enriched in nutrients that can cause intense phytoplankton blooms, thus regionally enhanced fluxes of particulate organic matter to the seafloor (Bauerfeind et al., 2009).
In light of this, a more extensive application of EC measurements for polar benthic ecosystems seems opportune. Only a few in situ benthic oxygen flux measurements exist for the high latitudes. For the Central Greenland Sea and the East Greenland Continental Margin Sauter et al. (2001) reported benthic O_2 fluxes estimated from in situ micropfiles in the order of 0.2 mmol O_2 m^{-2} d^{-1}. These fluxes differ by a factor of 5 to the ones obtained from our measurements, highlighting the need for further investigations in this region, especially as the Arctic Ocean is facing rapid alterations due to climate changes (e.g. Johannessen et al., 2004; Slagstad et al., 2011; Wassmann, 2011).

4.6 Conclusions

The results obtained with an EC system at 2500 m depth at the HAUSGARTEN observatory represent the deepest benthic O_2 exchange ever achieved with this non-invasive stand-alone technique. The applied data processing procedure (lowering of the ADV beam correlation threshold, applying the time shift correction and assessing significance to the correlations) were necessary to deal with the limiting conditions that were found

in these deep arctic sediments, i.e. clear waters with low turbulence and low sediment activity. The results from the EC were also compared with reference measurements carried out with a microprofiler and benthic chamber incubations showing good agreement. Therefore, we conclude that the EC technique is applicable in such extreme environments, and capable of measuring O_2 fluxes $<$ -1 mmol O_2 m^{-2} d^{-1}. The EC technique thus has a great potential for long-term autonomous measurements of O_2 fluxes at the seafloor, that would allow, for instance in the Arctic Ocean, to couple real time benthic O_2 fluxes to the concomitant dynamics of the water column (e.g. primary productivity and ice thickness). In order to express this potential, next generation EC systems should facilitate long-term measurements. Therefore the effort should be put in extending the stand-alone capability of the system (e.g. low power consumption, extend data capacity), and the stability of the O_2 measurements.

Acknowledgements

The authors are thankful to the scientific party and crew of RV Polarstern for their support with work at sea, Axel Nordhausen (MPI Bremen) for his help in the preparation and deployment of the benthic landers. We are grateful to the technicians of the Microsensor department at MPI (Bremen), for providing the microsensors used for this work, and to Ronnie Glud for his helpful contribution in discussing the data.
This work was financially supported by the EU 7^{th} FP HERMIONE project, the EU 7^{th} FP SENSEnet project and Helmholtz Alliance "ROBEX".

References

Archer, D., and A. Devol (1992). Benthic oxygen fluxes on the Washington shelf and slope: A comparison of in situ and chamber flux measurements, Limnology and Oceanography, 37, 614-629.

Bauerfeind E., Nothig, E.M., Beszczynska, A., Fahl, K., Kaleschke, L., Kreker, K., Klages, M., Soltwedel, T., Lorenzen, C. and J. Wegner (2009). Particle sedimentation patterns in the eastern Fram Strait during 2000-2005: results from the Arctic long-term observatory HAUSGARTEN. Deep Sea Research I 56:1471-1487.

Berg, P., Roy, H., Janssen, F., Meyer, V., J, B. B., Huettel, M. and D. de Beer (2003). Oxygen uptake by aquatic sediments measured with a novel non-invasive eddy correlation technique, Marine Ecology Progress Series, 261, 75-83.

Berg, P., Roy, H. and P.L. Wiberg (2007). Eddy correlation flux measurements: The sediment surface area that contributes to the flux, Limnology and Oceanography, 52, 1672-1684.

Berg, P., Glud, R. N., Hume, A., Stahl, H., Oguri, K., Meyer,V. and H. Kitazato (2009). Eddy correlation measurements of oxygen uptake in deep ocean sediments, Limnology and Oceanography Methods, 7, 576-584.

Berner, R. A. (1980) Early diagenesis: A theoretical approach, Princeton Univ. Press.

Cabrera, R., K. Deines, B. Brumley, and E. Terray (1987). Development of a practical coherent acoustic Doppler current profiler. Proc. Oceans ?87, Halifax, NS, Canada, IEEE Oceanic Engi- neering Society, 93-97.

Canfield, D. E. (1994). Factors Influencing organic carbon preservation in marine sediments, Chemical Geology, 114, 315-239.

Caroll, M.L. and J. Caroll (2003). The Arctic Seas. In: Black KD, Shimmield GB (eds) Biogeochemistry of marine systems. Blackwell, Oxford, pp 127-147.

Elgar, S., Raubenheimer, B. and R. T. Guza (2005). Quality control of acoustic Doppler velocimeter data in the surfzone. Measurement Science and Technology, 16, 1889-1893.

Fahrbach, E., Meincke, J., Osterhus, S., Rohardt, G., Schauer, U., Tverberg, V. and J. Verduin (2001). Direct measurements of volume transports through Fram Strait. Polar Research 20(2):217-224.

Forest, A., Wassmann, P., Slagstad, D., Bauerfeind, E., Nothig, E.M. and Klages, M. (2010). Relationships between primary production and vertical particle export at the

Atlantic-Arctic boundary (Fram Strait, HAUSGARTEN). Polar Biology, 33 (12), 1733-1746 .

Glud, R.N., Gundersen, J.K., Jørgensen, B.B., Revsbech, N.P. and Schulz, H.D. (1994). Diffusive and total oxygen uptake of deep-sea sediments in the eastern South Atlantic Ocean: in situ and laboratory measurements. Deep-Sea Research I 41, 1767-1788.

Glud, R. N., Forster, S. and M. Huettel (1996). Influence of radial pressure gradients on solute exchange in stirred benthic chambers. Mar. Ecology Progress Series, 141: 303-311.

Glud, R.N. and Blackburn, N., (2002). The effects of chamber size on benthic oxygen uptake measurements: a simulation study. Ophelia 56 (1), 23-31.

Glud, R.N., Gundersen, J. K., Røy, H. and B. B. Jørgensen (2003). Seasonal dynamics of benthic O2 uptake in a semi-enclosed bay: Importance of diffusion and fauna activity. Limnology and Oceanography, 48: 1265-1276.

Glud, R. (2008). Oxygen dynamics of marine sediments. Marine Biology Research 4, 243-289.

Glud, R. N., Berg, P., Hume, A., Batty, P., Blicher, M. E., Lennert, K. and S. Rysgaard (2010). Benthic oxygen exchange across hard- bottom substrates quantified by eddy correlation in a sub-Arctic fjord. Marine Ecology Progress Series, 417, 1-12.

Goring, D. G. and V. I. Nikora (2002), Despiking acoustic Doppler velocimeter data. Journal of Hydraulic Engineering, 128, 117-126.

Grasshoff, K., Ehrhardt, M. and Kremling, K. (1983). Methods of Sea Water Analysis. Verlag Chemie GmbH, Weinheim, pp 61-72.

Grenz, C., Denis, L., Boucher, G., Chauvaud, L., Clavier, J., Fichez, R. and O. Pringault (2003). Spatial variability in sediment oxygen consumption under winter conditions in a lagoonal system in New Caledonia (South Pacific). Journal of Experimental Marine Biology and Ecology, 285, 33 47.

Gundersen, J.K., Ramsing, N.B. and Glud, R.N., (1998). Predicting the signal of O2 microsensors from physical dimensions, temperature, salinity, and O2 concentration. Limnology and Oceanography 43, 1932-1937.

Hebbeln, D. (2000). Flux of ice-rafted detritus from sea ice in the Fram Street. Deep-Sea Research II 47:1,773-1,790.

Holtappels, M., Glud, R. N., Donis, D., Liu, B., Hume, A., Wenzhöfer, F. and M.M.M. Kuypers (2013). Effects of transient bottom water currents and oxygen concentrations

on benthic exchange rates as assessed by eddy correlation measurements. Journal of Geophysical Research: Oceans, 118(3), 1157-1169.

Hume, A. C., Berg, P., and K. J. McGlathery (2011). Dissolved oxygen fluxes and ecosystem metabolism in an eelgrass (Zostera marina) meadow measured with the eddy correlation technique. Limnology and Oceanography, 56, 86-96.

Jahnke, R.A. and M.B. Christiansen (1989). A free-vehicle benthic chamber instrument for seaf loor studies. Deep Sea Research, Part I , 36, 625-637.

Johannessen, O.M., Bengtsson, L., Miles, M.W., Kuzmina, S.I, Semenov, V.A., Alekseev, G.V. Nagurnyi, A.P., Zakharov, V.F, Bobylev, L.P., Pettersson, L.H., Hasselmann, K. and A.P. Cattle (2004). Arctic climate change: observed and modelled temperature and sea-ice variability. Tellus Series - Dynamic Meteorology and Oceanography 56(4):328-341.

Jørgensen, B.B. and N.P. Revsbech (1985). Diffusive boundary layers and the oxygen uptake of sediments and detritus. Limnology and Oceanography, 30: 111-122.

Jørgensen B.B. and D.J. Des Marais (1990). The diffusive boundary layer of sediments: Oxygen microgradients over a microbial mat Lmnol. Oceanogr., 35(6), 1343-135s.

Kuwae, T., Kamio, K., Inoue, T., Miyoshi, E. and Y. Uchiyama (2006). Oxygen exchange flux between sediment and water in an inter- tidal sandflat, measured in-situ by the eddy-correlation method. Marine Ecology Progress Series, 307, 59-68.

Lee, C., Murray, D.W., Barber, R.T., Buesseler, K.O., Dymond, J., Hedges, J.I., Honjo, S., Manganini, S.J., Marra, J., Moser, C., Peterson, M.L., Prell, W.L. and Wakeham, S.G., (1998). Particulate organic carbon fluxes: compilation of results from the 1995 US JGOFS Arabian Sea process study. Deep-Sea Research II 45, 2489-2501.

Lee, X., Massman, W. and B. Law (2004). Handbook of Micrometeorology: A Guide for Surface Flux Measurement and Analysis. Kluwer Academic Publishers.

Lhermitte, R. and U. Lemmin (1994). Open-channel flow and turbulence mea- surement by high-resolution Doppler sonar. Journal of Atmospheric and Oceanic Technology, 11, 1295-1308.

Li, Y.H. and S. Gregory (1974). Diffusion of ions in sea water and in deep-sea sediments. Geochimica et Cosmochimica Acta 38: 703-714.

Long, M.H., Berg, P., de Beer, D. and Zieman, J.C. (2013). In Situ Coral Reef Oxygen Metabolism: An Eddy Correlation Study. PLoS ONE 8(3): e58581.

Lorrai, C., McGinnis, D.F., Berg, P., Brand, A. and A. Wüest (2010). Application of oxygen eddy correlation in aquatic systems. Journal of Atmospheric and Oceanic Technology, 27:1533-1546.

Manley, O. (1995). Branching of Atlantic Water within the Greenland-Spitsbergen Passage: An estimate of recirculation. Journal of Geophysical Research 100 (C10):20627-20634.

McGinnis, D. F., Berg, P., Brand, A., Lorrai, C., Edmonds, T. and A. Wüest (2008). Measurements of eddy correlation oxygen fluxes in shallow freshwaters: Towards routine applications and analysis, Geophysical Research Letters, 35, 1-5.

Nodder, S.D., Boyd, P.W., Chiswell, S.M., Pinkerton, M.H., Bradford-Grieve, J.M. and Greig, M.J.N. (2005). Temporal coupling between surface and deep ocean biogeochemical processes in contrasting subtropical and subantarctic water masses, southwest Pacific Ocean. Journal of Geophysical Research, 110:C12017.

Pfannkuche, O. (1993). Benthic response to the sedimentation of particulate organic matter at the BIOTRANS station, 471N, 201W. Deep-Sea Research II 40, 135-149.

Rabouille, C., Denis, L., Dedieu, K., Stora, G., Lansard, B. and C. Grenz (2003). Oxygen demand in coastal marine sediments: comparing in situ microelectrodes and laboratory core incubation. Journal of Experimental Marine Biology and Ecology, 285, 49 69.

Ramseier, R. O., Garrity, C., Bauerfeind, E. and R. Peinert (1999). Sea-ice impact on long-term particle flux in the Greenland Sea's Is Odden-Nordbukta region, 1985-1996, Journal of Geophysical Research, 104(C3), 5329-5343.

Reimers, C.E., Fischer, K.M., Merewether, R., Smith Jr., K.L. and Jahnke, R.A. (1986). Oxygen microprofiles measured in situ in deep ocean sediments. Nature 320, 741-744.

Reimers, C. E., Tuba Ozkan-Haller, H., Berg, P., Devol, A., McCann-Grosvenor, K. and R. D. Sanders, (2012). Benthic oxygen consumption rates during hypoxic conditions on the Oregon continental shelf: Evaluation of the eddy correlation method, Journal of Geophysical Research, 117, 1-18.

Revsbech, N.P., Jørgensen, B.B. and T.H. Blackburn (1980). Oxygen in the sea bottom measured with a microelectrode. Science 207: 1355-1356.

Revsbech, N. P. (1989) An oxygen microsensor with a guard cathode. Limnology and Oceanography 34, 474-478.

Richardson, K., Markager, S., Buch, E., Lassen, M.F. and Kristensen, A.S. (2005). Seasonal distribution of primary production, phytoplankton biomass and size distribution in the Greenland Sea. Deep Sea Research I 52:979-999.

Rutgers van der Loeff, M.M., Friedrich, J. and U.V. Bathmann (1997). Carbon export during the spring bloom at the southern polar front determined with the natural tracer 4TDh. Deep Sea Research. Part I , 44,4 57-478.

Sakshaug, E. (2004). Primary and secondary production in the Arctic Seas. In: Stein, R., MacDonald R.W. (eds) The organic carbon cycle in the Arctic Ocean. Springer, New York, pp 57-81.

Sauter, E.J., Schlüter, M. and E. Suess (2001). Organic carbon flux and remineralization in surface sediments from the northern North Atlantic derived from pore-water oxygen microprofiles. Deep-Sea Research I 48(2):529-553.

Schauer, U., Beszczynska-Moeller, A., Walczowski, W., Fahrbach, E., Piechura, J. and Hansen, E. (2008). Variation of measured heat flothrough the Fram Strait between 1997 and 2006. In: Dickson R.R., Meincke, J., Rhines, P. (eds) Arctic-Subarctic Ocean Fluxes. Springer, Netherlands, pp 65-85.

Schewe, I. and T. Soltwedel (2003). Benthic response to ice-edge-induced particle flux in the Arctic Ocean. Polar Biology 26:610-620.

Schlüter, M., Sauter, E.J., Schr, A. and W. Ritzrau (2000). Spatial budget of organic carbon fl ux to the seafloor of the northern North Atlantic (60N- 80N). Global Biogeochemical Cycles 14:329-340.

Seiter, K., Hensen, C. and Zabel., M. (2005). Benthic carbon mineralization on a global scale. Global Biogeochemical Cycles 19:GB1010.

Shaw, W. J. and J. H. Trowbridge (2001). The direct evaluation of near- bottom turbulent fluxes in the presence of energetic wave motions. Journal of Atmospheric and Oceanic Technology, 18,1540-1557.

Slagstad D., Ellingsen, I. H. and Wassmann, P. (2011). Evaluating primary and secondary production in an Arctic Ocean void of summer sea ice: an experimental simulation approach. Progress in Oceanography 90:117-131.

Smith, K.L. and Hinga, K.R. (1983). Sediment community respiration in the deep sea. In: Rowe, G.T. (Ed.), The Sea, vol. 8. Wiley, New York, pp. 331-370.

Smith Jr., K.L., Kaufmann, R.S. and Baldwin, R.J. (1994). Coupling of near-bottom pelagic and benthic processes at abyssal depths in the eastern North Pacific Ocean. Limnology and Oceanography 34, 1101-1118.

Soltwedel, T., Baurfeind, E., Bergmann, M., Budaeve, N., Hoste, E., Jaeckisch, N., et al. (2005). HAUSGARTEN: multidisciplinary investigations at a deep-sea, long-term observatory in the Arctic Ocean. Oceanography, 18(3), 46-61.

SonTek, (2004) SonTek ADV Field Acoustic Doppler Velocimeter: Technical documentation. SonTek/YSI, SanDiego,CA, 186 pp.

Suess, E. (1980). Particulate organic carbon flux in the oceans-surface productivity and oxygen utilization. Nature 228, 260-263.

Tengberg, A., de Bovee, Hall, P., Berelson, W., Chadwick, D., Ciceri, G., Crassous, P., Devol, A., Emerson, S., Gage, J., Glud, R., Graziottini, F., Gundersen, J., Hammond, D., Helder, W., Hinga, K., Holby, O., Jahnke, R., Khripounoff, A., Liebermann, S., Nuppenau, V., Pfannkuche, O., Reimers, C., Rowe, G., Sahami, A., Sayles, F., Schurter, M., Smallman, D., Wehrli, B. and de Wilde, P., (1995). Benthic chamber and profiling landers in oceanography?a review of design, technical solutions and functioning. Progress in Oceanography 35, 253-294.

Van Oevelen, D., Bergmann, M., Soetaert, K., Bauerfeind, E., Hasemann, C., Klages, M., Schewe, I., Soltwedel, T. and N. E. Budaeva (2011). Carbon flows in the benthic food web at the deep-sea observatory HAUSGARTEN (Fram Strait). Deep-Sea Research I 58: 1069-1083.

Vinje, T.E. (1977). Sea ice conditions in the European sector of the marginal seas of the Arctic, 1966-75. Norsk Polarinstitutt Arbok 1975, pp. 163-174.

Vinje, T.E. (1985). Sea ice distribution 1971-80. Norsk Polarinstitutt Skifter 179D.

Wassmann, P. (2011). Arctic marine ecosystems in an era of rapid climate change. Progress in Oceanography. Volum 90 (1-4). ISSN 0079-6611.s 1 - 17.

Wenzhöfer, F. and R.N. Glud (2002). Benthic carbon mineralization in the Atlantic: a synthesis based on in situ data from last decade. Deep-Sea Research I, 49, 1255 1279.

Wilczak, J., Oncley, S. and S. Stage (2001). Sonic anemometer tilt correction algorithms. Boundary Layer Meteorology 99:127-150.

Witte, U. and O. Pfannkuche (2000). High rates of benthic carbon remineralisation in the abyssal Arabian Sea, Deep Sea Research, Part II, 47, 2785-2804.

Zedel, L., E. Hay and A. Lohrmann (1996). Performance of single beam pulse-to-pulse coherent Doppler profiler. IEEE J. Oceanic Engineering, 21, 290-299.

Figures

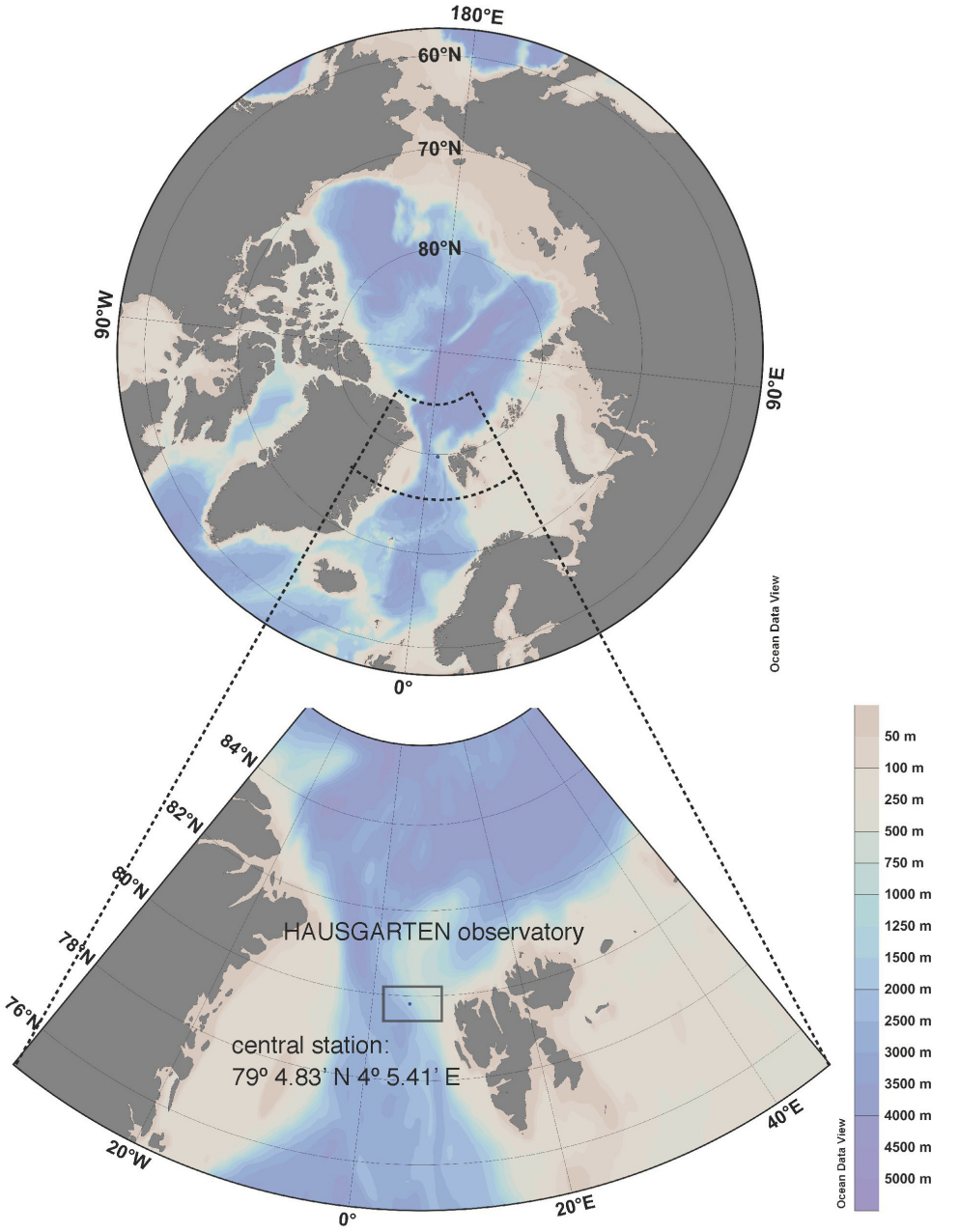

FIGURE 4.1: Map of the area where AWI deep sea long term observatory HAUSGARTEN is located. The coordinates indicates the central station at 2500 m depth where benthic oxygen fluxes were measured.

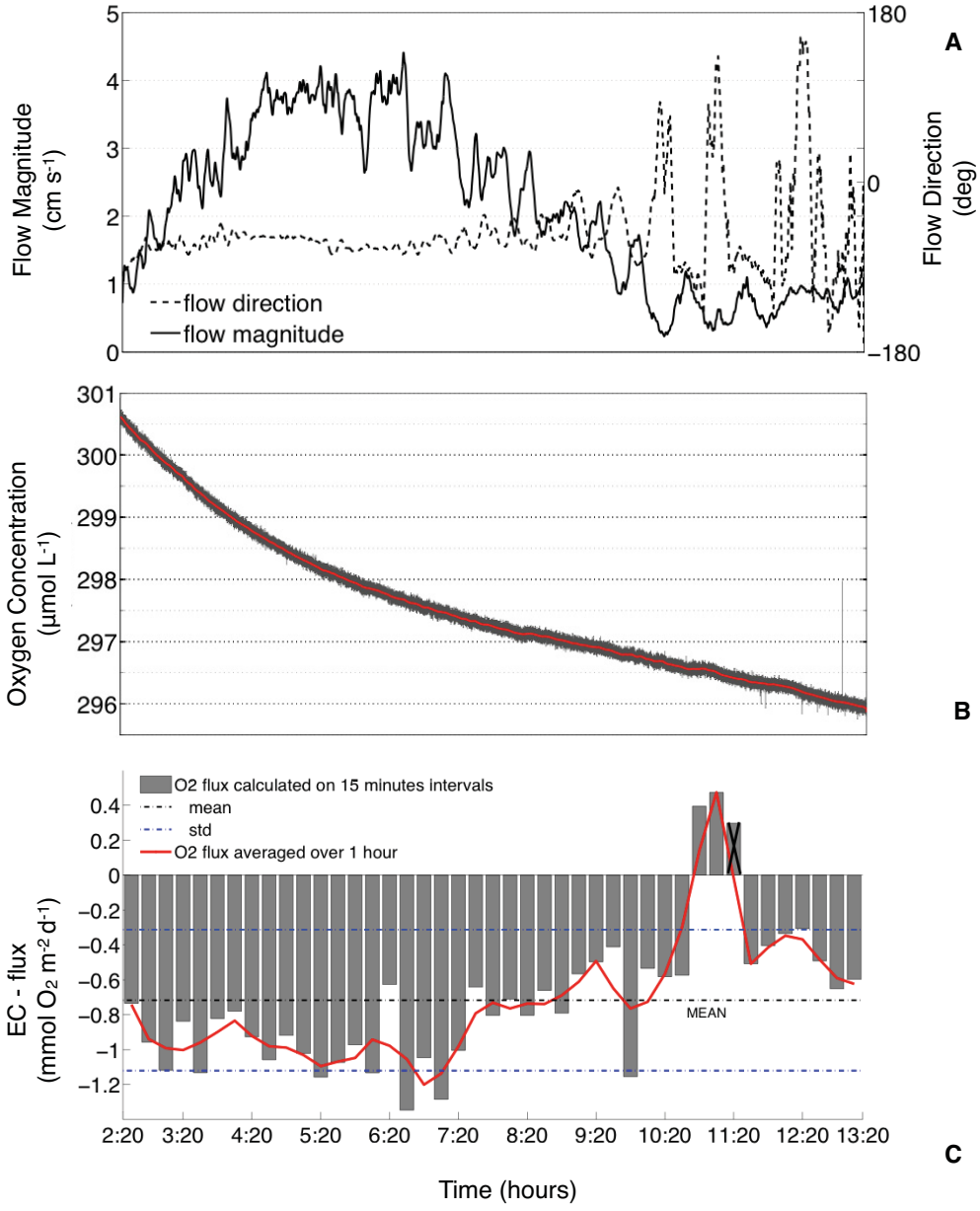

FIGURE 4.2: Results for EC deployment. A) current magnitude (solid line) and current direction (dashed line); B) oxygen concentration measured by the EC microelectrode; C) Oxygen fluxes calculated for 15 minutes bursts (bars), and averaged over 1 hour (red line). The black cross indicates a non significant flux ($p>0.05$).

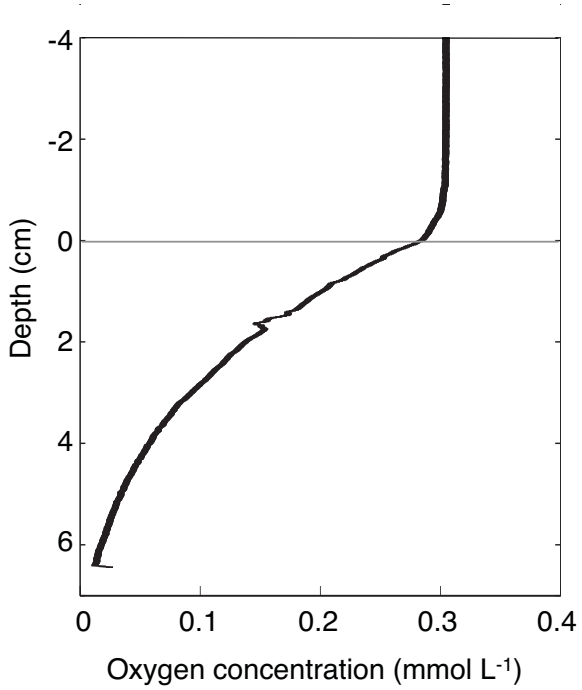

FIGURE 4.3: Average oxygen concentration of 16 micorprofiles from HAUSGARTEN central station (2500 m) used to calculate sediments dissolved oxygen uptake. The curve includes errorbars.

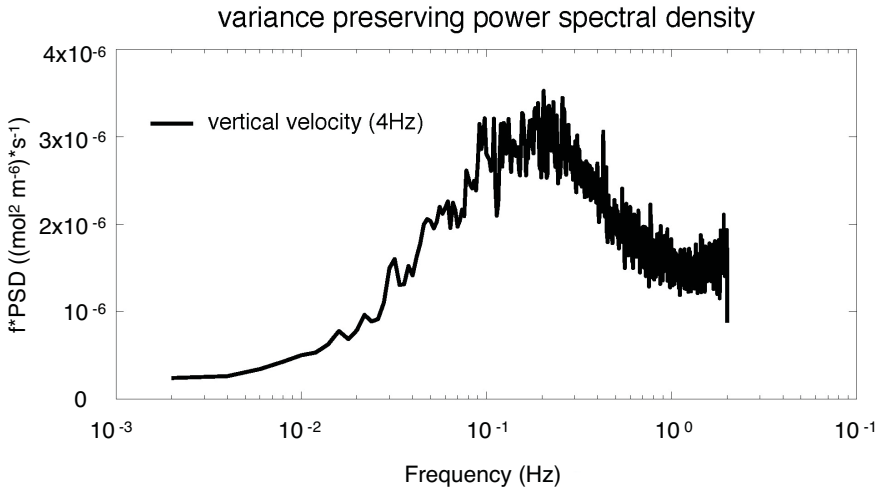

FIGURE 4.4: Variance preserving spectrum of vertical velocity measured by the ADV at 32 Hz and afterwards filtered (and de-spiked) at 4 Hz. The spectrum shows how the inertial subrange between 1 and 0.01 Hz is well resolved.

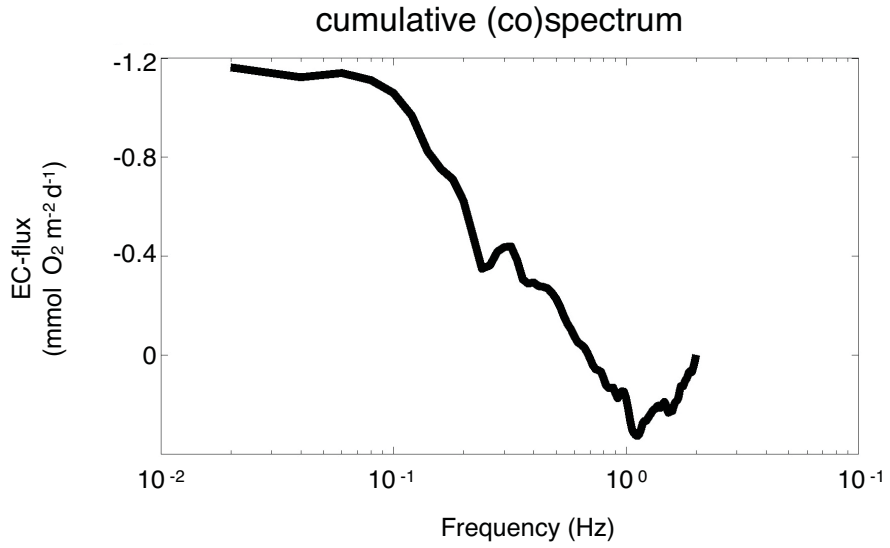

FIGURE 4.5: Cumulative (co)spectrum of w' C' showing the contribution of turbulent eddies to the vertical oxygen transport (negative, thus towards the sediment) between 1 and 0.01 Hz. The (co)spectrum also indicates a total O_2 flux of -1.2 mmol m^{-2} d^{-1}. (15 minutes burst)

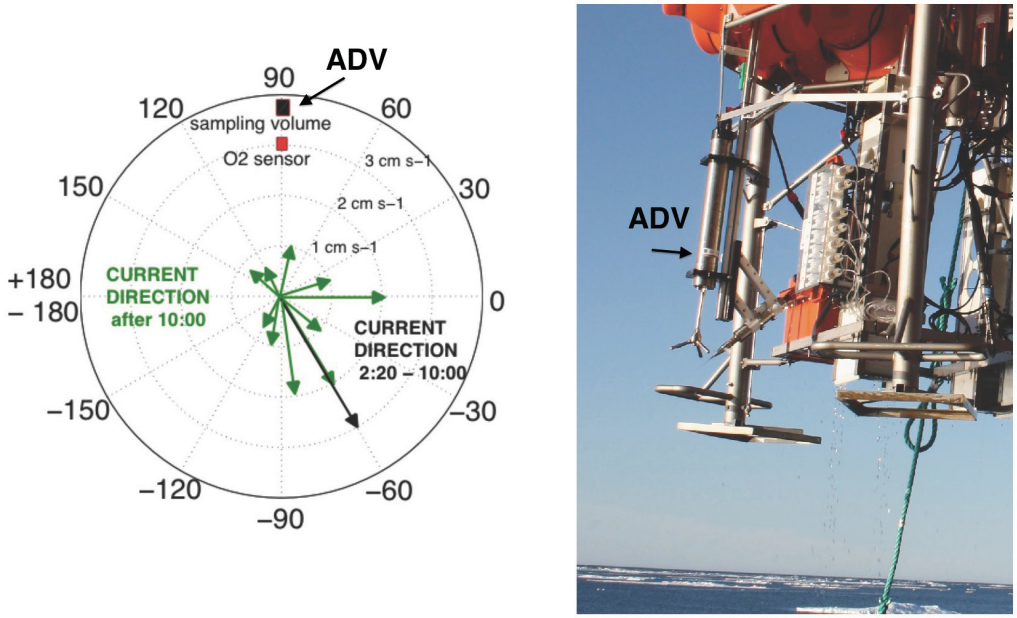

FIGURE 4.6: Left: Polar plot of the current direction during the deployment (from 2:20 to 13:00). The black and red squares indicate the position of the ADV sampling volume and the oxygen sensor respectively. The frame that held the EC system and the benthic chambers was located behind the red square. From 2:20 until 10:00 the main current was directed to -60 (deg) thus almost frontal to the EC system, and parallel to the sensors line. After 10:00 the current changed often direction, decreased its intensity reaching magnitudes < 1 cm s^{-1} and interfered with the frame when was directed to 60-120 (deg). On the right a picture of the EC system attached to the lander.

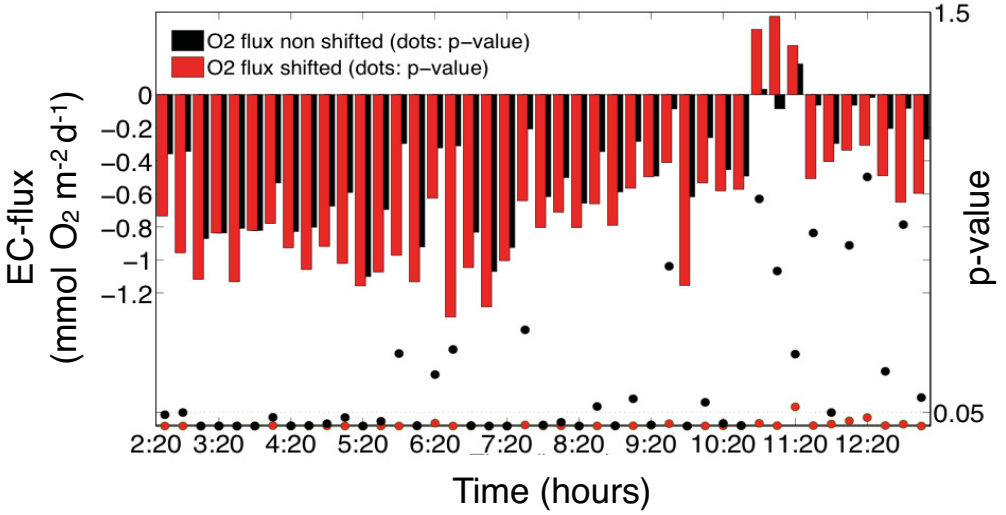

FIGURE 4.7: EC fluxes obtained without applying the time shift correction (black bars) and corrected for the time shift (red bars). The significance scale on the right axis (dots) indicates the robustness of the fluxes before and after time shift correction (same color code).

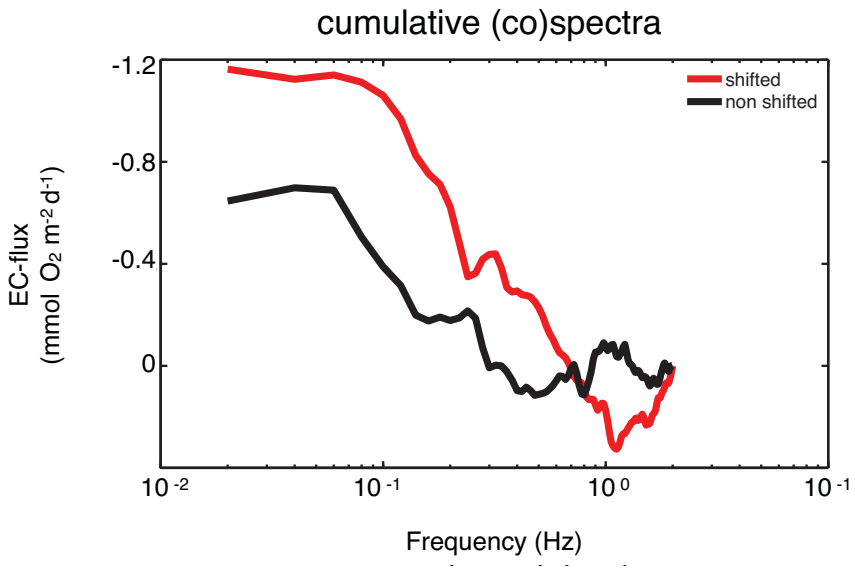

FIGURE 4.8: Cumulative (co)spectra as in Fig. 4.8, before (black) and after (red) shifting the time series w′ C′.

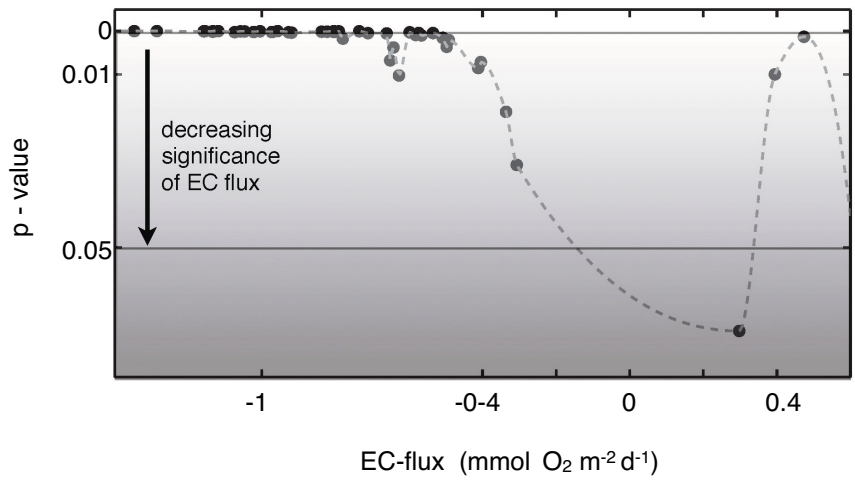

FIGURE 4.9: Magnitude of the EC fluxes (x axis) plotted against their significance (y axis) showing the increasing uncertainties related to fluxes between ± 0.4 mmol m^{-2} d^{-1}.

Chapter 5

Biogeochemical impact of submarine groundwater discharge on coastal surface sands of the southern Baltic Sea as revealed by in-situ SBC (stirred-benthic chamber) measurements

Daphne Donis[1,♣], Felix Janssen [1], Frank Wenzhöfer [1], Olaf Dellwig[2], Peter Escher [2], Michael E. Böttcher [2].

[1]HGF-MPG Joint Research Group for Deep Sea Ecology and Technology, Alfred Wegener Institute for Marine and Polar Research, Bremerhaven, Germany
[2] Leibniz Institute for Baltic Sea Research (IOW), Geochemistry and Isotope Geochemistry Group, Marine Geology Section, Warnemnde, Germany
♣Corresponding author

In preparation for Estuarine Coastal and Shelf Science

Abstract

By the use of stirred benthic chambers (SBC) integrated with seepage meters and combined with deep pore water profiles, this study evaluates the effect of submarine groundwater discharge (SGD) on mineralization pathways and net community production of sandy sediments (Hel bight, southern Baltic Sea). Measured seepage rates of 85±16 L $m^{-2}d^{-1}$ are in agreement with previous studies indicating that SGD is a durable feature of this site. Compared to the overlying water and to pore waters of an adjacent reference-site, the seep site groundwater (18 cm b.s.f.) was enriched in DIC, Mn^{2+}, PO_4^{3-}, SiO_4^{4-}, characterized by salinities <0.5 psu and depleted in Ca^{2+} and SO_4^{2-}. According to previous measurements the groundwater further contains dissolved CH_4 and HS-. Benthic flux measurements indicate that aerobic oxidation of organic matter represents the main mineralization pathway and similar rates of total oxygen uptake independent by SGD, (40 ± 15 and 42 ± 9 mmol O_2 $m^{-2}d^{-1}$ for the seep and reference site, respectively) are observed at both sites.

The main difference between biogeochemical processes at the two sites is driven by the supply of CH_4 by SGD at seep site, where a ratio of 0.8 between SO_4^{2-} deficiency to excess DIC, indicates anaerobic oxidation of methane (AOM) as an important process. The sulfide generated by sulfate reduction associated with AOM most likely reduces Fe^{3+} oxides that may trap additional sulfide as FeS.

Oxygen production was similar at both sites and governed by light rather than by nutrient availability. The supply of phosphate and silicate to the open water column that was observed at the seep site due to SGD, was not reflected on net primary productivity (106 ± 17 and 126 ± 33 mmol C $m^{-2}d^{-1}$ at the seep and reference site, respectively). However, the different nutrient load between the two sites probably affects the metabolic products of photoautotrophs that may lead to distinct trophic structures.

5.1 Introduction

The continental hydrological water cycle and the ocean are often connected by submarine groundwater discharge (SGD) in the coastal zone, a process that is primarily driven by hydraulic gradients between subterranean aquifers and the ocean (Burnett et al., 2003). SGD results in the mixing of waters with different salinities and chemical characteristics, similarly to what happens in surface estuarine systems. Indeed, the term "subterranean estuary" is used to describe the location of mixing between meteoric water and seawater in coastal aquifers, where the occurring chemical reactions may modify water's composition (Moore, 1999).

Seepage of groundwater in coastal sands is often diffuse and patchy, depending on the structure and permeability of the aquifer (Burnett et al., 2006; Holliday et al., 2007). Given the dispersive character of seepage, the quantification of discharge is not trivial and further complicated by an additional range of factors controlling the rates (e.g., spatial and temporal patterns of hydrostatic pressure and surface sediment permeability, seasonal changes in aquifer level) (Mulligan and Charette, 2009).

Methods for a direct measurement of SGD rates include seepage meters, piezometers and geochemical/geophysical tracers (Carr and Winter, 1980; Moore, 2005; Taniguchi et al., 2006), while indirect approaches include theoretical methods and numerical simulations, that are mainly used for basin-scale estimations of groundwater discharge into the ocean (see Santos et al. 2012 for a review of approaches and their limitations).

Globally groundwater discharge is thought to reach 6% of the total river input to the ocean (Burnett et al., 2003), being recognized as a phenomenon with a potentially large contribution to coastal-ocean geochemical budgets (Church, 1996; Moore, 2010 and references within). This is not necessarily relating to the volume being supplied, but due to enhanced concentrations of solutes found in the seeping ground waters (e.g., nutrients, contaminants, metals, carbon dioxide, hydrogen sulfide, and methane). Indeed, it is estimated that SGD is responsible for elemental fluxes between land to the ocean, in quantities that exceed the magnitude of river-borne fluxes (Burnett et al., 2003; Kim et al., 2005) and in some areas, may have pronounced ecological consequences (e.g., Costa et al., 2006).

It is thus not surprising that the assessment of groundwater discharge and its ecological effects on to the coastal ocean has been studied intensively over the past two decades (e.g.Bokuniewicz, 1992;Wilson, 2005; Burnett et al., 2006; Martin et al., 2006, 2007; McCoy et al., 2007a; Cable and Martin, 2008), and still is of high interest in particular in northern Europe, where these questions have not been in the focus for a long time.

Many studies were centred on methodological approaches of SGD quantification aside to its influence on the coastal nutrient and carbon budget (e.g. Beck et al., 2008; Moore 2010; Jeong et al., 2012; Rapaglia et al., 2012; Winde et al., 2013). Nutrients supplied

to coastal waters via SGD have been documented to alter the cycles of energy flow between benthic and pelagic zones (Nixon et al., 1986; Valiela et al.,1990; Gazeau et al., 2004; Opaliski et al., 2010) especially by influencing both sediment and water column primary productivity (Paerl, 1997; Hu et al., 2006) and increasing bacterial concentrations (Boehm et al., 2004, 2006). The biogeochemical reactions leading to carbon, nutrient and metal release are important aspects of SGD (Moore, 2010). Abiotic and microbially mediated reactions are usually occurring in aquifers, and through the flow path of SGD, including ion sorption, mineral dissolution and precipitation, and the remineralization of organic matter, depending to a certain extent on substrate availability, aquifer rock composition, and the residence time of ground water (Clark and Fritz, 1997; Appelo and Postma, 2005).

Most studies derive chemical fluxes associated to SGD from the characterization of the endmembers (i.e., wells and bottom water) and flow rates (e.g., Oberdorfer et al., 1990; Charette et al., 2001; Montlucon and Sanudo-Wilhelmy, 2001). However, the reactions that occur in the subterranean estuary can result in removal or addition of solutes (Moore, 1999) so that any non-conservative behavior must be accounted for when determining mass fluxes to the coastal ocean. It has been shown that without including non-conservative concentration changes chemical fluxes can be significantly over- or underestimated (Beck et al., 2007b).

Permeable coarse grained sands are characteristic for shallow water systems and have been estimated to cover two thirds of the continental shelves worldwide (Emery, 1968). By their nature, permeable sediments are more open to the advective transport of water, dissolved solutes and fine suspended particles that are circulated through the sediment pore space by hydrostatic pressures that result, e.g., from interactions of bottom flow with topographical features at the sediment-water interface (Huettel et al., 1996; Cook et al., 2007b). Owing to the fast exchange rates associated with this so called "pore water advection", solute fluxes to the overlying water column may be orders of magnitude greater than for fine-grained sediments despite the relatively low solute concentrations typically found in permeable sediments (Huettel and Gust, 1992; Huettel et al., 1996; Huettel and Rusch, 2000; Ret al., 2002; Janhke et al., 2003). Coastal sand-beds are now known to function as fast bioreactors where low organic carbon and nutrient concentrations reflect a high turnover rate rather than low activity (Huettel et al. 1998; de Beer et al., 2005). Despite the fact that permeable sediments are widespread in coastal regions that are often influenced by SGD, their role as zones of groundwater-related biogeochemical transformations have been largely overlooked (Charette and Bruesseler, 2004). The interactions between pore water advection and seepage adds complexity to SGD characteristics in permeable sediments (e.g. Beck et al., 2008). Both processes may be influenced by dynamic mechanisms such as tidal pumping and wave action that may add not only spatial but also temporally variability to seepage patterns and rates

(Santos et al., 2012).

In situ incubations of stirred benthic chambers represent a standard approach to estimate benthic respiration rates and fluxes. They leave sediments relatively undisturbed, may assess fluxes for any solute, include fauna-related processes and are able to reasonably represent natural hydrodynamic conditions in terms of diffusion properties and rates of pore water advection (Tengberg et al., 1995, 2005; Janssen et al., 2005; Cook et al., 2007b). DIC and oxygen day- and night-fluxes determined by means of benthic chambers provides an estimate for rates benthic carbon mineralization (Glud, 2008) and photosynthesis (Jahnke et al., 2000; Rascheed et al., 2004) while the O_2:DIC ratio provides information on the nature of remineralization processes. Areas of SGD in the Polish coastal zone were first observed in the early 1990s (Jankowska et al., 1994; Piekarek-Jankowska, 1996; Falkowska and Piekarek-Jankowska, 1999) in the area of the Puck Bay (southern Baltic Sea). The present study was carried out at Hel bight (Fig. 5.1), where several studies in the years 2009 and 2010 found in an area of near-shore permeable sandy sediments seep-type escapes of low-saline groundwaters into the bay (see Kotwicki et al., 2013, and references therein).

As part of the AMBER project of the BONUS+ initiative special focus was put on the biogeochemical impact of SGD on benthic processes at Hel bight. Investigations were centered on the comparison of ground water impacted and un-impacted sites (Vogler et al., 2010). Recent studies showed that SGD impacted sediments at Hel bight are characterized by high rates of production and emission of groundwater-derived methane. It was shown that the seepage affects the spatial distribution, abundance and taxonomic composition of benthic communities and may result in a significant reduction in meiofaunal density (Kotwicki et al., 2013).

This study addresses the effect of SGD on processes and rates in sandy sediments of Hel bight by the use of stirred benthic chambers combined with seepage meters as well as deep pore water profiles. Similar methods were used by Cook et al. (2007a), who investigated benthic fluxes and mineralization rates at Hel bight focusing on sediments not impacted by SGD. In the present wortk we compared a seepage "hot spot" to an adjacent site virtually unaffected by SGD. Seepage rates and benthic solute fluxes were measured simultaneously and compared to vertical solute distributions in order to assess aerobic and anaerobic mineralization as well as photosynthetic activity / net community production.

5.2 Materials and Methods

5.2.1 Study area and pore water investigations

The Polish Hel Peninsula forms a semi-enclosed basin (Puck Bay) in the western part of the Gulf of Gdansk (southern Baltic coast) (Fig. 5.1). A field campaign was conducted from August 25th to September 4th 2011 directly off the beach at the township of Hel (54° 3"25"N, 18° 47'57"E) at a water depth of 1 to 1.5 m. The tidal influence is minimal, and small changes in water level at the site are controlled by wind driven seiches (Cook et al., 2007a; Kotwicki et al., 2013). During the campaign, a recording current meter (Type Seaguard, AADI, Bergen, Norway) was deployed in direct vicinity of the chamber incubations. The instrument recorded current speed and direction, temperature, salinity, and dissolved oxygen approx. 20 cm above the sediment surface at 5 minute temporal resolution. It is known from previous studies that at Hel bight groundwater escapes from shallow water seeps in close proximity to the beach (Kotwicki et al., 2013). The extent and rates of seepage depend on several factors including sea level, wave action, precipitation and sea bottom relief (Santos et al., 2012). To locate the exact position of the seepage sites at the time of investigation the area was surveyed with a temperature and conductivity sensor. Conductivity measurements at approx. 10 cm sediment depth allowed to identify spots of high SGD impact where low salinity water escaped from the seafloor. These areas are referred to as "seep" sites while "reference" site designates the deployment sites in the surrounding area of low SGD impact (Fig. 5.3). The substrate of the study area is permeable medium sand. Mean grain size (d) and permeability (k) at the sites with strong SGD impact were reported to be slightly higher than at low impact areas with mean grain sizes of 388 and 314 μm and corresponding permeabilities of 1.95x10^{-11} m^2 and 2.32x10^{-11} m^2, respectively (Kotwicki et al., 2013). The sediments have a low organic matter content, with 0.15% of total organic carbon (TOC) in the top 2 cm of sediments at sites of high SGD (0.14 % averaged for the top 20 cm) and 0.17% at a non-impacted site (0.11% integrated on 20 cm) (Böttcher et al., unpublished data). Seep and reference site were sampled with a pore water lance (similar to the one described by Beck et al., 2007a) to determine vertical profiles of the pore water composition at 5 depth intervals up to 20 cm bsf (cm below surface). Pore water lances were inserted and left for at least 24 h to equilibrate before pore water sampling (25 mL).

5.2.2 In situ incubations

Six cylindrical benthic chambers were deployed for 21 hours each at the seep and reference site to investigate solute exchange of oxygen, dissolved inorganic carbon (DIC), sulfate and dissolved Manganese (Mn^{2+}) and Iron (Fe^{2+}). The 35 cm long acrylic chambers (ID = 18 cm) were provided with seepage bags to allow for SGD and to determine seepage rates. They were gently inserted into the sediment to a depth of 20 cm, enclosing approximately 0.026 m^2 of sediment with 15 cm of overlying water. Mixing of the overlying water was maintained by rotating acrylic stirrer discs (10 cm diameter). The volume of the overlying water was determined based on the dilution of Br- solution that was added prior to the start of the deployments according to the method described by Jahnke and Christiansen (1989). Two stirring modes were applied to compare seepage rates, and investigate whether the presence/absence of advective pore water exchange had an influence on seepage rates and biogeochemical processes in the enclosed sediments. In three chambers advective pore water exchange was maintained by stirring continuously at 40 rpm ("advective mode"). For the other three flux chambers, the stirring speed of the disk was set to a "non-advective mode" to ensure mixing without creating a significant pressure gradient (20 rpm, reversing rotational direction every 15 s). Relationships between stirring speed, stirrer disk to sediment distance and pressure gradient within the chamber have been characterized (Janssen et al., 2005). A 40 rpm stirring rate corresponds to a pressure gradient of approx. 2.5 Pa between the center and the rim of the flux chamber, which is in the range of pressure gradients that develop under moderate unidirectional flow over topographical features with heights in the cm range (Huettel et al., 1996; Janssen et al., 2012). To collect the groundwater seeping from the enclosed sediment patch into the overlying water polyethylene bags of 2 L volume were connected to the overlying water in the chambers by means of a 10 cm long PVC (Tygon®) tube (ID = 13 mm) attached to the wall of the chambers directly above the sediment surface. The bags were filled with 200 mL ultrapure water to ease filling and protected from ambient hydrodynamics by means of individual spacy plastic boxes. The boxes were provided with holes to allow for water displacement while the bags inflated and kept in place by ballast weights. The bags were replaced in the early morning after the first half of the deployment (after approx. 10 h), to allow for two separate seepage volume measurements covering the night and day, respectively. The collected water volumes were transferred into areal seepage rates. Dissolved oxygen inside the chambers was monitored continuously using fiber-optic oxygen microsensors that were inserted into the chamber lids (for the measuring principle, see Klimant et al., 1995, further setup and sensor characterization can be found in Janssen et al., 2005). Water samples of 50 or 100 mL were withdrawn from the overlying water of the flux chambers every 4 h through a stopcock, while a second opening in the lid allowed replacement of

the sample volume with ambient bottom water. Incubated water samples were filtered through 0.45 μm filters (except for samples dedicated to Winkler titration), stored and analyzed as described in "water sample analysis" section. Solute fluxes were calculated from the slope of linear regressions of solute concentration time series for dark and light periods. For the oxygen sensor readings these correspond to 21:30-3:00 and 7:00-14:00, while for samples to 21:00-5:00 and 9:00-17:00.

5.2.3 Mixing calculations

"Theoretical dilution lines" (TDL), i.e., the expected temporal changes in concentration (i.e., dilution / accumulation) of the different solutes in the chamber water were computed. The calculations were based on (1) the initial concentration of the target solute in the chamber water and the chamber water volume, (2) the groundwater endmember concentration (i.e., concentration in pore water samples extrapolated from concentration gradient as a function of conservative elements), and (3) the seepage rates (calculated from the bag content). The chosen approach assumed that (1) the chamber water was always fully mixed and (2) no mixing took place between the bag and the chamber, (3) that transport properties (advective mixing and diffusive transport) in the enclosed sediment were equal to conditions prior to chamber placement, and (4) that the solutes behaved conservatively in the surface sediment as well as in the overlying water (i.e., no conversions, ad-/desorption, precipitation, dissolution). To verify the reliability of the obtained seepage rates and to assess the feasibility of the calculation and the assumptions for a prediction of the seepage effect on chamber water properties the TDL of a conservative element (Cl-) was compared to the trend-line of concentrations measured in the samples taken during the incubation.

5.2.4 Prediction of conservative solute behavior based on salinity

To investigate the conservative or non-conservative behavior of the different solutes, changes in concentration with sediment depth (in pore water vertical gradients) and time (in chamber water time series) were compared to salinity as a conservative property. "Mixing curves" were constructed from predicted pore water concentrations of a target solute in the pore water (C_{mix}) that were calculated assuming simple mixing of groundwater and seawater (as in Fry, 2002):

$$C_{mix} = fC_g + (1 - f)C_s \tag{5.1}$$

where C denotes concentration of the target solute, the subscript g and s indicate groundwater and seawater, and f denotes the fraction of freshwater in each sample calculated

from the measured salinity S and the overlying water salinity Ss (i.e., $S_s = 7$):

$$f = \frac{(S_s - S)}{S_s} \tag{5.2}$$

5.2.5 Water sample analysis

Samples for oxygen measurements (V 10 mL) were fixed immediately in gas tight vials (Exetainer®, Labco, Lampeter, Ceredigion, UK) by addition of Winkler (I) and (II) reagents. Oxygen determination took place the same day in duplicates (5mL aliquots) following the standard Winkler titration procedure (Grasshoff, 1983). DIC samples were taken in the field as described by Winde et al. (2013) and preserved with saturated HgCl2 solution; DIC concentrations were quantified in the laboratory integrating the mass 44 signal on a Thermo Finnigan MAT 253 gas mass spectrometer. Results for samples were compared to artificial aqueous $NaHCO_3$ solutions. Samples for sulfate were fixed with 5% zinc acetate solution and stored at 4C. Sulfate concentrations were measured as total dissolved sulfur by means of ICP-OES (Thermo iCAP 6300 Duo). Samples for major and trace elements were filtered through 0.45 μm disposable filters and stored at 4C in PE vials. The main and trace elements were measured by ICP-OES (Thermo Fisher Scientific iCAP 6300 Duo) on acidified (nitric acid) samples. The accuracy and precision was routinely checked with the international CASS-4 reference standard (Kowalski et al., 2009; Winde et al., 2013). Salinity was calculated from Na+ concentrations using standard seawater ion concentrations at 35 psu taken from Bruland (1983).

5.3 Results

5.3.1 Water column parameters and SGD spatial patterns

The average steady flow as recorded by the recording current meter during the chamber deployments were slow with an average current speed of 2 cm s^{-1} and mainly directed parallel to the shoreline (southeast-northwest) (Fig. 5.2). Previous studies (Cook et al., 2007a) conducted at the same site at similar average steady flow (1.84 ± 1.05 cm s^{-1}) identified oscillating wave-driven currents with an average speed of 3.16 ±1.95 cm s -1 that were directed perpendicular to the shoreline, as the main flow component. The salinity was low (7 psu), reflecting the brackish nature of the Baltic Sea under impact of fresh waters. Dissolved oxygen concentrations were close to saturation with concentrations of 270-320 μmol $L^{-1}$and temperatures ranged between 18 during the night and 20 C at daytime (Fig. 5.2). Based on the conductivity survey well defined SGD areas could be identified. Based on the obtained high resolution map (approx. 1 m

resolution) a major Seepage site as well as a reference site (indicated in Fig. 5.3 as site A and B, respectively) were selected for pore water sampling and chamber deployments.

5.3.2 Pore water profiles and groundwater composition

Pore water gradients obtained at the seepage and the reference site are compared in Fig. 5.4. The geochemical analyses identify the deep pore water (18 cm b.s.f.) at the seep site as anoxic fresh groundwater. Compared to the overlying water and the reference-site pore waters at the same depth the seep site groundwater was enriched in DIC, Mn^{2+}, PO_4^{3-} and depleted in Ca^{2+} and SO_4^{2-} (Fig. 5.4). According to measurements of seep-site pore waters sampled during this and previous campaigns the groundwater further contains dissolved methane (Kotwicki et al., 2013; Böttcher and Gehre, unpublished data) and temporarily dissolved (Böttcher et al., unpublished data). At the reference site, the salinity in the pore waters did not show any freshening with depth but was constant throughout the upper sediment column and in equilibrium with the overlying water. The same is largely true for Mn^{2+} and Ca^{2+} while concentrations of PO_4^{3-} and DIC increase with depth. Fe^{2+} concentrations show a prominent subsurface concentration maximum at 5 cm b.s.f and is the only of the investigated solutes for which concentrations at depth are similar at the seep and the reference site. For all other solutes including conservative constituents (i.e., salinity), strong gradients existed at the seepage site, indicating the presence of upward migrating freshwater that is mixed with the overlying brackish water.
Recent studies in the summer season at this site reported similar sediment pore water salinity profiles (Kotwicki et al., 2013) implying that seepage-impacted geochemical conditions in surface sediments are commonly found in shallow water off Hel beach. For practical purposes, during this study, pore water samples characterized by salinity (S) <0.5 were attributed to essentially endmember groundwater, while those characterized by salinity $S = 7$, to the brackish seawater endmember.

5.3.3 Seepage rates

The volume of water collected in the bags attached to the 6 benthic chambers deployed at seep site, corresponded to discharge rates of 87 ± 16 L $m^{-2}d^{-1}$ for the 3 "advective" chambers that were stirred in "advective mode" at 40 rpm to exert a pressure on the sediment and to promote advective pore water exchange. Largely similar discharge rates of 83 ± 16 L $m^{-2}d^{-1}$ were also found for the other 3 "diffusive" chambers that were stirred in "non-advective mode" and where pore water exchange apart from seepage was restricted to diffusion. A minute groundwater seepage was also observed at the reference

site with rates of 8±4 and 9±3 L m^{-2} d^{-1} for the "advective" and "diffusive" chambers, respectively. The agreement between the rates determined at "advective" and "non-advective" stirring indicates that the pressure gradient did not affect the groundwater outflow (Fig. 5.5). Results for solutes time series and benthic fluxes will be shown only for the "advective" chambers, as this stirring mode is assumed to adequately reproduce conditions of pore water transport in shallow water permeable sands (Janssen et al., 2005; Cook et al., 2007a).

5.3.4 Flux chamber time series

Chloride fluxes seep and reference site: A comparison between the theoretical dilution line (TDL) and the measured temporal evolution of chloride in the chamber water time series gives an indication of the reliability of the obtained seepage rates and the feasibility of the approach to predict the effect of seepage on chamber water properties. In case of the reference site there was an excellent agreement between seepage-based predictions and Cl- measurements with the TDL falling within the standard deviation of the measured concentrations (Fig. 5.6-B). Chloride was hence only slightly decreasing over the time course of the deployment, confirming the absence of relevant SGD at this site. Also in case of the seep site the TDL was in fairly good agreement to the measurements. However, predicted concentrations show a slight tendency to underestimate the true dilution (equal to 8% of the initial Cl concentration in the end of the deployment after 20 hours; Fig. 5.6-A). The fact that the TDL lies outside the standard deviation of the measurements indicates that the plastic bags did not collect all seeping water leading to an underestimation of the true seepage rates or that the model and assumptions the TDL calculation was based upon did not cover all processes involved. The uncertainty has to be kept in mind when assessing the time series of the other solutes investigated.

Solute fluxes seep site: The temporal evolution of dissolved oxygen concentrations in the chamber water shows a clear temporal pattern with a shift at around 6:30 (i.e., 1 h after sunrise) from consumption at night-time to production during the day (Fig. 5.6-C). The obvious disagreement between optode measurements and TDL implies that the effect that oxygen consumption and production exert on chamber water oxygenation outweighs the effect of seeping anoxic waters. The abrupt rise in optode readings by approx. 100 μmol L^{-1}at around 9:00 is clearly an artifact that may be related to accidental mechanical disturbance of the optode electronics during chamber water sampling. This is confirmed by measurements on water samples (red circles in Fig. 5.6-C and D) that show that oxygen concentration at the end of the incubations was in fact approx. 100 μmol L^{-1}lower than the optode measurements. As the rates of increase in optode readings were largely similar before and after the increase it is assumed that

the shift in sensor signal did not compromise the measured oxygen trend. Hence both the time before and after the shift were included for the comparison of rates between day and night and between seep and reference site (below). Differently from oxygen, measured DIC and SO_4^{2-} concentrations plot close to the TDL (Fig. 5.6-E and G). This "quasi conservative behavior" indicates that seepage of DIC-enriched and SO_4^{2-} depleted groundwater dominated the temporal evolution of DIC and SO_4^{2-} concentrations in the chamber water. For more detailed biogeochemical analyses of trends in inorganic carbon and sulfate concentrations it has to be noted, however, that any changes are potentially obscured by the high initial concentrations of DIC and SO_4^{2-} exceeding, for example, initial oxygen concentrations by a factor of 5 and 10, respectively. While concentrations of reduced Iron were already low (approx. 1 μmol L^{-1}) in the groundwater initial Fe^{2+} concentrations in the chamber water were close to detection limit (0.07 μmol L^{-1}) and remained at that low level throughout the chamber incubation (Fig. 5.6-I). As for Fe^{2+}, Mn^{2+} concentrations in the chamber water were low and stayed fairly constant throughout the chamber incubation (approx. 0.2 μmol L^{-1}). However, as the pore water at depth was clearly enriched in reduced Mn^{2+} (5.4 μmol L^{-1}) as compared to bottom water, the TDL suggested an increase in Mn^{2+} concentration to approx. 2 μmol L^{-1}after 20 hours (Fig. 5.6-K). The strong discrepancy to measurements implies that Mn^{2+} removal by oxidation and precipitation were even more efficient as in case of Fe^{2+}. Groundwater PO_4^{3-} exceeded bottom water concentrations by two orders of magnitude (60 and 0.6 μmol L^{-1}, respectively). Consequently, the PO_4^{3-} concentrations substantially increased over the incubation period (to approx. 12 μmol L^{-1}after 20 h) although not to the degree expected from SGD rates and predicted by the TDL (approx. 20 μmol L^{-1}; Fig. 5.6-M). Hence processes other than mixing have to be involved that led to the observed non-conservative behavior of phosphate.

Solute fluxes reference site: Similar to the temporal pattern at the seep site oxygen concentrations depicted consumption during dark hours and production during the day (Fig. 5.6-D). Oxygen measurements in the replicate chambers strongly differed at the reference site, especially in the second half of the deployment, indicating pronounced patchiness in oxygen production or a bias calibration towards oxygen super-saturation in part of the optodes. A comparison with discrete oxygen measurements (red circles with error bars in Fig. 5.6-D) suggests that the average optode reading led to a slight overestimation of the oxygen concentration. DIC measurements did not produce consistent results at reference site, only three time points were available, that have a high standard deviation (0.9 $\pm$ 0.4 mmol L^{-1}; Fig. 5.6-F). In contrast to the strong decrease in concentrations observed at the seep site, sulfate at the reference site remained almost constant at approx. 5 mmol L^{-1}throughout the deployment (Fig. 5.6-H). This, however, largely agrees to the TDL that predicts only little dilution of the initial concentrations due to the low seepage rates at the reference site. Hence the behavior of sulfate

concentrations can again be considered "quasi conservative". Fe^{2+} and Mn^{2+} showed concentrations similar to the seep site and also changed only little with time (Figs. 6-J and L). Compared to conditions at the seep sites this again largely agrees with expectations based on the almost horizontal TDL. Similarly to iron and manganese, phosphate concentrations were in good agreement with the TDL and showed only a small increase over the time course of the deployment. Consequently, final concentrations were much lower than those measured at the seep site (2 and 10 μmol L^{-1}respectively).

5.3.5 Pore water and chamber water mixing

Figure 5.7 provides mixing plots that show chamber water time series and pore water profiles of DIC, SO_4^{2-}, Fe^{2+}, Mn^{2+}, and PO_4^{3-} relative to salinity for both seep and reference site. In this plot changes in solute concentration that cannot be explained by simple mixing between the two endmembers (i.e., bottom water and pore water at 18 cm b.s.f.) due to biological and chemical conversions (uptake, release, redox processes, changes in solubility and sorption) appear as excursions from the straight "mixing line" (dotted line in Fig. 5.7). Oxygen is left out as the non-conservative behavior is obvious already in Fig. 5.6. Plotting chamber water time series measurements of DIC and SO_4^{2-} obtained at the seep site versus salinity confirms that their concentrations in the chamber water were largely governed by conservative mixing with seeping groundwater (Figs. 7-A and C). This is in agreement with pore water profiles that also showed a largely conservative behavior and plot closely to the mixing line. Only at salinities of around 1 psu (corresponding to a sediment depth of 10 cm) concentrations diverged considerably from the conservative mixing found in the upper layers. Chamber water concentrations of Fe^{2+}, Mn^{2+} and PO_4^{3-} at the seep site plot well below the mixing line (Figs. 7-E,G and I). This indicates that chamber waters showed a relative depletion of these constituents that obviously - at least in part - are removed from the seeping groundwaters by e.g., uptake, precipitation, or sorption and are not transferred to bottom waters. Deviations of Fe^{2+} and Mn^{2+} pore water concentrations from the conservative mixing line (Figs. 7-E and G) demonstrate that these elements undergo release and removal processes at salinities of 0-6, i.e., at sediment depths between 5-18 cm. As expected from the missing pore water salinity gradient and the constant Cl- concentration in the chamber deployments at the reference site, none of the solutes depicted a trend relative to salinity (right panels in Fig. 5.7). As temporal changes and depth gradients at the reference site were generally small most concentrations plot in a small region. In agreement with Fig. 5.4, only pore water Fe^{2+} showed a wide range of concentrations that even exceeds the range of concentrations found at the seep site (Fig. 5.7-F).

5.3.6 Benthic oxygen and DIC fluxes

To investigate the contribution of aerobic respiration to organic matter (OM) mineralization as well as rates of benthic primary production, O_2 and DIC fluxes were determined from benthic chamber incubations at both seep and reference site. Figure 5.8 shows the total oxygen uptake (TOU) calculated at seep and reference site separated for night- and daytime. The net or total fluxes calculated directly from changes in oxygen concentrations in the chamber water (green bars in Fig. 5.8) represent all processes of oxygen removal and release. These include seepage of anoxic groundwater and loss to supply from the pore space by means of other transport processes (diffusion, advection, bioirrigation), respiration by aerobic microbes and metazoans, oxidation of reduced compounds (e.g., sulfide, reduced metals) and oxygen production during photosynthesis by benthic microalgae. The SGD-effect, i.e., the apparent flux due to the replacement of oxic chamber water with anoxic ground water (red bars in Fig. 5.8) was calculated directly from the seepage rate and the oxygen concentration and volume of the chamber water or, in other words, corresponds to the slope of the TDL times the height of chamber water column. The black bars correspond to the SGD-independent fluxes, i.e., the difference between the green and the red columns and, hence, represent O_2 release and removal due to biological production and respiration, non-SGD exchange processes, and the oxidation of reduced compounds.

SGD-independent O_2 uptake rates at night-time (upper panel of Fig. 5.8) were similar for both sites (40 $\pm$ 15 and 42 $\pm$ 9 mmol $m^{-2}d^{-1}$ for the seep and reference site, respectively). Similarly, the SGD-independent O_2 production at daytime (lower panel of Fig. 5.8) at the seep site (146 $\pm$ 9 mmol $m^{-2}d^{-1}$) compared well with values obtained at the reference site (168 $\pm$ 32 mmol $m^{-2}d^{-1}$). As a consequence, net community production (NCP; i.e., the rate of carbon fixation by oxygenic photosynthesis), estimated by subtracting O_2 consumption in the dark from production during daytime was in the same range for both sites (106 $\pm$ 17 and 126 $\pm$ 33 mmol C m-2 at the seep and reference site, respectively).

DIC fluxes at the seep site were analyzed in the same way as O_2 fluxes in order to separate SGD-related fluxes and fluxes induced by seepage independent processes (reference site DIC data were left out from the analysis due to their poor quality; see above). As expected from the close match between the TDL and the DIC concentration measured along the time course of the incubation at the seep site (Fig. 5.6) most of the DIC flux could be attributed to seepage of DIC rich waters by SGD. Consequently, the SGD-independent DIC flux contribution at nighttime (black bar in the upper panel of Fig. 5.9) represented a small fraction of the total flux (98 $\pm$ 22 mmol $m^{-2}d^{-1}$). Still, rates of DIC release during the night exceed those of oxygen uptake by approx. a factor of 2. Although hardly discernible in Fig. 5.6-E, the net DIC flux at daytime was reduced to

a value below the SGD-related DIC flux due to seepage of DIC-rich groundwater (206 ± 70 and 281 ± 30 mmol $m^{-2}d^{-1}$, respectively). This resulted in a negative value for the SGD-independent contribution of -75 ± 77 mmol $m^{-2}d^{-1}$ (i.e., a DIC flux from the water column to the sediment; black bar in the lower panel of Fig. 5.9). As during the night, SDG-independent DIC and O_2 flux at daytime are imbalanced with rates of DIC uptake being 25% lower compared to rates of oxygen release.

5.4 Discussion

5.4.1 Seepage rates

Collecting the water flowing from an enclosed sediment area of known size over a specific period of time is the only direct method available to evaluate rates and composition of SGD (Taniguchi et al., 2006).

Seepage meters used for this purpose can be designed in several ways as long as the flow from the sediment to the bag that collects the seeping water is not constrained, e.g., by too narrow tubing. Due to the pronounced spatial and temporal variability of SGD, replicate measurements are highly recommended (Fellows and Brezonik, 1980; Shaw and Prepas, 1990; Belanger and Montgomery, 1992; Libelo and MacIntyre, 1994). The stirred benthic chambers used in this study combined established seepage meter methodology with characteristics of sediment incubation chambers as they are typically used for studies of sediment processes and solute exchange across the sediment water interface (e.g. Tengberg et al., 1995, 2005). In comparison to standard seepage meters the chambers used in this study enclose a larger volume of overlying water. This helps to keep the settings for diffusive and advective transport in the chamber close to natural conditions by reducing changes in chemical composition of the overlying water due to solute exchange and by allowing for defined stirrer-induced flow conditions. Combining stirred benthic chambers with seepage meter functionality allowed to (1) investigate sediment processes and fluxes in seepage areas without blocking SGD and (2) compare sites with and without SGD using the same methodology. To our knowledge this study represents the first application of this combined method for this purpose.

Lee-type seepage-meters (Cable et al., 2008) were deployed in 2009 - 2010 and resulted in seepage rate estimates in the range of 50 to 150 L $m^{-2}d^{-1}$ for Hel Bight in summer / autumn (Kotwiki et al., 2013). These seepage rates are similar to those measured during this study (85±16 L $m^{-2}d^{-1}$) indicating that seepage is a stable and long-standing feature of this site. Upscaling these rates to area of the entire Puck Bay (520 km^2) results in seepage rates of approx. 0.1 - 0.3 km^3 y^{-1} which is several times higher than what previously estimated based on an hydrogeologic method for the Puck Bay (0.03

km^3 y^{-1}, Piekarek-Jankowska, 1994). This is probably due to the patchy nature of the seepage as it was identified by the salinity survey carried out in this and previous studies (Fig.2, Kotwicki et al., 2013). In addition, SGD is most likely most intense in shallow sandy areas, while more moderate, diffusive efflux can be expected for the muddy sediments in the deeper central Bay (Böttcher et al., unpublished data).
However, any seepage estimate that is referring only to discharge of fresh groundwater will underestimate the true volume of water passing the sediment-water interface as it does not account for the recirculated seawater component (Younger, 1996; Burnett et al., 2003). Several studies, including investigations carried out in Hel Bight, demonstrated that in permeable sands bottom water circulates through the sediment pore space (e.g. Huettel et al., 2003; Cook et al., 2007a). This advective pore water exchange will add to the directed seepage and intensify the connection between pore waters and the overlying water column.

5.4.2 Pore water mixing

In sandy sediments with permeabilities exceeding 10^{-11} m^2 pore water advection may represent the dominating transport mechanism for solutes across the sediment-water interface as well as in the sediments (Huettel and Gust, 1992; Huettel et al., 1996; Hutchinson and Webster, 1998). Pore water advection is typically caused by lateral pressure gradients that result from the interaction of bottom water flow with bottom roughness and topographical features at the sediment surface. In coastal areas where strong hydrodynamic regimes meet high permeabilities the resulting pore water advections results in rates of solutes transport that may exceed molecular diffusivion by up to three orders of magnitude (Huettel and Gust, 1992; Huettel and Webster 2001; Ret al., 2002; Janhke et al., 2003).
As driving forces of pore water advection origin at the sediment surface, mixing is strongest at the sediment-water interface and decreases with increasing sediment depth. Analyzing oxygen distributions in freshly retrieved sandy sediment cores from the North Sea Lohse et al. (1996) could show that mixing coefficients close to the surface were high, resulting in oxygen penetration depths of up to 50 mm. Deeper in the sediment mixing intensity dropped resulting in a sharp decline in oxygen concentration. Experimental studies on oxygenation of permeable sediments confirmed these findings and demonstrated that the oxygen distribution in these sediments is directly connected to topographical features at the sediment-water interface and that oxygen penetration depth increases as a function of bottom water flow velocity (Booij et al., 1991; Forster et al. 1992; Ziebis et al., 1996; Precht et al., 2004).
Deep oxygen penetration, ranging between 10 and 28 mm with an average of 17 mm in

summers was also observed in Hel bight sediments and attributed to pore water advection (Cook et al., 2007a). Later studies of bottom fauna confirmed that a significant contribution of bioirrigation by large pumping macrofauna can be excluded (Kotwicki et al. 2013).

In case of oxygen, vertical distribution patterns are determined by the interplay of rates of advective supply from the bottom water with consumption rates in the sediments. In SGD impacted sites similar characteristics can be expected also for conservative solutes. In this case distributions would be determined by rates of pore water advection, seepage rates, and the difference in concentration between ground and bottom water (i.e., the two endmembers). Assuming constant seepage rates and groundwater composition, the salinity distribution observed at the seep site indicates that mixing intensity decreases with depth (Fig. 5.4). From the sediment water interface to a sediment depth of approx. 7 cm intense advective transport keeps salinities close to seawater values (5-7 psu). The strong gradient in salinities observed between 7 and 10 cm sediment depth imply that rates of advective exchange between the pore water and the overlying water drops at this distance to the sediment surface. At sediment depths between 10-18 cm exchange with bottom waters hardly affected pore water composition and salinities were close to freshwater (<1 psu). Hence, at these depths the upward migration of groundwater clearly outcompetes vertical mixing. The vertical sequence of mixing conditions thus determines the two-layer structure encountered in pore water profiles (Fig. 5.4). Comparing the vertical distributions of the different solutes to the distribution of salinity as a conservative tracer already reveals strong differences in solute behavior. When pore water solutes are plotted relative to salinity that shows a simple two-endmember mixing between seawater and fresh groundwater to types of characteristics can be distinguished. While SO_4^{2-} and DIC exhibited quasi-conservative mixing (Fig. 5.7-A and C), Fe^{2+}, Mn^{2+} and PO_4^{3-} were characterized by non-conservative behavior with significant depletion at low salinities, i.e., at low sediment depths (Fig. 5.7-E, G and I).

5.4.3 Redox controlled solubility of porewater constituents with non-conservative behavior: Mn^{2+}, Fe^{2+} and PO_4^{3-}

Pore water distributions of Mn^{2+}, Fe^{2+} and PO_4^{3-} show pronounced similarities. All three solutes show slightly elevated concentrations deep in the sediment while they are virtually absent in the bottom water. Especially Fe^{2+} but to a lesser extent also Mn^{2+} and PO_4^{3-} show positive excursions from the conservative mixing line at sediment depths between 5 and 10 cm and reach concentrations in excess of the groundwater endmember. In addition to the input by pore waters this indicates a source for Mn^{2+}, Fe^{2+} and PO_4^{3-} at depth and a sink close to the surface. Advective transport of dissolved manganese

and iron and removal in the surface layer of sands has been shown in flume experiments (Huettel et al., 1998). Mn^{2+} and Fe^{2+} were transported upwards from deeper sediment layers where they accumulated under reduced conditions. Upon contact with oxygen in the upper sediment they precipitated and formed a layer at the interface between reduced and oxygenated sediments. A combination of a manganese and iron release under reducing conditions at depth and precipitation at oxygenated conditions close to the surface would also explain the distributions observed in this study - although at least in case of Mn^{2+} the groundwater would act as an additional source of its dissolved form. Processes involved in iron and manganese redox reactions and dissolution/precipitation are well known. The conversion of solid Mn^{4+} and Fe^{3+} into their reduced, soluble form may be microbially mediated as both are used as electron acceptors for microbial organic matter degradation once O_2 and NO_3^- are depleted. In other cases both iron and manganese may interact and be reduced abiotically by reduced species (e.g., H_2S) (Thamdrup et al., 1994; Böttcher et al., 2000). Manganese precipitation in the oxic surface layer of marine sediments typically takes place as manganese oxyhydroxides that occur in the form of amorphous materials and coatings on particles, often in close association with iron oxides (Burdige, 1993). Other than iron and manganese, phosphate does not change its oxidation state and does not precipitate under oxic conditions but can be taken up by organisms and hence removed from the dissolved phase. Uptake by organism at the sediment surface, e.g., by microphytobenthos could contribute to the depletion of phosphate observed in the chamber water. Non-conservative behavior in the sediment, i.e., release at depth and removal close to the surface are most likely associated with the Iron redox cycle. In surface sediments phosphate removal can take place via adsorption onto Fe-hydroxides. Charette and Sholkovitz (2002) and Charette et al. (2005) report scavenging of phosphates onto amorphous Fe-hydroxides that precipitate as fresh Fe-rich groundwater mixes with saline water. A similar sorption process or co-precipitation with Fe-hydroxides would explain the rapid pore water depletion in PO_4^{3-} above salinities of ~2 psu (from 60 to 0.8 μmol L^{-1}). In deeper sediment layers, under reducing conditions, PO_4^{3-} and Fe^{2+} accumulation shows similar patterns (Fig. 5.7-E and I) indicating that PO_4^{3-} accumulation is derived from reduction of Fe-oxides and release of associated P at depth in the sediment. This recycling of Fe and P in the sediment is well described for other near coastal and offshore marine systems (Sundby et al., 1992; Slomp et al., 1996; Anschutz et al. 1998). It has to be stated, however, that dissolved iron concentrations in the deep pore water are relatively low as compared to levels reported in anoxic groundwaters (Charette and Sholkovitz, 2006). This may indicate a relatively little relevance of iron cycling at these site with iron oxide concentrations that are below a level where a significant contribution of bacterial heterotrophic metal oxide reduction is expected (Thamdrup and Canefield, 2000). This may indicate that abiotic processes dominate iron cycling in Hel sediments. In case of manganese, relatively high concentrations (5.4

μmol L^{-1}) were found in the groundwater endmember and SGD clearly had a major impact on the Mn cycle with implications for geochemical gradients at the seep site (Fig. 5.4). The distribution of dissolved Mn suggests that the upward transport by SGD lead to the formation of a boundary between Mn^{2+} and Mn4+ between 5-10 cm depth. Above this horizon, contact to oxygenated water supplied to the sediment by advection may have promoted the precipitation process. Based on recent observations, formation of trivalent Mn(III) can not be ruled out, but will depend on the availability of compelxing lignads to stabilize this metastable species (Madison et al., 2013).
Irrespective of the biological or chemical processes dominating the iron, manganese and phosphorous cycle at the seep site, the deviations from the conservative mixing line in Mn^{2+}, Fe^{2+} and PO_4^{3-} indicate a net upward transfer of dissolved species which is not accounted for by solutes supplied by SGD. Assuming steady state this loss towards the upper sediment layers has to be compensated. Typically, downward transfer of particles by bioturbating fauna closes the loop. However, as previous studies indicate low abundances of large macrofauna (Kotwicki et al., 2013) physical redistribution of the upper sediment column at rough hydrodynamic conditions may be a more likely candidate. Such a replenishment of particulate / particle bound iron, manganese, and phosphate may regularly take place. Given that the main reduction / dissolution takes place at approx. 10 cm sediment depth it may well be that the cycle is largely closed by a "reset" of the system during the stormy season.
The accumulation or removal of groundwater constituents along the groundwater flowpath is vastly important in the interpretation of the ecological impact of SGD (Johannes, 1980; D'Elia et al., 1981; Valiela et al., 1990), and direct measurements such as the ones carried out in this study seem to be the most trustworthy approach. If possible conversions in the sediments are not included in the budgets, the calculation of chemical fluxes using samples from the most inland wells may result in false estimations of the true chemical flux.

5.4.4 Benthic oxygen consumption and net community production

In shallow coastal sediments benthic fluxes of oxygen are governed by decomposition of organic matter by aerobic microorganisms, oxidation of reduced products (e.g., Cai and Sayles, 1996; De Beer et al., 2005), benthic primary production (e.g., Jahnke et al. 2000), and fauna-related O_2 uptake. Apart from respiration, the main contribution of fauna to oxygen uptake takes place via bioirrigation and bioturbation (e.g. Forster and Graf, 1995; Hansen and Kristensen 1997; Glud et al. 2000b, 2003; Vopel et al., 2003) as the redistribution of solids and solutes stimulates aerobic microbial activity and chemical oxidation (e.g. Glud, 2008). As bioirrigation has been reported to be of

minor importance in Hel bight sediments (Kotwicki et al. 2013) it can be assumed, that pore water advection and molecular diffusion represent the main transport mechanisms and that most oxygen consumption takes place via aerobic microbial respiration and oxidation of reduced compounds unrelated to fauna. Due to the seepage measurements carried out in this study the effect of anoxic groundwater that seeps from the sediments and mixes with the overlying water can be quantified and subtracted in order to compare benthic oxygen consumption related to processes taking place in surface sediments of the two sites (black bars in Fig. 5.8, "SGD independent flux").

The SGD independent oxygen uptake at the seep site during the night compares well with rates measured at the reference site (-40 ±15 and -42±9 mmol $m^{-2}d^{-1}$ respectively) indicating that the seepage of groundwater did not change the overall activity of the benthic community. At the seep site, some of the oxygen consumption may be attributed to the re-oxidation of reduced compounds supplied by SGD. If reduced Mn^{2+} and Fe^{2+} contained in the groundwater (5.4 and 1 μmol L^{-1}, respectively) were entirely oxidized by O_2, the TOU fraction associated to this process - a few μmol O_2 L^{-1}- would however be negligible compared to consumptions measured in the chamber incubations (in the order of 100 μmol O_2 L^{-1}).

Oxygen consumption rates measured in this study agree well with O_2 fluxes measured in other coastal sediments (e.g. Callendar and Hammond 1982; Knoppers et al., 1996; Marinelli et al., 1998; De Beer et al., 2005). Using similar benthic chambers at 40 rpm stirring rate in Hel bight sediments not affected by SGD Cook et al. (2007a) reported a lower TOU (-16 mmol $m^{-2}d^{-1}$). The difference may be attributed to lower water temperatures as measurements of Cook and coworkers were carried out in spring and not in late summer like the measurement of this study. Besides, organic carbon content of the top sediment layer was 3 times higher at the time of our study, maybe due to the longer period available for benthic primary production (0.15 % in the top 2 cm compared to 0.05 % in the top cm reported by Cook et al., 2007a). It can thus be hypothesized that the higher oxygen uptake observed in the present study is a consequence of a higher organic carbon availability that fuelled higher rates of microbial respiration.

Similar to respiration rates, net community production (NCP) calculated from SGD independent oxygen fluxes during the day were in the same range for seep and reference site (106 ± 17 and 126 ± 33 mmol C $m^{-2}d^{-1}$ respectively). These values are in the upper range of annual averages reported for sandy and muddy sediments (e.g. 70 - 90 mmol C $m^{-2}d^{-1}$ respectively; Barranguet, 1998), and in the same range as rates reported from chamber experiments carried out by Rasheed et al. (2004) on permeable carbonate sands (98.0±40.7 mmol C $m^{-2}d^{-1}$). Comparing rates of aerobic respiration and oxygen consumption and considering the length of the day, both seep and reference site were clearly net autotrophic at the time of this study. This is already obvious from the overall increase in oxygen concentration during the almost complete day-night cycle

covered by the chamber incubations (Fig. 5.6C, D).

The fact that NCP was similar for the seepage and reference site is puzzling because of elevated concentrations of PO_4^{3-} as well as $SiO3^{2-}$ (data not shown) in the groundwater endmember. While some phosphorous probably got trapped in the oxidized upper sediments (see above) part of nutrients from the ground waters were most likely still available to the microphytobenthos. This is also indicated by the phosphate release from the sediments as observed in chamber water time series (Fig. 5.6M). Similar rates of oxygen release, however, contradict enhanced productivity at the seep site and indicate that microphytobenthos (MPB) in Hel bight is not nutrient limited. This is in agreement with observations for other coastal areas (e.g. Barranguet et al., 1998; Serodio and Catarino 2000, Migne et al. 2004). In a recent study carried out by Rao and Charette (2012), stirred benthic chambers (40 rpm, as for this study) were used to estimate TOU and nitrogen fluxes in sands in shallow waters of a semi enclosed estuary impacted by discharge of nutrient rich suboxic brackish water. Without collecting the seepage water, as in our case, pressure equalization was allowed through a capillary tube open to the surrounding bay water. Despite the load of nutrients supplied by the SGD, benthic photosynthesis (50 - 70 mmol C $m^{-2}d^{-1}$ in May and June) turned out to be mostly controlled by light availability. Light limitation of MPB productivity was also shown by other studies (e.g., Berg and Huettel 2008; Jahnke and Jahnke, 2008).

While NCP rates were similar at both sites it still seems plausible that, due to differences in nutrient availability, carbon fixation is channeled into different organic matter pools. At the seep site higher nutrient levels may facilitate biomass (i.e., particulate organic matter) production while at the reference site a larger share of the fixed carbon may have been secreted as extracellular polysaccharides. Direct transfer of carbon as exudates to the dissolved organic matter pool has been shown to occur, especially under nutrient limitation (e.g., Cook et al., 2007b) and may comprise up to 73 % of the total productivity (Goto et al., 2001). The similar respiration rates at the two sites suggest similar organic carbon remineralization rates. If our hypothesis of different carbon pools holds true this would indicate that nutrient poor dissolved organic matter is consumed at similar high rates as the P- and N-rich particulate organic matter. This is supported by Middelburg et al. (2000) who showed that exudates can be a significant labile carbon source for heterotrophs grazing on MPB. It could thus be hypothesized that SDG, while having no impact on rates of carbon fixation and mineralization, affects pathways of carbon fixation and the trophic structure of the sediment ecosystem. Additional studies are obviously needed to investigate this in more detail.

5.4.5 Aerobic and anaerobic sediment respiration

Dissolved inorganic carbon concentrations in coastal shallow sediments and interfacial fluxes of DIC are caused mainly by uptake of CO_2 during photosynthesis and by CO_2 release upon remineralization of organic compounds and dissolution of carbonates (e.g. Glud, 2008). As carbonate dissolution is considered negligible in Hel sediments (Cook et al., 2007a) the SGD-independent release of DIC at night at the seep site (98 ± 22 mmol $m^{-2}d^{-1}$) and the concurrent uptake of oxygen (see above) is probably largely representative of organic carbon oxidation as it was also shown in other studies (Anderson et al., 1986; Hulth et al., 1997).

Rates of DIC release measured in this study are in the upper range of rates reported from sandy sediments in other studies. Organic-poor marine sands, studied by open-top core incubations, showed rates of 18-40 mmol DIC $m^{-2}d^{-1}$ (Kristensen and Hansen, 1995), 126-150 mmol DIC $m^{-2}d^{-1}$ (Holmer, 1996), 35-41 mmol DIC $m^{-2}d^{-1}$ (Thomsen and Kristensen, 1997). In lab experiments with Mid Atlantic Bight sands, DIC was released at rates of up to 147 mmol DIC $m^{-2}d^{-1}$ (Rusch et al., 2006).

The high rates of this study may be attributed to the summer season where high water temperatures facilitate high rates or organic matter degradation and where most light is available for primary productivity and, hence, a high availability of fresh phytodetritus may be expected.

The ration of O_2:DIC fluxes measured at the seep site (0.4) indicates, that aerobic respiration did only account for 40% of the DIC being produced. Similar or even lower rates have been reported in the literature. Canfield et al. (1993a,b) found that in some temperate coastal sediments, O_2 consumption accounted for only 4-17% of total organic carbon oxidation.

The excess DIC production that is not balanced by oxygen consumption could be explained if organic matter in sediments is mineralized anaerobically using electron acceptors such as NO_3^- and SO_4^{2-}. However, measurements at the reference site indicated that this process probably contributes only little to total mineralization in Hel bight sediments (Wenzhöfer and Glud, unpubl. data), in agreement with no nitrate fouind in the groundwater (Nestler, 2011). Hence, sulfate reduction is the most likely candidate for anaerobic organic matter degradation at the seep site.

Oxygen penetration was not measured directly in this study.

However, the salinity profiles suggest intense flushing of at least the top 10 cm of the sediment, indicating that oxygen needed for aerobic oxidation of organic matter produced in the top layer should have been available. This seems to point to a deeper carbon source that fuelled sulfate reduction and the excess release of DIC. From previous campaigns it was assessed that groundwater contained methane up to the mM-range (Böttcher, Gehre Gentz, unpublished data) so that pore-water sulfate could be consumed by anaerobic

oxidation of methane (AOM; Reeburgh, 1976, Boetius et al., 2000) as an alternative to the oxidation or organic matter by means of sulfate that is referred to as sulfate reduction (SR; e.g., Brener, 1980). The stoichiometry of sulfate reduced per carbonate produced differs between the two processes. An SO_4^{2-}:DIC ratio of 2 is found in SR according to the following reaction:

$$2CH_2O + SO_4^{2-} \rightarrow 2HCO_3 + H_2S \tag{5.3}$$

$$CH_4 + SO_4^{2-} \rightarrow HCO_3 + HS^- + H_2O \tag{5.4}$$

AOM, on the other hand has a SO_4^{2-}:DIC ratio of 1:

Fig. 5.10 compares deviations from conservative mixing below 6.5 cm sediment depth for sulfate and DIC (i.e., ΔSO_4^{2-} and ΔDIC). The ratio of ΔSO_4^{2-}:ΔDIC = 0.8 indicates AOM as the major process consuming SO_4^{2-} in the anoxic sediments at the seep site. It may hence be suggested that SO_4^{2-} is primarily used to oxidize groundwater CH_4 to DIC rather than serve as an electron acceptor for organic matter remineralization.

It was shown by other studies how in methane-rich settings, AOM potentially consumes a significant portion of the interstitial sulfate pool, depleting sulfate more rapidly than oxidation of organic matter alone (Borowski et al., 1996).

Irrespective of the organic carbon pool being oxidized by sulfate reduction, sulfide would be produced at a 1:1 stoichiometry. No sulfide measurements have been performed as part of this study.

Pore water profiles measured in September 2009 in groundwater at the SGD impacted site showed concentrations of up to 150 μmol L^{-1}(Volger et al., 2010) and reported an SO_4^{2-} profile similar to what we have measured (Fig. 5.4).

Even higher sulfide concentrations of up to 480 μmmol $L^{-1}$are expected from the assessment of ΔSO_4^{2-} at 10 cm sediment depth (Fig. 5.10).

The sulfide produced in the sediment is obviously not oxidized by oxygen as the terminal electron acceptor. If this was the case DIC fluxes would have been balanced by oxygen fluxes and no excess DIC flux would have been found. Besides, oxygen consumption at night would have been higher at the seep site where methane for AOM was supplied by SGD. Hence, the fate of H_2S at the seep site sediments must therefore follow a different oxidation path. We hypothesize that sulfide was oxidized to sulfur by Fe^{3+} oxyhydroxides according to the following reaction:

$$2Fe(III)OOH + H_2S \rightarrow 2Fe^{2+} + S(0) + 2H_2O + 4OH^- \tag{5.5}$$

(e.g. Dos Santos and Stumm, 1992). For the reasons stated above this process was obviously not balanced by a concurrent (and oxygen-consuming) reoxidation of Fe^{2+} back to Fe^{3+} oxyhydroxides:

$$2Fe^{2+} + O_2 + 2H_2O \rightarrow 2FeOOH + 2H^+ \tag{5.6}$$

Instead we can hypothesize that the pool of Fe^{3+} oxyhydroxide necessary to oxidize and scavenge dissolved sulfide in the top sediments that were transported upwards by SGD was available in the sediment at the time of our study and is continuously replenished by oxygenated bottom waters penetrating the surface sediments (de beer et al., 2005). FeS may have been temporarily formed via reactions of Fe(II/III) with the excess of H_2S. This may also explain the low contents of dissolved Fe^{2+} that was measured (see Fig. 5.4 and 7E). In times of increased O_2 penetration or deep sediment redistribution at rough hydrodynamic conditions as discussed above, FeS would then be re-oxidized by oxygen to Fe(III)OOH and sulfate (von Rege, 1999).
For the reference site rates of O_2:DIC could not be calculated since we failed to determine reliable DIC fluxes in this study. An O_2:DIC ratio of 1.2 was determined from dark incubations in spring at sites not impacted by SGD (Cook et al., 2007a). This ratio suggests that all organic matter at the non-impacted sites was oxidized with O_2 as the terminal electron acceptor. According to Cook and coworkers it may further be assumed that the sulfur and the iron cycle were of minor importance at the reference site as in their study SR and Fe reduction accounted for only 2 and 10-20% of the total mineralization of organic matter, respectively.

5.5 Conclusions

At both the seep and the reference site aerobic oxidation of organic matter represents the main mineralization pathway and similar rates of total oxygen uptake are observed for both sites. Anaerobic oxidation by means of SO_4^{2-}, Mn, and Fe reduction are present but play a secondary role. The main difference between biogeochemical processes at the two sites is driven by the supply of CH_4 in the groundwater that was quantified by previous studies at the same site. At the reference site, oxidation of organic matter is the predominant reaction that controls interstitial sulfate concentrations. At the seep site where methane is provided by SGD, AOM could be identified as an important process based on a ratio of 0.8 between SO_4^{2-} deficiency to excess DIC. The DIC that is produced by AOM seeps from the sediment at rates that largely exceed oxygen uptake rates and obviously cannot be explained by aerobic oxidation of organic matter in the

surface sediments.

The sulfide generated by sulfate reduction associated with AOM most likely reduces Fe^{3+} oxides that may trap additional sulfide as FeS. From the excess in DIC relative to oxygen we can conclude that an oxidized iron pool existed in the sediment that was large enough to oxidize and trap the sulfide and not quantitatively replenished by the reoxidation of Fe^{2+} at the time of our study.

Small amounts of reduced iron and manganese as well as phosphate are provided by the seeping groundwater. At approx. 10 cm sediment depth additional Fe^{2+}, Mn^{2+}, and PO_4^{3-} is supplied - most likely by iron and manganese reduction and release of phosphate from iron oxides. Before reaching the sediment-water interface the metals are re-oxidized and most of the phosphate is being bound again or taken up, e.g., by microphytobenthos. As in the case of the iron oxides needed for sulfide removal, the mechanism replenishing particulate and oxidized metals as well as associated phosphate in the deeper sediment layers is unknown. As bioturbation is assumed to be of minor importance in Hel bight physical sediment redistribution and reoxidation at rough hydrodynamic conditions is considered most likely.

A moderate efflux of phosphate as well as silicate was observed at the seep site but was not reflected in elevated rates of net primary productivity. Oxygen production was similar at both sites and governed by light rather than by nutrient availability. It is hypothesized that lower nutrient supply at the reference site may favour the release of exudates by benthic phototrophs while more particulate organic matter may be produced at the seep site. Similar respiration rates at both sites during night-time, however, suggest that both carbon sources are utilized by aerobic heterotrophs. Key questions that need to be addressed in order to better understand the effect of SGD on the function of sedimentary ecosystems in Hel bight include (1) differences in primary products and their effect on the trophic structure, (2) seasonal patterns in iron cycling, and (3) the fate of volatile sulfur produced from sulfides upon the reduction of iron oxides.

Acknowledgements

We would like to thank Lechu Kotwicki, Beate Szymczycha and the staff working at Hel Marine Station (Institute of Oceanography in the Faculty of Oceanography and Geography at the University of Gdansk) for the support during the field campaign and Susan Volger for providing useful data. We thank Patrick Meyer for the great help during the work at sea, the technicians of the Microsensor department, Sea-Tech hall and electronic workshop (MPI, Bremen) for providing sensors and helping with the assembly of the instruments used in this work. Financial support for this work was

provided by the AMBER project (BONUS+ initiative), EU 7^{th} FP SENSEnet project and Max Plank Society.

References

Anderson, L. G., Hall, P. O. J., Iverfeldt, A., VanDerloeff, M.M.R., Sundby, B. and Westerlund, S. F. G. (1986). Benthic respiration measured by total carbonate production. Limnology and Oceanography 31: 319-329

Anschutz, P., Zhong S.J., Sundby B., Mucci A. and Gobeil C. (1998). Burial efficiency of phosphorus and the geochemistry of iron in continental margin sediments. Limnology and Oceanography 43: 53-64

Appelo, C.A.J. and Postma D. (2005). Geochemistry, groundwater and pollution, A.A. Balkema, Rotterdam

Barranguet, C., Kromkamp, J. and Peene, J. (1998). Factors controlling primary production and photosynthetic characteristics of intertidal microphytobenthos. Marine Ecology Progress Series, 173

Beck, M., Dellwig, O., Kolditz, K., Freund, H., Liebezeit, G., Schnetger, B. and Brumsack, H.-J. (2007a). In situ pore water sampling in deep intertidal flat sediments. Limnology and Oceanography Methods 5, 136-144

Beck, A.J., Tsukamoto, Y., Tovar-Sanchez, A., Huerta-Diaz, M., Bokuniewicz, H.J. and Sanudo-Wilhelmy, S.A. (2007b). Importance of geochemical transformations in determining submarine groundwater discharge-derived trace metal and nutrient fluxes. Applied Geochemistry 22:477-90

Beck, A.J., Rapaglia, J.P., Cochran, J.K., Bokuniewicz, H.J. and Yang, S., (2008). Submarine groundwater discharge to Great South Bay, NY, estimated using Ra isotopes. Marine Chemistry 109, 279-291

Belanger, T.V. and Montgomery, M.E. (1992). Seepage meter errors. Limnology and Oceanography 37:1787-95

Berg, P. and M. Huettel (2008). Monitoring the seafloor using the non invasive eddy correlation technique: Integrated benthic exchange dynamics, Oceanography, 21, 164-167

Boehm, A.B., Shellenbarger, G.G. and Paytan, A., (2004). Groundwater discharge: potential association with fecal indicator bacteria in the surf zone. Environmental science and technology, 38(13), pp.3558-66

Boehm, A.B., Paytan, A., Shellenbarger, G.G. and Davis, K.A. (2006). Composition and flux of groundwater from a California beach aquifer: Implications for nutrient supply to the surf zone, Continental Shelf Research, 26, 269-282

Boetius, A., Ravenschlag, K., Schubert, C.J., Rickert, D., Widdel, F., Gieseke, A., Amann, R., J, B.B., Witte, U. and Pfannkuche, O. (2000). A marine microbial consortium apparently mediating anaerobic oxidation of methane. Nature 407 (6804), 623-626

Bokuniewicz, H. J. (1992). Analytical descriptions of subaque- ous groundwater seepage. Estuaries, 15, 458-464

Booij, K., Helder, W. and Sundby B. (1991). Rapid redistribution of oxygen in a sandy sediment induced by changes in the flow velocity of the overlying water. Netherlands Journal of Sea Research 28: 149-165

Böttcher, M.E., Hespenheide, B., Llobet-Brossa, E., Beardsley, C., Larsen, O., Schramm, A., Wieland, A., Böttcher, G., Berninger, U.G. and Amann, R. (2000). The biogeochemistry, stable isotope geochemistry, and microbial community structure of a temperate intertidal mudflat: an integrated study. Continental Shelf Research 20:1749-1769

Borowski, W.S., Paull, C.K. and Ussler III, W., (1996). Marine pore-water sulfate profiles indicate in situ methane flux from underlying gas hydrate. Geology 24 (7), 655-658

Brener, R.A. (1980). Early Diagenesis-A Theroretical Approach. Princeton University Press

Bruland, K., (1983). Trace elements in seawater, in Chemical Oceanography, 2nd Edition, Vol. 8, ed. Riley, J. P., and Chester, R., pp. 147-220, Academic, London

Burdige, D.J. (1993). The biogeochemistry of manganese and iron reduction in marine sediments. Earth-Science Reviews 35, 249-284

Burnett, W.C., Bokuniewicz, H., Huettel, M., Moore, W.S. and Taniguchi, M. (2003). Groundwater and pore water inputs to the coastal zone. Biogeochemistry 66, 3-33

Burnett, W.C., Aggarwal, P.K., Bokuniewicz, H., Cable, J.E., Charette, M.A., Kontar, E., Krupa, S., Kulkarni, K.M., Loveless, A., Moore, W.S., Oberdorfer, J.A., Oliveira, J., Ozyurt, N., Povinec, P., Privitera, A.M.G., Rajar, R., Ramessur, R.T., Scholten, J., Stieglitz, T., Taniguchi,M. and Turner, J.V. (2006). Quantifying submarine groundwater discharge in the coastal zone via multiple methods. The Science of the Total Environment 367, 498-543

Cable, J.E. and Martin, J.B. (2008). In situ evaluation of nearshore marine and fresh pore water transport into Flamengo Bay, Brazil. Estuarine, Coastal and Shelf Science, 76(3), pp.473-483

Cai, W.-J. and Sayles, F.L. (1996). Oxygen penetration depths and fluxes in marine sediments. Marine Chemistry, 52, 123-131

Callender, E. and Hammond, D.E. (1982). Nutrient exchanges across the sediment water interface in the Potomac River Estuary. Estuarine Coastal and Shelf Science 15, 395-413

Canfield, D.E., J, B.B., Fossing, H., Glud, R., Gundersen, J., Ramsing, N.B., Thamdrup, B., Hansen, J.W., Nielsen, L.P. and Hall, P.O.J. (1993a). Pathways of organic carbon oxidation in three continental margin sediments. Marine Geology 113, 27-40

Canfield, D.E., Thamdrup, B. and Hansen, J.W. (1993b). The anaerobic degradation of organic matter in Danish coastal sediments: iron reduction, manganese reduction, and sulfate reduction. Geochimica et Cosmochimica Acta 57, 3867-3883

Carr, M.R. and Winter T.C. (1980). An annotated bibliography of devices developed for direct measurement of seepage. USGS Open-File Report 80-344, Denver, CO, 38pp

Charette, M.A., Buesseler, K.O. and Andrews, J.E. (2001). Utility of radium isotopes for evaluating the input and transport of groundwater-derived nitrogen to a Cape Cod estuary. Limnology and Oceanography 46(2), 465-470

Charette, M.A. and Sholkovitz, E.R. (2002). Oxidative precipitation of groundwater-derived ferrous iron in the subterranean estuary of a coastal bay. Geophysical Research Letters 29

Charette M.A. and Buesseler, K.O. (2004). Submarine groundwater discharge of nutrients and copper to an urban subestuary of Chesapeake Bay (Elizabeth River). Limnology and Oceanography 49:376-85

Charette, M.A., Sholkovitz E.R. and Hansel, C.M. (2005), Trace element cycling in a subterranean estuary: Part 1. Geochemistry of the permeable sediments, Geochimica et Cosmochimica Acta, 69, 2095-2109

Charette, M.A. and Sholkovitz, E.R. (2006). Trace element cycling in a subterranean estuary: Part 2. Geochemistry of the pore water, Geochimica et Cosmochimica Acta, 70, 811-826

Church, T. M. (1996). An underground route for the water cycle. Nature 380, 579-580

Clark, I.D. and Fritz, P. (1997). Environmental Isotopes in Hydrology. Lewis Publishers, New York, 328 pp

Cook, P. L. M.,Wenzhoefer, F., Glud, R. N., Janssen, F. and Huettel, M. (2007a). Benthic solute exchange and carbon mineralization in two shallow subtidal sandy sediments: Effect of advective pore-water exchange, Limnology and Oceanography 52(5), 1943-1963

Cook, P. L. M., Veuger, B., Boer, S. and Middelburg, J. J. (2007b). Effect of nutrient availability on carbon and nitrogen incorporation and flows through benthic algae and bacteria in near-shore sandy sediment, Aquatic Microbial Ecology 40, 165-180

Costa, O.S., Attrill, M.J. and Nimmo, M. (2006). Seasonal and spatial controls on the delivery of excess nutrients to nearshore and offshore coral reefs of Brazil. Journal of Marine Systems, 60(1-2), pp.63-74

D Elia, C.F., Webb, K.L., Porter, J.W., (1981). Nitrate-rich ground water inputs to Discovery Bay, Jamaica: a significant source of N to local reefs?. Bulletin of Marine Science 31, 903-910

De Beer, D., F. Wenzhoefer, T.G.Ferdelman, S.E.Boheme, M. Huettel, J.E.E. Van Beusekom, M.E. Böttcher, N. Musat, and N. Dubilier (2005). Transport and mineralization rates in North Sea sandy intertidal sediments, Sylt-RøBa- sin, Wadden Sea. Limnology and Oceanography 50: 113-127

Dos Santos, A.M. and Stumm, W. (1992). Reductive dissolution of iron(III) (hydr)oxides by hydrogen sulfide. Langmuir 8:1671-1675

Emery, K.O. (1968). Relict sediments on continental shelves of world. Am. Assoc. Pet. Geol. Bull. 52: 445-464

Falkowska, L. and Piekarek-Jankowska, H. (1999). Submarine seepage of fresh groundwater: disturbance in hydrological and chemical structure of the water column in the Gda?sk Basin. ICES Journal of Marine Science 56, 153-160

Fellows, C.R. and Brezonik, P.L. (1980). Seepage flow into Florida lakes. Water Resources Bulletin 16:635-41

Forster, S. and Graf, G. (1992). Continuously measured changes in redox potential influenced by oxygen penetrating from burrows of Callianassa subterranea. Hydrobiologia., 235/236, 527-532

Forster, S., Huettel, M. and Ziebis, W. (1996). Impact of boundary layer flow velocity on oxygen utilisation in coastal sediments. Marine Ecology Progress Series 143, 173-185

Fry, B. (2002). Conservative mixing of stable isotopes across estuarine salinity gradients: A conceptual framework for monitoring watershed influences on downstream fisheries production. Estuaries 25: 264-271

Gazeau, F., Smith, S.V., Gentill, B., Frankignoulle, M., Gattuso, J.-P., (2004). The European coastal zone: characterization and first assessment of ecosystem metabolism. Estuarine Coastal and Shelf Science, 60, 673-694

Glud, R.N., Risgaard-Petersen, N., Thamdrup, B., Fossing, H. and Rysgaard, S. (2000b). Benthic carbon mineralization in a high-artic sound (Young Sound, NE Greenland). Marine Ecology Progress Series 206, 59-71

Glud, R.N., Gundersen, J.K., Røy, H. and Jørgensen, B.B. (2003). Seasonal dynamics of benthic O_2 uptake in a semienclosed bay: Importance of diffusion and faunal activity. Limnology and Oceanography 48(3), 1265-1276

Glud, R.N. (2008). Oxygen dynamics of marine sediments. Marine Biology Research, 4(4), pp.243-289

Goto, N., Mitamura, O. and Terai, H. (2001). Bidegradation of photosynthetically produced extracellular organic carbon from intertidal benthic algae. Journal of Experimental Marine Biology and Ecology 257, 73-86

Grasshoff, K., Kremling, K. and Ehrhardt, M. (1983). Methods of seawater analysis. Wiley-VHC, Berlin, Germany, p. 419

Hansen, K. and Kristensen, E. (1997). Impact of macrofaunal recolonization on benthic metabolism and nutrient fluxes in a shallow marine sediment previously overgrown with macroalgal mats. Estuarine, Coastal and Shelf Science 45:613,28

Holliday, D., Stieglitz T.C., Ridd P.V. and Read W.W. (2007). Geological controls and tidal forcing of submarine groundwater discharge from a confined aquifer in a coastal sand dune system. Journal of Geophysical Research, 112, C04015

Holmer, M. (1996) Composition and fate of dissolved organic carbon derived from phytoplankton detritus in coastal marine sediments. Marine Ecology Progress Series 141, 217-228.

Hu, C., Muller-Karger, F.E. and Swarzenski, P.W. (2006). Hurricanes, submarine groundwater discharge, and Florida?s red tides. Geophysical Research Letters, 33(11), p.L11601

Huettel, M. and Gust, G. (1992). Impact of bioroughness on interfacial solute exchange in permeable sediments. Marine Ecology Progress Series, 89: 253-267

Huettel, M., Ziebis, W. and Forster, S. (1996). Flow-induced uptake of particulate matter in permeable sediments. Limnology and Oceanography 41, 309-322

Huettel, M., Ziebis, W., Forster, S. and Luther, G.W. (1998). Advective transport affecting metal and nutrient distributions and interfacial fluxes in permeable sediments. Geochimica et Cosmochimica Acta 62, 613-631

Huettel, M., Rusch, A., (2000). Transport and degradation of phytoplankton in permeable sediment. Limnology and Oceanography 45, 534-549.

Huettel, M., and Webster I.T. (2001). Porewater flow in permeable sediments, in The Benthic Boundary Layer: Transport Processes and Biogeochemistry, edited by B. P. Boudreau and B. B. J, pp. 144-177, Oxford Univ. Press, New York

Huettel, M., Roy, H., Precht, E. and Ehrenhauss, S. (2003). Hydronamical impact on biogeochemical processes in aquatic sediments. Hydrobiologia 494, 231-236

Hulth, S., Tengberg, A., Landen, A. and Hall P.O.J. (1997). Mineralization and burial of organic carbon in sediments of the Southern Weddell Sea. Deep-Sea Research I 44:955,81

Hutchinson, P.A. and Webster, I.T. (1998). Solute uptake in aquatic sediments due to current-obstacle interactions. Journal of Environmental Engineering 124: 419-426

Jahnke, R.A. and Christiansent, M.B. (1989). INSTRUMENTS AND METHODS A free-vehicle benthic chamber instrument for sea floor studies. Deep Sea Research, 36(4), pp.625-637

Jahnke, R.A., Nelson, J.R., Marinelli, R.L. and Eckman, J.E. (2000). Benthic flux of biogenic elements on the Southeastern US continental shelf: influence of pore water advective transport and benthic microalgae. Continental Shelf Research, 20: 109-127

Jahnke, R. A., Alexander, C. R. and Kostka, J. E. (2003). Advective pore water input of nutrients to the Satilla River Estuary, Georgia, USA. Estuarine Coastal and Shelf Science, 57, 641-653

Jahnke, D.B. and Jahnke R.A. (2008). Dynamics of seafloor processes: Advances from benthic observing technologies. Oceanography 21(4):162-163

Jankowska, H., Matciak, M. and Nowacki, J. (1994). Salinity variations as an effect of groundwater seepage through the seabed (Puck Bay, Poland). Oceanologia 36 (1), 33-46

Janssen, F., Huettel, M. and Witte, U. (2005). Pore-water advection and solute fluxes in permeable marine sediments (II): Benthic respiration at three sandy sites with different permeabilities (German Bight, North Sea). Limnology and Oceanography, 50(3), pp.779-792

Janssen, F., Cardenas, M. B., Sawyer, A. H., Dammrich, T., Krietsch, J. and de Beer, D. (2012). A comparative experimental and multiphysics computational fluid dynamics study of coupled surface-subsurface flow in bed forms, Water Resources Research 48: W08514

Jeong, J., Kim, G. and Han, S. (2012). Influence of trace element fluxes from submarine groundwater discharge (SGD) on their inventories in coastal waters off volcanic island, Jeju, Korea. Applied Geochemistry, 27(1), pp.37-43

Johannes, R. E. (1980) The ecological significance of the submarine discharge of groundwater. Marine Ecology Progress Series, 3, 365-373

Kim, G., Ryu, J., Yang, H. and Yun, S. (2005). Submarine groundwater discharge (SGD) into the Yellow Sea revealed by Ra and Ra isotopes: implication for global silicate fluxes. Earth Planet. Sci. Lett. 237, 156-166

Klimant, I., Meyer, V. and Kühl, M. (1995). Fiber-optic oxygen microsensors, a new tool in aquatic biology. Limnology and Oceanography, 40(6), pp.1159-1165

Knoppers, B., Landim De Souza Weber, F., Landim De Souza Marcelo, F., Rodriquez Eliane, G., Landim Elisa Fatima Da Cunha, V. and Vieira Antonio, R. (1996). In situ measurements of benthic primary production, respiration and nutrient fluxes in a hypersaline coastal lagoon of SE Brazil. Revista Brasileira de Oceanografia 44, 155-165

Kotwicki, L., Grzelak, K., Czub, M., Dellwig, O., Gentz, T., Szymczycha, B., Böttcher, M. (2013). Submarine groundwater discharge to the Baltic coastal zone: Impacts on the meiofaunal community. Journal of Marine Systems.

Kowalski, A. F., Hawley, S. L., Hilton, E. J., Becker, A. C., West, A. A., Bochanski, J. J. and Sesar, M. (2009). Dwarfs in Sloan Digital Sky Survey Stripe 82: Photometric Light Curves and Flare Rate Analysis B. 2009, AJ, 138, 633

Kristensen, E. and Hansen, K. (1995). Decay of plant detritus in organic-poor marine sediment: Production rates and stoichiometry of dissolved C and N compounds. Journal of Marine Resources, 53, 675-702

Libelo, E.L. and MacIntyre, W.G. (1994). Effects of surface-water movement on seepage-meter measurements of flow through the sediment-water interface Hydrogeology Journal, 2:49-54

Lohse, L., Epping E.H.G., Helder, W. and VanRaaphorst, W. (1996). Oxygen pore water profiles in continental shelf sediments of the North Sea: turbulent versus molecular diffusion. Marine Ecology Progress Series 145:63-75

Madison, A.S., Tebo, B. M., Mucci, A., Sundby, B. and Luther III, G.W. (2013). Abundant porewater Mn(III) is a major component of the sedimentary redox system. Science (New York, N.Y.), 341(6148), pp.875-8.

Marinelli, R.L., Jahnke, R.A., Craven, D.B., Nelson, J.R. and Eckman, J.E. (1998). Sediment nutrient dynamics on the South Atlantic Bight continental shelf. Limnology and Oceanography 43: 1305-1320

Martin, J.B., Cable, J.E., Jaeger, J., Hartl, K. and Smith, C.G. (2006). Thermal and chemical evidence for rapid water exchange across the sediment-water interface by bioirrigation in the Indian River Lagoon, Florida. Limnology and Oceanography 51, 1332-1341

Martin, J.B., Cable, J.E., Smith, C., Roy, M. and Cherrie, J. (2007). Magnitudes of submarine groundwater discharge from marine and terrestrial sources: Indian River Lagoon, Florida. Water Resources Research, 43(5)

McCoy, C., Corbett, D.R., Cable, J.E. and Spruill, R.K. (2007). Hydrogeological characterization of southeast coastal plain aquifers and groundwater discharge to Onslow Bay, North Carolina (USA). Journal of Hydrology, 339(3-4), pp.159-171

Middelburg, J.J., Barranguet, C., Boschker, H.T.S., Herman, P.M.J., Moens, T. and Heip, C.H.R. (2000). The fate of intertidal micro- phytobenthos carbon. An in situ 13C labelling study. Limnology and Oceanography 45, 1224-1234

Mign., Spilmont, N. and Davoult, D. (2004). In situ measurements of benthic primary production during emersion: seasonal variations and annual production in the Bay of Somme (eastern English Channel, France). Continental Shelf Research, 24(13-14), pp.1437-1449

Montlucon, D. and Sanudo-Wilhemey, S. A. (2001) Influence of net groundwater discharge on the chemical composition of a coastal environment: Flanders Bay, Long Island, New York. Environmental Science and Technology, 35, 480-486

Moore, W. S. (1999) The subterranean estuary: A reaction zone of ground water and sea water. Marine Chemistry 65, 111-125.

Moore, W.S. and Wilson, A.M. (2005). Advective flow through the upper continental shelf driven by storms, buoyancy, and submarine groundwater discharge. Earth and Planetary Science Letters, 235(3-4), pp.564-576

Moore, W.S. (2010). The Effect of Submarine Groundwater Discharge on the Ocean. Annual Review of Marine Science, 2(1), pp.59-88

Mulligan, A.E. and Charette, M.A. (2009). Groundwater flow to the coastal ocean. Encyclopedia of Ocean Science 2009;32:3842-51

Nestler, S. (2011). Diploma thesis, University of Rostock.

Nixon, S.W., Oviatt, C.A., Frithsen, J. and Sullivan, B. (1986). Nutrients and the productivity of estuarine and coastal marine ecosystems. J. Limnol. Soc. South Africa 12, 43-71

Oberdorfer, J.A., Valentino, M.A. and Smith, S.V. (1990). Groundwater Contribution to the Nutrient Budget of Tomales Bay, California. Biogeochemistry 10(3), 199-216

Opalinski, K.W., Maciejewska, K., Urban-Malinga, B. and Weslawski, J.M. (2010). The oxygen fluxes of sandy littoral areas: Quantifying primary and secondary producers in the Baltic Sea. Marine Pollution Bulletin, 61, 211-214

Paerl, H.W. and Carolina, N. (1997). Coastal eutrophication and harmful algal blooms?: Importance of atmospheric deposition and groundwater as ? new ? nitrogen and other nutrient sources. Limnology and Oceanography, 42

Piekarek-Jankowska, H., Matciak, M. and Nowacki, J. (1994). Salinity variations as an effect of ground- water seepage through the seabed (Bay of Puck, Poland). Oceanologia; 36:33-46

Piekarek- Jankowska, H. (1996). Hydrochemical effects of submarine groundwater discharge to the Puck Bay. Geographia Polonica, 67, 103-119

Precht, E., Franke, U., Polerecky, L. and Huettel, M. (2004). Oxygen dynamics in permeable sediments with wave-driven pore water exchange. Limnology and Oceanography. 49: 693-705

Rao, A.M.F. and Charette, M.A. (2012). Benthic Nitrogen Fixation in an Eutrophic Estuary Affected by Groundwater Discharge. Journal of Coastal Research coas-28-05-22.3d

Rapaglia, J., Koukoulas, S., Zaggia, L., Lichter, M., Manfe, G. and Vafeidis, A.T. (2012). Quantification of submarine groundwater discharge and optimal radium sampling distribution in the Lesina Lagoon, Italy. Journal of Marine Systems, 91, 11-19

Rasheed, M., Wild, C., Franke, U. and Huettel, M. (2004). Benthic photosynthesis and oxygen consumption in permeable carbonate sediments at Heron Island, Great Barrier Reef, Australia. Estuarine, Coastal and Shelf Science 59, 139-150

Reeburgh, W.S. (1976). Methane consumption in Cariaco Trench waters and sediments. Earth Planet. Science Letters, 28, 337-344

Røy, H., Huettel, M. and Jørgensen B. B. (2002). The role of small-scale sediment topography for oxygen flux across the diffusive boundary layer. Limnology and Oceanography, 47:837-847

Rusch, A., Huettel, M.,Wild, C. and Reimers, C. E. (2006). Benthic oxy- gen consumption and organic matter turnover in organic-poor, permeable shelf sands, Aquatic Geochemistry, 12, 1-19

Santos, I. R., Cook, P. L. M., Rogers, L., de Weys, J. and Eyre, B. D. (2012). The ??salt wedge pump??: Convection-driven pore-water exchange as a source of dissolved organic and inorganic carbon and nitrogen to an estuary , Limnology and Oceanography, 57(5), 1415-1426

Serodio, J. and Catarino, F. (2000). Modelling the primary productivity of intertidal microphytobenthos?: time scales of variability and effects of migratory rhythms. Marine Ecology Progress Series , 192, pp.13-30

Shaw, R.D. and Prepas, E.E. (1990). Groundwater-lake interactions: I. Accuracy of seepage meter estimations of lake seepage. Journal of Hydrology 119, 105-120

Slomp, C. P., Epping, E. H. G., Helder, W. and Van Raaphorst, W. (1996). A key role for iron-bound phosphorus in authigenic apatite formation in North Atlantic continental platform sediments. Journal of Marine Research, 54, 1179-1205

Sundby B., Gobeil Ch., Silverberg N. and Mucci A. (1992). The phosphorus cycle in coastal marine sediments, Limnology and Oceanography, 37, 1129-1145

Taniguchi,M., Ishitobi,T., Shimada, J. and Takamoto,N. (2006). Evaluations of spatial distribution of submarine groundwater discharge. Geophysical Research Letters, 33 (6)

Tengberg, A., De Bovee, F., Hall, P., Berelson, W., Chadwick, D., Ciceri, G., Crassous, P., Devol, A., Emerson, S., Gaga, J., Glud, R., Graziottini, F., Gundersen, J., Hammond, D., Helder, W., Hinga, K., Holby, O., Jahnke, R., Khripounoff, A., Lieberman, S., Nuppenau, V., Pfannkuche, O., Riemers, C., Rowe, G., Sahami, A., Sayles, F., Schurter, M., Smallman, D., Wehrli, B. and De Wilde, P. (1995). Benthic chamber and profiling landers in oceanography - a review of design, technical solutions and functioning. Progress in Oceanography, 35, 253-294

Tengberg, A., P.O.J. Hall, U. Andersson, B. Liden, O. Styrenius, G. Boland, F. de Bovee, B. Carlsson, S. Ceradini, A. Devol, G. Duineveld, J.U. Friemann, R.N. Glud, A. Khripounoff, J. Leather, P. Linke, L. Lund-Hansen, G. Rowe, P. Santschi, P. de Wilde and U. Witte. (2005). Intercalibration of benthic flux chambers II. Hydrodynamic characterization and flux com- parison of 14 different designs. Marine Chemistry, 94: 147-173

Thamdrup, B., Fossing, H. and Jørgensen, B.B. (1994). Manganese, iron, and sulphur cycling in a coastal marine sediment, Aarhus Bay, Denmark. Geochimica et Cosmochimica Acta, 58, 5115-5129

Thamdrup, B. and Canfield, D.E. (2000). Benthic respiration in aquatic sediments. In: Sala, O.E., Jackson, R.B., Mooney, H.A., Howarth, R.W. (Eds.), Methods in Ecosystem Science. Springer, New York, pp. 86-103

Thomsen, U. and Kristensen, E. (1997). Dynamics of SCO_2 in a surficial sandy marine sediment: The role of chemoautotrophy. Aquatic Microbial Ecology, 12, 165-176

Valiela, I., Costa, J., Foreman, K., Teal, J.M., Howes, B. and Aubrey, D. (1990). Transport of groundwater-borne nutrients from watersheds and their effects on coastal waters. Biogeochemistry 10, 177-197

Vogler, S., Szymczycha, B., Gentz, T., Dellwig, O., Kotwicki, L., Endler, R., Pempkowiak, J., Weslawski, J.M., Schlüter, M. and Böttcher, M.E. (2010). The impact of submarine ground water discharge on a coastal ecosystem of the southern Baltic Sea: Results from the BONUS+ project AMBER. Geophysical Research Abs. 12, 2974

Von Rege, H. (1999). Bedeutung von Mikroorganismen des Schwefelkreislaufes fur die Korrosion von Metallen. Univ. of Hamburg

Vopel, K., D. Thistle and R. Rosenberg (2003). Effect of the brittle star Amphiura filiformis (Amphiuridae, Echinodermata) on oxygen flux into the sediment, Limnology and Oceanography, 48, 2034-2045

Younger, P.L. (1996). Submarine groundwater discharge. Nature 382, 121-122

Ziebis, W., M. Huettel and S. Forster (1996). Impact of biogenic sediment topography on oxygen fluxes in permeable seabeds. Marine Ecology Progress Series, 140: 227-237

Wilson, A.M. (2005). Fresh and saline groundwater discharge to the ocean: Aregional perspective. Water Resources Research 41.

Winde, V., Böttcher, M. E., Escher, P., Böning, P., Beck, M., Liebezeit, G. and Schneider, B. (2013). Tidal and spatial variations of DI13C and aquatic chemistry in a temperate tidal basin during winter time. Journal of Marine Systems.(accepted)

Figures

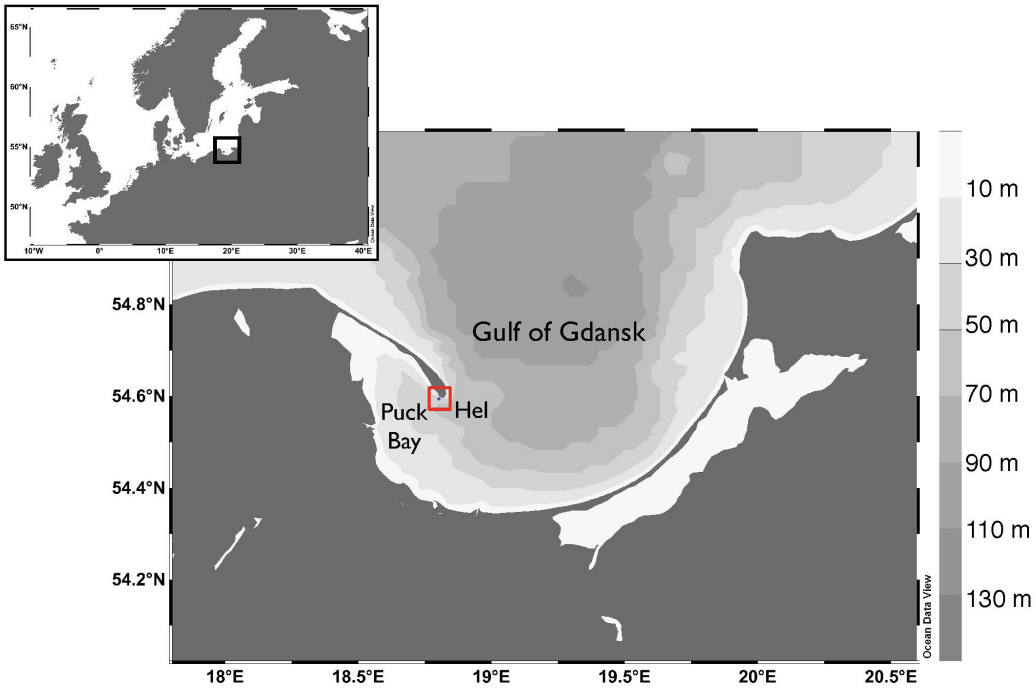

FIGURE 5.1: Map of the study site, Hel bight (red square) in southern Baltic Sea, Poland.

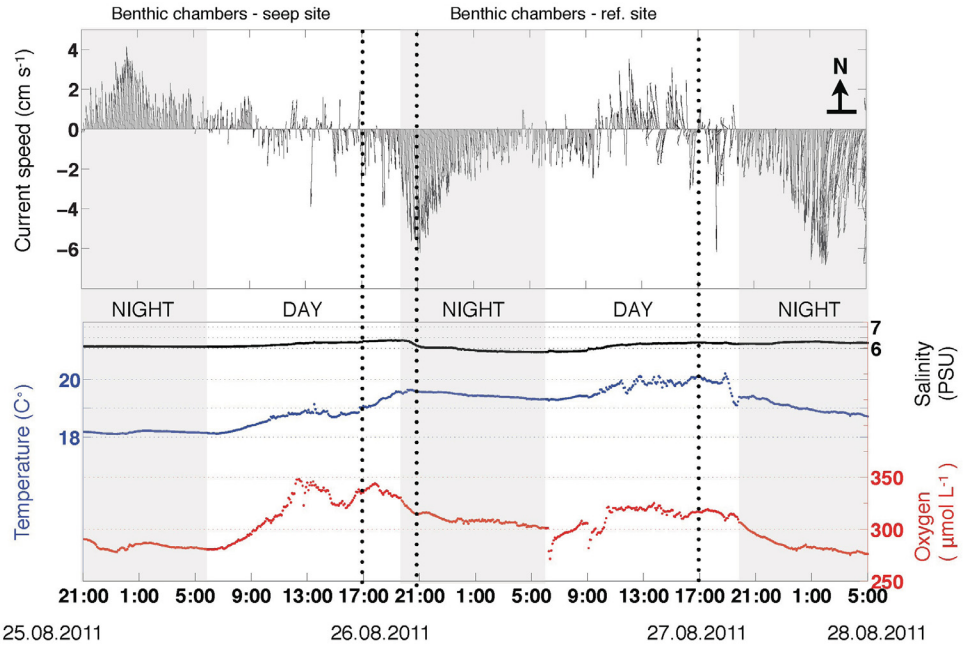

FIGURE 5.2: Time series of in situ current speed and direction (top panel), temperature, salinity, and O_2 concentrations (lower panel), measured using a Seaguard RCM data logging device concomitantly to the deployment of benthic flux chambers (deployment time marked by dotted lines) at Hel bight (1.5 m depth).

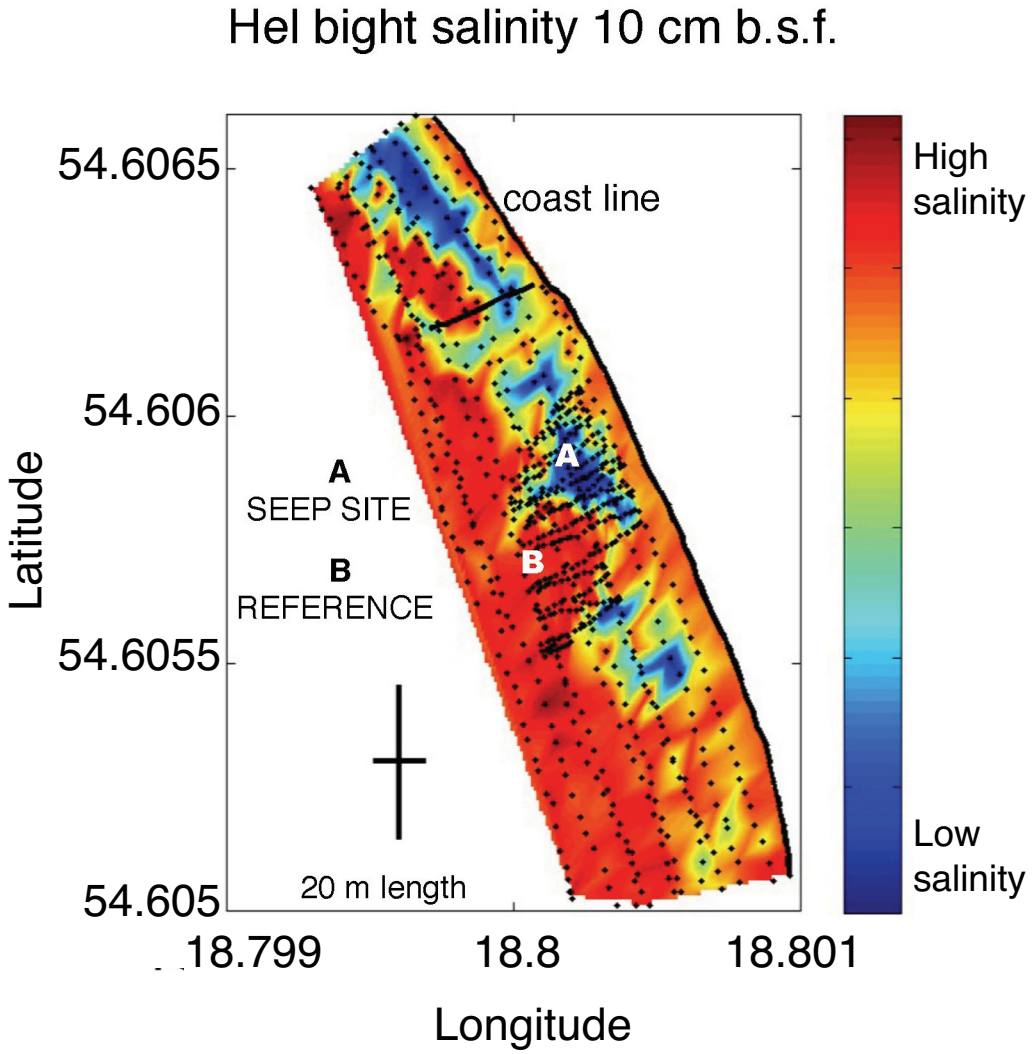

FIGURE 5.3: Map of the main seepage areas at Hel bight obtained by high resolution survey with a temperature and conductivity sensor. Black dots indicate the spots where conductivity and temperature were measured in situ at 10 cm b.s.f. The areas in blue indicate sites of major groundwater discharge (the 20 m length is referred to the vertical line of the cross).

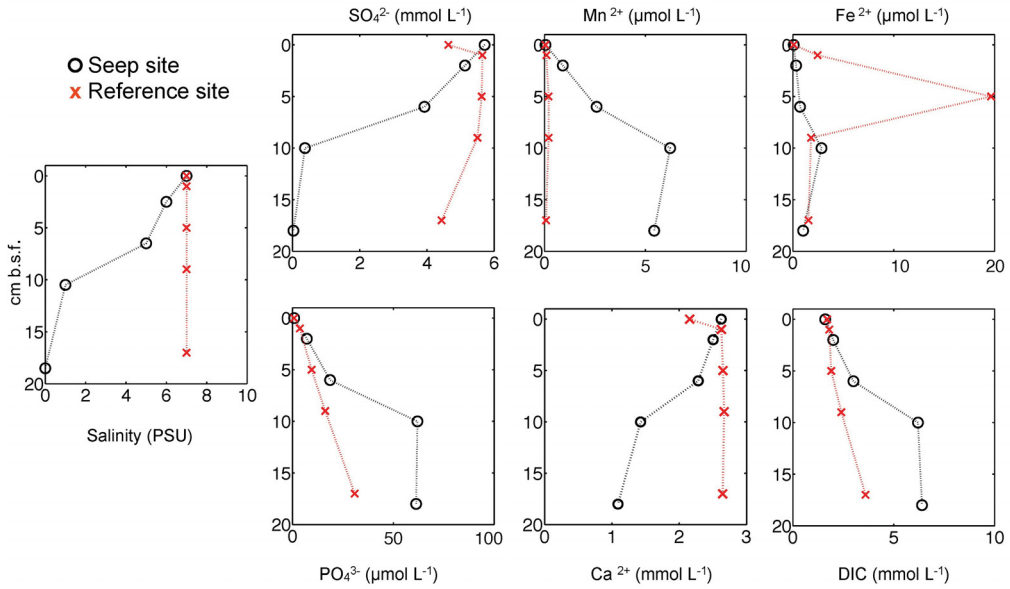

FIGURE 5.4: Porewater distribution of salinity, SO_4^{2-}, Fe^{2+}, Mn^{2+} ,PO_4^{3-} ,Ca^{2+} and DIC until 18 cm below the seafloor, at the site impacted by SGD (seep site, black circles) and site non impacted by SGD (reference, red crosses).

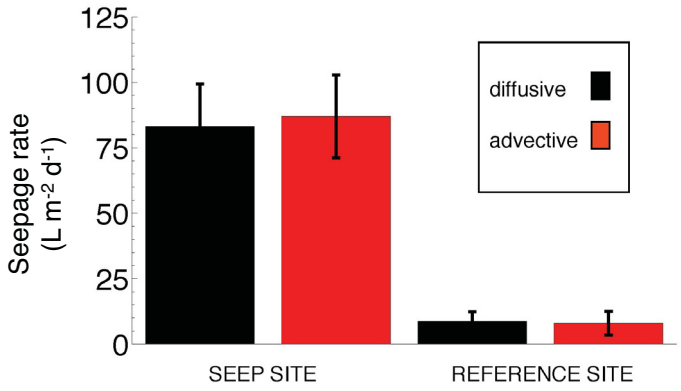

FIGURE 5.5: Seepage rates at seep and reference site estimated from benthic chambers with advective stirring (red bar) and non-advective (diffusive) stirring (black bar).

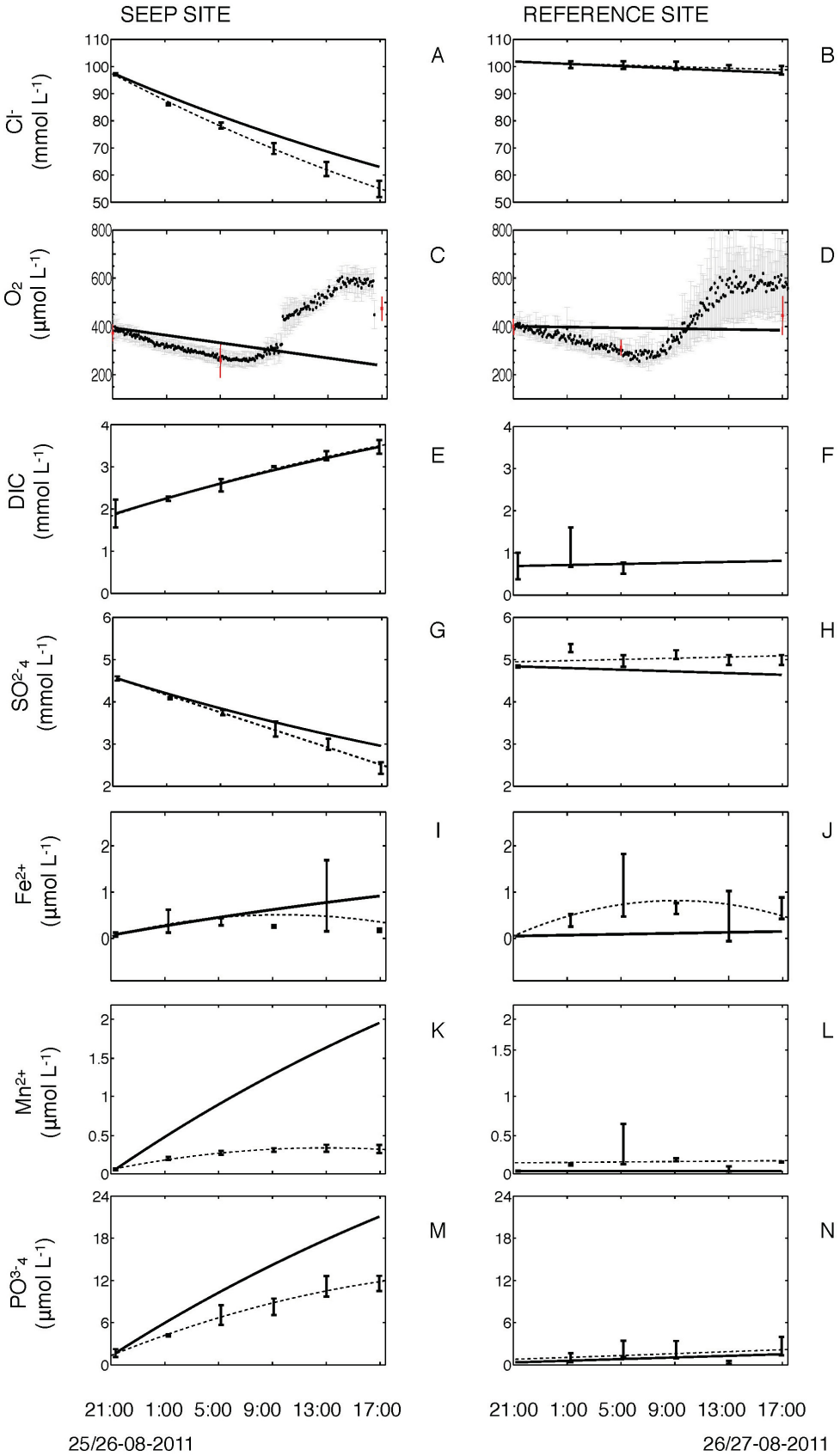

FIGURE 5.6: Time series for Cl^-, O_2, DIC, SO_4^{2-}, Fe^{2+}, Mn^{2+} and PO_4^{3-} concentrations along flux chambers incubation period compared to the theoretical dilution (solid line) at the site impacted by SGD (seep) and non impacted by SGD (reference). Error bars represent standard deviations for the average among 3 chambers, while the trend lines for discrete measurements are calculated by 2nd order polynomial fit. The O_2 plot includes concentrations with error bars from Winkler titration (red dots).

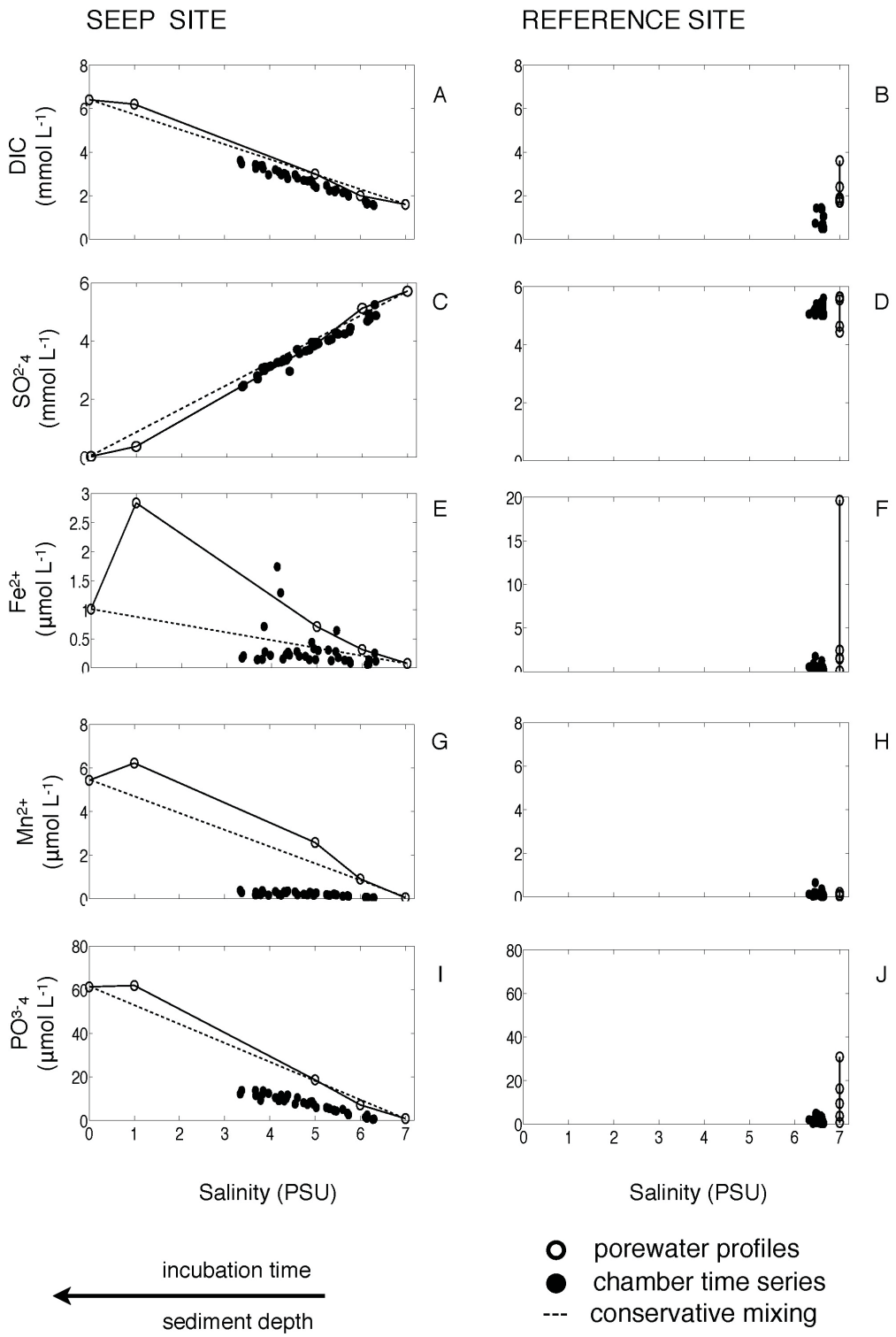

FIGURE 5.7: Distribution of selected variables in chamber incubated water (full circles) and in porewater (empty circles), along the salinity gradient (inversely related to chambers incubation time) at seep and reference site. Conservative mixing is indicated by the dashed line. Iron plots have different y axis scale.

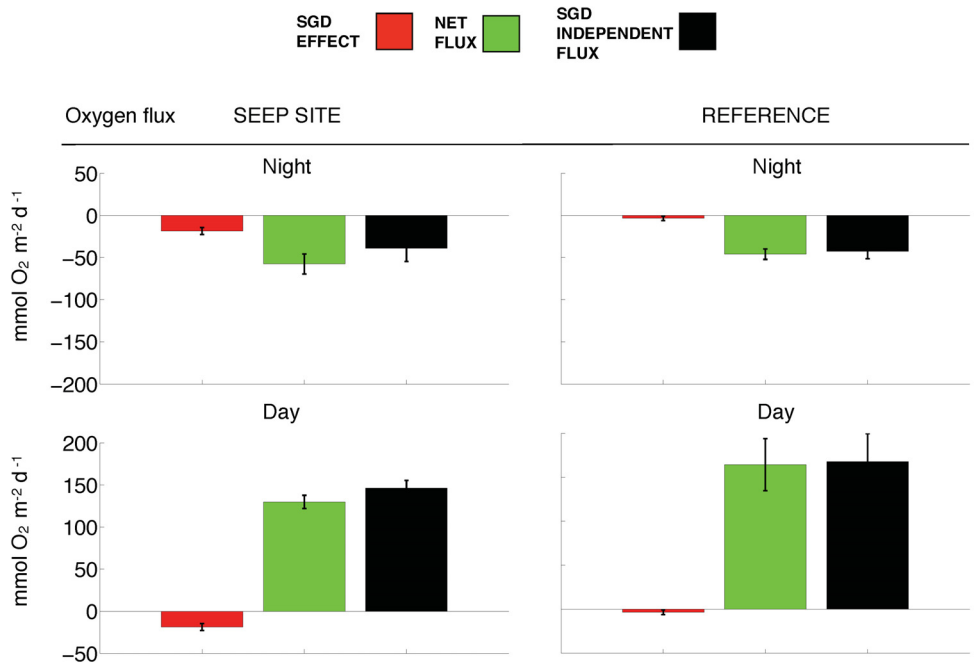

FIGURE 5.8: Oxygen fluxes measured with benthic chambers at seep and reference site. Red bars indicate the oxygen depletion due to supply of anoxic water to the chamber by SGD; green bars the total oxygen consumption/production as determined by optode readings; black bars the O_2 consumption/production independent of the supply of anoxic waters by SGD, i.e. due to biological activity and oxidation of reduced species.

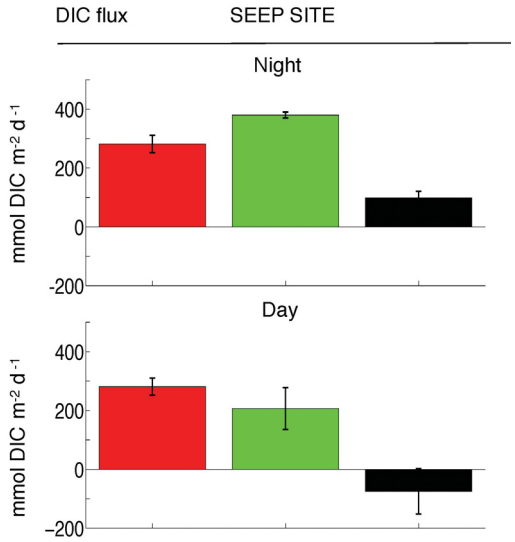

FIGURE 5.9: DIC fluxes measured with benthic chambers at seep site. Red bars indicate the DIC supplied by SGD; green bars the total DIC consumption/production as determined by analysis on the incubated water samples; black bars the contribution independent from SGD, i.e. estimation of biological respiration, since dissolution and precipitation of $CaCO_3$ is assumed negligible.

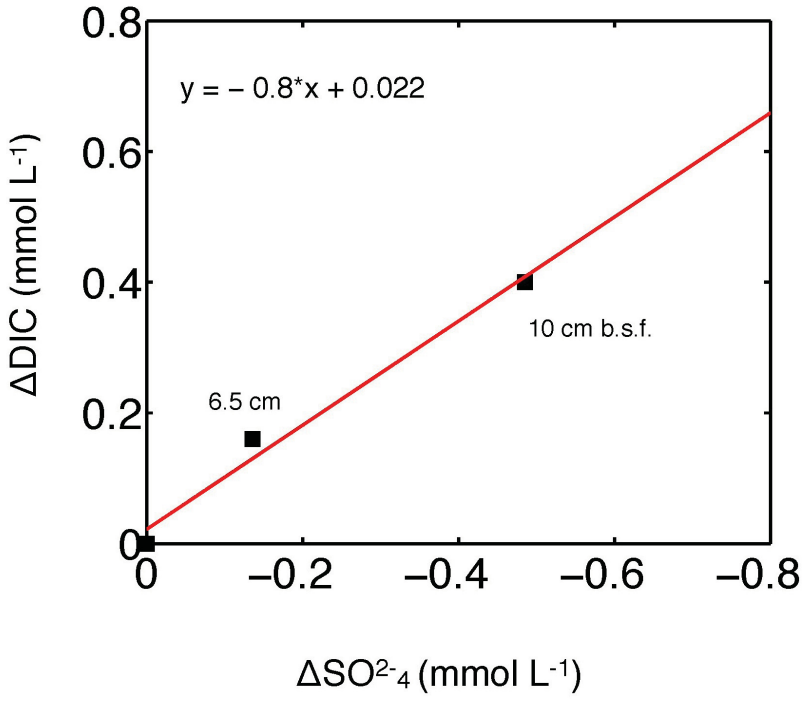

FIGURE 5.10: Pore water sulfate versus DIC deviation form conservative mixing line (as visible for each compound in Fig. 5.7). The linear regression line indicates 0.8 ratio of DIC produced to sulfate consumed.

Chapter 6

Discussion and Perspectives

In situ measurements for the investigation of solute exchanges at the sediment water-interface play an important role in the field of marine biogeochemical studies. In this context, benthic flux chambers and microprofilers are well-established methods (section 1.3). In recent years the eddy correlation (EC) has gained acceptance as a valid technique for determining dissolved oxygen (DO) fluxes between aquatic sediments and overlying water masses.

These techniques are suitable for certain biogeochemical processes and spatial-temporal scales. Benthic chambers and microprofilers can provide reasonable flux estimates especially in non-bioturbated sediments of limited permeability whereas EC has the potential for directly estimating benthic oxygen fluxes for those sediments where advection is the controlling factor for mineralization (Berg et al., 2013, McGinnis et al., in prep.).

Fully understanding benthic oxygen dynamics in deep-sea sediments is not an easy task with traditional technologies, given that mineralization rates can often be at, or below, measurement detection limits (that requires long in situ incubation times) and the expensive, expertise demanding platforms needed to reach thousands meter depths. ECs could be a convenient approach for those remote ecosystems with respect to benthic chambers and microprofilers, because they can potentially measure in standalone mode over several weeks or even months. However, being a relatively novel method, EC applications are still relatively scarce (although increasing), and only very recently some of the sources of measurement uncertainties have been investigated (Reimers et al., 2012, Holtappels et al., 2013, Rheuban and Berg, 2013).

One of the main objectives of this work was to improve the confidence in the assessment of EC fluxes. The reason behind this is that a more robust interpretation of aquatic EC data would certainly lead to a better integration with other flux methods to achieve

insights into benthic biogeochemical processes and achieve long-term flux measurements from benthic systems that are still overlooked in the context of global carbon budgets.

The results shown in this work derive from the application to coastal sands as well as to deep-sea sediments of different in situ benthic flux measurement methods. By this, we present considerations on site-related method limitations, with special emphasis on EC technique.

6.1 In situ benthic fluxes estimation for permeable coastal sediments

In sediments with permeability of approx. 10^{-12} to 10^{-11} cm^2 , advection dominates porewater transport (Huettel and Webster, 2001; Reimers et al., 2004). It was shown that transport processes at the sediment-water interface may be induced by bottom current–sediment interactions (Huettel et al., 1996) and by pore pressure variations due to surface gravity waves (Precht and Huettel, 2004). It is now obvious that when measuring benthic fluxes in permeable sediments, it is crucial to resolve the hydrodynamic setting.

Nevertheless, in situ benthic flux studies that include highly variable hydrodynamic conditions encountered in the near-shore habitats are still rather scarce. As a consequence, in situ porewater exchange and flow rates, and their effect on biogeochemical cycling in coastal shelf environments are still poorly quantified (Jahnke, 2005, Santos et al., 2012).

In our study at Hel bight we used stirred benthic chambers to investigate oxygen and dissolved inorganic carbon fluxes in coastal sediments (permeability=$2x10^{-11}cm^2$) that are influenced by groundwater in some localized areas of the bight. A pressure gradient of 2.5 Pa was imposed by the rotation of a stirring plate inside the chambers that did not affect the groundwater seepage rate (see Ch.5). In this way we accounted for the natural pressure gradient that develops under a unidirectional flow over the investigated topographical features at the dominant current magnitude measured at the site, i.e. 3 cm s^{-1} (as shown in Cook at al., 2007; Janssen et al. 2012).

Such measurements allowed us to establish that aerobic oxidation of organic matter represents the main mineralization pathway for these sediments, under a single flow field geometry and flushing rate. However it was shown that organic matter degradation pathways in sands can be highly variable, ranging from predominantly aerobic to predominantly sulfate reduction, and depend on temperature, the availability of degradable organic matter in the sediment, sediment permeability, sediment topography, and boundary layer flow velocity (Section 1.2). These variables change on different timescales (from minutes to weeks) and can be influenced by episodic events such as major storms.

The state-of-the-art EC technique is the only method that can resolve benthic fluxes accounting for the variability of the hydrodynamic setting, because fluxes can be obtained without disturbing the natural flow conditions and they will capture the in situ effects of pore-water flushing. Furthermore, because the footprint (the sediment surface area that contributes to the flux) covers a relatively large area (typically 10–100 m^2; Berg et al. 2007), it integrates spatial heterogeneities found in most benthic systems (Fenchel and Glud, 2000; Wenzhöfer and Glud, 2004; Thouzeau et al., 2007). These important features encouraged the application of EC for permeable sediments (Donis et al., 2012; McGinnis et al. in prep.). A recent application of EC to permeable sediments confirmed the link between oxygen uptake and current flow for the first time through direct in situ measurements (Berg et al., 2013), while so far it was largely investigated only with flume experiments and chamber studies (Huettel and Gust 1992; Reimers, 1996; Precht and Huettel, 2003). Berg et al., measured an EC oxygen flux 20 times greater than diffusive oxygen uptake, indicating that vertical oxygen transport was almost exclusively advective. However, Berg et al. (2013) have considered only current-driven flows and omitted the complex effect of wave action, although they stressed the importance of including it in the future.

It was previously shown that the large variability between the eddy fluxes derived for individual bursts can be due to internal waves, or other low-frequency mixing events, that cause intermittent advection (Brand et al., 2008, Lorke et al, 2012, Reimers et al., 2012). Because EC measurements resolve all dynamic processes that contribute a net nonzero flux of oxygen into/from the seabed, the presence of high frequency waves over permeable sediments brings several major considerations: 1) Wave orbital velocities near a rippled sandy bed may induce significant flow velocities through the bed, allowing water of lower oxygen concentration to be returned to the water column leading to oxygen consumption not related to remineralization processes (Reimers et al., 2004). 2) Net flux computations across wave frequencies can be significantly biased if the observation platform is not oriented perfectly in the vertical direction (Lorke et al. 2013). Any rotation errors will result in components of the horizontal velocities associated with surface waves being superimposed to the vertical velocities (Shaw and Trowbridge, 2001) and can potentially lead to large errors in the flux estimates. Thus one may consider, when correcting for wave action, removing the entire wave contribution (e.g., Shaw and Trowbridge, 2001) or distinguishing between the real wave contribution (that may include processes not related to remineralization of organic matter) and the apparent wave bias due to rotation errors (Reimers et al., 2012).

An important aspect to be considered when comparing total oxygen uptake between EC and benthic chambers (TOU_{EC} and TOU_{Ch}) is the inhomogeneity of the seabed. When we applied EC at Hel sands impacted by submarine groundwater discharge (unpublished

data, see Appendix A), we removed the wave contribution and obtained TOU_{EC} comparable to TOU_{Ch} (-77 and -55 $\pm$ 15 mmol O_2 m^{-2} d^{-1} , respectively). As shown in Chapter 5, the investigated bight is characterized by a patchy distribution of anoxic, fresh groundwater discharge locations. Therefore, chamber incubations may represent the localized impact of the seepage while the area contributing to the EC-flux (approx. 20 m^2) most likely integrated an inhomogeneous area, composed by spots of higher and lower oxygen consumption. However, we measured the TOU_{Ch} at sites with higher and negligible seepage impact, and did not observe significantly different rates.

Reimers et al. (2012) explained with the "inhomogeneity effect" the results obtained for 80 m depth in permeable sediments of a hypoxic region on the Oregon shelf. The magnitudes of TOU_{EC} (-10 mmol O_2 m^{-2} d^{-1}) compared with TOU_{Ch} (-8 mmol O_2 m^{-2} d^{-1}), and both were greater (as expected) than diffusive flux estimates from oxygen microelectrode profiles (-2.4 mmol O_2 m^{-2} d^{-1}). It was suggested that the chambers may have sampled a localized "hot spot", ascribed to an inhomogeneous distribution of decomposing phytodetritus (e.g., as in Glud et al., 2009). It is as well possible that TOU_{EC} was not higher than TOU_{Ch}, (as hypothesized and found for a 2 m depth sandy site by Berg et al. (2013)) because shallow sites are under nearly air-saturated waters and experience regularly strong tidal currents, exhibiting a greater degree of advective oxygen flux enhancement than the 80 m depth Oregon shelf sites studied under late spring and summer conditions by Reimers et al. (2012).

It can be concluded that when we want to address biogeochemical processes for well-determined conditions at an inhomogeneous seafloor, chamber incubations (such as those used in this study) still provide the most trustful insight into interactions between pore-water advection, solute fluxes, and reaction rates in permeable sediments. EC appears as a suitable approach for a broader scale investigation, that would include the high dynamic processes of coastal benthic systems. The two techniques therefore in this context are complementary.

More studies are however necessary to assess the procedures needed to avoid/correct the effects that physical variables, such as the density gradients induced by groundwater discharge, may have on EC-flux measurements. It is plausible that, for this instance, the EC-flux measurement height above the seabed is determinant under a spectrum of turbulent conditions that can be certainly tested and assessed with further studies.

6.2 In situ benthic fluxes estimation for cohesive and deep-sea sediments

The measurement of in situ benthic fluxes is virtually easier for cohesive sediments, as some of the mentioned uncertainties encountered for estimations in permeable sediments can be excluded. The agreement between oxygen flux measurements carried out with benthic chambers, microprofilers and EC is an indication that, in terms of remineralization rates, the area under study is homogeneous.

Our study at HAUSGARTEN (2500 m depth), showed good agreement between oxygen fluxes obtained by the three techniques (DOU = -1.2 ± 0.1, TOU_{Ch}= -1.2 ± 0.3, TOU_{EC} = -0.9 ± 0.2 mmol O_2 m^{-2} d^{-1}), confirming what has been obtained by previous comparative studies on cohesive sediments (Berg et al., 2003, 2009). The results, in addition, confirm that deep-sea sediments at this oligotrophic site, are characterized by a low oxygen uptake, and the faunal contribution to remineralization of organic matter is small. This finding is relevant in light of the few flux studies existing for Arctic deep sea sediments (Schluster et al., 2000; Sauter et al., 2001).

Our achievement, i.e. measuring low oxygen sediment uptake rates (< 1 mmol O_2 m^{-2} d^{-1}) with EC, assessing their significance, is particularly relevant in the perspective of in situ long term measurements of benthic biogeochemical activity at deep-sea sites. Indeed, future flux studies may need to be expanded to open oceans and polar regions. Long-term high-resolution time series of benthic oxygen exchanges are required for better understanding the quantitative importance of episodic events in the upper water column (e.g. ice melting) for the annual oxygen and carbon budgets (Thiel et al., 1994; Pfannkuche and Linke 2003).

6.3 Towards an improved confidence of eddy correlation measurements

Depending on the aim of the study, comparative measurements between benthic chambers, microprofilers and EC can be convenient to gain insights on sediments activity, with different spatial and temporal resolution. Nevertheless it should be possible to avoid side measurements when deploying an EC system. Firstly, because it is expensive and time consuming, and secondly, because for several benthic ecosystems, the comparison between fluxes obtained by the three methods is barely achievable (e.g. highly permeable sediments and hard substrates). Since EC measurements are already providing results on benthic processes from systems that previously were difficult to address

quantitatively (e.g. ice subsurface mass and oxygen exchange with the ocean, Long et al., 2012, coral reefs, Long et al., 2013), it appears urgent to establish common protocols for EC data quality control that are so far missing.

Oxygen fluxes obtained from EC measurements often show extensive short-term variability, that is poorly explained by benthic community response. The variability of EC fluxes for shallow sediments is recognized as naturally dynamic, as for instance, the variations due to the shifting from autothrophic to heterotrophic metabolism of benthic communities (Berg et al., 2013). In order to use oxygen exchange as a proxy for total carbon mineralization and production in benthic systems (Canfield et al., 1993) it is therefore recommended to integrate EC measurements over considerable periods of time (weeks) to be considered representative of the system trophic status.

However, since EC measurements are usually performed at 10-15 cm above the seafloor, a short outflow of oxygen depleted porewater from the ripple crests in permeable sediments would alter temporarily the vertical concentration gradient at the measuring point. It is therefore suggested that averaging EC fluxes over a time scale of hours, would help counter the biases (Berg et al., 2013).

Even though is not yet established whether the current-induced pore water outflow would affect EC measurements, it is true that environmental conditions that nullify the assumption of a steady state oxygen concentration may occur often, especially in coastal waters, where strong oxygen sinks and sources prevail. This issue was faced in Chapter 3, where we examined the effect of transient oxygen concentration (and current magnitude) on EC-fluxes.

We showed how changes of 5–10 μmol O_2 L^{-1} h^{-1} can result in transient EC-fluxes of 6–12 mmol O_2 m^{-2} d^{-1}, which is comparable to the oxygen uptake on shelf sediments. We additionally show that for horizontal gradients, the bias increases with the distance between the measuring volume and the seabed. Thus, measurements closer to the sediment would reduce the errors, however reducing the size of the area contributing to the flux as well as the "blending height" (EC footprint, Berg et al., 2007).

Our results suggest to carefully analyze the velocity and oxygen concentration time series recorded during EC-deployments and resolve their rate of change to estimate how this may confound the true benthic flux (Holtappels et al., 2013, Chapter 3 and 4). However, coherently with Berg et al., (2013) for EC measurements in highly permeable sediments, we conclude that the probability of an erroneous flux estimation during transient conditions is higher for short deployments, while extended sampling periods would average out the biases due to increasing and decreasing velocities or concentrations.

The recommended procedure of averaging EC fluxes over long periods (for the mentioned cases of permeable sediments and transient conditions) applies as well to the case of low frequency waves. It is in fact assumed that a sufficiently long deployment period would capture multiple cycles of low-frequency motions and would therefore lead to a low-frequency flux that averages to zero in the long term (Reimers et al., 2012).

After these considerations, it appears obvious that the potential for EC measurements to achieve flux estimates with high temporal resolution (e.g. on a fraction of hour), is limited to those systems where strong discontinuities in the current field and concentrations gradients are excluded. We think that this must be considered for future novel applications of EC measurements. Due to the characteristics of EC systems (largely described in this study), one of the most challenging application of this technique is the estimation of respiration rates on hard seabed substrates and coral reefs.

Similarly to what has been described for highly permeable sediments, coral reefs, with many cavities and organisms colonizing inhomogeneously the surface, can easily induce (under the effect of changing current flow regimes) bursts of oxygen enriched/depleted interstitial waters, leading to unsteady boundary concentration gradients. Nevertheless, a recent study by Long et al. (2013) reports high-temporal resolution EC oxygen fluxes of a coral reef. The aim here was to incorporate contributions of all of the organisms within and on the reef structure and correlate respiration rates to changes in environmental conditions.

Given the inhomogeneity of such substrates, the area that contributes to the vertical oxygen flux (footprint) has to be precisely defined, which is not a n easy task. The EC footprint is typically large, but is also narrow with a width on the order of a few meters, and changes with the current direction. Even small changes in the current direction can yield an entirely different footprint, therefore the authors had to analyze the flux as a function of current directions.

The high variance of the resolved EC fluxes (up to 4 times the minimum flux) was attributed to the change in the footprint relative to the current, i.e. to the different composition of the sediments/corals and of the benthic community contributing to the oxygen flux. However, as we show in Chapter 2, some of the variability of EC fluxes can be related to the orientation of the sensors (the oxygen sensor tip and the velocity sampling volume) with respect to the current direction. We suggest that an underestimation of benthic fluxes by EC may occur when the system is oriented perpendicularly to the current direction, due to the miss sampling of turbulent structures. This eventuality requires further analysis to determine the order of magnitude of the smallest eddies contributing to the flux, and compare it to the distance between the sensors.

In the study by Long et al. (2013) on the coral reef, oxygen measurements were taken 7 cm apart from the velocity sampling volume (personal communication), with local current magnitudes of 2-5 cm s^{-1}. Given the high drag coefficient of coral reefs, even with such low mean currents, the energy dissipation is expected in the order of 10^{-5} W kg^{-1}. Thus, as reported in Lorrai et al. (2010), the smallest eddies contributing to the turbulent flux can easily be < 1 cm. In the case of 7 cm distance between the sensors, it is plausible that a significant loss of high frequency signal occurs when the mean current is perpendicular to the sensors.

We showed in Chapter 2 that even for the ideal orientation (i.e. sensors oriented downstream with respect to the mean current) the correction of the time shift due to the physical distance of the measured time series, w' C', may not be sufficient to align the sensor readings to the same water parcel. This is because increasing distances between the sensors also increases the mismatch of the spatial overlay of corresponding velocity-concentration pairs (w' and C'), and may constitute a weak point especially under non-uniform conditions.

We suggest indeed that the oxygen sensor tip distance from the velocity sampling volume should be as small as possible, especially if the current direction is expected to change during the deployment of an EC system. These considerations, together with the application of correction procedures shown in Chapter 2 and 3, are needed if we want to be able to assess EC fluxes without a reliable reference measurement. When we evaluated the flow field direction and correlate it with the significance of the EC fluxes for the deployment in Arctic deep sea sediments (Chapter 4), we could increase the confidence of the obtained fluxes by a 30%. This represents a next step for the amelioration of EC use for non-ideal conditions, opening to a better estimation of benthic exchange processes on longer time scales, compared to what is achievable by traditional methods.

6.4 Technical improvements for aquatic eddy correlation

In Chapter 2 we point out how the orientation of an EC system with respect to the current direction can cause (for high turbulence) a significant underestimation of the measured flux, which has been so far overlooked. Is not possible however to establish a criterium for which a certain loss of precision in the flux estimation corresponds to a given orientation, since it depends not only on the direction of the current but also on the scale of the smallest turbulent structures contributing to the flux.

For non-ideal conditions, as high turbulence and variable mean flow directions, the best way to achieve a higher precision of flux measurements with EC is to keep the sampling

volumes as close as possible, and oriented downstream to the current for the whole deployment period. For this instance EC frames could be adapted to rotate the system towards the current. This implies either a freely orientating EC-system, mounted on a rotating pole provided with a fin that helps the alignment towards the mean flow, or a motor (and a dedicated routine) that calculates the current direction and rotates the system accordingly.

For the first solution, it was shown that the induced vibrations would spoil the measurements by introducing fluctuations that have the same order of magnitude as the ones needed to calculate the turbulent fluxes (McCann, 2010). The second solution instead would fix the system at a given orientation avoiding the vibration problem, but on the other hand requires additional payload on the power consumption and is prone to electronic problems. However, with the availability of new generation batteries (e.g. higher capacity/volume ratio), this may represent the best solution.

We showed that low oxygen fluxes at deep-sea sediments are measurable with EC, and as well pointed out how continuous, long-term benthic flux measurements would raise new questions concerning benthic responses to water column dynamics. For this instance, a crucial requirement for EC measurements is to have stable signals, i.e. sensors with minimal electronic drift, not easily breakable and resistant to biofouling. For oxygen measurements, optodes have several advantages over microelectrodes. Provided they are fast enough to capture the oxygen fluctuations that drive the turbulent flux, optodes are less susceptible to signal drift, and are more durable in the field conditions, less expensive to fabricate and reparable. Moreover, no oxygen is consumed during the measurements, thus is independent of the flow (no stirring sensitive). A recent study by Chipman et al. (2012) showed EC (optode-based) fluxes in a range of 20-100 mmol O_2 m^{-2} d^{-1}, confirming that the existing technology makes the oxygen optode a suitable sensor for EC measurements in aquatic environments.

One limitation concerns the accuracy of the oxygen concentration measurements which is currently better for microelectrodes than for optodes ($\pm$ 0.5 and 2.5 μmol L^{-1} , respectively). For the purpose of measuring small fluxes at low turbulent regimes, as the ones we have measured in deep-sea Arctic sediments, optode accuracy would thus be not sufficient. However highly sensitive chemistries are being tested, that will further improve optode performance, and it is likely that these sensors will become the most suitable for EC measurements in aquatic environments.

Bibliography

Aller, R. C. (1994). Bioturbation and remineralization of sedimentary organic matter: effects of redox oscillation. Chemical Geology, 114(3-4), 331-345.

Aller, R.C., and J. Y. Aller. (1998). The effect of biogenic irrigation intensity and solute exchange on diagenetic reaction rates in marine sediments. Journal of Marine Research. 56: 905-936.

Anderson, L.G., Hall, P.O.J., Iverfeldt, A., Rutgers van der Loeff, M.M., Sundby, B. and Westerlund, S.F.G., (1986). Benthic respiration measured by total carbonate production. Limnology and Oceanography. 31(2), 319-329.

Anderson, J. J. and Devol, A. H.(1987). Extent and intensity of the anoxic zone in basins and fjords, Deep-Sea Research. Pt. I, 34, 927-944.

Antoine, D., Andre, J.-M., Morel, A., (1996). Oceanic primary production. 2. Estimation at global scale from satellite (coastal zone color scanner) chlorophyll. Global Biogeochemical Cycles 10, 57-69.

Archer, D. and Devol, A. (1992). Benthic oxygen fluxes at the Washington shelf and slope: A comparison of in situ microelectrode and chamber flux measurements. Limnology and Oceanography 37, 614-629.

Archer, D., Maier-Reimer, E. (1994). Effect of deep-sea sedimentary calcite preservation on atmospheric CO_2 concentration. Nature 367, 260-263.

Aubinet, M., A. Grelle, A. Ibrom, Ü.Rannik, J.Moncrieff, T. Foken, A.S.Kowalski, P. H.Martin, P. Berbigier, C. Bernhofer, R. Clement, J.Elbers, A.Granier, T. Grünwald, K.Morgenstern, K.Pilegaard, C. Rebmann, W. Snijders, R.Valentini, and T. Vesala. (2000). Estimates of the annual net carbon and water exchange of forests: The EUROFLUX methodology. Advances in Ecological Research. 30: 113-175.

Berner, R.A. (1978). Sulfate reduction and the rate of deposition of marine sediments. Earth and Planetary Science Letters 37, 492-498.

Berner, R. A. (1980). Early diagenesis: A theoretical approach, Princeton Univ. Press.

Berner, R.A., (1990). Atmospheric carbon dioxide levels over Phanerozoic times. Science 249, 1382-1386.

Berner R.A. and D.E. Canfield (1989). A model for atmospheric oxygen over phanerozoic time. American Journal of Science, 289, 333-361.

Bender, M. L., and D. T. Heggie. (1984). Fate of organic carbon reaching the deep sea floor: A status report. Geochimica et Cosmochimica Acta 48: 977-986.

Bender, M.L. and Heggie, D.T. (1984). Fate of organic carbon reaching the deep sea floor: a status report. Geochimica et Cosmochimica Acta, 48: 977-986.

Bender, M., Jahnke, R., Weiss, R., Martin, W., Heggie, D., Orchardo, J., and Sowers, T., (1989). Organic carbon oxidation and benthic nitrogen and silica dynamics in San Clemente Basin, a continental borderland site. Geochimica et Cosmochimica Acta, 53, 685-697.

Berelson, W., Hammond, D., and Johnson, K. (1987). Benthic fluxes and the cycling of biogenic silica and carbon in two southern California borderland basins. Geochimica et Cosmochimica Acta, 51(6), 1345-1363.

Berelson,W. (2002). Particle settling rates increase with depth in the ocean, Deep Sea Research Part II, 49, 237-251.

Berg, P., Risgaard-Petersen, N., and Rysgaard, S. (1998). Interpretation of measured concentration profiles in sediment pore water - Limnology and Oceanogaphy 43(7), 1500-1510.

Berg, P., Røy, H., Janssen, F., Meyer, V., Jørgensen, B., Huettel, M., and De Beer, D. (2003). Oxygen uptake by aquatic sediments measured with a novel non-invasive eddy-correlation technique. Marine Ecology Progress Series, 261, 75-83.

Berg, P., Røy, H., Wiberg, P. L. (2007). Eddy correlation flux measurements: The sediment surface area that contributes to the flux. Limnology and Oceanography, 52(4), 1672–1684

Berg, P., and M. Huettel, (2008). Monitoring the seafloor using the non-invasive eddy correlation technique: Integrated benthic exchange dynamics. Oceanography, 21, 164-167.

Berg, P., Glud, R. N., Hume, A., Stahl, H., Oguri, K., and Meyer, V. and H. Kitazato (2009). Eddy correlation measurements of oxy- gen uptake in deep ocean sediments. Limnology and Oceanography: Methods 7:576-584

Berg, P., Long, M. H., Huettel, M., Rheuban, J. E., Mcglathery, K. J., Howarth, R. W., Foreman, K. H., et al. (2013). Eddy correlation measurements of oxygen fluxes in permeable sediments exposed to varying current flow and light. Limnology and Oceanography 58(4), 1329-1343.

Berger, W.H., Fischer, K., Lai, C., Wu, G., (1987). Ocean productivity and organic carbon flux. I. Overview and Maps of Primary Production and Export Production. University of California, San Diego, SIO Reference, 87-30, 67pp.

Betzer, P.R., Showers, W.J., Laws, E.A., Winn, C.D., Dituillio, G.R., Kroopnick, P.M., (1984). Primary productivity and particle fluxes on a transect of the Equator at 1533W in the Pacific Ocean. Deep-Sea Research 31, 1-11.

Biles CL, Paterson DM, Ford RB, Solan M, Raffaelli DG (2002). Bioturbation, ecosystem functioning and community structure. Hydrology and Earth System Science 6:999-1005.

Blackburn T.H, N.D Blackburn, K. Jenssen, and N. Risgaard-Petersen (1994). Simulation model of the coupling between nitrification and denitritication in a freshwater sediment. Applied and Environmental Microbiology. 60: 3089-3095.

Boudreau B. P. and Ruddick B. R. (1991). On a reactive continuum representation of organic matter diagenesis. American Journal of Science. 291, 507-538.

Boudreau, B. P.(1996). The Diffusive Tortuosity of Fine-Grained Unlithified Sediments, Geochimica et Cosmochimica Acta, 60, 3139-3142.

Boudreau, B. P.(1997). Diagenetic Models and Their Implementation, Springer, Berlin,.

Boudreau, B. P. (2001). Solute transport above the sediment-water interface, p. 104-143. In B. P. Boudreau and B. B. Jørgensen [eds.], The benthic boundary layer. Oxford Univ. Press.

Boudreau, B.P., Jørgensen, B.B., (2001). The Benthic Boundary Layer: Transport Processes and Biogeochemistry. Oxford University Press, Oxford.

Boudreau, B.P., Huettel, M., Forster, S., Jahnke, R., McLachlan, A., Middelburg, J., Nielsen, P., Sansone, F., Taghon, G., Van Raaphorst, W., Webster, I., Marcin Weslawski, J., Wiberg, P., Sundby, B. (2001). Permeable marine

sediment: overturning an old paradigm. Estuarine Coastal and Shelf Science 82:133-136.

Bouldin, D. R. (1968). Models for describing the diffusion of oxygen and other mobile constituents across the mud-water interface. Journal of Ecology 56, 77-87.

Brand, A., Mcginnis, D. F., Wehrli, B., and Wu, A. (2008). Intermittent oxygen flux from the interior into the bottom boundary of lakes as observed by eddy correlation. Limnology and Oceanography 53(5), 1997-2006.

Brutsaert, W. (1982). Evaporation into the atmosphere. D. Riedel Publishing Co. Dordrecht, Holland. 300 p.

Burdige, D.J., (2007). The preservation of organic matter in marine sediments: controls, mechanisms and an imbalance in sediment organic carbon budgets? Chemical Reviews 107, 467-485.

Cai, W.-J., Sayles, F.L., (1996). Oxygen penetration depths and fluxes in marine sediments. Marine Chemistry 52 (2), 123-131.

Caldwell, D.R., and T. M. Chriss (1979). Viscous sublayer at the sea-floor. Science 205: 1131-1132.

Canfield, D.E. (1993a). Organic matter oxidation in marine sediments. In: Wollast, R., Chou, L., Mackenzie, F. (Eds.), Interactions of C, N, P, and S Biogeochemical Cycles. Springer, Berlin, Heidelberg, pp. 333-363.

Canfield,D.E, Jørgensen, B.B, Fossing, H., Glud, R., Gundersen, J., Ramsing, N.B., Thamdrup, B., Hansen, J.W, Nielsen, L.P., Hall, P.O.J. (1993b). Pathways of organic carbon oxidation in three continental margin sediments, Marine Geology, (113) 27-40.

Canfield, D. E. 2005 The early history of atmospheric oxygen. Annual Reviews in Earth Planetary Scence. 33, 1-36.

Canfield, D. E., and Thamdrup, B. (2009). Towards a consistent classification scheme for geochemical environments, or, why we wish the term “suboxic” would go away. Geobiology, 7(4), 385-92.

Chipman, L., Huettel, M., Berg, P., Meyer, V., Klimant, I., Glud, R., Wenzhöefer, F. (2012). Oxygen optodes as fast sensors for eddy correlation measurements in aquatic systems. Limnology and Oceanography: Methods, 10, 304–316. doi:10.4319/lom.2012.10.304

Cook, P. L. M., Wenzhöfer, F., Glud, R. N., Janssen, F., Huettel, M., Glud, A. (2007). Benthic solute exchange and carbon mineralization in two shallow subtidal sandy sediments : Effect of advective pore-water exchange. Limnology and Oceanography 52(5), 1943-1963.

Crusius, J., Berg, P., Koopmans, D. J., and Erban, L. (2008). Eddy correlation measurements of submarine groundwater discharge. Marine Chemistry, 109(1-2), 77-85.

Dade, W. B., A. J. Hogg, and B. P. Boudreau. (2001). Physics of flow above the sediment-water interface, p. 3-43. In B. P. Boudreau and B. B. Jørgensen [eds.], The benthic boundary layer. Oxford Univ. Press.

Dauwe, B., Middelburg, J. J., and Herman, P. (2001). Effect of oxygen on the degradability of organic matter in subtidal and intertidal sediments of the North Sea area. Marine Ecology Progress Series, 215, 13-22.

Davis R. B. (1974). Tubificids alter profiles of redox potential and pH in profundal lake sediments. Limnology and Oceanography 19:342-346

De Beer, D., Wenzhöfer, F., Ferdelman, T. G., Boehme, S. E., Huet- tel, M., Van Beusekom, J. E. E., Böttcher, M. E., Musat, N., and Dubilier, N. (2005). Transport and Mineralization Rates in North Sea Sandy Intertidal Sediments, Sylt-Romo Basin,Wadden Sea, Limnology and Oceanography, 50, 113-127.

De Haas, H., T. C. E. Van Weering, and H. De Stigter. (2002). Organic carbon in shelf seas: Sinks or sources, processes and products. Continental Shelf Research 22: 691-717.

Devol, A. H., and J. P. Christensen. (1993). Benthic fluxes and nitrogen cycling in the sediments of the continental margin of the eastern North Pacific. Journal of Marine Research 51: 345- 372.

Donis, D., Janssen, F., B/"ottcher, M.E., McGinnis, D., Holtappels, M., Wenzhöefer, F. (2012). Application of an eddy correlation system for the estimation of oxygen benthic fluxes in coastal permeable sediments impacted by submarine groundwater discharge. Geophysical Research Abs. Vol. 14, EGU2012-11471-2.

Dunne, J. P., Armstrong, R. A, Gnanadesikan, A., and J. L. Sarmiento (2005). Empirical and mechanistic models for the particle export ratio, Global Biogeochemical Cycles, 19, GB4026.

Fenchel, T. and R.N. Glud (2000). Benthic primary production and O_2-CO_2 dynamics in a shallow water sediment: spatial and temporal heterogeneity. Ophelia 53: 159–171.

Fischer, J., Ferdelman, T.G., D'Hondt, S., Røy, H., Wenzhöfer, F., (2009). Oxygen penetration deep into the sediment of the South Pacific. Biogeosciences 6, 1467-1478.

Foken, T., (2008) Micrometeorology. Springer, Berlin/Heidelberg, 308 pp

Foken T., Aubinet, M., Leuning, R. (2012): The eddy covariance method. in Aubinet et al., (eds), Eddy Covariance: A Practical Guide to Measurement and Data Analysis, Springer Atmospheric Sciences.

Froelich P. N., Klinkhammer G. P., Bender M. L., Ludtke N. A., Heath G. R., Cullin D., Dauphin P., Hammond D., Hartman B., and Maynard V. (1979). Early oxidation of organic matter in pelagic sediments of the eastern equatorial Atlantic: suboxic diagenesis. Geochimica et Cosmochimica Acta, 1075-1090.

Gattuso, J.-P., Frankignoulle, M., Wollast, R., (1998). Carbon and carbonate metabolism in coastal aquatic ecosystems. Annual Review of Ecology and Systematics 29, 405-434.

Glud, R. N., J. K. Gundersen, B. B. Jørgensen, N. P. Revsbech,and H. D. Schulz. (1994). Diffusive and total oxygen-uptake of deep-sea sediments in the eastern south-atlantic ocean - in-situ and laboratory measurements. Deep-Sea Research. I 41:1767-1788.

Glud, R. N., J. K. Gundersen, N. P. Revsbech,B.B. Jørgensen, and M. Huttel. (1995). Calibration and performance of the stirred flux chamber from the benthic Lander Elinor. Deep-Sea Research. I. 42: 1029-1042.

Glud, R. N., Forster, S., and Huettel, M.(1996). Influence of Radial Pres- sure Gradients on Solute Exchange in Stirred Benthic Chambers, Marine Ecology Progress Series, 141, 303-311.

Glud, R.N., Gundersen, J.K., Røy, H. and Jørgensen, B.B., (2003). Seasonal dynamics of benthic O uptake in a semienclosed bay: Importancd of diffusion and faunal activity. Limnology and Oceanography, 48, 1265 1276.

Glud, R. N., Berg, P., Fossing, H., and Jørgensen, B. B. (2007). Effect of the diffusive boundary layer on benthic mineralization and O_2 distribution: A theoretical model analysis. Limnology and Oceanography, 52(2), 547-557.

Glud, R. N. (2008). Oxygen dynamics of marine sediments. Marine Biology Research, 4(4), 243-289.

Glud, R. N., P. Berg, A. Hume, P. Batty, M. E. Blicher, K. Lennert, and S. Rysgaard. (2010). Benthic O_2 exchange across hard-bottom substrates quantified by eddy correlation in a sub-Arctic fjord. Marine Ecology Progress Series 417: 1-12

Goodman, L., E. R. Levine, and R. G. Lueck, (2006). On measuring the terms of the turbulent kinetic energy budget from an AUV. J. Atmospheric and Oceanic Technology, 23, 977-990

Graf G, Rosenberg R (1997). Bioresuspension and Biodeposition - A Review. Journal of Marine Systems 11: 269-278

Grantham, B. A., Chan, F., Nielsen, K. J., Fox, D. S., Barth, J. A., Huyer, A., Lubchenco, J., and Menge, B. A.(2004). Upwelling-driven nearshore hypoxia signals ecosystem and oceanographic changes in the northeast Pacific, Nature, 429, 749-754.

Grenz, C., Denis, L., Boucher, G., Chauvaud, L., Clavier, J., Fichez, R. and Pringault, O. (2003). Spatial variability in sediment oxygen consumption under winter conditions in a lagoonal system in New Caledonia (South Pacific). Journal of Experimental Marine Biology and Ecology, 285, 33-47.

Green, M.A., Aller, R.C., Aller, J.Y., (1993). Carbonate dissolution and temporal abundances of foraminifera in Long-Island Sound sediments. Limnology and Oceanography 38, 331-345.

Gruber N. (2004). The dynamics of the marine nitrogen cycle and its influence on atmospheric CO_2.In The ocean carbon cycle and climate, ed. M. Follows, T. Oguz, pp. 97-148. Dordrecht: Kluwer Academic

Gundersen, J.K., and B. B. Jørgensen. (1990). Microstructure of diffusive boundary layers and the oxygen uptake of the sea floor. Nature 345: 604-607.

Güss, S. (1998), Oxygen uptake at the sediment water interface simultaneously measured using a flux chamber method and microelectrodes: Must a diffusive boundary layer exist? Estuarine Coastal Shelf Science, 46, 143-156.

Hammond D.E., McManus J., Berelson W.M., Kilgore T.E. and Pope RH. (1996). Early diagenesis of organic material in equatorial Pacific sediments: stoichiometry and kinetics. Deep-Sea Research I 43:1365-412.

Hecker B. (1990). Photographic evidence for the rapid flux of particles to the sea floor and their transport down the continental slope. Deep-Sea Research I, 37:1773-82.

Heip, C. H. R., Goosen, N. K., Herman, P. M. J., Kromkamp, J., Middelburg, J. J., and Soetaert, K.(1995). Production and consumption of biological particles in temperate tidal estuaries. Marine Biology, 33, 1-150.

Higashino, M., Stefan, H.G., Gantzer, C.J., (2003). Periodic diffusional mass transfer near sediment/water interface: theory. Journal of Environmental Engineering 129 (5), 447-455.

Hinrichs, K.-U., and A. Boetius. (2002). The anaerobic oxidation of methane: new insights in microbial ecology and biogeochemistry, p. 457-477. In G. Wefer, D. Billett, D. Hebbeln, B. B. Jørgensen, M. Schlüter, and T. C. E. van Weering (ed.), Ocean margin systems. Springer-Verlag, Berlin, Germany.

Hedges, J.I., Oades, J.M., (1997). Comparative organic geochemistries of soils and marine sediments. Organic Geochemistry 27, 319-361.

Heggie, D., Maris, C., Hudson, A., Dymond, J., Beach, R., Cullen, J. (1997). Organic carbon oxidation and preservation in NW Atlantic continental margin sediments. Geological Society, London, Special Publications 01/1987; 31(1):215-236

Hensen, C., Zabel, M. and Schulz, H.D., (2000) A comparison of benthic nutrient fluxes from deep-sea sediments off Namibia and Argentina. Deep-Sea Research II, 47, 2029-2050.

Herbert R. A. (1999). Nitrogen cycling in coastal marine ecosystems. FEMS Microbiology Reviews 23:563-590

Holtappels, M., and A. Lorke (2011), Estimating turbulent diffusion in a benthic boundary layer, Limnology and Oceanography Methods, 9, 29-41.

Holtappels, M., Kuypers, M. M. M., Schlüter, M., and Brüchert, V. (2011). Measurement and interpretation of solute concentration gradients in the benthic boundary layer. Limnology and Oceanography Methods. 9: 1-13.

Holtappels, M., Glud, R. N., Donis, D., Liu, B., Hume, A., Wenzhöefer, F., Kuypers, M. M. M. (2013). Effects of transient bottom water currents and oxygen concentrations on benthic exchange rates as assessed by eddy correlation measurements. Journal of Geophysical Research: Oceans, 118(3), 1157–1169.

Huettel, M. (1990) Influence of the lugworm Arenicola marina on porewater nutrient profiles of sand flat sediments. Marine Ecology Progress Series, 62, 241-248.

Huettel, M., Gust, G., (1992). Impact of bioroughness on interfacial solute exchange in permeable sediments. Marine Ecology Progress Series, 89, 253-267.

Huettel, M., Ziebis, W., Forster, S., (1996). Flow-induced uptake of particulate matter in permeable sediments. Limnology and Oceanography 41 (2), 309-322.

Huettel, M., Webster I.T. (2001). Porewater flow in permeable sediments. In: Boudreau BP, Jørgensen BB (eds) The benthic boundary layer. Oxford University Press, New York, p 144-179

Huettel, M., R/oy, H., Precht, E., Ehrenhauss, S., (2003). Hydrodynamical impact on biogeochemical processes in aquatic sediments. Hydrobiologia 494, 231-236.

Hulth, S., Tengberg, A., Landen, A., Hall, P.O.J. (1997). Mineralization and burial of organic carbon in sediments of the Southern Weddell Sea. Deep-Sea Research I, 44:955-81.

Hume, A.C., Berg, P. and McGlathery, K.J. (2011). Dissolved oxygen fluxes and ecosystem metabolism in an eelgrass (Zostera marina) meadow measured with the eddy correlation technique. Limnology and Oceanography, 56(1), 86-96.

Jahnke, R.A., Reimers, C.E. and Craven, D.B., (1990). Intensification of recycling of organic matter at the sea floor near ocean margins. Nature, 348: 50-54.

Jahnke, R.A., Craven, D.B., McCorkle, C.D., Reimers, C.E., (1997). $CaCO_3$ dissolution in California continental margin sediments: the influence of organic matter remineralization. Geochimica et Cosmochimica Acta 61, 3587-3604.

Jahnke R. A., Alexander C. R., and Kostka J. E. (2003). Advective pore water input of nutrients to the Satilla River Estuary, Georgia, USA. Estuarine Coastal and Shelf Science 57, 641-653.

Jahnke, R., M. Richards, J. Nelson, C. Robertson, A. Rao, and D. Jahnke (2005). Organic matter remineralization and porewater exchange rates in permeable South Atlantic Bight continental shelf sediments, Continental Shelf Research 25, 1433-1452.

Janssen, F., Huettel, M., and Witte, U. (2005). Pore-water advection and solute fluxes in permeable marine sediments (II): Benthic respiration at three sandy sites with different permeabilities (German Bight, North Sea). Limnology and Oceanography, 50(3), 779-792.

Janssen, F., Faerber, P., Huettel, M., Meyer, V., and Witte, U. (2005a). Pore-Water Advection and Solute Fluxes in Permeable Marine Sediments (I): Calibration and Performance of the Novel Benthic Chamber System Sandy, Limnology and Oceanography, 50:768-778.

Janssen, F., Cardenas, M. B., Sawyer, A. H., Dammrich, T., Krietsch, J., de Beer, D. (2012), A comparative experimental and multiphysics computational fluid dynamics study of coupled surface–subsurface flow in bed forms. Water Resources Research 48: W08514

Johnson, K. S., J. P. Barry, L. J. Coletti, S. E. Fitzwater, H. W. Jannasch, and C. F. Lovera (2011). Nitrate and oxygen flux across the sediment-water interface observed by eddy correlation measurements on the open continental shelf, Limnology and Oceanography Methods, 9: 543-553.

Jørgensen, B.B., (1978). A comparison of methods for the quantification of bacterial sulfate reduction in coastal marine sediments, II. Calculation from mathematical model. Geomicrobiology Journal, 1: 129-47.

Jørgensen, B. B. (1982). Ecology of the bacteria of the sulphur cycle with special reference to anoxic-oxic interface environments. Philosophical Transactions of the Royal Society of London B 298:543-561

Jørgensen B.B. (1983) Processes at the sediment-water inter- face. In: Bolin B, Coock R.B. (eds) The major biochemical cycles and their interactions. John Wiley and Sons, New York, p 477-515

Jørgensen, B. B., and Revsbech, N. P. (1985). Diffusive boundary layers and the oxygen uptake of sediments and detritus. Limnology and Oceanography 30, 11-21.

Jørgensen, B. B., and Des Marais, D. J. (1990). The diffusive boundary layer of sediments: oxygen microgradients over a microbial mat. Limnology and Oceanography, 35(6), 1343-55.

Jørgensen B.B. (2000). Bacteria and marine biogeochemistry. In Marine Geochemistry, ed. H.D. Schulz, M. Zabel, pp. 173-207. Berlin: Springer

Kaimal, J.C., Finnigan, J.J., (1994). Atmospheric boundary layer flows: their structure and measurement. Oxford University Press, Oxford, 289 pp.

Klimant, I., Meyer, V., and Kühl, M. (1995). Fiber-optic oxygen microsensors, a new tool in aquatic biology. Limnology and Oceanography, 40(6), 1159-1165.

Kolmogorov, A. N., (1941). The local structure of turbulence in in- compressible viscous fluid for very large Reynolds numbers. Doklady Akademii Nauk SSSR, 30, 301-305.

Kristensen, E. (1985). Oxygen and inorganic nitrogen ex- change in a Nereis virens (Polychaeta) bioturbated sediment-water system. Journal of Coastal Research 1: 109-116

Kuwae, T., Kamio, K., Inoue, T., Miyoshi, E., and Uchiyama, Y. (2006). Oxygen exchange flux between sediment and water in an intertidal sandflat , measured in situ by the eddy-correlation method. Marine Ecology Progrees Series 307, 59-68.

Lee, C. (1992). Controls on organic carbon preservation: The use of stratified water bodies to compare intrinsic rates of decomposition in oxic and anoxic systems. Geochimica et Cosmochimica Acta, 56(8), 3323-3335.

Lee, X., Massman, W., and B. Law (2004). Handbook of Micrometeorology: A Guide for Surface Flux Measurement and Analysis. Kluwer Academic Publishers.

Lohrer AM, Thrush SF, Gibbs MM (2004) Bioturbators enhance ecosystem function through complex biogeochemical interactions. Nature 431:1092-1095.

Lohse L., Malschaert J. F. P., Slomp C. P., Helder W., Van Raaphorst W. (1993) Nitrogen cycling in North-Sea sediments - Interaction of denitrification and nitrification in offshore and coastal areas. Marine Ecology Progress Series. 101:283-296

Lohse, L., Epping, E., Helder, W., and Van Raaphorst, W. (1996). Oxygen pore water profiles in continental shelf sediments of the North Sea:turbulent versus molecular diffusion. Marine Ecology Progress Series, 145, 63-75.

Long, M. H., Koopmans, D., Berg, P., Rysgaard, S., Glud, R. N., and S, D. H. (2012). Oxygen exchange and ice melt measured at the ice-water interface by eddy correlation. Biogeosciences, 9(6), 1957-1967.

Long, M. H., Berg, P., De Beer, D., and Zieman, J. C. (2013). In situ coral reef oxygen metabolism: an eddy correlation study. PloS one, 8(3), e58581.

Lopez G. R. and Levinton J. S. (1987). Ecology of deposit-feeding animals in marine sediments. The Quarterly Review of Biology. 62: 235-260.

Lorke, A., Umlauf, L., Jonas, T., and A. Wüest (2002). Dynamics of turbulence in low-speed oscillating bottom-boundary layers of stratified basins. Environmental Fluid Mechanics 2:291-313.

Lorke, A., Mu, B., Maerki, M., and Wu, A. (2003). Breathing sediments : The control of diffusive transport across the sediment - water interface by periodic boundary-layer turbulence. Limnology and Oceanography 48(6), 2077-2085.

Lorke, A., McGinnis, D. F., Maeck, A., and H. Fischer (2012). Effect of ship locking on sediment oxygen uptake in impounded rivers, Water Resources Research. 48, W12514

Lorke, A., McGinnis, D.F., Maeck, A. (2013). Eddy-correlation measurements of benthic fluxes under complex flow conditions: Effects of coordinate transformations and averaging time scales. Limnology and Oceanography Methods. 11:425-437.

Luther III, G.W., Sundby, B., Lewis, B.L., Brendel, P.J., Silverberg, N., (1997). Interactions of manganese with the nitrogen cycle: alternative pathways to dinitrogen. Geochimica et Cosmochimica Acta 61, 4043-4052.

Lorrai, C., McGinnis, D. F., Berg, P., Brand, A., and Wüest, A. (2010). Application of Oxygen Eddy Correlation in Aquatic Systems. Journal of Atmospheric and Oceanic Technology, 27(9), 1533-1546.

Mackenzie, F.T., Lerman, A., Andersson, A.J. (2004). Past and present of sediment and carbon biogeochemical cycling models. Biogeosciences 1, 11-32.

McCann, K., (2010) Title: Eddy Correlation Benthic O2 Exchange Rates and Characterization of Sediment Properties from the Central Oregon Shelf at 30 Meters. MSc Thesis submitted to Oregon State University.

McCave, I. N. (1984). Size spectra and aggregation of suspended particles in the deep ocean. Deep-Sea Research 31: 329-352.

McGinnis, D. F., Berg, P., Brand, A., Lorrai, C., Edmonds, T. J., and Wüest, A. (2008). Measurements of eddy correlation oxygen fluxes in shallow freshwaters: Towards routine applications and analysis. Geophysical Research Letters, 35(4), L04403.

McGinnis, D. F., S. Cherednichenko, S. Sommer, P. Berg, L. Rovelli, R. Schwarz, R. N. Glud, P. Linke (2011): Simple, robust eddy correlation amplifier for aquatic dissolved oxygen and hydrogen sulfide flux measurements. Limnology and Oceanography:Methods, 9, 340-347.

Maerki, M., B. Wehrli, C. Dinkel, and B. Müller. (2004). The influence of tortuosity on molecular diffusion in freshwater sediments of high porosity. Geochimica et Cosmochimica Acta 68:1519-1528.

Marinelli, R.L., Jahnke, R.A., Craven, D.B., Nelson, J.R., Eckman, J.E., (1998). Sediment nutrient dynamics on the South Atlantic Bight continental shelf: The importance of benthic photosynthesis, nutrient regeneration, bioirrigation and porewater advection. Limnology and Oceanography 43, 1305-1320.

Marinelli R. L., Lovell C. R., Wakeham S. G., Ringelberg D. B., White D. C. (2002) Experimental investigation of the control of bacterial community composition in macrofaunal burrows. Marine Ecology Progress Series 235:1-13

Martin, J. H., G. A. Knauer, D. M. Karl, and W. W. Broenkow. (1987). Vertex: Carbon cycling in the northeast Pacific. Deep-Sea Research 34: 267- 285.

Mermillod-Blondin, F., Rosenberg, R., Francois-Carcaillet, F., Nor- ling, K., Mauclaire, L., (2004). Influence of bioturbation by three benthic infaunal species on microbial communities and biogeo- chemical processes in marine sediment. Aquatic Microbial Ecology. 36, 271-284.

Meysman, F. J. R., Middelburg, J. J., and Heip, C. H. R. (2006). Bioturbation: a fresh look at Darwin's last idea, Trends Ecology and Evolution, 21, 688-695,.

Michaud, E., Desrosiers, G., Mermillod-Blondin, F., Sundby, B., and Stora, G. (2005). The functional group approach to bioturbation: The effects of biodiffusers and gallery-diffusers of the Macoma balthica community on sediment oxygen uptake. Journal of Experimental Marine Biology and Ecology, 326(1), 77-88.

Middelburg, J.J., (1989). A simple rate model for organic mat- ter decomposition. Geochimica et Cosmochimica Acta, 53:1577- 1581.

Middelburg, J.J., (1991). Organic carbon, sulphur and iron in recent, semi-euxinic sediments of Kau Bay, Indonesia. Geochimica et Cosmochimica Acta, 55:815-828.

Middelburg, J. J., C. M. Duarte and J.-P. Gattuso, (2005). Respiration in coastal benthic communities. In Del Giorgio, P. A. and P. J. LeB. Williams (eds), Respira- tion in Aquatic Ecosystems, Oxford University Press, New York, 206-224.

Middelburg, J.J., Meysman, F.J.R., (2007). Burial at sea. Science 316, 1294-1295.

Middelburg, J. J., and Levin, L. A. (2009). Coastal hypoxia and sediment biogeochemistry. Biogeosciences, 6(7), 1273-1293.

Moodley, L., Middelburg, J.J., Boschker, H.T.S., Duineveld, G.C.A., Pel, R., Herman, P.M.J., Heip, C.H.R., (2002). Bacteria and Foraminifera: key players in a short- term deep-sea benthic response to phytodetritus. Marine Ecology Progress Series 236, 23-29.

Moodley, L., Middelburg, J.J., Soetaert, K., Boschker, H.T.S., Herman, P.M.J., Heip, C.H.R., (2005a). Similar rapid response to phytodetritus deposition in shallow and deep-sea sediments. Journal of Marine Research 63, 457-469.

Morales, C. E., Hormazabal, S. E., and Blanco, J. L. (1999). Interannual variability in the mesoscale distribution of the depth of the upper boundary of the oxygen minimum layer off northern Chile (18- 24S): Implications for the pelagic system and biogeochemical cycling. Journal of Marine Research, 57, 909-932.

Müller, B., M. M/"arki, C. Dinkel, R. Stierli, and B. Wehrli. (2002). In situ measurements in lake sediments using ion-selective electrodes with a profiling lander system, p. 126 - 143. In M. Taillefert and T. F. Rozan [eds.], Environmental electrochemistry - Analyses of trace element biogeochemistry. American Chemical Society.

Münster, U. and de Haan, H., (1998). The role of microbial extracellular enxymes in the transformation of dissolved organic matter in humic waters. In: Hessen, D.O. and Tranvik, L.J.(eds.) Aquatic humic substances: Ecology and biogeochemistry. Springer- Verlag, Berlin. pp. 199257.

Naqvi, S.W. A., Jayakumar, D. A., Narvekar, P.V., Naik, H., Sarma, V. V. S. S., D'Souza, W., Joseph, S., and George, M. D (2000). Increased marine production of N_2O due to intensifying anoxia on the Indian continental shelf. Nature, 408, 346-349.

Pfannkuche, O., Linke, P. (2003). GEOMAR landers as long-term deep-sea observatories. Sea Technology 44:50.

Precht E, Huettel M (2003). Advective pore water exchange driven by surface gravity waves and its ecological implications. Limnology and Oceanography 48:1674-1684

Precht, E., and M. Huettel. (2004). Rapid wave-driven advective pore water exchange in a permeable coastal sediment. Journal of Sea Research 51: 93-107.

Priestley MB (1992) Spectral analysis and time series. Academic Press, London

Rabouille, C., Denis, L., Dedieu, K., Stora, G., Lansard, B., and Grenz, C. (2003). Oxygen demand in coastal marine sediments: comparing in situ microelectrodes and laboratory core incubations. Journal of Experimental Marine Biology and Ecology, 285-286, 49-69.

Rasmussen, H., and Jørgensen, B. B. (1992). Microelectrode studies of seasonal oxygen uptake in a coastal sediment : role of molecular diffusion. Marine Ecology Progress Series 81, 289-303.

Reichardt W. (1988) Impact of bioturbation by Arenicola marina on microbiological parameters in intertidal sediments.Marine Ecology Progress Series 44:149-158

Reimers, C. E., K. M. Fischer, R. Merewether, K. L. Smith, Jr., and R.A. Janhke. (1986). Oxygen microprofiles measured in situ in deep ocean sediments. Nature 320: 741-744.

Reimers, C.E., (1987). A in situ microprofiling instrument for measuring interfacial pore water gradients: methods and oxygen profiles from the North Pacific Ocean. Deep-Sea Research 34, 2019-2035.

Reimers C. E., R. A. Jahnke and D. C. McCorkle (1992) Carbon Ruxes and burial rates over the continental slope and rise off Central Califronia with implications for the global carbon cycle. Global Byogeochemical Cycles. 6: 199-224.

Reimers, C.E., Ruttenberg, K.C., Canfield, D.E., Christiansen, M.B., Martin, J.B., (1996). Porewater pH and authigenic phases formed in the uppermost sediments of the Santa Barbara Basin. Geochimica et Cosmochimica Acta 60, 4037–4057.

Reimers, C.E., Jahnke, R.A., Thomson, L., (2001). In situ sampling in the benthic boundary layer. In: Boudreau, B.P., J/orgensen, B.B. (Eds.), The Benthic Boundary Layer-Transport Processes and Biogeochemistry. Oxford University Press, Oxford, pp. 245-268.

Reimers C. E., Stecher III H. A., Taghon G. L., Fuller C. M., Huettel M., Rusch A., Ryckelynck N. and Wild C. (2004). In situ measurements of advective solute transport in permeable shelf sands. Continental Shelf Research, 24, 183-201.

Reimers, C. E., H. T. Ozkan-Haller, P. Berg, A. Devol, K. McCann-Grosvenor, and R. D. Sanders (2012). Benthic oxygen consumption rates during hypoxic conditions on the Oregon continental shelf: Evaluation of the eddy correlation method. Journal of Geophysical Research. 117:1-18.

Revsbech NP. (1989). An oxygen microsensor with a guard cathode. Limnology and Oceanography 34: 474-478.

Rheuban, J. E., Berg, P. (2013). The effects of spatial and temporal variability at the sediment surface on aquatic eddy correlation flux measurements. Limnology and Oceanography: Methods, 11, 351–359.

Ridgwell, A., Zeebe, R.E., (2005). The role of the global carbonate cycle in the regulation and evolution of the Earth system. Earth and Planetary Science Letters 234, 299-315.

Ridgwell, A. and Hargreaves, J. C. (2008) Regulation of atmospheric CO_2 by deep-sea sediments in an Earth system model, Global Biogeochemmical Cycles, 21, GB2008.

Riedl RJ, Ott JA (1972) Water movement through porous sediments In: Fanning KA, Mannheim FT (eds) The dynamic environment of the ocean floor Lexington Books, Toronto, p 29-55.

Roberts, J., and A. Mcminn. (2004). Marine diffusive boundary layers at high latitudes. Limnology and Oceanography 49: 934-939.

Røy H., Huettel M., and J/orgensen B. B. (2002). The role of small-scale sediment topography for oxygen flux across the diffusive boundary layer. Limnology and Oceanography 47, 837-847.

Røy, H., Huettel, M., and Jørgensen, B. B. (2004). Transmission of oxygen concentration uctuations through the diffusive boundary layer overlying aquatic sediments. Limnology and Oceanography, 49(3), 686-692.

Rowe, G. T., G. S. Boland,W. C. Phoel, R. F. Anderson, and P. E. Biscaye (1994). Deep-sea floor respiration as an indication of lateral input of biogenic detritus from continental margins, Deep Sea Research, Part II, 41, 657-668.

Rysgaard, S., and Berg, P,. (1996). Mineralization in a northeastern Greenland sediment: Mathematical modelling, measured sediment pore water profiles and actual activities. Aquatic Microbial Ecology 11: 297-305.

Ryther, J.H., (1969). Photosynthesis and fish production in the sea. Science 166, 72-76.

Shaw, T.J., Gieskes, J.M., Jahnke, R.A., (1990). Early diagenesis in differing depositional environments: The response of transition metals in pore water. Geochimica et Cosmochimica Acta, 54: 1233- 1246.

Santos, I. R., Cook, P. L. M., Rogers, L., de Weys, J., Eyre, B. D. (2012). The "salt wedge pump": Convection-driven pore-water exchange as a source of dissolved organic and inorganic carbon and nitrogen to an estuary. Limnology and Oceanography, 57(5), 1415–1426. doi:10.4319/lo.2012.57.5.1415

Shaw, W. J., and J. H. Trowbridge (2001). The direct evaluation of near- bottom turbulent fluxes in the presence of energetic wave motions, Journal of Atmospheric and Oceanic Technology 18,1540–1557

Schlüter, M., Sauter, E.J., Schäfer, A. and W. Ritzrau (2000). Spatial budget of organic carbon fl ux to the seafloor of the northern North Atlantic (60N- 80N). Global Biogeochemical Cycles 14:329-340.

Schnitzer, M., (1991) Soil organic matter: the next 75 years. Soil Science 151, 41-58.

Schulz, H.D. and Zabel, M. (2006). Marine Geochemistry. (H. D. Schulz and M. Zabel, Eds.). Berlin/Heidelberg: Springer-Verlag.

Siegenthaler, U., Sarmiento, J.L., (1993) Atmospheric carbon dioxide and the ocean. Nature 365, 119-125

Sauter, E.J., Schlüter, M., and E. Suess (2001). Organic carbon flux and remineralization in surface sediments from the northern North Atlantic derived from pore-water oxygen microprofiles. Deep-Sea Research I 48(2):529-553.).

Soetaert, K., Herman, P.M.J., Middelburg, J.J., (1996). A model for early diagenetic processes from the shelf to abyssal depths. Geochimica et Cosmochimica Acta 60, 1019-1040.

Soetaert, K., J. J. Middelburg, P. M. J. Herman, and K. Buis. (2000). On the coupling of benthic and pelagic biogeochemical models. Earth Science Reviews, 51:173-201.

Stahl, H., Tengberg, A., Brunnegard, J., Bjornbom, E., Forbes, T. L., Josefson, A. B., Kaberi, H. G., Hassellov, I. M. K., Olsgard, F., Roos, P., and Hall, P. O. J. (2004). Factors influencing organic carbon re cycling and burial in Skagerrak sediments. Journal of Marine Research, 62(6):867-907.

Stull, R. B. (1988). An introduction to boundary layer meteorology. Kluwer.

Swinbank, W. C. (1951). The measurement of vertical transfer of heat and water vapor by eddies in the lower atmosphere. Journal of Meteorology 8:135-146.

Tegelaar, E.W., de Leeuw, J.W., Derenne, S., Largeau, C., (1989). A reappraisal of kerogen formation. Geochimica et Cosmochimica Acta 53, 3103-3106.

Thamdrup B., Glud R. N., and Würgler Hansen J. (1994) Manganese oxidation and in situ manganese fluxes from a coastal sediment. Geochimica et Cosmochimica Acta 58: 2563-2570.

Thamdrup, B., (2000). Bacterial manganese and iron reduction in aquatic sediments. In: Schink, B. (ed.), Advances in microbial ecology, Volume 16. Kluwer Academic Publishers, New York, p. 41 84.

Thiel, H., Kirstein, K.O., Luth, C., Luth, U., Luther, G., Meyerreil, L.A., et al. (1994). Scientific requirements for an abyssal benthic laboratory. Journal of Marine Systems 4:421-39

Thorpe S.A., (2007) An Introduction to Ocean Turbulence. Cambridge University Press.

Thouzeau, G., J. Grall, J. Clavier, Chauvaud, L., Jean, F., Leynaert, A., Longphuirt, S., Amice, E., Amoroux, D. (2007). Spatial and temporal variability of benthic biogeochemical fluxes associated with macrophytic and macrofaunal distributions in the Thau lagoon (France). Estuarine Coastal and Shelf Science 72: 432–446

Thrush SF, Gray JS, Hewitt JE, Ugland KI (2006) Predicting the effects of habitat homogenization on marine biodiversity. Journal of Applied Ecology 16:1636-1642.

Trimmer, D. C. O., G. J. C. Underwood, and D. B. Nedwell.(1999). Effect of illumination and emersion period on the ex-change of ammonium across the estuarine sediment-water interface. Marine Ecology Progress Series 184: 11-20.

Viollier, E., Rabouille, C., Apitz, S.E., Breuer, E., Chaillou, G., Dedieu, K., Furukawa, Y., Grenz, C., Hall, P., Janssen, F., Morford, J.L., Poggiale, J.C., Roberts, S., Shimmield, T., Taillefert, M., Tengberg, A., Wenzhöfer, F., Witte, U., (2003). Benthic biogeochemistry: state of the art technologies and guidelines for the future of in situ survey. Journal of Experimental Marine Biology and Ecology 286, 5-31.

von Karman, T. (1930), Mechanische /"ahnlichkeit und Turbulenz, pp. 85-105, Proceedings of the Third International Congress of Applied Mechanics.

Wakeham, S.G., Lee, C., Hedges, J.I., Hernes, P.J., Peterson, M.L., (1997) Molecular indicators of diagenetic status in marine organic matter. Geochimica et Cosmochimica Acta 61, 5363-5369.

Wenzhöfer F., Adler M., Kohls O., Hensen C., Strotmann B., Boehme S. and Schulz H.D. (2001) Calcite dissolution driven by benthic mineralization in the deep-sea: In situ measurements of Ca^{2+}, pH, pCO_2 andO_2. Geochimica et Cosmochimica Acta, 65, pp. 2677- 2690.

Wenzhöfer, F., and R. N. Glud (2002). Benthic carbon mineralization in the Atlantic: A synthesis based on in situ data from the last decade, Deep-Sea Research I, 49(7), 1255-1279.

Wenzhöfer F., and Glud, R.N. (2004). Small-scale spatial and temporal variability in coastal benthic O2 dynamics: Effects of fauna activity. Limnol. Oceanogr. 49: 1471–1481.

Wetzel, R.G., (2001). Limnology Lake and river ecosystems. Academic Press, San Diego. pp. 1006.

Witte U, Aberle N, Sand M, Wenzhöfer F. (2003). Rapid responseof a deep-sea benthic community to POM enrichment: an in situ experimental study. Marine Ecology Progress Series 251:27-36

Wollast R. (1991). The coastal organic carbon cycle: fluxes, sources, and sinks. In Ocean Margin Processes in Global Change (eds. R. F. C. Mantoura, J. M. Martin and R. Wollast). John Wiley and Sons, New York.

Wollast, R., (1998). Evaluation and comparison of the global carbon cycle in the coastal zone and in the open ocean. In: Brink, K.H., Robinson, A.R. (Eds.), The Sea, vol. 10. Wiley, New York, pp. 213E252.

Wollast, R. (2002). Continental margins - review of geochemical settlings, in: Ocean margin systems, edited by: Wefer, G., Billet, D., Hebbeln, D., Jørgensen, B. B., Schl E., Springer.

Wüest, A., and Lorke, A. (2003). Small Scale Hydrodynamics in Lakes. Annual Review of Fluid Mechanics, 35(1), 373-412.

Zhang, J., Gilbert, D., Gooday, a. J., Levin, L., Naqvi, S. W. a., Middelburg, J. J., Scranton, M., et al. (2010). Natural and human-induced hypoxia and consequences for coastal areas: synthesis and future development. Biogeosciences, 7:5, 1443-1467.

Ziebis, W., M. Huettel, and S. Forster. (1996). Impact of biogenic sediment topography on oxygen fluxes in permeable seabeds. Marine Ecology Progress Series 140:227-237.

Acknowledgements

The first Thank You goes to Frank Wenzhöfer, because one day, some years ago, he picked me, so that I could join an extraordinary project named SENSEnet, living an adventure that brought me in so many places - playing research - side to side to a number of outstanding, curious and helpful scientists. Unbelievable. Thank You Doug Connely and Carla Sands for turning something so demanding as an EU project can be, into such a relaxed and at the same time efficiently-profitable experience.

My supervisor Antje Boetius, I sincerely Thank You for being so inspiring. To have you in the vicinity is to feel the wind (polar perhaps)- you keep us motivated, you show the way with enthusiasm and sharpness - I couldn't wish for anyone more encouraging.

Thank You Dieter Wolf-Gladrow, for accepting to follow the progress and to review my work. With the first thesis committee meeting I promptly smashed your hope for attending brilliant results! Nevertheless you gave me brightness. From there on I magically got on the right track.

Thank You so much to Claudio Richter, who accepted to be part of the defense committe...

...as did Moritz Holtappels. Thank You especially for having helped me a lot and for being so peaceful and brilliant. Our sampling campaign in Askö was genuinely great. I hope I've learned form you to look into things with the time it takes to understand them, with no fear and no rush.

I was very lucky and honored to have Ronnie Glud keeping an eye on my progresses, with kindness and honesty; a reliable and competent mentor. Thank You.

When sparkling-genius Dan McGinnis showed up on my path (or better I caught him, begging to be my advisor) my understanding of what I was dealing with made a huge step forward. There must be a reason if I call you my GURU. Only few mysteries are left now between me and eddy correlation! I thank you more or less every couple of weeks... I'd gladly do it one more time: Thank You.

At MPI I discovered a world of true commitment to science that is a treasure for life- It will be really hard to work anywhere else. Where else can I get a Felix Janssen..WHERE? You are my favorite- you know. I wish I could have 1% of your dedication and critical thinking. Thank You for your help, your support, for understanding my lame jokes... and exchanging.

Thanks to Per Hall, Michael Böttcher and Volker Brüchert who facilitate and took part to some of the best field campaigns I've joined, providing much of the support and knowledge. Ketil Koop-Jakobsen, we had some amazingly tough field work on Sylt. I'll never forget the carrying of such ridiculously heavy instrumentation across the dunes..in the middle of the night... with the storm..and the tide rising fast! that-was-insane. Especially since we didn't get anything out of it-that's science too baby. Right?

I truly thank Patrick Mayer for the patience and the great help on each field campaign.

Thank You to our wonder-makers: Volker Meyer, Paul Farber and Arald Osmers.

Thank You to our awesome technicians: Axel, Volker, Marc, Rafael, Erika, Gabi, Wiebke...

Thank You to Josephine and Rebecca, you're lovely.

Thanks to all the ones I haven't directly work with, who made things so much easier- Alban, Christina, Gunter, Mari, Felix, Emil, Janine, Katy... from most of you I had learned a lot by listening to your talks, participating to the commitment to your interests, seeking new perspectives for looking at the world (micro-or mega)..over a lunch break. Well..there is no need to tell you how binding is for an Italian to prepare meals- exchange recipes - unravel ingredients- analyze combinations and finally share the pleasure of a taste. (yes, most of the time it was snubbing mensa's delicacies. But still, it's never merely food!)

Oh Gerd! The beautiful layout of this book is a perfect metaphor for the smile that bloomed on my face since you arrived: neither of those things would have been so easy to achieve without you.

Paula -I'm your simpatica pesada, para siempre, Natalie -we made it through a lot lady bella, we are sisters, Petra - dear I'm so glad I found you, Antoni - first Blanes then Bremen..what comes next?

Machu Picchu?

You all make worth living here 10 more years. Yes. 10 more years in Bremen. You know how strong is this declaration! And I mean it.

Appendix

Appendix A

Additional studies and Secondments

Cruise participations

R/V M.S.Merian MSM 15/1, Black Sea (7 April-8 May 2010)

Waddensea Island Sylt (Field Campaign), Germany (26 July - 08 August 2010)

Hel Peninsula (Field Campaign), Poland (30 September – 10 October 2010; 25 August-5 September 2011)

A.1 Additional studies not included as manuscripts

The following studies were included in periodic reports for the EU SENSEnet project

Benthic exchanges at groundwater seepage sites by eddy correlation technique

A study was carried out at a site where 2 characteristics are relevant for the application of EC: permeable sediments and submarine groundwater discharge (SGD). The first because understanding the role of permeable sediments in the coastal cycles of matter requires approaches that take into account the tight coupling between the interfacial fluxes and variable boundary layer flows. The second because SGD is often patchy, diffuse and temporarily variable, thus an approach that is representative of a wide area

can lead the estimation of the impact of SGD on benthic oxygen consumption to an ecosystem level.

After accurate spectral analyses of EC measurements, we detected the cases for which the resulting flux term (the product of vertical velocity and oxygen concentration fluctuations, w'C') contained contributions from turbulence as well as from wave induced processes. We corrected the net flux by calculating the energy dissipation (from which we can derive the time scale for the smallest eddies contributing to the turbulent flux) and cut the bias caused by the high frequency wave contribution.

Fluxes obtained by stirred benthic chamber incubations performed at this SGD site provide us the only possible comparison to give consistency to the novel application of the eddy correlation technique in high energetic ecosystems (chambers = -55 $\pm$ 12 N=3, EC= -77 , N=1, mmol $m^{-2}d^{-1}$). Next step will be to compare EC fluxes to heat fluxes measured with another EC system in the proximity and verify whether the seepage of grounwater produced stratification in the water column. Although the sampling site was very shallow (approx. 1 mt) and energetic.

Adaptation of the EC system for other flux measurements

The EC system was adapted for the measurement of small-scale temperature changes and used to identify and quantify fresh water seeps in coastal sandy sediments (Hel, Poland). The development of an EC system for heat flux measurements in 2010 was successful but the first results did not show a significant difference in the magnitude of the heat fluxes between the seepage and the reference site. Only small temperature differences between the water column (13.2 °C) and the pore water (13°C) as well as harsh sea conditions causing a fast mixing of the seepage and bottom water might be responsible for this.

For this reason the EC system has then been modified to host two amplifiers. This allows combining temperature and conductivity measurements at the same spot and time. The new system was tested in August 2011 during the second field campaign in Hel (Poland). Unfortunately, technical problems during the deployment lead to a miss-functioning of the conductivity sensor which did not resolve the high frequency fluctuations. The only application of temperature measurements for the aim of determining SGD rates is possible, however, more suitable for seepage of freshwater at greater depths , where the energy of the water column mixing is lower (i.e having a stronger temperature gradient at the sediment water interface). Moreover, at depths of 1.5 m (such as for Hel's SGD study site), to the heat flux generated by the seepage, is superimposed a strong flux

produced by the heat exchange between the relatively small volume of the water column and the atmosphere (especially during summer).

The EC system was also adapted for sulphide flux measurements and a first attempt for performing measurements was made during the cruise in the ByFjord (Baltic Sea, October 2010). Unfortunately the deployment was not successful because of the extremely soft sediment. The entire frame with the sensors sank into the sediment preventing any valuable data. The next attempt to test the application of EC for sulphide flux measurements took place in August 2011 in Hel (Poland) at the groundwater seepage site. Here the instrument could be easily controlled and additional parameters were measured by chamber incubations. However, during summer Hel campaign the outflow of H_2S was hardly detectable, most probably because the oxidation of H_2S took place within the oxygenated surface permeable sediments. The penetration of oxygen in sandy sediments depends on the energy of the hydrodynamics involved (i.e. on the flushing rate), and it was shown that at Hel the extension of the oxic sediment layer can reach 10 cm.

A.2 Secondments

University of Gothenburg, Sweden

R/V Skagerak in Byfjorden (Oct 25-30th 2010) The aim was to investigate the temporal and spatial dynamics of the oxygen transport and turnover rates and their effects on biogeochemistry and composition of the benthic communities. The EC was deployed in a sill fjord (ByFjord, Sweden) characterized by brackish conditions, intermittent water exchanges, and periodically low oxygen concentrations. During the cruise the EC system was deployed two times at 7 meters together with a benthic chamber lander (UGot). We learned that in systems where the hydrodynamic conditions are highly variable, turbulent O_2 transport between the bottom boundary layer and the fjord interior might not be related to benthic exchanges. For such environments it is therefore important to obtain long time-series to capture all environmental conditions and to correctly average O_2 exchange. Moreover, heat flux measurements at the same time resolution must be coupled to the oxygen flux measurements. By this it should be possible to separate the benthic oxygen flux from the flux related to water mass exchange.

University of Stokholm, Sweden

Askö Marine Station (Himmelfjärden) November 11 – 21, 2011 The general purpose was to measure bottom boundary layer nutrient profiles, and to determine the sediment O_2 uptake rates using three different methods: Eddy correlation, bottom boundary layer profiling, and by ex-situ measurements of sediment cores. In addition, an Eddy device with a conductivity sensor was tested and 15N tracer experiments were performed on intact cores and slurries. The collected data are under analysis process.

Appendix B

Workshops and Conferences

B.1 Workshops

SENSEnet workshop 1: "Sensors in the marine environment" (12-14th May 2010), Southampton, UK Workshop

SENSEnet workshop 1: "Sensor technology in marine research – General use and data analysis. Part I", (23-27th August 2010) Bremen Germany

SENSEnet workshop 2: "Sensor technology in marine research – General use and data analysis. Part II ", (September 2011) Sylt, Germany

SENSEnet workshop: "Data Management", (11-15 October 2011) NOC Southampton, UK.

SENSEnet workshop : "From research-based discovery to business", (26-27 March 2011), Aarhus, Denmark.

Workshop on eddy correlation system: flume experiments (September 2011). Landau University, Germany.

B.2 International conferences: oral presentations

Donis, D., Holtappels, M., McGinnis, D.F., Wenzhöefer, F.
"BENTHIC OXYGEN EXCHANGE RATES IN DEEP SEA ARCTIC SEDIMENTS: A DIRECT EDDY CORRELATION MEASUREMENT".
Ocean Sciences Meeting. Salt Lake City, Utah, U.S.A, 19 - 24 February 2012.

Donis, D., Janssen, F., Böttcher, M., McGinnis, D.F., Holtappels, M, Wenzhöfer, F.
"IN SITU OXYGEN BENTHIC FLUX MEASUREMENTS IN COASTAL PERMEABLE SEDIMENTS IMPACTED BY SUBMARINE GROUNDWATER DISCHARGE".
European Geosciences Union General Assembly 2012. Vienna, Austria, 22 – 27 April 2012.

Donis, D., Holtappels, M., Noss, C., Wenzhöfer, F., Hancke, K., Lorke, A., Glud, R. N., Meysman, F., and D.F. McGinnis
"IMPROVING PRECISION AND CONFIDENCE OF AQUATIC EDDY CORRELATION BENTHIC SOLUTE EXCHANGE MEASUREMENTS - FROM FLUMES TO THE DEEP SEA".
ASLO 2013 Aquatic Sciences Meeting. New Orleans, U.S.A, 17-22 February 2013

Donis, D. "EDDY CORRELATION APPLIED TO BENTHIC SOLUTE EXCHANGE MEASUREMENTS UNDER VARYING BENTHIC BOUNDARY LAYER CONDITIONS"
ASLO 2013 - SENSEnet Showcase

Erklärung

Hiermit erkläre ich, Daphne Donis, dass ich

1. die Arbeit ohne unerlaubte fremde Hilfe angefertigt habe,

2. keine anderen als die von mir angegebenen Quellen und Hilfsmittel benutzt habe und

3. die den benutzten Werken wörtlich oder inhaltlich entnommenen Stellen als solche kenntlich gemacht habe.